Spatio-temporal feedbacks between soil legacies and the rhizosphere microbiome of maize

Inaugural-Dissertation

zur

Erlangung des Doktorgrades

der Mathematisch-Naturwissenschaftlichen Fakultät

der Universität zu Köln

vorgelegt von

Daniela Niedeggen

angenommen im Jahr 2025

Abstract

The rhizosphere is the narrow layer of soil around roots, where root respiration and rhizodeposits continually restructure the physicochemical conditions, fuelling microbial growth. Bottom-up carbon release operates alongside top-down trophic consumers across interlinked feedback loops: mucilage at growing tips and exudates along older zones trigger bacterial and fungal proliferation, and, subsequently, protist grazers restructure the emerging assemblage. Senescing roots leave behind biological and structural legacies, microbial propagules and empty root channels (biopores), that influence root architecture and rhizosphere microbiomes of subsequent plants. These dual legacies may accelerate beneficial interactions but may also favour host-specific pathogens under continuous monoculture.

This thesis first quantified how maize carbon release structures the rhizosphere. Respiration-kinetics assays showed that microbial growth is initiated at 60 % of microbial-biomass carbon for simple sugars but requires 250–630 % for complex rhizodeposits, indicating substrate-specific activation thresholds that confine activity to the immediate root zone. PET-MRI, combined with DNA-SIP, traced photo-synthesised carbon into bacterial, fungal, and protistan communities, revealing discrete hotspots that select for specific sub-communities. A five-year field chronosequence monitored protist succession across two soil textures (sand and loam), while complementary column experiments used the pre-conditioned monoculture field soil to observe a full growth–decay–regrowth cycle, testing how biopore recycling and legacy inocula jointly influence rhizosphere microbial community assembly. Field data demonstrated that continuous maize steadily enriched potentially pathogenic oomycete species as well as heterotrophic Cercozoa, confirming that soil legacy drives microbial succession. Loam promoted an enhanced soil legacy effect by facilitating compositional shifts in protist communities. By contrast, sand exhibited more stochastic and drought-sensitive behaviour. Column imaging revealed that 10 % of biopores were reused by new roots. During regrowth, these recycled biomes shifted from decomposer communities back towards rhizosphere communities, though they hosted microbiomes with elevated beta dispersion.

Overall, the results showed that the location of microbial niches is determined by the availability of carbon, while inherited inocula and pore architecture influence the assembly of communities, which is further defined by exudate patterns. The interaction between these factors creates spatiotemporal feedback loops that can maintain the resilience of the maize rhizosphere microbiome or cause it to become vulnerable under continuous monoculture.

Table of content

Introduction

The self-organising rhizosphere

Since the concept of the rhizosphere was first introduced 100 years ago by Hiltner (1904) as the region around roots affected by rhizodeposition, our understanding of this interface has evolved to recognise it as a self-organising system maintained by tightly interlaced feedback loops (Kuzyakov and Razavi 2019, Vetterlein et al. 2020).

The rhizosphere forms a narrow soil layer surrounding the root where root respiration and the secretion of rhizodeposits, ranging from simple carbohydrates and amino acids to organic acids, phenolics and antimicrobial compounds, substantially modify physico-chemical conditions (Collins and Reilly 1968, Santangeli et al. 2024). These inputs act as energy sources, chemotactic signals, pH buffers and chelators that mobilise mineral nutrients (Oburger et al. 2011), shaping the composition and activity of plant associated microbial communities (Zhalnina et al. 2018). Carbon (C) release from growing roots is heterogeneous in both space and time. At the centimetre scale, root growth creates a mosaic of C hotspots across the root system (Kuzyakov and Blagodatskaya 2015), while radial diffusion, sorption and microbial mineralisation establish steep concentration gradients within just a few millimetres of the root surface. Simultaneously, as roots grow, they physically displace soil particles and release mucilage reshaping pore geometry and hydraulic connectivity (Hinsinger et al. 2009). Over time, the interaction of these physical and chemical processes produces distinct patterns: biopores in the soil matrix, localised microbial assemblages of varying abundance and trophic structure, and local pH, redox and nutrient gradients (Garcia Arredondo et al. 2024). These emergent features then feed back on root physiology and, ultimately, whole-plant performance.

Based on a current theory, the plant and its associated root microbiota are considered as a single dynamic entity—the plant holobiont (Vandenkoornhuyse et al. 2015, Mesny et al. 2023). This collective view posits that the functions and interactions of root-associated microorganisms cannot be disentangled from those of the host plant; rather, they form an integrated system that experiences selection and adapts as one evolutionary unit (Zilber-Rosenberg and Rosenberg 2008). Others caution that this framing may overstate harmony because the same microbial pool contains soilborne pathogens that can reduce host fitness (Raaijmakers et al. 2009).

Recent multiscale modelling approaches have demonstrated that self-organised rhizosphere patterns can be resolved and quantified only when processes are represented continuously from

the pore to the whole-root scale, explicitly coupling three-dimensional root architecture, rhizodeposition, soil water flow and root-induced mechanical deformation (Landl et al. 2021, Schnepf et al. 2022). However, most models simplify the biotic domain by reducing it to a single 'microbial pool' directed by a linear decay term (i.e. a rate directly proportional to the current pool size). This approach omits functional groups, trophic links and facilitative interactions. Recognising this gap is key to achieving a more systematic understanding, as the microbiome provides the plant with additional metabolic capabilities, expanding their gene pool that can be adapted to local conditions through interactions within and between microbial groups (Hassani et al. 2018).

Nevertheless, the composition of rhizosphere communities is primarily driven by local environmental factors, particularly soil properties and their inherent microbial structure, which explain more variance than plant genotype (Bulgarelli et al. 2012, Lundberg et al. 2012, Schlaeppi et al. 2014). Host identity, however, still imposes a measurable genotype-specific influence, as cultivar-comparison studies across several crop species have shown (Bouffaud et al. 2014, Ofek et al. 2014), suggesting the existence of a consistent core microbiome (Schlaeppi et al. 2014, Toju et al. 2018). The plant reduces taxonomic diversity in the rhizosphere through rhizodeposition, which fosters the growth of certain fast-growing copiotroph bacteria (Fierer et al. 2007, Bulgarelli et al. 2012). Additionally, it is suggested that plants may actively recruit a subset of plant growth promoting rhizobacteria (PGPR) by adjusting the quantity and chemical composition of their exudates (Bais et al. 2006). These beneficial microbes may suppress pathogens, mobilise nutrients, synthesise growth-regulating phytohormones, and activate host defences via induced systemic resistance. They can also detoxify allelochemicals and mitigate abiotic stresses, such as drought and heavy metal toxicity (Trivedi et al. 2020). However, because many beneficial plant traits depend on costly 'public goods', they remain vulnerable to 'signal-blind' or non-producing cheaters that exploit these goods without paying their metabolic cost (Denison et al. 2003, Jousset et al. 2009).

Previous work on this research project has already started to map out how self-organisation occurs in the maize rhizosphere. At the edaphic scale, soil texture emerged as a central filter: coarse substrates promoted lateral-root proliferation, restricted primary-root elongation and sharpened microbial selectivity (Rüger et al. 2023a). Superimposed on this environmental backdrop, the microbial community oscillated along the individual roots. This process was orchestrated by specific plant organs, such as the root cap (Rüger et al. 2023b). The young root tip environment is rich in resources and hosts taxonomically diverse assemblages, largely shaped by

priority effects. In contrast, older root segments had more organised communities, shaped by resource limitation and protistan predation (Rüger et al. 2021). Greater protist diversity enhanced trophic complementarity among protists, thereby modifying bacterial community structure (Rüger et al. in prep). Together, these findings emphasised that trophic interactions, particularly predation by protists, alongside root architectural traits and soil texture, jointly organise the maize rhizosphere. Building on this understanding, the present thesis explored the influence of biological and physical soil legacies, as well as spatial, quantitative and qualitative variations in C exudation, on rhizosphere microbiome assembly.

Protists grazing and pathogen dynamics

Soil protists are increasingly recognised as key players in rhizosphere processes. Despite occupying pivotal trophic positions that couple microbial turnover to nutrient fluxes (Clarholm 1981, Clarholm 1985, Bonkowski 2004), research on soil microbial communities has been dominated by studies of bacteria and fungi (Zhalnina et al. 2018, Epp Schmidt et al. 2022, Gong et al. 2023). Functionally, protists are very diverse and encompass a wide range of trophic strategies (Pawlowski et al. 2012, Geisen et al. 2018). As predators, heterotrophic protists connect microbial primary producers and decomposers to higher trophic levels, placing them at the centre of soil food webs (Rosenberg et al. 2009, Rüger et al. 2021, Rüger et al. 2023b). This drives the microbial loop, accelerating nitrogen turnover, and releases mineral nutrients that plants can re-capture (Bonkowski 2004). Predation imposes deterministic shifts in bacterial traits and community structure (Rosenberg et al. 2009, Jousset 2012, Geisen et al. 2017). As pathogens, such as oomycetes (*Pythium*, *Phytophthora*) or Phytomyxea (*Plasmodiophora*), they can act as parasites with worldwide economic importance, for example by infecting the roots of important crop species (Dixon 2009, Neuhauser et al. 2014, Thines 2014, Schwelm et al. 2018). Of the many protist lineages found in soil, Cercozoa and Oomycota play two ecologically important roles: microbial grazing and plant pathogenesis (Geisen et al. 2017). Cercozoa dominate the pool of free-living bacterivores and fungivores in arable soils; their diverse feeding modes, coupled with well-developed group-specific primers and reference databases (Fiore-Donno et al. 2018), allow detailed investigation of grazing-driven interactions. Within Cercozoa, the subgroup Phytomyxea harbours obligate plant pathogens such as *Plasmodiophora* and *Spongospora* (Neuhauser et al. 2014). Oomycota, by contrast, include many of the most damaging root pathogens (e.g. *Pythium*, *Phytophthora*) and combine saprotrophic with parasitic lifestyles (Kamoun et al. 2015).

Analyses incorporating protists demonstrated that predation acts as a sensitive bioindicator and network hub (Zhao et al. 2019); that grazing transforms seemingly stochastic bacterial patterns

into predictable, predator-driven results (Bonkowski et al. 2021); and revealed top-down controls that would otherwise overstate the importance of resource supply (Guo et al. 2022). Therefore, their inclusion is essential for any mechanistic framework aimed at predicting rhizosphere self-organisation. Accordingly, this thesis placed an emphasis on protist-mediated trophic feedback in its investigation of the maize rhizosphere.

Carbon hotspots and microbial growth

A substantial share of the photosynthetically fixed C is transferred below-ground (Kuzyakov and Domanski 2000, Pausch and Kuzyakov 2018), where it enters the soil in the form of border cells shed from the root cap, mucilage from growing tips, or exudates from older root segments (Bais et al. 2006). Mucilage, a viscous polysaccharide matrix, is actively secreted at the root tips to lubricate the advancing root tip. It consists of high-molecular-weight compounds such as polysaccharides, proteins, phenolic acids, and lipids (Bacic et al. 1987). By contrast, the more soluble exudate fraction, consisting of low-molecular-weight compounds such as sugars, amino acids, organic acids and phenolic compounds, as well as high-molecular-weight compounds like proteins, dominates along older root segments (Collins and Reilly 1968, Walter et al. 2003). This fraction greatly increases the diversity of rhizodeposits and undergoes significant changes as the root and season progress (Santangeli et al. 2024). Rhizodeposits are the primary energy source for the rhizosphere microbiome (Brimecombe et al. 2000). Released in pulses that diffuse only millimetres from the root surface (Lohse et al. 2021), they generate sharp spatial and temporal gradients, producing short-lived *hot moments* and microbial *hotspots* of elevated activity relative to bulk soil (Kuzyakov and Blagodatskaya 2015). Because roughly 90 % of bulk-soil microorganisms are dormant (Stenström et al. 2001), a fresh C pulse first triggers a 5–15 h lag phase in which respiration spikes while catabolic enzymes are up-regulated before exponential growth begins (Anderson and Domsch 1978, Panikov 1995).

In maize, a crop with a strongly hierarchical root architecture, the spatial pattern of C release changes as the plant develops. As the root system progresses from a single primary root through seminal roots to successive whorls of crown roots, the growth dynamics, cell-wall architecture and gene-expression profiles of each root class differ, indicating functional specialisation and suggesting root-type-specific C release patterns (Tai et al. 2016). Architectural diversity therefore translates into a patchwork of hotspots whose C concentration and chemical composition vary over centimetres in space and over hours to days in time (Kuzyakov and Razavi 2019). These concentration gradients matter because microbial growth is triggered only when the local C addition reaches a soil-dependent threshold of approximately 50 %–150 % of microbial-biomass

carbon (C_{mic}) (Anderson and Domsch 1985, Bremer and Kuikman 1994, Sawada et al. 2008). As C_{mic} accumulates, this threshold increases, linking hotspot strength to community size and nutrient status; it rises even further when N or P is limiting (Reischke et al. 2015). Notably, these thresholds have been derived almost exclusively from glucose assays. Comparable kinetics for complex rhizodeposits remain unquantified, creating a significant gap in our understanding of, and ability to accurately model, substrate-specific microbial activation in the rhizosphere.

Research using Positron Emission Tomography-Magnetic Resonance Imaging (PET-MRI) has shown that ^{11}C-labelled assimilates reach individual maize root tips within minutes, yet neighbouring roots displayed different temporal uptake patterns: some tips accumulated tracer continuously, whereas others received it in successive pulses (Jahnke et al. 2009). Three-dimensional MRI subsequently linked this heterogeneity to the spatial arrangement of primary, seminal and crown roots (van Dusschoten et al. 2016). In regions further behind the tip, where the total supply of freshly fixed photosynthate is lower, the relevance of specific exudate compounds, which are often more soluble, increases. Together, these intra-root mosaics are likely to create patchy *carbon niches* in the surrounding soil, fuelling microbial hotspots. In this work, the spatial C patches were linked to their specific microbial consumers by combining in-situ PET-MRI tracer imaging with DNA stable-isotope probing (DNA-SIP), which enabled photosynthate to be traced from fixation into microbial biomass.

Root channel legacies under continuous cropping

Each crop leaves behind living and structural imprints that accumulate over time, shaping the roots and microbiomes of subsequent plants (Bever et al. 1997, Donn et al. 2015, Bonkowski et al. 2021). This is known as soil legacy (Bakker et al. 2018, Frouz 2024). Two complementary dimensions can be distinguished. A biological legacy consists of resident microbiota, such as spores, cysts, dormant hyphae and bacterial cells, which survive root senescence and regain activity once resources reappear. These persistent consortia can accelerate the establishment of beneficial interactions, but can equally favour the build-up of host-specific pathogens under continuous cropping (Bever et al. 2012, van der Putten et al. 2013, Bakker et al. 2018). A physical legacy arises from the network of empty root channels, or biopores, left in the soil matrix after root senescence (Ehlers et al. 1983). In biopore recycling, new roots preferentially re-enter these pre-formed channels (Atkinson et al. 2020). The reused pores lower mechanical impedance and improve aeration and drainage (Lucas et al. 2019), serving as ‘root highways’ that promote deeper soil exploration and directed microbial transfer between plant generations (Passioura 2002).

Soilborne legacies can steer plant performance in contrasting directions. Resident microbiomes may exert positive feedback, for example when nutrient-mobilising or pathogen-suppressive consortia persist and benefit the next crop (Mariotte et al. 2018, Wubs and Bezemer 2018, Hannula et al. 2021). Equally, they can impose negative feedback when root-specific pathogens or antagonistic nutrient cycles build up and hinder subsequent plant growth (Kardol et al. 2007, Li et al. 2019). These effects are agriculturally important: the microbiome assembled by one crop can raise or lower the yield of the next (Roy et al. 2021, Liu et al. 2023). Continuous monoculture tends to amplify negative legacies. For example, lower diversity, disrupted nutrient cycling and greater pathogen pressure have been documented in maize and other crops (Frindte et al. 2020, Yang et al. 2020, Mao et al. 2021, Zhao et al. 2021). Traditional crop rotation mitigates this build-up (Bullock 1992, Krupinsky et al. 2002), further diversification strategies such as intercropping dilute specialist pathogens and broaden the chemical landscape of root exudates, reshaping microbial interaction networks in favour of plant immunity (Li et al. 2021, Pelissier et al. 2021, Oburger et al. 2022). Complex, well-connected microbial networks can protect crops against abiotic stress (Toju et al. 2018, Wagg et al. 2019). However, microbial communities themselves respond to climate variables such as temperature, moisture, and soil texture (Williams and Rice 2007, Bauke et al. 2022, Yim et al. 2022, Zhao et al. 2024).

Physical and biological legacies together lead to a spatio-temporal feedback loop that links past root activity to the current state of the microbiome. Column-scale studies refine this picture by isolating specific mechanisms. In rhizotron experiments, for example, young maize roots exhibited a strong tendency to re-enter pre-existing channels. Once inside, contact with decaying root walls promoted the rapid colonisation of filamentous Actinobacteria (Watt et al. 2006). However, roots that grew quickly beyond old pores were not affected by 'legacy infiltration' (Watt et al. 2003).

Therefore, deciphering how biological and physical legacies arise and interact with environmental drivers is key to understanding the spatio-temporal feedbacks that govern rhizosphere self-organisation, and to applying this knowledge in the design of resilient agricultural systems. This thesis examined how microbial succession and biopore recycling occur across successive seasons of continuous maize cultivation and how these processes contribute to legacy formation at different scales. A five-year field chronosequence was analysed to capture the evolution of legacies under authentic climate and management regimes (Vetterlein et al. 2021). A column-scale study was conducted to examine the locally specific influence of biopore recycling on subsequent rhizosphere microbiomes.

Aims and hypotheses

This thesis was conducted within the DFG Priority Programme 2089 “Rhizosphere Spatiotemporal Organisation – a Key to Rhizosphere Functions”. The programme views the rhizosphere as a self-organising system in which feedback loops among C release, microbial activity and soil structure generate patterns that shape plant resilience. Building on this concept, the thesis investigated how spatio-temporal feedbacks between soil legacies and the maize rhizosphere microbiome drive the self-organisation of emergent community patterns and functions.

Maize roots deliver pulsed C inputs: mucilage at growing tips and exudates along older root zones. These bottom-up pulses fuel bacterial and fungal growth; subsequent top-down grazing by protists rearranges the assemblage and feeds back on the predators themselves. We suggest that this trophic loop is a key factor in rhizosphere self-organisation and that its outcome is further modulated by biological legacies (dormant microbial propagules) and physical legacies (re-used biopores) inherited from previous crops.

To investigate these processes, the study used laboratory assays to quantify the kinetics of microbial growth across maize rhizodeposit concentration gradients. PET-MRI tracer imaging and DNA-SIP were employed to trace the movement of photosynthate from fixation into specific bacterial and protist consumers. Field chronosequences monitored microbial succession and pathogen build-up over successive maize seasons. Finally, mechanistic column experiments used MRI to track root growth and tested the influence of biopore recycling on community assembly. By including bottom-up C supply response dynamics, top-down control in trophic networks, and legacy feedback, we aimed to describe how self-organisation emerges and evolves in the maize rhizosphere under continuous monoculture.

The hypotheses of this thesis were as follows:

H1 Where rhizodeposit carbon falls below substrate-specific activation thresholds, microbial growth is restricted.

H2 Patchy photosynthate allocation along roots establishes discrete carbon niches that structure trophic networks.

H3 Soil legacy (i.e. microbial residues) directs microbial succession over successive growth seasons.

H4 Biopores recycling intensifies negative plant–soil feedback by transmitting legacy-borne microbes.

H5 Pathogenic protists accumulate progressively during continuous maize cultivation, thereby reinforcing negative plant–soil feedback loops.

Chapter Summary

Chapter I: Microbial utilization of maize rhizodeposits

Microbial utilisation of maize rhizodeposits applied to agricultural soil at a range of concentrations

Microbial growth dynamics were measured in order to quantify the response of soil microbes to root-derived substrates applied at a concentration gradient. The results showed the activation thresholds for complex rhizodeposits to be higher than for simple sugars. Adding N and P lowered activation thresholds. Early-season exudates behaved like complex C sources, whereas late-season exudates behaved like simple sugars. The defined kinetic functions enable the temporal and spatial aspects of microbial growth and rhizodeposit mineralisation to be incorporated into models. This allows more accurate predictions of how rhizodeposition drives microbial C and nutrient dynamics in the soil.

Chapter II: Photosynthate hotspots structure rhizosphere microbiota

Photosynthate distribution determines spatial patterns in the rhizosphere microbiota of the maize root system.

PET–MRI tracking of ^{11}C photosynthate revealed uneven hotspots among different types of maize root. Follow-up $^{13}CO_2$ pulse labelling and DNA-SIP showed that rhizodeposition mirrored internal carbon allocation and that bacterial, fungal and cercozoan communities segregated accordingly. ^{13}C-enriched consumers were found at high-C tips, while distinct assemblages were found in older zones. Thus, intra-root C hotspots define discrete microbial habitats and organise trophic food webs in the maize rhizosphere, highlighting the importance of carbon flow as a spatial and temporal selector.

Chapter III: Protist community shifts under maize monoculture

Continuous maize cropping reshapes rhizosphere protist communities through soil legacy effects.

In a five-year field experiment, rhizosphere protist communities were tracked to investigate how continuous maize cultivation shapes the belowground community. Soil legacy effects progressively altered community composition. Maize-specific potential pathogenic oomycetes (e.g., *Pythium arrhenomanes* and *P. monospermum*) accumulated and there was an increase in variability among heterotrophic cercozoan consumers, including potential pathogen antagonists such as *Platyreta* and Trinematidae. Meanwhile, obligate non-maize-specific plant-pathogenic Phytomyxea declined. These shifts in community composition were modulated by soil texture and interannual climate variability: communities in loam underwent gradual, cumulative changes, whereas those in sand responded in a more seasonal, drought-driven manner.

Chapter IV: Root legacies govern the maize rhizosphere

Decay legacies and biopore recycling drive rhizosphere succession in maize monocultures.

To disentangle the influence of biological (resident microbiota) and physical (root biopores) legacies on rhizosphere assembly and plant performance, high-resolution MRI was used to track maize roots through growth, decay and regrowth in columns containing either fresh or maize monoculture-conditioned ‘legacy’ soil. Microbial succession followed three phases: (i) distinct rhizosphere microbiomes during growth; (ii) a community shift after decomposition; and (iii) an imperfect return to rhizosphere microbiomes during regrowth since root decay shifted rhizosphere community composition. About 10 % of new roots re-entered existing biopores, boosting rooting depth and microbial heterogeneity. Communities in legacy and fresh soil were always distinct, demonstrating the influence of previous cropping history.

Chapter I: Microbial utilization of maize rhizodeposits

Microbial utilisation of maize rhizodeposits applied to agricultural soil at a range of concentrations

Reference:

Niedeggen, D., Rüger, L., Oburger, E., Santangeli, M., Ahmed, M., Vetterlein, D., Blagodatsky, S., Bonkowski, M. (2024). Microbial utilisation of maize rhizodeposits applied to agricultural soil at a range of concentrations. *European Journal of Soil Science*, *75*(4), e13530. https://doi.org/10.1111/ejss.13530

Author contributions:

Daniela Niedeggen: Conceptualization; formal analysis; methodology; validation; visualization; writing – review and editing; writing – original draft; data curation. Lioba Rüger: Conceptualization; methodology. Eva Oburger: Validation; writing – review and editing; supervision. Michael Santangeli: Writing – review and editing; methodology. Mutez Ahmed: Validation; methodology; conceptualization. Doris Vetterlein: Writing – review and editing; conceptualization. Sergey Blagodatsky: Validation; writing – review and editing; formal analysis; supervision; methodology. Michael Bonkowski: Conceptualization; validation; writing – review and editing; writing – original draft; project administration; supervision; funding acquisition.

The PDF of the article and supplementary material for Chapter I can be viewed and downloaded here: https://uni-koeln.sciebo.de/s/DK1NsXCQPfXK4WD

Received: 2 February 2024 | Revised: 17 June 2024 | Accepted: 19 June 2024

DOI: 10.1111/ejss.13530

RESEARCH ARTICLE

European Journal of Soil Science WILEY

Microbial utilisation of maize rhizodeposits applied to agricultural soil at a range of concentrations

Daniela Niedeggen[1,2] | **Lioba Rüger**[1,2] | **Eva Oburger**[3] | **Michael Santangeli**[3,4] | **Mutez Ahmed**[5] | **Doris Vetterlein**[6] | **Sergey Blagodatsky**[1,2] | **Michael Bonkowski**[1,2]

[1]Institute for Zoology, Terrestrial Ecology, University of Cologne, Cologne, Germany

[2]Cluster of Excellence on Plant Sciences (CEPLAS), University of Cologne, Cologne, Germany

[3]Institute of Soil Research, BOKU University, Tulln an der Donau, Austria

[4]Institute of Analytical Chemistry, BOKU University, Vienna, Austria

[5]School of Life Sciences, Root-Soil Interaction, Technical University Munich –TUM, Freising, Germany

[6]Dept. Soil System Science, Helmholtz Centre for Environmental Research GmbH –UFZ, Halle/Saale, Germany

Correspondence
Daniela Niedeggen, University of Cologne, Institute for Zoology, Terrestrial Ecology, Cologne, Germany.
Email: daniela.niedeggen@uni-koeln.de

Funding information
Deutsche Forschungsgemeinschaft, Grant/Award Number: 403635931

Abstract

Rhizodeposition fuels carbon (C) and nutrient cycling in soil. However, changes in the dynamics of microbial growth on rhizodeposits with increasing distance from the root is not well studied. This study investigates microbial growth on individual organic components of rhizodeposits and maize root-derived exudates and mucilage from agricultural soil. By creating a gradient of substrate concentrations, we simulated reduced microbial access to rhizosphere C with increasing distance to the root surface. We identified distinct C-thresholds for the activation of microbial growth, and these were significantly higher for rhizodeposits than singular, simple sugars. In addition, testing for stoichiometric constraints of microbial growth by supplementing nitrogen (N) and phosphorus (P) showed accelerated and increased microbial growth by activating a larger proportion of the microbial biomass. Early and late season exudates triggered significantly different microbial growth responses. The mineralization of early-season exudates was induced at a high C-threshold. In contrast, the mineralization of late-season exudates showed 'sugar-like' properties, with a low C-threshold, high substrate affinity, and a reduced maximum respiration rate of microorganisms growing on the added substrate. Mucilage exhibited the highest C-threshold for the activation of microbial growth, although with a short lag-period and with an efficient mucilage degradation comparable to that of sugars. By determining kinetic parameters and turnover times for different root-derived substrates, our data enable the upscaling of micro-scale processes to the whole root system, allowing more accurate predictions of how rhizodeposition drives microbial C and nutrient dynamics in the soil.

KEYWORDS

carbon cycling, microbial growth, microbial respiration, mucilage, rhizosphere, root exudates, *Zea mays*

1 | INTRODUCTION

More than a century ago, the rhizosphere was defined as the region around roots influenced by rhizodeposition (Hiltner, 1904), but still today the precise boundaries of the rhizosphere remain elusive (Finzi et al., 2015). The release of labile organic carbon (C) from roots creates temporally a specific hotspot with significantly enhanced microbial activity and growth (Jones et al., 2004; Kuzyakov & Blagodatskaya, 2015; Ma et al., 2018). The microbial activity decreases strongly with distance from the root surface (Vetterlein et al., 2020). The spatial expansion of the rhizosphere is influenced by the amount and composition of rhizodeposits, their diffusion and sorption in soils, which is a function of plant age, photosynthetic activity, root morphology and soil texture but also depends on their degradation by microbial activity (Hertenberger et al., 2002; Ma et al., 2018; Molina et al., 2001; Santangeli et al., 2024).

Rhizodeposits are typically divided into actively secreted mucilage, lubricating the advancing root tip, and mostly passively released exudates (Nguyen, 2003). Exudates, which are both low-molecular-weight compounds such as sugars, amino acids, organic acids, phenolics and high molecular weight compounds, like proteins, contribute significantly to the diversity of rhizodeposits (Collins & Reilly, 1968; Lohse et al., 2021; Walter et al., 2003). Less diverse is the mucilage, a viscous substance actively secreted at the root tip, consisting of high molecular weight compounds such as polysaccharides, proteins, phenolic acids and lipids (Bacic et al., 1987). These rhizodeposits provide the primary energy source for microbial activity in the rhizosphere (Brimecombe et al., 2000).

Whilst physical factors are integrated into existing rhizosphere models (Kuppe et al., 2022), the consideration of biological factors, such as consumption and mineralisation of rhizodeposits by microorganisms, remains a challenge. Current models either lack an explicit representation of microbial degradation activities or follow simplified linear degradation kinetics (Kirk et al., 1999; Landl et al., 2021). More advanced models (Chertov et al., 2022; Finzi et al., 2015) need to be rigorously validated against experimental data obtained in the plant–soil environment, as the microbial parameters in rhizosphere models are traditionally derived from pure culture studies (Zelenev et al., 2000). Integrating biological activity into rhizosphere models remains a challenge due to the lack of quantitative data, leaving a gap in the modelling of rhizosphere processes (Schnepf et al., 2022).

Because the vast majority of microorganisms in bulk soil are dormant (Stenström et al., 2001), microbial growth is initiated only 5–15 h after the C-pulse from rhizodeposition (Anderson & Domsch, 1978; Anderson & Domsch, 1985; Reischke et al., 2015). The transition of microorganisms from a stationary dormant to an active growth stage is associated with a dramatic change in their metabolism. After encountering an accessible C source, the dormant soil microorganisms must first upregulate their enzymatic machinery for mineralising the growth substrates, which is characterised by a typical lag-period with significantly increased microbial respiration before the onset of microbial growth (Panikov, 1995). The lag-period depends on the proportion of dormant microbial biomass, and microbial respiration increases with the concentration of the C source until the 'maximum initial respiratory response' (MIRR) is reached at maximum or excess availability of C (Anderson & Domsch, 1978). Microbial mineralisation and growth responses have mainly been studied using glucose, a common component of rhizodeposits (Jones et al., 2009). Previous studies have shown that microbial growth in response to glucose is triggered only when the concentration of carbon exceeds a threshold value that depends on the soil microbial biomass (Cmic) (Anderson & Domsch, 1985; Reischke et al., 2015; Sawada et al., 2008). The studies have reported a C-threshold of approximately 50%–150% Cmic. However, microbial responses to glucose versus rhizodeposits, the latter being a diverse mixture of different compounds, have not been compared in a single experimental set-up, and microbial growth kinetics on rhizodeposits have not been studied at all. We argue that mineralisation dynamics and C-thresholds governing microbial growth in response to rhizodeposition differ from those associated with glucose and require further investigation. In addition, the C-rich rhizodeposits are anticipated to influence the stoichiometric requirements of the rhizosphere microorganisms. As N and P are essential for the synthesis of biomolecules and the facilitation of cellular processes, their limitation can severely inhibit microbial growth.

Highlights

- Growth thresholds for rhizodeposits were significantly higher than for singular, simple sugars.
- Even at high concentrations, root exudates did not induce distinct microbial growth.
- Mucilage was degraded after a short lag-phase as efficiently as sugars if added at high concentrations.
- Microbial growth on exudate components was co-limited by N and P in agricultural soils.

This study aims to provide quantitative information on the microbial respiration response to natural maize rhizodeposits and its most common single compounds in agricultural soil. Microbial responses to single C sources, such as simple sugars, organic acids or amino acids, will be compared with those to complex sources, such as exudates or mucilage, in a single setup. With high temporal resolution, we measured the kinetics of microbial respiration in response to single C sources, including mono- and polysaccharide sugars, amino and organic acids, as well as complex substrates such as maize root-derived exudates or mucilage, quantifying the microbial growth responses to these different carbon sources. A gradient of substrate concentration was created to simulate reduced microbial access to C with increasing distance from the root surface. Further nutrient limitations were tested by supplementing nitrogen (N) and/or phosphorus (P) along the concentration gradient at a stoichiometric ratio of C:N:P 10:2:1. This study aims for the first time to provide information to accurately calibrate models of rhizosphere microbial growth dynamics with increasing distance from the root surface.

2 | MATERIALS AND METHODS

2.1 | Sampling of soil and origin of rhizodeposits

A loamy agricultural soil was sampled from the upper horizon (0–10 cm) of the experimental field platform of the DFG priority programme 2089 'Rhizosphere Spatiotemporal Organisation – a key to rhizosphere functions' near Bad Lauchstädt, Germany. After sampling in June 2022, the sample was transported to Cologne, Germany, where it was sieved (2 mm) and stored at 4°C until use. As in the previous 3 years, the field was planted with maize at the time of sampling. The soil had a pH of 5.6, and a C:N ratio of 10.85, containing 0.80% C and 0.07% N. See Vetterlein et al. (2021) for a more detailed soil description. The extractable organic C (EOC), denoting the potentially available, organic C for microbial growth, was determined by extracting samples of 5 g field-moist soil with 20 mL of 0.025 M K_2SO_4 on a horizontal shaker at 250 rpm for 30 min. Subsequently, samples were centrifuged for 30 min at 4420 g and EOC was measured using an EOC-TN Analyser (Multi-N/C 2100S, Analytik Jena, Germany).

The individual components of maize rhizodeposits tested in this study, including the sugars glucose ($C_6H_{12}O_6$, VWR), sucrose ($C_{12}H_{22}O_{11}$) and arabinose ($C_5H_{10}O_5$), the amino acid aspartate ($C_4H_7NO_4$, Serva) and the organic acids citric acid ($C_6H_8O_7$) and oxalic acid ($C_2H_2O_4$) (Chaboud, 1983; Collins & Reilly, 1968), are recognised as major compounds in the literature but do not accurately reflect the composition of the root-derived exudates analysed in this study. For measuring mineralisation kinetics of the latter two organic acids, soils were buffered by a citrate buffer (0.1 M $C_6H_8O_7$, 0.1 M $C_6H_5Na_3O_7 \cdot 2H_2O$) to keep the pH 5.6 of the soil constant. All reagents used in this study were analytical grade and purchased from Sigma Aldrich (Merck, Darmstadt, Germany) unless otherwise stated.

Exudates and mucilage of maize (*Zea mays* B73 wild type) were collected in the same field experiment as described above (Vetterlein et al., 2021). Exudates were collected in the early vegetation period during leaf development (BBCH 14), and in the late vegetation period at the first ripening stage (BBCH 83) (Lancashire et al., 1991) by a soil hydroponic-hybrid approach as described in Santangeli et al. (2024). Briefly, soil-grown plants were grown in perforated soil columns in the field which allowed excavation of the entire intact maize plants. The root system was gently rinsed with tap water for 30 min to remove soil particles. Root exudates were then collected hydroponically for 1 h in 0.5 and 7.5 L of deionised water at BBCH 14 and BBCH 83, respectively. Finally, the solution was filtered (0.2 µm, cellulose acetate OE 66, Whatman, UK) to remove all root debris, to capture only the soluble exudate fraction. Four replicates of the filtered exudates were divided into aliquots, frozen at −20°C and stored at −80°C until analysis. Exudate C contents were determined on a Shimadzu TOC-5050 from freeze-dried subsamples. Immediately before mineralisation measurements, the remaining freeze-dried material was dissolved in ultra-pure H_2O to obtain the desired C concentration. The replicate samples were pooled at this step.

Mucilage collection followed the procedure in Ahmed et al. (2015), with slight modifications. Briefly, nodal roots were carefully detached from the maize root systems at the end of tassel emergence (BBCH 59) and cleaned from soil with deionised water. Nodal roots with intact tips were submerged in deionised water for 24 h to allow mucilage hydration. Subsequently, the excess water was discarded through a fine sieve and hydrated mucilage was aspirated using syringes and frozen at −20°C until use. The C and N content of the mucilage was analysed by combustion using a C/N elemental analyser (Thermo Flash EA 2000, Fisher Scientific). The remaining material of two replicate samples was mixed and dissolved in ultra-pure H_2O to obtain the desired C concentrations.

2.2 | Measurements of microbial substrate utilisation

Microbial utilization of single rhizodeposit components, maize exudates, and mucilage (hereinafter referred to as 'substrates') was measured by an electrolytic O_2 microcompensation apparatus as described in Scheu (1992). To mimic the decrease of rhizodeposits and the resulting

lower C supply to the soil microorganisms with increasing distance from the root surface, the individual substrates were diluted with ultrapure H_2O according to their C content to form a concentration gradient of 1600, 400, 200, 100 and 40 μg C g^{-1} soil dry wt. For mucilage, mineralization of four additional concentrations of 1200, 1000, 800, and 600 μg C g^{-1} soil was measured. For early and late season exudates the 200 μg C g^{-1} soil concentration step was omitted.

Portions of field soil, equivalent to 3 g dry weight, were adjusted to 60% of their maximum water holding capacity (corresponding to a gravimetric water content of 30%) to ensure uniform water content. The samples were either amended with a substrate or left without substrate for further measurements of microbial basal respiration (μg CO_2–C g^{-1} h^{-1}). Thus, equivalent amounts of water were used to add different quantities of C. Oxygen consumption rates at 22°C were monitored every 15 min for the next 24–48 h with three replicates, each. To assess the C mineralisation of the substrates, the microbial O_2 consumption was converted into respired CO_2–C according to the ideal gas law and assuming a respiratory quotient of 1. In addition, the extent to which the microbial mineralisation of the added C substrates was limited by the availability of N and P was determined by amending the soils in a factorial combination with solutions of $(NH_4)_2SO_4$ or/and KH_2PO_4, corresponding to an optimal microbial C:N:P stoichiometry of 10:2:1 (Griffiths et al., 2012).

2.3 | Calculations of substrate mineralisation kinetics

To analyze the mineralization of rhizodeposits, microbial kinetic substrate-induced respiration (KSIR) was measured from the respiration curves (Blagodatsky et al., 2000) (Figure 1). The addition of a substrate causes an immediate significant upregulation of microbial respiration above the level of basal respiration prior to the onset of microbial growth. During this lag-period, the MIRR (Anderson & Domsch, 1978) was calculated as the mean of the three lowest respiration measurements. Microbial biomass C (Cmic) was calculated from the mean MIRR value after the addition of 1600 μg C g^{-1} glucose according to Equation (1) (Beck et al., 1997):

$$\text{Cmic} = 38.0 * \text{MIRR} \quad (1)$$

The specific respiration (qCO_2) could then be calculated as the ratio between basal respiration and Cmic (μg CO_2–C μg Cmic-C^{-1}).

Substrate supply in excess of microbial demand allowed for the unrestricted exponential growth of microorganisms but the growth of microbial biomass decreased

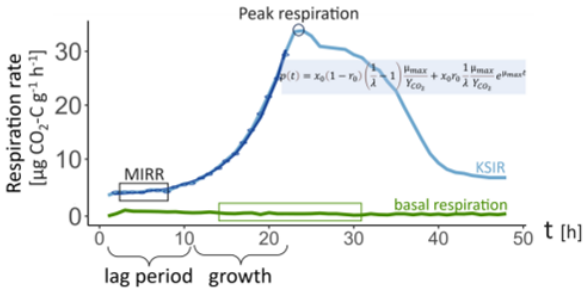

FIGURE 1 Explanatory graph for the definition of respiration measurements by microbial growth behaviour. MIRR is the maximal initial respiratory response, calculated as the mean of the three lowest lag-period measurements. KSIR is microbial kinetic substrate-induced respiration. With the kinetic model by Wutzler et al. (2012) the respiration curve is fitted to the respiration rates and used to calculate microbial parameters.

with the stepwise reduction of the C supply until no further growth occurred. The time span of the lag-period until the exponential increase of respiration during microbial growth and its decrease during the microbial depletion of the substrate were covered by the measurements. The differences in substrate application rates enabled the determination of the C-threshold, which reflects the transition from maintenance to active growth of the microorganisms (Panikov, 1995). Therefore, our approach allows the calculation of the following microbial mineralization characteristics: (i) the C-threshold needed to initiate microbial growth, which was determined according to Anderson and Domsch (1985) as the concentration that merely triggered an increase in respiration, which remained constant for several hours before decreasing, but at which the C supply was insufficient for microbial growth and (ii) the peak respiration, which was set as the first peak in microbial growth, typically occurring between 10 and 30 h after the addition of the substrate. Additionally, (iii) the maximum specific growth rate (μ_{max}) and (iv) the active microbial fraction were estimated using KSIR analysis. The KSIR analysis was based on the respiration measurements in response to the C concentration that gave the highest peak respiration for each substrate (Blagodatsky et al., 2000). Following the model presented in Wutzler et al. (2012), the measured respiration rates were described in Equation (2) and best-fit parameters were estimated.

$$p(t) = x_0(1-r_0)\left(\frac{1}{\lambda}-1\right)\frac{\mu_{max}}{Y_{CO_2}} + x_0 r_0 \frac{1}{\lambda}\frac{\mu_{max}}{Y_{CO_2}} e^{\mu_{max} t} \quad (2)$$

where $p(t)$ is the respiration rate at time t, expressed as respired C per time, μ_{max} is the maximum specific growth

rate of the growing microorganisms, r_0 (from 0 to 1) is the initial physiological state of microbial biomass and x_0 is the microbial biomass at the moment of substrate addition. As suggested in Wutzler et al. (2012), (2) was used as a three-parameter equation, accepting the following assumptions: first, λ was assumed to be a basic stoichiometric constant of 0.9 during unrestricted growth (Akimenko et al., 1983). Secondly, $Y_{CO_2} = Y/(1\text{-}Y)$ can be assumed to be a constant of 1.5 during unlimited growth (Blagodatsky et al., 2000). These values were subsequently used to calculate the lag-period (t_{lag}) as described in Baranyi and Pin (1999). T_{lag} is inversely proportional to μ_{max} and depends on r_0. It was determined using Equation (3):

$$t_{lag} = -\ln(r_0/\mu_{max}) \quad (3)$$

For each substrate, a Michaelis–Menten model curve was fitted to the MIRR values of the different concentration steps, relating the added substrate concentration to the initial microbial respiration rate. This model was used to calculate the maximum respiration rate (V_{max}), which indicates the theoretical microbial peak CO_2 production during MIRR for a specific substrate, and the Michaelis–Menten constant (K_m), which describes the affinity of microorganisms to mineralise the given substrate, with low values indicating high microbial substrate mineralisation at low substrate concentrations. The turnover time (T_t) of the applied substrate is the total time required by the microbial community to metabolise the applied substrate at K_m plus the concentration of soil indigenous C, measured as EOC. This estimation was made using Equation (4) (Blagodatskaya et al., 2009):

$$\mathrm{Tt\,[h]} = \frac{\mathrm{Km} + \mathrm{Sn}}{\mathrm{Vmax}} \quad (4)$$

Two-way ANOVA was used to analyse differences between MIRR and peak respiration dependent on substrate and nutrient limitation, with Tukey's test for post-hoc pairwise comparisons. Calculations were performed using R statistical software (version 4.2.1, 2022-06-23; 'Funny-Looking Kid'). The following R packages were utilised for various aspects of the analysis: 'ggplot2' for data visualization (Wickham et al., 2018), 'dplyr' to arrange the data (Wickham et al., 2020), 'reshape2' for melting data (Wickham, 2007), 'nlstools' for Michaelis–Menten analysis (Baty et al., 2015) and 'twKinresp' for KSIR.

3 | RESULTS

3.1 | Microbial mineralisation of rhizodeposits at varying substrate concentrations

The loamy agricultural soil had a microbial biomass of 158 μg Cmic-C g^{-1} with basal respiration of 0.18 μg CO_2–C g^{-1} h^{-1}. Accordingly, the specific respiration (qCO_2) was 1.14 μg CO_2–C g^{-1} Cmic-C. The maize mucilage contained 357 μg C g^{-1} and 16.2 μg N g^{-1} (C:N ratio = 22), whilst early season exudates (BBCH 14) and late season exudates (BBCH 83) had C contents of 10.9 and 12.8 μg C mL^{-1}, respectively.

Microbial respiration was increased well above basal respiration after the addition of sugars and amino acids, with a characteristic lag-period lasting until the onset of exponential microbial respiration when the substrate supply exceeded the substrate-specific C-threshold for microbial growth (Figure 1, Suppl.-Figure 1). The extent of this increased microbial respiration was dependent on the concentration of substrate added. In response to the sugars applied, respiration increased 12-fold above basal maintenance levels during the first 10 h to a MIRR of 2.25 μg CO_2–C g^{-1} h^{-1} after the addition of 1600 μg C g^{-1} glucose or sucrose, and 9-fold to 1.65 μg CO_2–C g^{-1} h^{-1} in response to 1600 μg C g^{-1} arabinose (Table 1, Figure 2). The lag-phase, characterised by an increase in respiration, transitioned into an exponential phase of respiration response at the onset of microbial growth. The C-threshold for microbial growth on glucose and sucrose was 100 μg C g^{-1}. For arabinose, the threshold C concentration required to initiate microbial growth was lower with 40 μg C g^{-1} (Suppl.-Table 1). Microbial respiration peaked 22 h after the addition of glucose. Higher substrate levels resulted in higher rates of peak respiration, indicating higher microbial growth. Below the C-threshold for microbial growth, however, the initial upregulation of respiration after glucose addition dropped off without exhibiting the typical exponential phase seen at higher substrate levels (Figure 2). At peak respiration, approximately 0.01% of the total amount of added sugar–C was respired per hour (Table 1, Figure 2). The total (cumulative) CO_2–C respired from sugars at peak respiration amounted to between 7% and 9% of the added C. Peak respiration following arabinose addition at 27 h was delayed by 5 and 7 h longer compared to glucose and sucrose, respectively (Table 1, Figure 2).

The C-thresholds for microbial growth on citric and oxalic acid were 40 and 100 μg C g^{-1}, respectively. The addition of organic acids to buffered soils at concentrations above 400 μg C g^{-1} inhibited microbial activity, with growth starting only after 20–21 h.

TABLE 1 Microbial mineralization response parameters to the different substrates without and with nutrient supplementation.

Substrate			MIRR		Peak respiration		Cumulative CO_2 respiration until peak		Time of peak respiration (h)
	+	μg C g^{-1}	μg CO_2–C g^{-1} h^{-1}	SE	μg CO_2–C g^{-1} h^{-1}	SE	μg CO_2–C g^{-1}	SE	
Glucose		1600	2.23	0.09	16.20	1.31	127.23	14.73	22.00
	P	1600	2.09	0.06	19.87	0.39	152.64	7.37	23.33
	N	1600	2.41	0.43	22.84	1.15	188.98	8.82	22.33
	NP	1600	1.80	0.24	21.15	1.46	199.02	12.69	22.67
Sucrose		1600	2.28	0.11	15.92	0.15	112.04	2.50	19.67
	P	1600	2.32	0.18	17.31	0.81	110.83	4.05	19.33
	N	1600	2.25	0.30	28.35	1.02	218.82	16.11	20.67
	NP	1600	2.17	0.68	19.67	5.57	195.26	7.32	20.50
Arabinose		1600	1.65	0.07	17.55	0.83	146.44	6.32	27.00
	P	1600	1.41	0.20	11.56	0.21	82.97	6.66	24.00
	N	1600	1.87	0.07	16.89	0.31	122.63	1.99	24.00
	NP	1600	1.22	0.91	10.73	2.87	99.34	27.34	26.00
CiAcid		400	0.98	0.13	4.33	0.44	39.49	3.69	19.67
OxAcid		400	1.04	0.12	1.87	0.16	19.42	2.66	15.33
Aspartate		100	1.77	0.13	6.47	0.46	60.85	5.02	21.00
	P	100	1.06	0.45	4.48	1.77	56.44	4.52	23.00
Early exudates		1600	2.05	0.04	3.88	0.19	68.19	3.23	26.33
Late exudates		1600	1.65	0.24	3.50	0.21	81.34	6.85	34.00
Mucilage		1600	2.92	0.18	15.13	1.58	143.55	20.75	19.25

Note: Only the values for each substrate that correspond to the C concentration resulting in the highest peak respiration are displayed. Results are the average of 3 replicates.
Abbreviations: MIRR, maximum initial respiratory response; SE, Standard error of the mean.

The highest peak respiration of 4.3 μg CO_2–C g^{-1} h^{-1} was observed after the addition of 400 μg C g^{-1} citric acid, which is the same magnitude as the respiration peak in response to an addition of sugars at 400 μg C g^{-1}. The cumulative respired CO_2 at peak respiration after the addition of citric acid amounted to 10% of the total added C whilst for oxalic acid it was 5% of the total added C.

The soil microorganisms mineralised the amino acid aspartate more efficiently than sugars. The C-threshold for microbial growth was 40 μg C g^{-1} aspartate. The addition of 100 μg C g^{-1} aspartate resulted in a peak respiration rate of 6.5 μg CO_2–C g^{-1} h^{-1}. This means that 0.07% of the substrate_C was respired per hour at peak respiration, leading to a cumulative C respiration of 61% of the added C until peak respiration, 21 h after substrate addition (Table 1). However, aspartate concentrations above 400 μg C g^{-1} inhibited microbial growth.

Patterns of microbial mineralisation of root-derived C sources such as exudates and mucilage were more complex. The threshold for microbial growth was only exceeded in response to 400 and 100 μg C g^{-1} of early and late season exudates, respectively (Suppl.-Table 1). However, even when the C-threshold for exudates was exceeded, the microbial respiration did not enter an exponential growth phase as with the other substrates, but merely a steady increase was observed (Figure 2). This led to a peak respiration of about 3–4 μg CO_2–C g^{-1} h^{-1} in response to exudates at 1600 μg C g^{-1} (Table 1). For mucilage, the C-threshold for microbial growth was at 1000 μg C g^{-1} (Suppl.-Table 1), leading to a peak respiration almost as high as for sugars (up to 13.4 μg CO_2–C g^{-1} h^{-1}) (Table 1). Early season exudates and mucilage caused two respiratory growth peaks at this highest C concentration (Figure 2). The first peak was observed 24 h after substrate addition as for the other substrates and the second peak was observed 30–35 h after substrate addition. Microbial respiration at the highest concentrations of late-season exudates decreased very slowly after the initial peak, without showing the typical decline in microbial activity after 1 day. The cumulative respired CO_2–C at peak respiration was about 4% of the added C in early and late season exudates, and 9% of the added C for mucilage (Table 1).

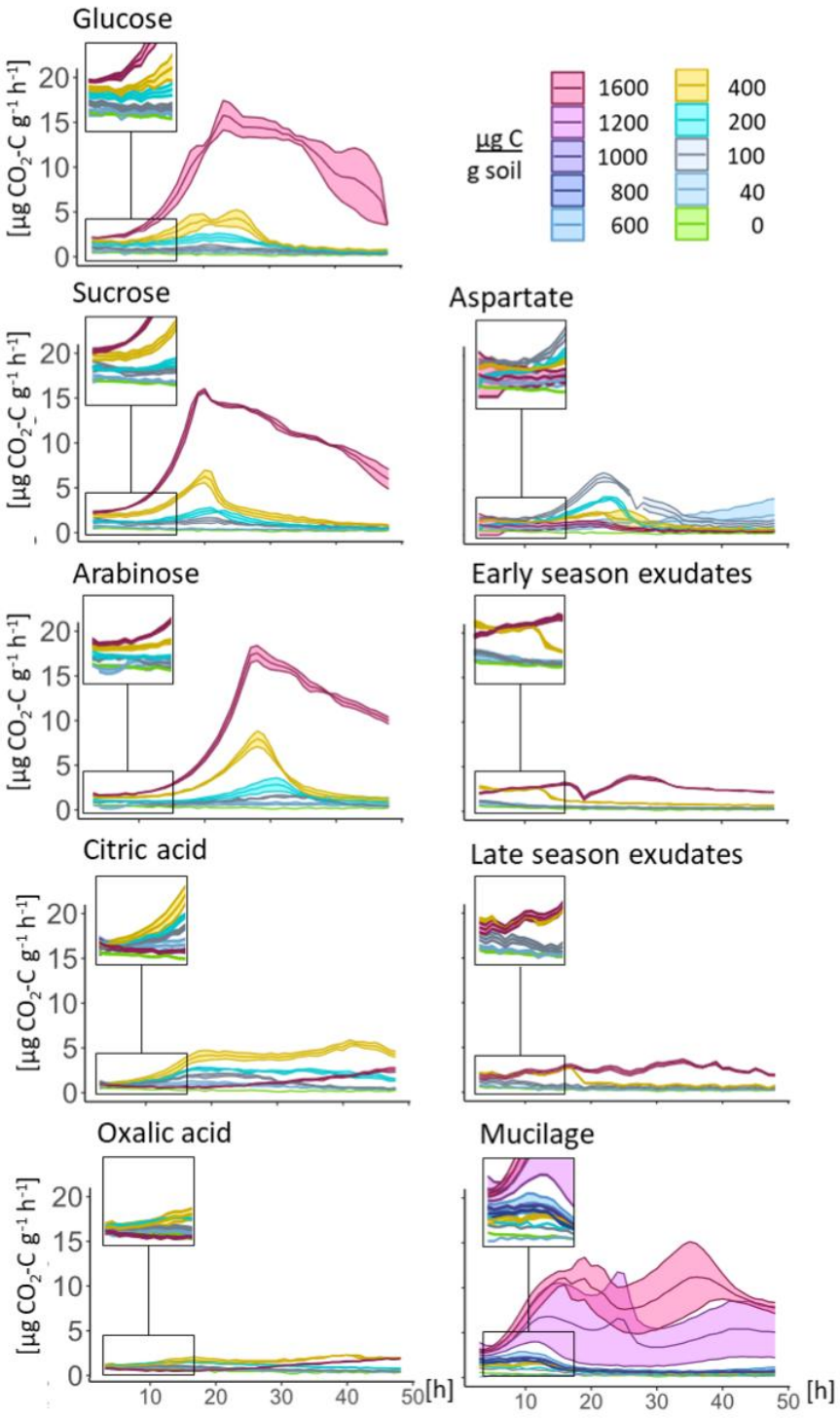

FIGURE 2 Microbial growth in response to different root-derived substrates: glucose, sucrose, arabinose, aspartate, critic and oxalic acid, mucilage, and early and late exudates. Each curve represents the mean of three replicates ± standard error. The lag-period is enlarged in the top left corner of each graph, with the scale of the enlargement indicated by rectangles.

Overall, the microbial mineralisation of rhizodeposits showed more complex patterns as compared to sugars, with multiple growth peaks and generally requiring higher C concentrations to initiate microbial growth.

3.2 | Microbial growth kinetics

The kinetic variables obtained from the model fitting of the respiration curves showed high similarity amongst

the sugars (Suppl.-Table 3). The specific growth rate (μ_{max}) of the microbial community on the monosaccharide sugars glucose ($\mu_{max} = 0.21$) and arabinose ($\mu_{max} = 0.20$) was slightly lower than the specific growth rate on the disaccharide sucrose with 0.26 (Figure 4). Microbial growth on aspartate also showed a high μ_{max} (0.27), but with a longer lag-period compared to sugars, and aspartate stimulated a very low active fraction of Cmic (Figure 5). In response to mucilage, microorganisms showed a relatively low μ_{max} of 0.18. Mucilage stood out due to its notably brief lag time of 58 min and a more than 10-fold higher active fraction of Cmic than any of the other tested substrates (Figure 5). Due to the absence of a distinct growth phase, the respiration curves of organic acids and exudates could not be fitted to assess the lag-period, μ_{max}, and the active fraction of microbial biomass according to the Wutzler model.

3.3 | Michaelis–Menten kinetics

The relationship between the quantity of substrate added and MIRR, shown by Michaelis–Menten kinetics (Figure 3), confirms significant variation in the mineralisation of different rhizodeposit substrates. Across a range of substrates, respiration showed a sharp increase up to roughly 250 µg C g^{-1} before reaching a plateau near V_{max}. As expected, microorganisms showed a high affinity to sugars and exudates with low K_m values at around 100 µg C g^{-1} (Figure 4, Suppl.-Table 2). Glucose, sucrose and early-season exudates had a high V_{max} value of around 2.5 µg CO_2–C g^{-1} h^{-1} and T_t about 3 h, whereas the late-season exudates and arabinose had lower V_{max} values, falling below 2 µg CO_2–C g^{-1} h^{-1} and T_t about 4 h. The Michaelis–Menten model was successful in fitting the mineralisation of the easily decomposable sugars and exudates but no K_m values could be determined for aspartate, the organic acids and mucilage (Figure 3).

The model was more robust for calculations of V_{max} (Suppl.-Table 2), except for mucilage, where the initial upregulation of microbial respiration (MIRR) increased linearly with the added amount (MIRR = 0.30 + 1.74 * µg C mucilage g^{-1}, $R^2 = 0.75$) without reaching a plateau at the highest concentration of 1500 µg C g^{-1} soil (Figure 2).

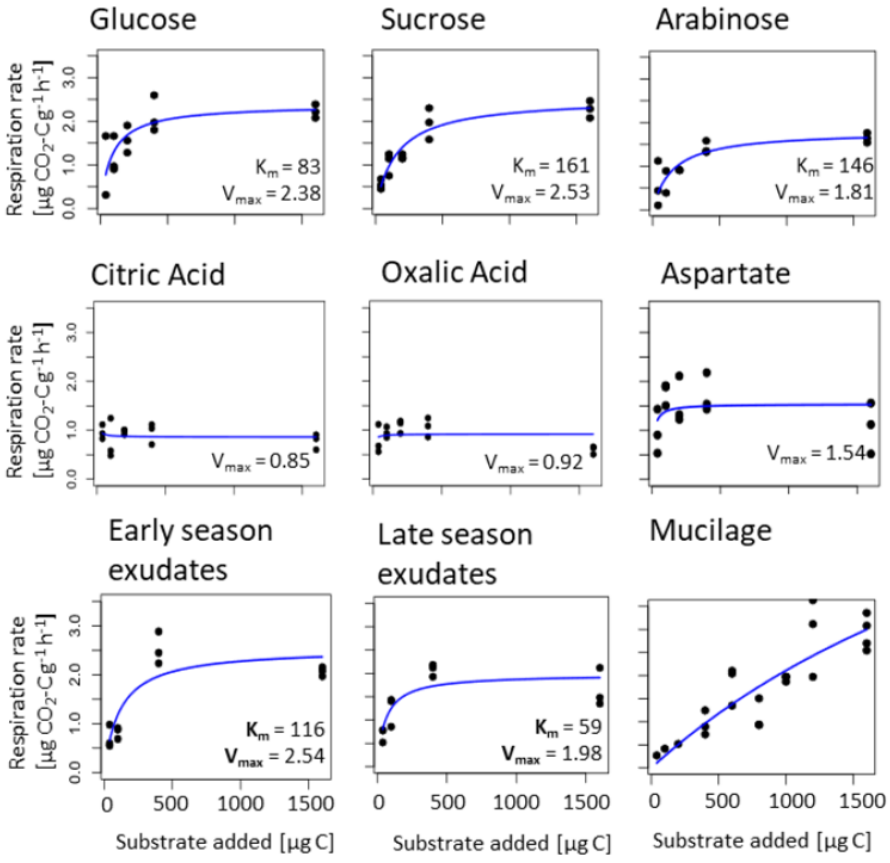

FIGURE 3 Michaelis–Menten kinetics, Model of MIRR (µg CO_2–C g^{-1} h^{-1}) to a gradient of substrate concentrations (µg C) (glucose, sucrose, arabinose, aspartate, citric acid, oxalic acid, early season exudates, late season exudates and mucilage), K_m and V_{max} values are displayed if significant.

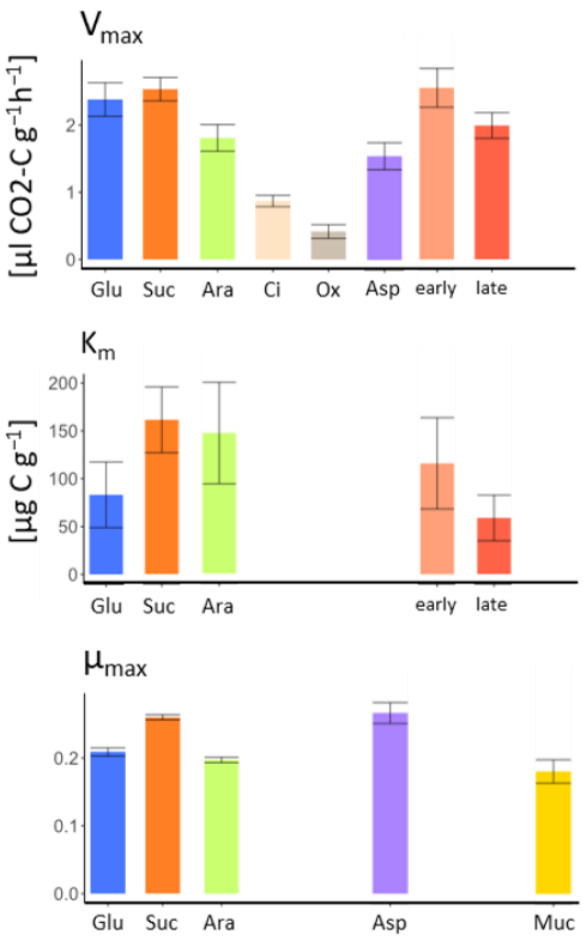

FIGURE 4 Community properties in response to different substrates. The bar graphs show the Michaelis–Menten model-based parameters for V_{max} and K_m, and the KSIR model-based parameters for μ_{max}, with a standard error of V_{max} and K_m and a standard deviation of μ_{max}. Substrates include Glu (Glucose), Suc (Sucrose), Ara (Arabinose), Ci (Citric acid), Ox (Oxalic acid), Asp (Aspartate), early and late (early and late season exudates) and Muc (Mucilage).

3.4 | Effect of nutrient addition on substrate-induced respiration response

Microbial growth in the soil is mainly limited by C and was therefore strongly stimulated by the C-rich rhizodeposits. The addition of N and P on top of the C input by glucose or sucrose showed a significant increase in peak respiration in response to the combination of C and N, demonstrating a strong shift in nutrient limitation of microbial growth to N (Figure 5). However, a microbial co-limitation of N and P was indicated by the amplification of peak respiration and a decrease of the C-threshold required for microbial growth when both nutrients together were added with glucose (Suppl.-Figure 1, Table 1, Suppl.-Table 1). By the addition of N, P or both to glucose, microbial growth was initiated already at 40% of the threshold concentration required without it (Suppl.-Table 1). Notably, in response to sucrose a reduction of the C-threshold was only observed with N-supplementation. In contrast, nutrient addition to arabinose raised the C-threshold for the transition from maintenance to microbial growth, corresponding to an increment to the next substrate concentration level, for example, from 40 to 100 µg C g^{-1} with the addition of nutrients (Suppl.-Table 1).

Overall, the lag-period was reduced by 50%–75% and the active fraction of the microbial biomass increased 2.5- to 6-fold with the addition of both N and P (Figure 5, Suppl.-Table 3).

4 | DISCUSSION

Rhizodeposits are a diverse mixture of organic compounds released by plant roots that stimulate microbial activity and influence the physical and chemical properties of the rhizosphere (Carminati & Vetterlein, 2013; Nazari, 2021). However, studies investigating microbial responses to substrate inputs into the soil often use glucose as a model substrate (Anderson & Domsch, 1985; Reischke et al., 2015; Sawada et al., 2008; Stenström et al., 2001) and sometimes other single components of rhizodeposits such as organic acids (van Hees et al., 2002). We observed a typical dynamic of the microbial degradation of sugars with a clear lag-period before the exponential growth takes place at peak respiration at 22 h. The observed patterns confirm a strong sugar affinity of the microbes and high mineralisation rates. The aldopentose arabinose, however, was utilised with a slower turnover by fewer active microbes. Apparently, the bulk soil microbiome was not well adapted for the rapid metabolisation of arabinose. Although arabinose is a common constituent of rhizodeposits, it is far less abundant than glucose (Chaboud, 1983; Nazari et al., 2020). The difference from the other sugars may be due to potentially less abundant or fewer activated transporters involved in arabinose mineralisation compared to glucose transporters (Mayer & Boos, 2005; Ryu & Trinh, 2018).

From a stoichiometric perspective, amino acids provide both C and N for optimal microbial growth. Accordingly, microbial growth was significantly increased at 100 µg C g^{-1} of aspartate, but elevated concentrations of aspartate did inhibit microbial growth. Amino acid uptake may be also hampered by physiological limitations of non-adapted microbial bulk soil communities (Koskella & Vos, 2015), as the numbers and activity of specific ABC transporters restrict the microbial uptake of amino acids (Hosie & Poole, 2001).

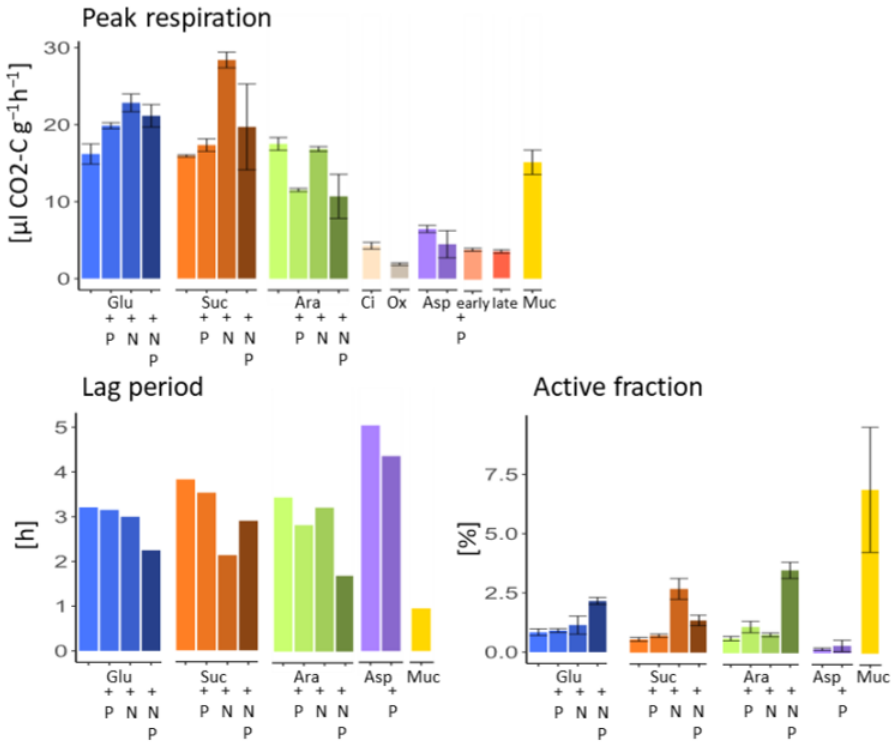

FIGURE 5 Parameter for microbial growth on different substrates with and without nutrient limitations. Substrates include 1600 µg C g^{-1} Glu (Glucose), 1600 µg C g^{-1} Suc (Sucrose), 1600 µg C g^{-1} Ara (Arabinose), 400 µg C g^{-1} Ci (Citric acid), 400 µg C g^{-1} Ox (Oxalic acid), 100 µg C g^{-1} Asp (Aspartate), 1600 µg C g^{-1} early and late (early and late season exudates) and 1600 µg C g^{-1} Muc (Mucilage). The bar graph shows the measured value of peak respiration, the KSIR model-based parameters for lag-period (h) before exponential growth, and active fraction (the active part of the total biomass), $n = 3$, with standard error of peak respiration and standard deviation of difference for active fraction.

The adaptation of different microbial taxa to degrade individual substrates and the complexity of substrates may explain the temporal variation in the microbial mineralisation of exudates and mucilage in our study. Rhizodeposits could trigger microbial growth through the provision of readily available C substrates but they also contain chemical inhibitors of microbial growth (Nazari, 2021; Oburger et al., 2011; Wiesenbauer et al., 2023). Two distinct growth peaks in response to early season exudates and to mucilage indicate interactions between taxa that utilise different C sources at different times, and potentially the influence of compounds that delay substrate utilisation (Badri & Vivanco, 2009; Baetz & Martinoia, 2014). In particular, the late season exudates did exhibit multiple small respiration peaks, some of which may be superimposed and therefore not visible, but still contributing to the rugged pattern of microbial growth on late season exudates (Figure 2).

The assembly of the rhizosphere microbiome starts at the root tip and was shown to change along the root axis towards older root sections (Dupuy & Silk, 2016; Rüger et al., 2021). The bulk soil microbial community is mostly dormant and its small active part is dominated by K-strategists, strictly adapted to resource-limited conditions (Soler-Bistue et al., 2023). As the root extends into the bulk soil, the secretion of mucilage at root tips activates the dormant bulk soil microbiota and creates a first temporally and spatially restricted hotspot of microbial activity (Kuzyakov & Blagodatskaya, 2015). The brief lag-phase following mucilage addition with a low μ_{max} indicates the growth of a significant proportion of K-strategists (Couso et al., 2023). Due to their lower energy requirements, these K-strategists are capable of immediate growth upon encountering a mucilage-coated root tip. However, these K-strategists do not reproduce as efficiently as r-strategists, reflected by their relatively low μ_{max} for the immediate microbial growth response to mucilage supplementation. In addition, soluble exudates are released behind the root tip into the soil matrix, where mucilage has already induced the growth of a significant proportion of the microbial biomass. The majority of maize exudates are composed of sugars (Santangeli et al. (2024), and therefore one would intuitively expect their rapid microbial metabolisation, and a replacement of K-strategists by r-strategists with faster turnover rates. Interestingly, after the typical initial up-regulation of microbial metabolism in response to root exudates, the expected exponential microbial growth was not realised. Secondary metabolites in exudates repeatedly have been found to restrict the growth of rhizosphere microbiota (El Zahar Haichar et al., 2014; Khashi u Rahman et al., 2019; Sasse et al., 2018). One likely reason is that plants hinder the rapid degradation of substances with functional potential by involving antibiotics and microbial inhibitors in rhizodeposition (Bais et al., 2006; Hawes et al., 2000). The rather slow microbial growth rate on root exudates fit well with a recent study by (Zhalnina et al., 2018), who inferred from a codon-

usage bias in members of the rhizosphere microbiome of the grass *Avena*, and later confirmed by culturing studies, that the majority of rhizosphere bacteria had much longer generation times than would be expected from fast-growing r-strategists.

There is further a spatial component in addition to the temporal utilisation of rhizodeposits. The C supply to microorganisms by rhizodeposits is decreasing rapidly with distance from the root surface (Alphei et al., 1996), this was mimicked by the stepwise addition of lower concentrations of rhizodeposits to soil. When confronted with a limiting C-source, microorganisms make strategic choices, as the uptake of substrate and its conversion into storage compounds requires less energy than the synthesis of cellular structural compounds during growth (Sawada et al., 2008). This results in a critical threshold that differentiates between the microbial use of C for storage, or its use for growth when a critical C-threshold is exceeded (Bremer & Kuikman, 1994). As the microbial biomass increases, the required C-threshold also tends to increase as well (Reischke et al., 2015) and lies approximately at 30% of Cmic, according to Anderson and Domsch (1985). Therefore, any C-threshold obtained should be normalised by the soil's Cmic content to make studies on different soils comparable. Our data show a Cmic-specific threshold between 25% and 63% to trigger microbial growth in response to sugars (Suppl.-Table 1), aligning with previous studies (Anderson & Domsch, 1985; Reischke et al., 2015; Sawada et al., 2008). In addition, the C-threshold for microbial growth varies with the type of C-substrate. The C-thresholds for late season exudates were not different from those for sugars, amino acids and organic acids. This corresponds to the findings of Santangeli et al. (2024) reporting that late-season exudates consist of over 50% of soluble carbohydrates. On the other hand, the C-thresholds for microbial growth in response to early season exudates and mucilage were an order of magnitude higher, at 2.53 and 6.33 μg C μg Cmic-C^{-1}, respectively, indicating that these rhizodeposits were less supportive for microbial growth. It has been shown that the composition of the rhizosphere microbiome is closely linked to the bouquet of exudates that plants release to recruit members of the bulk soil microbial community. However, only plants during their active growth period (e.g., BBCH 14) will benefit from any plant-protective or growth-promoting microbial traits whilst after flowering all resources are redirected to seed formation (e.g., BBCH 83) (Keith et al., 1986; Swinnen et al., 1994). The decrease of secondary phenolic compounds in late season exudates at ripening (BBCH83) of maize (Santangeli et al., 2024) may be an indication of the switch from microbiome selection to general microbial growth promotion by rhizodeposits. When relating substrate concentration to the initial microbial response using Michaelis–Menten kinetics, microbial growth on early season exudates showed a more effective substrate turnover (lower T_t) due to the activation of a larger fraction of the microbial community (higher V_{max}), but with reduced affinity to the substrate, leading to an increased C-threshold for growth on early season exudates. Microbial growth dynamics on early season exudates thus resembled the pattern of the disaccharide sucrose (Figure 3). Late season exudates in contrast supported the growth of microorganisms with a lower K_m and a longer T_t.

Also, for stoichiometric reasons, it may not be in the interest of plants that their rhizodeposits fuel microbial growth too rapidly. The C-supply from roots lifts the C-limitation of the soil microorganisms, whose growth then becomes nutrient-limited. Unfortunately, the amount of rhizodeposits available was not sufficient to measure the nutrient limitation of microbial growth. However, the increased peak respiration after amending sugars with N and P demonstrates the hypothesised switch towards strong N-limitation of microbial growth (Figure 5), leading to strong nutrient competition with plants (Hodge et al., 2000). The reduced lag-phase and the strongly increased fraction of microorganisms activated by the substrate, especially when supplied with both N and P (Figure 5), give further proof of how strongly the microbial mineralisation of these substrates was nutrient-limited. For mucilage, where we could obtain measurements of C and N contents, its C:N ratio of 22 was much wider than the C:N of 5 applied to soils. Mucilage, despite much lower N-availability, exhibited the shortest lag-period and activated the largest fraction of the soil microbial biomass (Figure 5). Thus not only nutrients but additional components within the mucilage likely accelerated the rapid activation of a high fraction of the microbial biomass, perhaps aided by enzymes that facilitate the breakdown of polysaccharides for microbial use and nutrient uptake (Pozzo et al., 2018), or by the recruitment of special microorganisms, like those containing glycosyl hydrolases to degrade polysaccharides (Amicucci et al., 2019).

5 | CONCLUSION

The microbial mineralisation of rhizodeposits showed more complex temporal patterns than investigations on individual model substrates would suggest. A high C-concentration of 1000 μg C mucilage g^{-1} was needed to stimulate exponential microbial growth, but then mucilage stimulated two growth peaks as high as in

response to sugars. Contrary and unexpected was the low microbial growth on exudates, and the remarkable differences in the microbial use of early and late season exudates. Overall, the initiation of microbial growth required surpassing a critical C-threshold, whilst lower C availability primarily stimulated microbial respiration. Accordingly, at a greater distance to the root surface, where the C-supply via rhizodeposition falls below this critical threshold, the rhizosphere microorganisms preferentially respire the assimilated C without converting it to biomass. By identifying kinetic parameters of a variety of root-derived substrates, our data allow more accurate calibration of models that consider the temporal and spatial extent of microbial growth and the mineralisation of rhizodeposits in the rhizosphere.

AUTHOR CONTRIBUTIONS

Daniela Niedeggen: Conceptualization; formal analysis; methodology; validation; visualization; writing – review and editing; writing – original draft; data curation. **Lioba Rüger:** Conceptualization; methodology. **Eva Oburger:** Validation; writing – review and editing; supervision. **Michael Santangeli:** Writing – review and editing; methodology. **Mutez Ahmed:** Validation; methodology; conceptualization. **Doris Vetterlein:** Writing – review and editing; conceptualization. **Sergey Blagodatsky:** Validation; writing – review and editing; formal analysis; supervision; methodology. **Michael Bonkowski:** Conceptualization; validation; writing – review and editing; writing – original draft; project administration; supervision; funding acquisition.

ACKNOWLEDGEMENTS

We thank Irene Brockhaus for her technical support. This project was carried out in the framework of the priority programme 2089 "Rhizosphere spatiotemporal organization – a key to rhizosphere functions" funded by the Deutsche Forschungsgemeinschaft (project number 403635931). Open Access funding enabled and organized by Projekt DEAL.

CONFLICT OF INTEREST STATEMENT

None declared.

DATA AVAILABILITY STATEMENT

The data that support the findings of this study are available from the corresponding author upon reasonable request.

ORCID

Daniela Niedeggen https://orcid.org/0000-0003-4376-3473
Lioba Rüger https://orcid.org/0000-0001-7168-0005

REFERENCES

Ahmed, M. A., Holz, M., Woche, S. K., Bachmann, J., & Carminati, A. (2015). Effect of soil drying on mucilage exudation and its water repellency: A new method to collect mucilage. *Journal of Plant Nutrition and Soil Science*, *178*, 821–824.

Akimenko, V. K., Trutko, S. M., Medentsev, A. G., & Korobov, V. (1983). Distribution of cyanide-resistant respiration among yeasts and bacteria and its relation to oversynthesis of metabolites. *Archives of Microbiology*, *136*, 234–241.

Alphei, J., Bonkowski, M., & Scheu, S. (1996). Protozoa, Nematoda and Lumbricidae in the rhizosphere of Hordelymus europaeus (Poaceae): Faunal interactions, response of microorganisms and effects on plant growth. *Oecologia*, *106*, 111–126.

Amicucci, M. J., Galermo, A. G., Guerrero, A., Treves, G., Nandita, E., Kailemia, M. J., Higdon, S. M., Pozzo, T., Labavitch, J. M., Bennett, A. B., & Lebrilla, C. B. (2019). Strategy for structural elucidation of polysaccharides: Elucidation of a maize mucilage that harbors Diazotrophic bacteria. *Analytical Chemistry*, *91*, 7254–7265.

Anderson, J. P. E., & Domsch, K. H. (1978). A physiological method for the quantitative measurement of microbial biomass in soils. *Soil Biology and Biochemistry*, *10*, 215–221.

Anderson, T. H., & Domsch, K. H. (1985). Maintenance carbon requirements of actively-metabolizing microbial populations under in situ conditions. *Soil Biology & Biochemistry*, *17*, 197–203.

Bacic, A., Moody, S. F., McComb, J. A., Hinch, J. M., & Clarke, A. E. (1987). Extracellular polysaccharides from shaken liquid cultures of Zea mays. *Functional Plant Biology*, *14*, 633–641.

Badri, D. V., & Vivanco, J. M. (2009). Regulation and function of root exudates. *Plant, Cell & Environment*, *32*, 666–681.

Baetz, U., & Martinoia, E. (2014). Root exudates: The hidden part of plant defense. *Trends in Plant Science*, *19*, 90–98.

Bais, H. P., Weir, T. L., Perry, L. G., Gilroy, S., & Vivanco, J. M. (2006). The role of root exudates in rhizosphere interactions with plants and other organisms. *Annual Review of Plant Biology*, *57*, 233–266.

Baranyi, J., & Pin, C. (1999). Estimating bacterial growth parameters by means of detection times. *Applied and Environmental Microbiology*, *65*(2), 732–736.

Baty, F., Ritz, C., Charles, S., Brutsche, M., Flandrois, J. P., & Delignette-Muller, M. L. (2015). A toolbox for nonlinear regression in R: The package nlstools. *Journal of Statistical Software*, *66*, 1–21.

Beck, T., Joergensen, R. G., Kandeler, E., Makeschin, F., Nuss, F., Oberholzer, H. R., & Scheu, S. (1997). An inter-laboratory comparison of ten different ways of measuring soil microbial biomass C. *Soil Biology and Biochemistry*, *29*, 1023–1032.

Blagodatskaya, E. V., Blagodatsky, S. A., Anderson, T. H., & Kuzyakov, Y. (2009). Contrasting effects of glucose, living roots and maize straw on microbial growth kinetics and substrate availability in soil. *European Journal of Soil Science*, *60*, 186–197.

Blagodatsky, S. A., Heinemeyer, O., & Richter, J. (2000). Estimating the active and total soil microbial biomass by kinetic respiration analysis. *Biology and Fertility of Soils*, *32*, 73–81.

Bremer, E., & Kuikman, P. (1994). Microbial utilization of 14C[U] glucose in soil is affected by the amount and timing of glucose additions. *Soil Biology & Biochemistry*, *26*, 511–517.

Brimecombe, M. J., de Leij, F. A., & Lynch, J. M. (2000). The effect of root exudates on rhizosphere microbial populations. In *The rhizosphere* (pp. 111–156). CRC Press.

Carminati, A., & Vetterlein, D. (2013). Plasticity of rhizosphere hydraulic properties as a key for efficient utilization of scarce resources. *Annals of Botany*, *112*, 277–290.

Chaboud, A. (1983). Isolation, purification and chemical composition of maize root cap slime. *Plant and Soil*, *73*, 395–402.

Chertov, O., Kuzyakov, Y., Priputina, I., Frolov, P., Shanin, V., & Grabarnik, P. (2022). Modelling the rhizosphere priming effect in combination with soil food webs to quantify interaction between living plant, soil biota and soil organic matter. *Plants*, *11*, 2605.

Collins, J. C., & Reilly, E. J. (1968). Chemical composition of the exudate from excised maize roots. *Planta*, *83*, 218–222.

Couso, L. L., Soler-Bistue, A., Aptekmann, A. A., & Sanchez, I. E. (2023). Ecology theory disentangles microbial dichotomies. *Environmental Microbiology*, *25*, 3052–3063.

Dupuy, L. X., & Silk, W. K. (2016). Mechanisms of early microbial establishment on growing root surfaces. *Vadose Zone Journal*, *15*, 1–13.

El Zahar Haichar, F., Santaella, C., Heulin, T., & Achouak, W. (2014). Root exudates mediated interactions belowground. *Soil Biology & Biochemistry*, *77*, 69–80.

Finzi, A. C., Abramoff, R. Z., Spiller, K. S., Brzostek, E. R., Darby, B. A., Kramer, M. A., & Phillips, R. P. (2015). Rhizosphere processes are quantitatively important components of terrestrial carbon and nutrient cycles. *Global Change Biology*, *21*, 2082–2094.

Griffiths, B. S., Spilles, A., & Bonkowski, M. (2012). C: N: P stoichiometry and nutrient limitation of the soil microbial biomass in a grazed grassland site under experimental P limitation or excess. *Ecological Processes*, *1*, 1–11.

Hawes, M. C., Gunawardena, U., Miyasaka, S., & Zhao, X. (2000). The role of root border cells in plant defense. *Trends in Plant Science*, *5*, 128–133.

Hertenberger, G., Zampach, P., & Bachmann, G. (2002). Plant species affect the concentration of free sugars and free amino acids in different types of soil. *Journal of Plant Nutrition and Soil Science*, *165*, 557–565.

Hiltner, L. (1904). Über neuere Erfahrungen und Probleme auf dem Gebiete der Bodenbakteriologie und unter besonderer Berücksichtigung der Gründüngung und Brache. *Arbeiten der Deutschen Landwirtschaftlichen Gesellschaft*, *98*, 59–78.

Hodge, A., Robinson, D., & Fitter, A. (2000). Are microorganisms more effective than plants at competing for nitrogen? *Trends in Plant Science*, *5*, 304–308.

Hosie, A. H. F., & Poole, P. S. (2001). Bacterial ABC transporters of amino acids. *Research in Microbiology*, *152*, 259–270.

Jones, D., Hodge, A., & Kuzyakov, Y. (2004). Plant and mycorrhizal regulation of rhizodeposition. *New Phytologist*, *164*, 459–480.

Jones, D. L., Nguyen, C., & Finlay, R. D. (2009). Carbon flow in the rhizosphere: Carbon trading at the soil–root interface. *Plant and Soil*, *321*, 5–33.

Keith, H., Oades, J. M., & Martin, J. K. (1986). Input of carbon to soil from wheat plants. *Soil Biology & Biochemistry*, *18*, 445–449.

Khashi u Rahman, M., Zhou, X., & Wu, F. (2019). The role of root exudates, CMNs, and VOCs in plant–plant interaction. *Journal of Plant Interactions*, *14*, 630–636.

Kirk, G., Santos, E., & Findenegg, G. (1999). Phosphate solubilization by organic anion excretion from rice (Oryza sativa L.) growing in aerobic soil. *Plant and Soil*, *211*, 11–18.

Koskella, B., & Vos, M. (2015). Adaptation in natural microbial populations. *Annual Review of Ecology, Evolution, and Systematics*, *46*, 503–522.

Kuppe, C. W., Schnepf, A., von Lieres, E., Watt, M., & Postma, J. A. (2022). Rhizosphere models: Their concepts and application to plant-soil ecosystems. *Plant and Soil*, *474*, 17–55.

Kuzyakov, Y., & Blagodatskaya, E. (2015). Microbial hotspots and hot moments in soil: Concept & review. *Soil Biology and Biochemistry*, *83*, 184–199.

Lancashire, P. D., Bleiholder, H., Boom, T. V. D., LangelÜDdeke, P., Stauss, R., Weber, E., & Witzenberger, A. (1991). A uniform decimal code for growth stages of crops and weeds. *Annals of Applied Biology*, *119*, 561–601.

Landl, M., Haupenthal, A., Leitner, D., Kroener, E., Vetterlein, D., Bol, R., Vereecken, H., Vanderborght, J., Schnepf, A., Evers, J., & Long, S. P. (2021). Simulating rhizodeposition patterns around growing and exuding root systems. *Silico Plants*, *3*(2), diab028.

Lohse, M., Haag, R., Lippold, E., Vetterlein, D., Reemtsma, T., & Lechtenfeld, O. J. (2021). Direct imaging of plant metabolites in the rhizosphere using laser desorption ionization ultra-high resolution mass spectrometry. *Frontiers in Plant Science*, *12*, 753812.

Ma, X., Liu, Y., Zarebanadkouki, M., Razavi, B. S., Blagodatskaya, E., & Kuzyakov, Y. (2018). Spatiotemporal patterns of enzyme activities in the rhizosphere: Effects of plant growth and root morphology. *Biology and Fertility of Soils*, *54*, 819–828.

Mayer, C., & Boos, W. (2005). Hexose/pentose and hexitol/pentitol metabolism. *EcoSal Plus*, *1*, 10–1128.

Molina, J. A. E., Clapp, C. E., Linden, D. R., Allmaras, R. R., Layese, M. F., Dowdy, R. H., & Cheng, H. H. (2001). Modeling the incorporation of corn (Zea mays L.) carbon from roots and rhizodeposition into soil organic matter. *Soil Biology & Biochemistry*, *33*, 83–92.

Nazari, M. (2021). Plant mucilage components and their functions in the rhizosphere. *Rhizosphere*, *18*, 100344.

Nazari, M., Riebeling, S., Banfield, C. C., Akale, A., Crosta, M., Mason-Jones, K., Dippold, M. A., & Ahmed, M. A. (2020). Mucilage polysaccharide composition and exudation in maize from contrasting climatic regions. *Frontiers in Plant Science*, *11*, 587610.

Nguyen, C. (2003). Rhizodeposition of organic C by plants: Mechanisms and controls. *Agronomie*, *23*, 375–396.

Oburger, E., Leitner, D., Jones, D. L., Zygalakis, K. C., Schnepf, A., & Roose, T. (2011). Adsorption and desorption dynamics of citric acid anions in soil. *European Journal of Soil Science*, *62*, 733–742.

Panikov, N. S. (1995). *Microbial growth kinetics*. Chapman and Hall.

Pozzo, T., Higdon, S. M., Pattathil, S., Hahn, M. G., & Bennett, A. B. (2018). Characterization of novel glycosyl hydrolases discovered by cell wall glycan directed monoclonal antibody screening and metagenome analysis of maize aerial root mucilage. *PLoS One*, *13*, e0204525.

Reischke, S., Kumar, M. G. K., & Bååth, E. (2015). Threshold concentration of glucose for bacterial growth in soil. *Soil Biology and Biochemistry*, *80*, 218–223.

Rüger, L., Feng, K., Dumack, K., Freudenthal, J., Chen, Y., Sun, R., Wilson, M., Yu, P., Sun, B., Deng, Y., Hochholdinger, F., Vetterlein, D., & Bonkowski, M. (2021). Assembly patterns of the rhizosphere microbiome along the longitudinal root Axis of maize (Zea mays L.). *Frontiers in Microbiology*, *12*, 614501.

Ryu, S., & Trinh, C. T. (2018). Understanding functional roles of native pentose-specific transporters for activating dormant pentose metabolism in Yarrowia lipolytica. *Applied and Environmental Microbiology*, *84*(3), e02146-17.

Santangeli, M., Steininger-Mairinger, T., Vetterlein, D., Hann, S., & Oburger, E. (2024). Maize (Zea mays L.) root exudation profiles change in quality and quantity during plant development—A field study. *Plant Science*, *338*, 111896.

Sasse, J., Martinoia, E., & Northen, T. (2018). Feed your friends: Do Plant exudates shape the root microbiome? *Trends in Plant Science*, *23*, 25–41.

Sawada, K., Funakawa, S., & Kosaki, T. (2008). Soil microorganisms have a threshold concentration of glucose to increase the ratio of respiration to assimilation. *Soil Science and Plant Nutrition*, *54*, 216–223.

Scheu, S. (1992). Automated measurement of the respiratory response of soil microcompartments: Active microbial biomass in earthworm feaces. *Soil Biology and Biochemistry*, *24*, 1113–1118.

Schnepf, A., Carminati, A., Ahmed, M. A., Ani, M., Benard, P., Bentz, J., Bonkowski, M., Knott, M., Diehl, D., Duddek, P., Kröner, E., Javaux, M., Landl, M., Lehndorff, E., Lippold, E., Lieu, A., Mueller, C. W., Oburger, E., Otten, W., ... Vetterlein, D. (2022). Linking rhizosphere processes across scales: Opinion. *Plant and Soil*, *478*, 5–42.

Soler-Bistue, A., Couso, L. L., & Sanchez, I. E. (2023). The evolving copiotrophic/oligotrophic dichotomy: From Winogradsky to physiology and genomics. *Environmental Microbiology*, *25*, 1232–1237.

Stenström, J., Svensson, K., & Johansson, M. (2001). Reversible transition between active and dormant microbial states in soil. *FEMS Microbial Ecology*, *36*, 93–104.

Swinnen, J., van Veen, J. A., & Merckx, R. J. S. B. (1994). 14C pulse-labelling of field-grown spring wheat: An evaluation of its use in rhizosphere carbon budget estimations. *Soil Biology & Biochemistry*, *26*, 161–170.

van Hees, P. A., Jones, D. L., & Godbold, D. L. (2002). Biodegradation of low molecular weight organic acids in coniferous forest podzolic soils. *Soil Biology & Biochemistry*, *34*, 1261–1272.

Vetterlein, D., Carminati, A., Kögel-Knabner, I., Bienert, G. P., Smalla, K., Oburger, E., Schnepf, A., Banitz, T., Tarkka, M. T., & Schlüter, S. (2020). Rhizosphere spatiotemporal organization—A key to rhizosphere functions. *Frontiers in Agronomy*, *2*, 8.

Vetterlein, D., Lippold, E., Schreiter, S., Phalempin, M., Fahrenkampf, T., Hochholdinger, F., Marcon, C., Tarkka, M., Oburger, E., Ahmed, M., Javaux, M., & Schlüter, S. (2021). Experimental platforms for the investigation of spatiotemporal patterns in the rhizosphere—Laboratory and field scale. *Journal of Plant Nutrition and Soil Science*, *184*, 35–50.

Walter, A., Feil, R., & Schurr, U. (2003). Expansion dynamics, metabolite composition and substance transfer of the primary root growth zone of Zea mays L. grown in different external nutrient availabilities. *Plant, Cell & Environment*, *26*, 1451–1466.

Wickham, H. (2007). Reshaping data with the reshape package. *Journal of Statistical Software*, *21*, 1–20.

Wickham, H., Chang, W., Henry, L., Pedersen, T. L., Takahashi, K., Wilke, C., & Woo, K. (2018). ggplot2: Create Elegant Data Visualisations Using the Grammar of Graphics. R Package, Version 335.

Wickham, H., François, R., Henry, L., & Müller, K. (2020). dplyr: A Grammar of Data Manipulation. R package version 1.0.0.

Wiesenbauer, J., König, A., Gorka, S., Marchand, L., Nunan, N., Kitzler, B., Inselsbacher, E., & Kaiser, C. (2023). A pulse of simulated root exudation alters the composition and temporal dynamics of microbial metabolites in its immediate vicinity. *Soil Biology and Biochemistry*, *189*, 109259.

Wutzler, T., Blagodatsky, S. A., Blagodatskaya, E., & Kuzyakov, Y. (2012). Soil microbial biomass and its activity estimated by kinetic respiration analysis–Statistical guidelines. *Soil Biology and Biochemistry*, *45*, 102–112.

Zelenev, V. V., van Bruggen, A. H., & Semenov, A. M. (2000). "BACWAVE", a spatial-temporal model for traveling waves of bacterial populations in response to a moving carbon source in soil. *Microbial Ecology*, *40*, 260–272.

Zhalnina, K., Louie, K. B., Hao, Z., Mansoori, N., da Rocha, U. N., Shi, S., & Brodie, E. L. (2018). Dynamic root exudate chemistry and microbial substrate preferences drive patterns in rhizosphere microbial community assembly. *Nature Microbiology*, *3*, 470–480.

SUPPORTING INFORMATION

Additional supporting information can be found online in the Supporting Information section at the end of this article.

How to cite this article: Niedeggen, D., Rüger, L., Oburger, E., Santangeli, M., Ahmed, M., Vetterlein, D., Blagodatsky, S., & Bonkowski, M. (2024). Microbial utilisation of maize rhizodeposits applied to agricultural soil at a range of concentrations. *European Journal of Soil Science*, *75*(4), e13530. https://doi.org/10.1111/ejss.13530

Chapter II: Photosynthate hotspots structure rhizosphere microbiota

Photosynthate distribution determines spatial patterns in the rhizosphere microbiota of the maize root system

Reference:

Schultes, S., Rüger, L., **Niedeggen**, **D.**, Freudenthal, J., Frindte, K., Becker, M., Metzner, R., Pflugfelder, D., Chlubek, A., Hinz, C., van Dusschoten, D., Bauke, S., Bonkowski, M., Watt, M., Koller, R., Knief, C. Accepted. Photosynthate distribution determines spatial patterns in the rhizosphere microbiota of the maize root system. Nature Communications manuscript ID NCOMMS-24-55118A

Author contributions:

S.R.S., R.K., M.W. and C.K. conceptualized the study. S.R.S. performed the experiments and data analysis. L.R., **D.N.**, and K.F. contributed to amplicon and qPCR data generation and analysis. M.F.B., K.F., J.F., M.B. and S.L.B. contributed to data analysis and interpretation. A.C. and S.R.S. performed $^{13}CO_2$ labeling. D.P. and D.v.D. performed MRI measurements and contributed to the data analysis. R.M., C.H. and A.C. performed ^{11}C-PET labeling and contributed to the data analysis. S.R.S., R.K. and C.K. wrote the manuscript with input from **all authors**.

The supplementary material for Chapter II can be viewed and downloaded here:

https://uni-koeln.sciebo.de/s/DK1NsXCQPfXK4WD

Photosynthate distribution determines spatial patterns in the rhizosphere microbiota of the maize root system

Sina R. Schultes[1], Lioba Rüger[2], Daniela Niedeggen[2], Jule Freudenthal[2], Katharina Frindte[1], Maximilian F. Becker[1], Ralf Metzner[3], Daniel Pflugfelder[3], Antonia Chlubek[3], Carsten Hinz[3], Dagmar van Dusschoten[3], Sara L. Bauke[4], Michael Bonkowski[2], Michelle Watt [3,5], Robert Koller[3,*], Claudia Knief[1,*]

[1]Institute for Crop Science and Resource Conservation (INRES), Molecular Biology of the Rhizosphere, University of Bonn, Bonn, Germany

[2]Institute of Zoology, Terrestrial Ecology, Cluster of Excellence on Plant Sciences (CEPLAS), University of Cologne, Cologne, Germany

[3]Institute of Bio- and Geosciences, IBG 2: Plant Sciences, Forschungszentrum Jülich GmbH, Jülich, Germany

[4]Institute for Crop Science and Resource Conservation (INRES), Soil Sciences, University of Bonn, Bonn, Germany

[5]Adrienne Clarke Chair of Botany, School of BioSciences, Faculty of Science, University of Melbourne, Melbourne, Australia (present)

*Correspondence:

Prof. Dr. Claudia Knief, knief@uni-bonn.de

INRES – Molecular Biology of the Rhizosphere

University of Bonn, Nussallee 13, 53115 Bonn, Germany

Dr. Robert Koller, r.koller@fz-juelich.de

Institute of Bio- and Geosciences, IBG 2: Plant Sciences

Forschungszentrum Jülich GmbH, Wilhelm-Johnen-Straße, 52428 Jülich, Germany

Abstract

The spatial variation and underlying mechanisms of pattern formation in the rhizosphere microbiome are not well understood. We demonstrate that specific patterns in the distribution of recently fixed carbon within the plant root system influence the spatial organization of the rhizosphere microbiota. Non-invasive analysis of carbon allocation in the maize root system by ^{11}C tracer-based positron emission tomography combined with magnetic resonance imaging reveals high spatial heterogeneity with highest ^{11}C-signal accumulations at root tips and differences between root types. Strong correlations exist between root internal carbon allocation and rhizodeposition as evident from $^{13}CO_2$ labelling. These patterns are reflected in the bacterial, fungal and protistan community structure in rhizosphere soil with differences depending on root structure and related spatial heterogeneities in carbon allocation. Especially the active consumers of ^{13}C-labeled rhizodeposits are responsive to photosynthate distribution with differences in ^{13}C-labelling according to their spatial localization within the root system. Thus, root photosynthate allocation supports distinct habitats in the plant root system and is a key determinant of microbial food web development, evident from ^{13}C-labeling of diverse bacterial and protistan predators, especially at root bases, resulting in characteristic spatiotemporal patterns in the rhizosphere microbiome.

1 Introduction

The assembly of the rhizosphere microbiome is the result of complex interactions between the plant and microorganisms. It is further affected by abiotic and biotic factors such as soil properties and interactions between microorganisms in the rhizosphere. It is suggested that microbiome enrichment by the plant host is, for a large part, mediated by rhizodeposition of various compounds into the rhizosphere[1,2]. Plants exude a substantial amount of carbon into the rhizosphere[3], and different exudate compounds have been reported to attract specific microbial consumers[4-6]. These microbial consumers of rhizodeposits have been identified using $^{13}CO_2$ labeling followed by DNA-based stable isotope probing (DNA-SIP)[7].

The root system is mostly sampled as a whole, but no studies have yet systematically unraveled how spatially heterogeneous carbon allocation and rhizodeposition within the root system affect microbiome establishment and lead to spatial patterns in the rhizosphere microbiome. Rhizodeposition is known to be spatially heterogeneous within the root system [8,9]. It varies along the root axis [8,10] and root exudates have been reported to differ between root types[11,12]. Similarly, evidence exists for heterogeneities in the rhizosphere microbiome within plant root systems[13-16], and differences have likewise been reported for microbial communities along the root axis[10] and between root types[11,12]. These heterogeneities in rhizodeposition and microbial community composition suggest the presence of consistent, small-scale selection mechanisms in the rhizosphere, likely driven by substrate preferences of the rhizosphere microbiota[2]. However, apart from the notion that a specific bacterial reporter strain profited primarily from photosynthate distribution at the root tips[17], dependencies within the root system remain largely unresolved at the small scale. It is unclear to what extent spatial variation in the rhizosphere microbiome is related to spatial patterns in carbon allocation within the root system and to rhizodeposition. This leads to the question where in the root system specific microbial taxa are particularly supported by rhizodeposits. Such small-scale dependencies will guide microbial community establishment and processes in the rhizosphere. This in turn has possible implications for the whole food-web that is fueled by rhizodeposits and possibly for plant performance, considering that the rhizosphere microbiome includes taxa with potential benefits for the plant[1,18].

Here, we assess congruencies between spatial patterns in root carbon allocation, rhizodeposition and the rhizosphere microbiota within the maize root system. Maize has a complex root system consisting of different root types with seed-borne (primary and seminal) roots and shoot-borne (crown) roots that develop sequentially over time from different nodes (Figure S 1)[19,20]. Root carbon allocation was studied by $^{11}CO_2$ pulse labeling of plants coupled with

positron emission tomography (PET) and magnetic resonance imaging (MRI). The short-lived carbon radioisotope ^{11}C ($t_{1/2}$ = 20.4 min) allows for tracing recently fixed carbon in vivo and enables detailed time series of ^{11}C tracer allocation processes in the root system[21-23]. Using image-guided sampling for destructive sample collection, data on photosynthate allocation were integrated with microbial data from community compositional analysis (study I). In a second study, this approach was complemented by photosynthate labeling using $^{13}CO_2$ as stable isotopic tracer to track the transfer of carbon from the root into the rhizosphere and its microbiota, followed by DNA-based stable isotope probing (SIP) to identify key microbial consumers of rhizodeposits (Fig 1). We analyzed the prokaryotic, fungal and cercozoan consumers, the latter representing a major group of soil protists[24]. We hypothesize that (I) photosynthates are heterogeneously distributed in the root system, especially along the longitudinal root axis and between root types. (II) Root-internal heterogeneity in carbon allocation extends into the rhizosphere with a largely congruent pattern. (III) The rhizosphere microbiota is expected to develop specific spatial patterns in the rhizosphere in response to carbon allocation. (IV) Microbial taxa are particularly supported by rhizodeposits related to their localization within the root system. This would make photosynthate distribution a central driver of microbial small-scale heterogeneity in the rhizosphere of a root system.

2 Results

2.1 PET-MRI imaging reveals highly heterogeneous distribution of recently fixed carbon

In the two experimental studies, the root systems of all plants were regularly imaged by PET-MRI to non-invasively collect data on photosynthate allocation and root growth. ^{11}C-PET in combination with MRI measurements revealed that recently fixed carbon was heterogeneously distributed in the plant root system over time (Fig 2). Nevertheless, consistent patterns were observed among the $^{11}CO_2$ labeled plants in study I (Figure S 2) and study II (Figure S 3).

We evaluated the spatial patterns in ^{11}C-photosynthate allocation into the root system at three different plant developmental stages in study I. After 6 days of plant development, no ^{11}C tracer was detected in the root system, indicating that recently fixed carbon was not yet allocated into the roots (Fig 2A). In contrast, intensive and heterogeneous belowground allocation of carbon was observed in plants of 13 and 20 days of age, with primary, seminal and crown root tips exhibiting high levels of ^{11}C tracer signal. Tips of the most recently emerged crown roots held particularly strong accumulations of the tracer. On day 13, the tips of crown roots of the second node were rapidly supplied with recently fixed carbon and showed the highest ^{11}C signal intensity. On day 20, the newly emerging crown roots of the third and fourth node showed particularly high

signal intensity, while intensity in crown roots of the second node had declined as the roots matured. Lateral root tips also showed photosynthate accumulations, but this was more difficult to resolve due to their high number and overlapping tracer signals.

Belowground ^{11}C-photosynthate allocation into the root system occurred very rapidly (Fig 2B, Video S 1), with the first photosynthates being detected in the primary root at around 10-15 min after the start of the pulse labeling (Fig 2B, white arrow). The first accumulations of labeled photosynthates at root tips were detected in the youngest crown roots (Fig 2B, green arrow). Once established, these accumulations at root tips generally persisted over the total measurement time, whereas the tracer signal disappeared at the root bases of some roots over time including the primary root, which had received the tracer first.

2.2 Root photosynthate allocation as main driver of rhizodeposition

To relate carbon allocation inside of the roots to carbon allocation in the rhizosphere, the ^{11}C-PET analysis was complemented by stable isotope labeling of shoots with $^{13}CO_2$ and EA-IRMS measurements of root tissue and rhizosphere samples from root tips (2 cm length) and bases (upper 10 cm of a root) after destructive sampling in study II. The $^{11}CO_2$ labeling pulse was again 6 min long, whereas plants were exposed to 12-hour $^{13}CO_2$ pulses daily for the preceding six days to achieve good label incorporation into the microbiota for subsequent DNA-SIP.

As observed in ^{11}C-PET imaging, the mass fraction of ^{13}C in the root tissue and rhizosphere soil was noticeably higher in most root tips compared to their bases, except for the root tissue from the youngest crown roots (Fig 3a, b). Differences were also evident between different root types, whereby the root tissue and rhizosphere soil at the root bases showed a consistent increase in mass fraction of ^{13}C from the primary root over the seminal roots to the different generations of crown roots. A comparison of the mass fraction of ^{13}C between root tissues and corresponding rhizosphere samples revealed consistently higher values in root tissue, along with a significantly positive Pearson correlation ($r = 0.77$, $p < 0.001$) (Fig 3c). When this was analyzed separately for root tips and bases, it became evident that this correlation was primarily driven by a very strong correlation in samples from the root bases ($r = 0.96$, $p < 0.001$; Fig 3d), whereas correlation at the root tips was clearly weaker and not significant anymore ($r = 0.44$, $p = 0.054$). The absence of a significant correlation at the root tips resulted from differences in carbon allocation. In the root tips, the mass fraction of ^{13}C was higher for younger roots compared to older ones, being highest in the first generation of crown roots. In contrast, mass fractions of ^{13}C in the rhizosphere soil were less distinct and in case of the primary and seminal roots more heterogeneous. The decline in ^{13}C in the root tips of the youngest (third) generation of crown roots compared to the first and second generation appeared to be in contrast to the observed highest

^{11}C signals in these youngest roots. This can be explained by the fastest growth of these roots, along with the lag period between the last $^{13}CO_2$ pulse and sample collection, which was required for ^{11}C-PET and MRI imaging. This resulted in further biomass formation at the root tips with unlabelled photosynthates. However, this lag period after ^{13}C pulse labelling does not explain the absence of correlation at the root tips, because the exclusion of the youngest, fastest growing crown root tips from the correlative analysis did not result in significant findings. The mass fraction of ^{13}C in unlabeled controls matched closely the isotope's natural abundance of approximately 1.1% (Figure S 4).

2.3 Root architectural factors and photosynthate level determine microbial community composition

To investigate how photosynthate allocation, root type and root section affect the composition of the rhizosphere microbiota, we sampled root tips and bases from all root types and defined for these samples three levels of photosynthate allocation based on ^{11}C signal intensities (Figure S 1). We distinguished between root tips with high signal intensity, root tips with medium signal intensity and basal root sections with low signal intensity. The community compositional analysis targeted prokaryotes, fungi and Cercozoa. In study I, the communities were directly analyzed by amplicon sequencing, whereas the focus in study II was on the communities that incorporated ^{13}C-labeled photosynthates to more closely link carbon allocation patterns to the benefiting microbial taxa. ^{13}C-incorporating taxa were represented by ^{13}C-labeled DNA obtained from a heavy fraction upon density gradient centrifugation of the DNA. In both experimental studies, the composition of the prokaryotic, fungal and cercozoan communities differed according to root type, root section and the ^{11}C signal categories, which was confirmed by permutational analysis of variance (PERMANOVA) (Tab 1, Table S 1). The statistical model "root type * ^{11}C level" had the best explanatory power in study I. Thereby, root section could be excluded from the model, because the other two factors covered the variation by root section. When root section was introduced as first term in the model, significant variation was assigned to this factor and ^{11}C level could be eliminated.

The non-metric multidimensional scaling (NMDS) plots revealed clear clustering according to root type, especially for bacteria (Fig 4a, Figure S 5). Even the different generations of crown roots formed discernable clusters. This patterning became more pronounced in the microbiota represented by the ^{13}C-labeled DNA fraction in study II, especially in case of fungi, whereas the clustering of Cercozoa related to root type remained less distinct. A sample grouping related to root type was likewise seen in the PERMANOVA results with R^2-values ranging in study I from 0.13 – 0.20 and in study II from 0.14 – 0.26 plus, in case of bacteria and fungi, an increased interaction

term in study II (Tab 1). Sample clustering by root type in the NMDS plots even reflected the chronology of root emergence from the primary root over the seminal roots towards the first, second, third and fourth generation of crown roots. This successive clustering in the NMDS plot was also particularly evident for the bacteria in study II. Further, it was very well reflected in R^2-values of PERMANOVA post-hoc comparisons between all individual root types, though the rather low sample number per root type along with the correction for multiple comparisons did not support the significance of most R^2 values (Figure S 6). Moreover, the successiveness across root types was seen in the analysis of differentially abundant taxa (Figure S 6, Data S 1,Table S 2). This revealed a couple of abundant genera with monotonic changes in relative abundance in the rhizosphere from older towards younger roots. For example, the bacterial genera *Mizugakiibacter, Chujaibacter, Pseudolabrys, Hyphomicrobium, Porphyrobacter, Catenulispora* and *Massilia* as well as the fungal genus *Mortierella* increased in relative abundance towards the younger roots, whereas a few taxa like *Methylotenera* and *Ralstonia* showed the opposite pattern.

Clustering of samples according to root sections was also clearly noticeable in the NMDS plots, whereas sample clustering according to ^{11}C-photosynthate allocation was rather weak, especially in study I (PERMANOVA R^2 between 0.07 and 0.09). It increased substantially in study II (R^2 between 0.34 and 0.47), where we focused on the analysis of DNA in the ^{13}C-heavy fraction, which represents predominantly the consumers of rhizodeposits. This was reflected in the NMDS plots (Fig 4a), where samples clustered according to ^{11}C tracer level as well as root section along the first axis and root type along the second axis. The explanatory power of recent photosynthate allocation in study II was also higher in the unlabeled control samples in this study, but values were not as high as for the ^{13}C-heavy fraction (mean R^2 of 0.28; Table S 3). For reasons of direct comparability with study I, we applied the same PERMANOVA model in study II (Tab 1,Table S 3), though the explanatory power of the model "^{11}C level * root type" was slightly better with even higher R^2 values for the factor ^{11}C level with R^2 values of 0.39 (fungi), 0.43 (bacteria) and 0.59 (Cercozoa).

Next, we evaluated whether ^{13}C quantified in the rhizosphere was an even better explanatory factor for variation in microbial community composition than the ^{11}C tracer signals. The EA-IRMS-derived data on mass fraction of ^{13}C reflects C allocation into the rhizosphere over a longer labeling period than the ^{11}C signal in the root. The replacement of ^{11}C label categories by ^{13}C content in the PERMANOVA model resulted in almost equal R^2 values of 0.31 to 0.37 for the ^{13}C mass fractional data (Tab 1). In the NMDS plots, it became evident that sample clustering according to ^{13}C content coincided strongly with the clustering by root type and section, which is most clearly visible for bacteria (Fig 4b). This demonstrates that recent photosynthate allocation

in the root and rhizosphere is indeed strongly related to major spatial patterns in the microbiota according to root section and root type, over short periods of time, i.e. hours, as well as over days.

Seeing that quite some variation existed in microbial beta diversity but remained unexplained, especially in study I, we assessed community assembly by iCAMP to gain insight into the relevance of stochasticity in community assembly within the root system (Figure S 8). This revealed a strong dominance of stochastic processes, especially drift (68.5-89 % for bacteria and 19.8-86.7 % for fungi), whereas deterministic processes were less relevant and dominated by homogenous selection (7.2-16.2 % for bacteria and 0.16-19.3 % for fungi). The homogenous selection was slightly higher for bacterial communities at root tips compared to bases, which became a bit more pronounced when analyzing the community data of the ^{13}C-heavy fraction in study II. Likewise, homogenous selection gained relevance in fungal communities at root tips in study II. Additionally, dispersal limitation became relevant as stochastic process in the bacterial community at root tips (7.8 %), whereas homogenizing dispersal gained substantial relevance in the fungal community at root bases (42.5 %).

Study I included an analysis of alpha diversity and abundance. The Shannon diversity indices of the prokaryotic, fungal and cercozoan communities showed significant differences in response to photosynthate level, root type and root section, whereby the prokaryotes showed the strongest variation and Cercozoa the weakest (Figure S 9). A reduced diversity was observed with increasing ^{11}C allocation, decreasing age of root types and at the root tips. For the prokaryotes and fungi, this was the consequence of a decrease in richness and evenness in response to the ^{11}C-photosynthate level and root region, whereas the differences related to root type were primarily driven by a decline in evenness. For Cercozoa, changes were primarily related to decreased evenness, but not richness. Concerning prokaryotic and fungal abundance, a strong increase in target gene copy numbers was seen in all rhizosphere samples compared to bulk soil, but strong patterns related to ^{11}C allocation or root section were not evident (Figure S 10). Only trends were seen, which suggest that higher bacterial abundances appear to be related to higher carbon availability, which was likewise reflected by variation according to root type and region. Further, a negative correlation between alpha diversity and abundance was seen for bacteria (Pearson correlation r = -0.23, p = 0.029) and fungi (Kendall correlation = -0.24, p = 0.001) (Figure S 11).

2.4 Heterogeneity in photosynthate allocation impacts microbial consumers of ^{13}C-labeled photosynthates

To reliably identify specific taxa of microbial ^{13}C incorporators, we applied further statistical analysis with the DESeq2 algorithm. We therefore grouped samples in two different ways. In one approach, samples were grouped into four categories based on the quantified mass fractions of ^{13}C in the rhizosphere (Category 1: 1.5 % - 6.9 %; Category 2: 6.9 % - 12.3 %, Category 3: 12.3 % - 17.7 %; Category 4: 17.7 % - 23.1 %; Figure S 12). This enabled the identification of taxa that became uniformly and thus significantly labeled related to the amount of carbon transferred into the rhizosphere. Alternatively, samples were grouped according to their origin in the root system, i.e. from tips or bases of seed-borne (primary and seminal roots) and shoot-borne (crown) roots, respectively. This grouping allowed the identification of labeled taxa with consistent label incorporation according to root architecture. Overall, the number of identified taxa ranged from 2 - 18 per amplified clade and category (Table S 4). More labeled taxa were detected in the groups of bacteria and Cercozoa than fungi. Most taxa identified as ^{13}C-labeled were identified by both approaches (Fig 5, Figure S 13), underlining that their labeling was strongly related to both, the spatial location of the taxa in the root system and the amount of ^{13}C rhizodeposition. Several of the ^{13}C-labeled taxa had been identified as responsive to ^{11}C level and/or root type already in study I, confirming the strong responsiveness of these taxa to one or both of these factors. Among others, the bacterial genera *Paenibacillus*, *Massilia*, *Methylotenera* and *Rhodotorula* as well as the fungal genera *Fusarium*, *Trichoderma* or *Ustilago* were identified in both studies (Fig 5,Figure S 6).

Several fungal amplicon sequencing variants (ASVs) were exceptionally strongly labeled in samples with the highest ^{13}C signature in the rhizosphere soil, while their labeling was significantly lower than that of bacteria and Cercozoa in samples with low ^{13}C content in the rhizosphere (i.e., label categories 1 and 2; Fig 5A). The alternative approach, during which ^{13}C incorporators were identified upon sample grouping based on their origin in the root system, showed that this intensive fungal labeling occurred at root tips (Fig 5B), and thus, taken together, at root tips with highest carbon allocation. Bacterial and cercozoan taxa showed less variation in label intensity between the four defined categories, regardless of the underlying sample grouping strategy (Fig 5A, B).

Visualizing ^{13}C consumer label intensity for each significantly labeled taxon revealed that several ASVs represented ^{13}C consumers of the bacterial class *Bacilli*, especially the genus *Paenibacillus* was identified in samples with high ^{13}C content in rhizosphere soil, i.e. in ^{13}C-label category 3 and

4 (Fig 5C). In contrast, almost all ^{13}C-labeled ASVs within the *Gammaproteobacteria* (e.g. *Pseudomonas, Methylotenera, Massilia* and unidentified *Oxalobacteraceae*) and *Actinobacteria* were detected in the weakly labeled category 1 samples. The *Bacilli,* especially *Paenibacillus,* showed the highest relative abundance in the labeled fraction of root tip samples (Figure S 14), whereas the *Gammaproteobacteria* with *Massilia* as well as unidentified *Oxalobacteraceae* and *Comomonadaceae* were particularly prominent in root base samples (Figure S 15). For some taxa, a further differentiation between seed- and shootborne root bases was seen, especially in the case of ASVs from the Rhizobium group, occurring preferentially as labeled at the seed-borne root bases.

Among the fungi, the most intensively labeled ASVs were represented by the class *Sordariomycetes*, especially the genus *Fusarium* (Fig 5C), resulting in the high fold-change for fungi in ^{13}C-label category 4 (Fig 5A). This category is represented by tips of seminal and crown roots of the first node (Figure S 12), but *Fusarium* occurred also in the ^{13}C-heavy fraction of other root tips (Figure S 14). Also striking was the ^{13}C labeling of some ASVs representing non-identified members of the *Lobulomycetes* (*Chytridiomycota*) (Fig 5C) with high relative abundance in rhizosphere soil samples of ^{13}C-label category 1 to 3, i.e. at root bases and tips of the crown roots (Figure S 14). Among the Cercozoa, most ^{13}C-labeled operational taxonomic units (OTUs) represented members of the *Cercomonadida* and *Glissomonadida*, but in contrast to the highlighted bacterial and fungal taxa, these did not show very particular enrichment or abundance patterns related to the mass fraction of ^{13}C in the rhizosphere or related to the root system (Fig 5). Their labeling and relative abundances were more balanced.

Lastly, we combined the amplicon data of the three microbial groups and explored the role of ^{13}C-labeled taxa within the community by network analysis (Fig 6). This was done separately for the root tip and root base microbiota, as major differences were observed between samples from these two root sections in the SIP amplicon dataset (Fig 4). Networks were calculated at species level resolution and aggregated at phylum (bacteria, fungi) / order (Cercozoa) level (Fig 6) or at genus level (Figure S 15). Compared to the network constructed for the root tip (49 associations), the network for the root base showed more associations between bacteria and Cercozoa (63 associations), especially between bacteria and *Glissomonadida* (22 and 29 associations, respectively) (Fig 6). In contrast, many fungal taxa disappeared from the root base network. To assess the role of the ^{13}C-labeled taxa within these networks, we analyzed their connectivity and compared it to non-labeled taxa. While there were no significant differences observed in the root tip network, the labeled taxa showed a higher degree, radiality and centrality in the network of the

microbiota associated to the root bases (Table S 5), indicating that these had more prominent positions in the network.

3 Discussion

$^{11}CO_2$ labeling in combination with PET and MRI allowed the integration of tomographic data on photosynthate distribution with root structural information at high spatial and temporal resolution[21]. Applied to 6-day old maize plants, it revealed that recently assimilated photosynthates remained in the shoot and were not translocated into the roots, which is explained by the early developmental stage at which the root system is still supplied by seed reserves[25]. In 13 and 20-day old plants, the recent photosynthates were rapidly transferred into the entire root system. The primary root received the recently fixed carbon most rapidly after the $^{11}CO_2$ pulse, indicating an efficient reorganization from seed- to shoot-derived carbon supply until day 13. It is assumed that the reorganization from heterotrophy to autotrophy occurs in maize around day 10[25]. The observed fast transition ensures the further development and functionality of the seed-borne roots. At the two later time-points, we observed the hypothesized heterogeneities in carbon allocation within the root system.

Within the individual roots, the allocation of recently fixed carbon varied strongly along the longitudinal root axis with most intensive accumulations at the root tips. This was seen in ^{11}C-PET images (Fig 2A) and confirmed by ^{13}C analysis of the root tips as well as for the associated rhizosphere soil (Fig 3). The intensive photosynthate accumulations in and around root tips align with previous studies using ^{14}C[26,27] and ^{13}C approaches[15] and can be linked to the energy demanding processes occurring at root tips, including cell division in the apical meristem, mucilage synthesis at the root cap and membrane transport. The related high photosynthate accumulations in the rhizosphere are the consequence of different rhizodeposition processes with photosynthate loss at the root tips due to exudation, mucilage production and border cell shedding[9,26,28,29].

We also detected clear differences in photosynthate allocation between root types, whereby the youngest crown roots showed particularly high ^{11}C signal intensity, especially at their tips. This indicates that these young roots are already well connected to leaves via the phloem and efficiently supplied by recent photosynthates, supporting their high elongation rates[30] and dominant role in soil exploration[31]. The $^{13}CO_2$ labeling confirmed that photosynthate accumulations at root tips decreased consistently for root types of increasing age (Fig 3b). This can be explained by the development of lateral roots as additional local sinks, therewith reducing the initially very high accumulations at the main root tip. It is assumed that both, root elongation

and the emergence of lateral roots contribute to the total photosynthate sink strength of a root, and these processes are thought to be regulators of root photosynthate transport in the root system[32,33].

At the root bases, the recent photosynthates merely passed through according to ^{11}C-PET imaging (Video S 1). Also, the $^{13}CO_2$ labeling over several photoperiods showed that root bases did not accumulate much of the ^{13}C tracer, especially not the primary and seminal roots (Fig 3). These roots were already established with the full length that we sampled for the base section when the $^{13}CO_2$ labeling period began. In the younger roots, part of the sampled base section developed during the ^{13}C labeling period and incorporated ^{13}C-labeled photosynthates into the tissue, explaining the consistent increase in ^{13}C content of root samples with decreasing age. Further, the mass fraction of ^{13}C within the root system was very closely correlated to that in the rhizosphere at the root bases (Fig 3d) pointing to tightly coupled processes for photosynthate allocation within the root and their release into the rhizosphere. This aligns with our hypothesis and the knowledge about reduced rhizodeposition with increasing root maturity along the root axis, which comes with a stricter control of diffusion and increasing relevance of specific secretion mechanisms[9,34]. These obviously link root internal photosynthate allocation tightly with allocation in the rhizosphere. At the root tips, the root internal and external ^{13}C tracer accumulations were not well correlated (Fig 3d), merely because the rhizosphere samples from different root types showed less distinct patterns and more variation between replicate samples than the root tissue samples did. Differences in microbial carbon mineralization might have contributed to this discrepancy, considering that we observed root type specific variation in the microbiota at the root tips (Fig 4, Figure S 5).

As an asset of the temporal resolution of ^{11}C-PET imaging, we observed heterogeneity regarding the arrival of the short-lived ^{11}C tracer signal in the individual roots. This may indicate differences in flow velocity between individual roots. In combination with the variation in photosynthate accumulation at root tips, it indicates that specific mechanisms play a role in determining the distribution of recent photosynthates within the root system. Intensely debated in this context are functional differences between the roots[15], root length and diameter[15,28], as well as root growth rates[35]. Further, anatomical traits such as phloem diameter and processes including phloem loading and unloading may contribute to this.

As rhizodeposits present a major energy source for microorganisms[36] and microbial taxa have specific substrate preferences in the rhizosphere[2], we hypothesized that the observed variation in photosynthate allocation within the roots and into the rhizosphere should have consequences for

the rhizosphere microbiota. We have multiple lines of evidence that the spatial patterns observed in the microbiota according to root type and root section were closely related to photosynthate allocation. Root section, root type and the two isotopic tracer levels, taken as a proxy for recent photosynthate allocation in the root system, explained jointly variation in microbial community composition according to PERMANOVA. Likewise, the NMDS plots revealed that sample clustering occurred according to root section and root type, and in addition to the ^{11}C tracer level and the amount of ^{13}C quantified in the rhizosphere. The taxa that were identified as significantly labeled by the DESeq2 algorithm were largely the same, independent of the grouping of samples according to their origin in the root system or the ^{13}C tracer category.

The most striking differences in photosynthate allocation were observed along the root axis with accumulations at the root tips (Fig 2A). These patterns were reflected by differences in community composition of bacteria, fungi and Cercozoa between root tips and bases (Fig 4, Figure S 5)and a reduced alpha diversity of prokaryotes and fungi at root tips (Figure S 9). Differences in the microbiota between root tip and base reflect stages of a successive community developmental process along the axis, related to rhizodeposition processes[10,37]. The population size of bacteria and fungi in the rhizosphere did not differ substantially between root base with low recent photosynthate accumulation and root tips with high accumulations, indicating a very rapid population build-up at root tips, supported by the high substrate availability at root tips[38-40]. This comes along with a decline in alpha diversity, i.e. reduced richness and evenness, explained by a specific enrichment of selected fast-growing taxa[41], such as *Paenibacillus* or *Fusarium*, as identified by DNA-SIP.

Root type was the second major factor that differed in recent photosynthate allocation and to which variation in microbial community structure was related (Tab 1). Evidence for root type dependent differences in microbial communities of cereals is recently accumulating[11,42,43]. For maize, differences in bacterial communities have been reported to exist between primary and crown roots[12]. Beyond these root type related differences, we demonstrate with our results a successive change in community composition from the oldest, primary root to the most recently emerged crown roots for bacteria, Cercozoa and, with more variability, for fungi (Fig 4, Figure S 5). Similarly, a successive decrease in alpha diversity from the oldest to youngest roots was seen, especially for bacteria, primarily a decline in evenness (Figure S 9). These successive changes can also be explained by community development, based on the observation that several taxa showed consistent increases in relative abundance across root types and related to the chronology of root emergence (Figure S 7, Data S 1, Table S 2). The development is likely driven by different

processes, including root type specific exudation patterns, which have been reported to exist in maize[12], and time-related processes as roots and rhizosphere mature. The sequential emergence of the roots gives more time for community assembly, competitive outcomes, plant-selection processes and top-down control by predators along the root axis towards the bases for older roots compared to younger roots. Our samples from root bases include this temporal aspect, as they differ not only with regard to root type, but also in rhizosphere age.

Root type related patterns were not only observed at the root bases but likewise seen at the root tips. While this can be seen for bacteria in study I, the results of study II show this even more clearly for the communities of bacteria, fungi and Cercozoa that profited from rhizodeposits (Fig 4a). This demonstrates that root-type related differences in the microbiota develop already at a very early stage of rhizosphere establishment. Considering that differences existed between all analyzed root types including the different generations of crown roots, the underlying mechanism leading to these differences is not necessarily only related to root type, but likewise defined by further processes, probably related to root length, root age or root growth rate[44].

Despite reproducible spatial patterns in the rhizosphere microbiota, substantial variation in beta diversity remained unrelated to root type, root region and carbon allocation patterns. The quantitative analysis of community assembly processes revealed a strong dominance of stochastic processes, especially drift (Figure S 8). This may appear unexpected, considering the important role of rhizodeposits in shaping the rhizosphere microbiome, but high variability in the rhizosphere microbiota between individual plants and substantial drift, in part along with other stochastic processes, was likewise seen in other pot experiments and enforced under certain growth conditions and during early plant growth stages[45-47]. It indicates that stochastic processes such as drift are likely to be high in small-scale (pot) experiments and to increase further at even smaller spatial scales, i.e. within a root system of an individual plant. It can result from processes such as competitive exclusion and priority effects, which have been proposed to contribute to microbiome assembly especially at root tips due to the rich amount of rhizodeposits that are released[41]. However, our data showed that stochastic processes and more specifically drift is nearly equally relevant at root tips and bases. Instead, we observed a slight increase in homogenous selection at root tips, which was enforced in the ^{13}C-heavy fraction of study II. It also increased with inclining ^{13}C label intensity in the rhizosphere (Figure S 8B). This indicates that part of the microbial community becomes specifically enriched by deterministic processes related to rhizodeposition, whereas the enrichment of many other taxa is affected by stochastic processes, therewith introducing heterogeneities. The ^{13}C-heavy fraction of the bacterial community showed

in addition dispersal limitation at root tips, which may also be related to priority effects, when early-arriving taxa limit the establishment of later-arriving taxa. In contrast to the bacteria, the ^{13}C-labeled fungal communities showed high homogenizing dispersal at root bases under conditions of more limited carbon supply. Fungi may compensate spatial heterogeneities and carbon limitation in the rhizosphere by their hyphal growth, but not yet at root tips, rather over time at root bases.

The focus on taxa with significant ^{13}C label incorporation allowed to confirm the fourth hypothesis and revealed an exceptionally high labeling of fungi in rhizosphere regions that received highest levels of ^{13}C-labeled photosynthates, i.e. the root tips (Fig 5, Figure S 13). While bacteria have traditionally been considered the prime consumers of rhizodeposits, recent studies reported that fast-growing "sugar" fungi can also profit from this plant-derived carbon[48, 49]. Our data indicate that this occurs in particular in rhizosphere regions with highest rhizodeposition. Towards the root base, competition between fungi and bacteria for the more limited rhizodeposits increases, giving an advantage to bacteria over fungi, demonstrated by higher log2 fold changes in this root region for bacteria than fungi (Fig 5A) and the disappearance of fungal taxa from the co-occurrence network. A particularly high ^{13}C labeling in samples with highest ^{13}C-photosynthate rhizodeposition was linked to *Fusarium* (Fig 5C), which was apparently very efficient at obtaining organic carbon from rhizodeposition in these regions, i.e. root tips. The genus *Fusarium* includes different species of commensals as well as potential beneficials[50,51] and maize pathogens[52,53] It is tempting to speculate that these fungi can establish in the rhizosphere preferentially in regions that provide ample amounts of organic carbon and that do not yet host a very competitive microbiome, conditions they encounter at root tips. Besides, root tips are known to represent a good entry point for pathogens[54]. Along with *Fusarium*, potentially beneficial fungi such as *Trichoderma* were also labeled in samples with high ^{13}C-photosynthate deposition[55]. In contrast, the very high relative abundance of unidentified *Lobulomycetales* within the labeled fungal community indicates that not all fungi follow the same pattern, because this not yet well-known taxon was prominently present and labeled at all root bases and the tips of shoot-borne roots (Figure S 14). The different colonization pattern of this taxon was reflected in the co-occurrence network, where it remained visible in the network of the root base with only positive associations to other taxa, whereas many other fungal taxa disappeared (Figure S 15). Members of the *Chytridiomycota*, to which the *Lobulomycetales* belong, have been reported to profit from rhizodeposits in grassland soil and is was speculated that these might be secondary consumers rather than primary consumers of rhizodeposits[49]. Our data for the unidentified *Lobulomycetales* support this assumption considering their rather weak labeling and their position and positive

connectedness in the co-occurrence network, suggesting that these fungi may be more competitive as secondary consumers than as primary consumers at root bases.

Among the bacteria, the most intensive ^{13}C label incorporation was observed for *Paenibacillus* in rhizosphere samples with high ^{13}C content, which reflects the pattern of *Fusarium* and *Trichoderma* and is well in line with their copiotrophic lifestyle, enabling a rapid proliferation in root regions with high photosynthate supply[56]. Indeed, *Paenibacillus* was prominent at both, seed-borne and shoot-borne root tips (Figure S 13) and showed high ASV diversity, to which operon heterogeneity within strains likely contributed to some extent[57,58]. The ^{13}C-labeled taxon with the highest relative abundance among the labeled taxa in the ^{13}C-heavy DNA fractions was *Massilia*, which became labeled in particular at the bases of shootborne roots (Figure S 13). Further taxa with this pattern included different rhizobia*,* some of the *Paenibacillus* ASVs and other *Oxalobacteraceae*. All these genera have previously been identified as carbon consumers in the rhizosphere by DNA-SIP studies[7,59]. These genera are known to include beneficial taxa[4,60], which may be particularly supported in root regions more distant from the tip, where overall fewer photosynthates are released, but the secretion or diffusion of specific compounds gains relevance compared to root tips[61,62]. These compounds may more specifically support beneficial taxa, as reported for *Oxalobacteraceae*, which benefit from flavonoids and can improve plant nutrient aquisition[4]. The fact that labeled taxa had prominent positions within the network at the root bases underlines that these became particularly well established at the root bases upon community succession along the root axis.

Among the bacteria, not only primary consumers became ^{13}C-labeled, but also the predatory bacterial genera *Vampirovibrio* and *Bdellovibrio* as secondary consumers. They were labeled at the root bases, where they were detected at rather low relative abundance (Figure S 13), but with an intermediate ^{13}C label enrichment compared to the other ^{13}C-labeled bacterial taxa (Fig 5). This aligns with a report that these bacterial predators can be highly active[63]. They may thus represent relevant players in the microbial food webs of the rhizosphere besides eukaryotic predators. The latter, studied here with a focus on cercozoan predators, became significantly ^{13}C-labeled in all different root regions. Although Cercozoa integrate the ^{13}C label at a higher trophic level, their mean label log2 fold changes followed closely the patterns of the bacterial communities (Fig 5A, B). This was also seen in the community compositional variation of the total ^{13}C-heavy DNA fraction, which reflected very well the pattern of their bacterial prey (Fig 4a). Further, a tight association of protist grazers with potential bacterial prey was seen in the co-occurrence network (Fig 6), where the main ^{13}C-lableled cercozoan consumers of labeled prokaryotic prey were small

flagellates in the *Glissomonadida* and *Cercomonadida*. These have short generation times and specific grazing impacts on bacterial communities[64,65]. With their establishment along the root axis, they have likely modulated the labeling patterns of some taxa that serve as prey. These findings indicate significant top-down control of the maize microbiome by predatory bacteria, protists and likely also fungi, especially towards the root bases.

In summary, the combination of isotope-based approaches to document recent photosynthate allocation within the root system and into the rhizosphere along with image-guided destructive spatially resolved rhizosphere sampling allowed to link this allocation with heterogeneities in microbial community structure. The spatial patterning in photosynthate allocation within the maize root system is dominated by strong photosynthate allocation at root tips and a tight correlation between root internal and external allocation especially at the root bases. The rhizosphere microbiota responds to this with notable changes in community structure along the root axis and differences between root types. Thus, photosynthate availability is an important factor driving habitat differentiation within the maize root system and causing spatial variation in the rhizosphere microbiome. Fast-growing taxa, here in particular *Paenibacillus*, benefit strongly from photosynthates at the root tips, likewise as some fungal taxa, including potentially pathogenic fungi like *Fusarium* that exploit these root sections efficiently. Towards the root bases, the microbiota undergoes a succession, whereby other taxa are particularly supported by rhizodeposits, including bacterial taxa with potential benefits for the plant, whereas fungal taxa become less competitive under the more limited photosynthate availability. Further, the development of the microbiota is modulated by a range of prokaryotic and eukaryotic secondary consumers that thrive in the rhizosphere, known or predicted predators that exert top-down control on the community. Community compositional differences exist between root types and between each generation of crown roots, evident at root bases as well as tips. This points to mechanisms and processes that are not only root-type specific, but change related to the age of the root or the rhizosphere or are related to other traits such as root length. It requires further analyses to resolve the underlying mechanisms in more detail, whereby processes that define the composition of the rhizodeposits, which fuel the microbiota, will require particular attention. Taken together, the existence of spatiotemporal patterns in photosynthate allocation and the composition of rhizodeposits and the resulting differences in rhizosphere microbial food webs implies that processes in the rhizosphere are spatially and temporally defined. It requires spatiotemporal resolution to understand microbiota assembly and precisely assess microbially driven processes within the root system, including those that provide potential benefits for the

plant, which may be very locally supported in the root system by the plant. This knowledge is crucial for developing effective management strategies for root microbiomes.

4 Methods

4.1 Soil preparation and plant cultivation

Soil columns were established according to Vetterlein et al. 2021[66]. Briefly, 16.7 % loam soil derived from a Haplic Phaeozem (Schladebach, Germany) was mixed with 83.3 % quartz sand (WF33, Quarzwerke GmbH, Frechen, Germany). This growth substrate was dried, sieved to <1 mm and fertilized[66] before homogeneously filling PVC columns (20 cm height, 8 cm diameter) up to a bulk density of 1.47 g cm $^{-3}$. *Zea mays* seeds (line B73) were surface sterilized in 10 % H_2O_2 for 10 min, primed in a saturated $CaSO_4$ solution for 3 h and sown at 1.5 cm depth. Plants were grown in a climate chamber for 22 days as described[66], while upholding a volumetric soil water content of 18 %.

4.2 $^{13}CO_2$ labeling of plants

Stable isotope labeling to trace photosynthates into the rhizosphere and its microbiota was conducted in two Perspex® chambers adapted from Hünninghaus et al. 2009[7] (Fig 1). Eight plants were transferred into each labeling chamber at day 15 after sowing and either exposed to $^{13}CO_2$ or unlabeled CO_2, (referred to as $^{12}CO_2$). Plants were continuously labeled during the whole 12-hour light period for 6 days. Both chambers were initially scrubbed of ambient CO_2 by passing air through a soda lime cartridge at each labeling day before $^{12}CO_2$ or 99 % $^{13}CO_2$ (Linde GmbH, Pullach, Germany) were pumped into the respective chambers and evenly dispersed by ventilators. In both chambers, constant gas concentrations of 407 ± 20 ppm were established using an automated system combining $^{12}CO_2$ and $^{13}CO_2$ gas analyzers ($^{12}CO_2$ = Li-820, LI-COR Biosciences – GmbH, Bad Homburg, Germany, 13CO2, S710, Sick AG, Waldkirch, Germany) (Figure S 16). Temperature within chambers was regulated to maintain 18 °C at night and 23 °C during the light period, ± 2°C. At the end of each labeling day, the labeling gasses within the chambers were scrubbed by passing through a soda lime cartridge and the chambers were opened to allow for inflow of ambient CO_2.

4.3 Radioactive $^{11}CO_2$ labeling and PET-MRI scanning

Plants were supplied with ^{11}C ($t_{1/2}$≈20 min) labeled CO_2 and scanned by PET (Fig 1) to non-invasively visualize the short-term photosynthate distribution in the root system. Due to the short half-life of ^{11}C, it is produced on site with a dedicated cyclotron. The night before PET scanning,

plants were transferred to the *pheno*PET facility[67] and mounted in an environmentally controlled labeling cuvette connected to the gas exchange system with the roots in the field of view of the *pheno*PET. The shoot was subjected to labeling with ~200 MBq (study I) or 100MBq (study II) $^{11}CO_2$ for 6 min after the start of the 2.5 h PET measurement. Data processing and image reconstruction is based on Hinz et al. 2024[67]. The image reconstruction was done in 5-min frames. Scatter and attenuation corrections were not applied. Images were decay-corrected. PET measurements were complemented by transferring the plant to MRI to non-invasively monitor root system architecture. We used a 4.7-T vertical bore magnet (Magnex Scientific, Oxford, United Kingdom) equipped with a 21-cm gradient system up to 400 mT/M (MR Solutions, Guildford, United Kingdom) and a 10-cm RF coil (Varian, Palo Alto, CA) as previously described[68]. To counter imaging artifacts observed in this soil, the imaging parameters were set to: Spin-Echo Multi-Slice (SEMS) sequence, Bandwidth = 400 kHz, 4 averages, Field of view = 96 mm, 0.5 mm resolution, 1 mm slice thickness, echo time TE = 9 ms, repetition time TR = 2.8 s. MRI data were analyzed using the program NMRooting[68]. We restricted root tree analysis to the axial roots, i.e. the primary root, seminal roots and crown roots, thus excluding all lateral roots and quantified root length (Figure S 17). For further analysis and to enable image-guided sampling, overlays of the PET and MRI 3D-scans were constructed in the MeVisLab environment (MeVis Medical Solutions AG, Bremen, Germany).

4.4 Image-guided root and rhizosphere soil sampling

Before sampling, the soil was brought to the targeted volumetric water content to ensure comparable extension of the rhizosphere. Soil cores were pushed out of the pots and MRI images were used for orientation and identification of root and rhizosphere samples. We took root tip samples of about 2 cm length and root base samples of about 10 cm length to capture the largest possible variation of both root sections (Figure S 1) from every root, while distinguishing between the primary root, seminal roots, and crown roots from the first to the third or fourth underground node. The length of the root base sample was slightly reduced for the third generation of crown roots, whereas the fourth generation base samples were not yet available. PET scans enabled us to roughly categorize root samples according to three ^{11}C tracer signal intensity levels. Image evaluation by visual assessment resulted in a distinction between root tips with high signal intensity, root tips with medium signal intensity and basal root sections with low signal intensity. Lateral roots were cut off to avoid mixed root type signals. As the youngest crown roots were very small on the day of sampling, only root tip samples were taken from this root type. Rhizosphere samples were taken by dipping the root pieces in 0.3 % sterile NaCl solution. To sediment the

rhizosphere soil, the suspension was centrifuged at 5000 x g and 4 °C for 30 min. Root tissue samples were further cleaned upon dipping by vortexing the root pieces in 0.3 % sterile NaCl for 15 seconds. The pelleted rhizosphere soil samples and the washed root pieces were stored at -80 °C.

Analyses were done in study I for individual roots from a total of three plants, whereas the same type of root sample, i.e. roots of each root type and section, from two plant replicates was pooled in study II to obtain enough material for all analyses (Figure S 1). The previously obtained PET-MRI scans ensured that the photosynthate allocation and development of sampled roots were comparable (Figure S 3). Using 16 plants in total, this resulted in four replicate ^{13}C-labeled sample sets and four corresponding ^{12}C-control sets covering all root types, root sections and photosynthate allocation categories in study II (Table S 6).

4.5 Determination of mass fractions of ^{13}C in root and rhizosphere samples

A subsample of each rhizosphere and root sample was dried for 4 days at 50 °C and ground to a fine powder by hand. Approximately 70 mg of rhizosphere soil and 0.5 mg of root material was used for $^{13}C/^{12}C$ isotope analysis with an elemental analyzer (Flash EA 1112; Thermo Fisher GmbH, Bremen, Germany) coupled to an isotope ratio mass spectrometer (Delta V Advantage; Thermo Fisher Scientific, Waltham, MA, USA). We calibrated results against the reference materials calcite (IAEA 603; $\delta^{13}C$ = 2.46‰) and corn starch (Schimmelmann Research, Indiana University; $\delta^{13}C$ = -11.01‰). Results are presented as mass fraction of ^{13}C in percent (mass of ^{13}C relative to the total mass of C in each sample), as calculated based on Teste et al. 2009[69].

4.6 DNA extraction

DNA was extracted from ~500 mg of wet rhizosphere sample using the FastDNA™ SPIN Kit For Soil (MP Biomedicals™, Santa Ana, Canada) following the protocol of Tournier et al. 2015[70] with minor alterations (2 x 45 s cell disruption, 100 µl elution volume). The DNA was quantified using the QuantiFluor dsDNA System on a Quantus™ Fluorometer (Promega, Madison, WI, USA).

4.7 DNA stable isotope probing

DNA-SIP was performed for 36 ^{13}C-labeled samples and 36 corresponding ^{12}C-control samples following the protocol of Lueders et al. 2010[71] with minor alterations. Per sample, ~1.5 µg of DNA was loaded onto CsCl (≥99.999 % p.a., Carl Roth, Karlsruhe, Germany) suspensions with a starting density of 1.721 g ml^{-1}. Samples were randomly assigned to different ultracentrifuge runs

to compensate for possible run-related variation. Gradients were spun at 20°C and 177.000 x g for 38 h in an Optima™ XPN-80 ultracentrifuge with VTi 65.2 rotor (Beckman Coulter, Brea, CA, USA). Gradients were fractionated from bottom (heavy) to top (light) into 12 fractions (~400 µl) by displacement of the gradient solution with bromophenol blue stained DEPC-water. The buoyant density of each fraction was determined by measuring the temperature-corrected refractive index (nDTC) of a small sample aliquot on an AR200 refractometer (Reichert, Depew, NY, USA). Depending on sample origin (root type, root section), we observed that light, unlabeled DNA peaked at densities around 1.705 - 1.710 g ml^{-1} and heavy, ^{13}C-labeled DNA peaked at buoyant densities of around 1.720 – 1.728 g ml^{-1} (Figure S 17). The DNA in each fraction was precipitated by adding 2 Vol of 30 % PEG 6.000 in 1.6 M NaCl and 1 µl of glycogen (20 µg; Roche, Basel, Switzerland) before incubating the samples at room temperature for 2 h. This was followed by 40 min of centrifugation at 4 °C and 21.000 x g, a washing step in 70 % EtOH and a second centrifugation step of 25 min before the pellet was eluted in 25 µl of 10 mM Tris-HCl and stored at -80 °C. After centrifugation, one heavy and one light fraction of each sample was selected for amplicon sequencing. The selection was done individually for bacteria, fungi and Cercozoa based on quantitative PCR (qPCR) data generated for all fractions. When DNA was similarly abundant in two neighboring fractions, the more extreme one was selected for sequencing - the lighter fraction with lower density and the heavier fraction with higher density. Plotting the 16S rRNA, ITS1 and 18S rRNA copy numbers against the buoyant density revealed the fractions that contained peaks of ^{13}C- and ^{12}C-DNA, respectively (Figure S 17).

4.8 Quantitative PCR and amplicon sequencing

Quantitative PCR assays were performed as previously described[72] using 10-fold diluted DNA solutions with slightly adapted thermal cycling protocols (Table S 7) and the same primers as for amplicon sequencing (Table S 8).

Prokaryotic 16S rRNA gene amplicons, fungal ITS1 amplicons and cercozoan SSU/18S rRNA gene amplicons were generated following group-specific two-step PCR protocols (Table S 8, Table S 9, Table S 10). As ITS1 amplification products showed several unspecific bands on a 1.5 % agarose gel, correct bands were excised after the first round of PCR and purified using the NucleoSpin® Gel and PCR Clean-up Kit (Macherey-Nagel, Düren, Germany) Prokaryotic and fungal amplification products were quantified using the QuantiFluor dsDNA System on a Quantus™ Fluorometer and pooled at equimolar concentrations. 18S rRNA gene amplicons were processed using the SequalPrep Normalisation Plate Kit (Invitrogen GmbH, Karlsruhe, Germany). Pooled PCR products were purified with the CleanNA magnetic bead system (GC-Biotech, Waddinxveen, the

Netherlands). Library preparation and sequencing of the amplicons was performed by the West German Genome Center (WGGC) and the Cologne Center for Genomics (Cologne, Germany), on MiSeq instruments (Illumina, San Diego, Canada) generating 2x300 bp paired-end reads.

4.9 Sequence data analysis

The raw sequence reads were preprocessed using a customized bash script with Cutadapt version 4.2 to demultiplex the samples[73]. Primer trimming was performed using QIIME 2, version 2022.11[74] and denoised ASVs were created for bacteria and fungi using the DADA2 pipeline[75]. The denoising step also comprised forward and reverse read merging and chimera removal. Sequence alignment was performed using the MAFFT software[76]. The SILVA database (version 138) was used for prokaryotic taxonomy assignment[77] and the UNITE database (version 9) for fungal taxonomy assignment[78]. Data were exported into R (version 4.2.3) and analyzed with the packages *phyloseq*[79], *vegan*[80] and *microbiome*[81]. Singletons and reads unclassified above class level were removed from the data sets (Table S 11).

Cercozoan raw sequence reads were processed using the custom MOTHUR pipeline v.39.5[82]. After demultiplexing and primer- and tag-sequence trimming, the remaining reads were clustered into OTUs using VSEARCH[83] with an abundance-based greedy clustering algorithm (agc) at a similarity threshold of 97 %. Clusters with fewer than 214 reads were removed to eliminate potential amplification or sequencing noise[24]. OTUs were assigned to taxa using BLAST+[84] with an e-value cutoff of 1e-50 and the PR2 database[85], retaining only the best hit. Non-target sequences were excluded. Sequences were aligned using the provided template[24] allowing gaps of up to five nucleotides, and cleaned for chimeras using UCHIME[86].

4.10 Statistical evaluation

Alpha diversity was analyzed using rarefied datasets and differences were assessed by ANOVA and Tukey-HSD posthoc tests or Mann-Whitney U-tests with Benjamini-Hochberg correction. Beta diversity was assessed by NMDS plots based on Bray-Curtis dissimilarities calculated from rarefied datasets. Differences in community structure were evaluated by PERMANOVA using the function adonis2 of the *vegan* package. Pairwise PERMANOVA was applied to compare microbial community composition between different root types, using the pairwise.adonis() function of the *pairwiseAdonis* package.

To identify microbial consumers of ^{13}C-labeled recent photosynthates, we employed the HR-SIP function from the R package HTSSIP[87]. To increase statistical power, we grouped samples in two different ways. In one approach, samples were grouped into four categories based on their mass fraction of ^{13}C in the rhizosphere as measured by EA-IRMS (Figure S 12). Alternatively, samples were classified into four categories based on their origin within the root system: seed-borne root tip, seed-borne root base, shoot-borne root tip, and shoot-borne root base. A separate HR-SIP analysis was conducted for each category using non-rarefied sequence datasets. HR-SIP utilizes the differential gene expression analysis from the R package DESeq2[88] to identify ASVs that are significantly enriched in high buoyant density fractions (BD of 1.72 – 1.75 g ml^{-1}) of ^{13}C-labeled samples compared to the high buoyant density fractions of unlabeled control samples[87].

We conducted co-occurrence network analyses to explore associations between bacterial, fungal and cercozoan communities in the rhizosphere of the root tip and base sections for the ^{13}C-labeled plants. Prior to network calculation, sequence read counts were summarized at species level. Species that were present in less than 1/4 of all samples were summed into one pseudo taxon to reduce spurious edges[89]. Additionally, the location of the sample within the root system and the mass fraction of ^{13}C in the rhizosphere were included in the network calculation. To account for the compositionality of community data, the bacterial, fungal and cercozoan datasets were individually normalized by centered log-ratio transformation. Further, z-transformation was applied to the numeric metadata, while categorical metadata were hot-encoded. The networks were calculated using FlashWeave v.0.18.0[90] with parameters for homogeneous data (sensitive = true and heterogeneous = false) and without normalization. The species networks were summarized in R to genus and order level and visualized in Cytoscape v.3.9.0[91]. The node parameters were assessed with the NetworkAnalyzer[92] implemented in Cytoscape.

Microbial community assembly mechanisms were analyzed using the icamp.big() function from the iCAMP package in R, applying phylogenetic bin-based null modeling with bin-specific confidence intervals and βNTI as turnover metric. To minimize phylogenetic bias, null model randomizations were confined within taxonomic bins (max size: 12). Relative contributions of ecological processes were compared across root sections and ^{13}C label categories, with statistical significance assessed via 1,000 bootstrap iterations using the icamp.boot() function.

4.11 Data availability

The MRI/PET dataset is available under this DOI: https://doi.org/10.26165/JUELICH-DATA/Q4NWVE. The amplicon sequencing data generated in this study have been deposited in the Sequence Read Archive (SRA; bioproject number PRJNA1145186). Processed sequencing data (as .RDS) and representative sequences for each ASV (as .FASTA) are available on GitHub (https://github.com/sinaschultes/photosynthate-distribution-maize-rhizosphere-microbiota). Source data are provided with this paper.

4.12 Code availability

Custom scripts and all required data files to run them are available on GitHub (https://github.com/sinaschultes/photosynthate-distribution-maize-rhizosphere-microbiota).

5 References

1 Hu, L. *et al*. Root exudate metabolites drive plant-soil feedbacks on growth and defense by shaping the rhizosphere microbiota. *Nature Communications* 9, 1-13 (2018).

2 Zhalnina, K. *et al*. Dynamic root exudate chemistry and microbial substrate preferences drive patterns in rhizosphere microbial community assembly. *Nature microbiology* 3, 470-480 (2018).

3 Pausch, J. & Kuzyakov, Y. Carbon input by roots into the soil: Quantification of rhizodeposition from root to ecosystem scale. *Global Change Biology* 24, 1-12 (2018).

4 Yu, P. *et al*. Plant flavones enrich rhizosphere Oxalobacteraceae to improve maize performance under nitrogen deprivation. *Nature Plants* 7, 481-499 (2021).

5 Schütz, V. *et al*. Differential impact of plant secondary metabolites on the soil microbiota. *Frontiers in Microbiology* 12, 666010 (2021).

6 Thoenen, L. *et al*. The lactonase BxdA mediates metabolic specialisation of maize root bacteria to benzoxazinoids. *Nature Communications* 15, 6535 (2024).

7 Hünninghaus, M. *et al*. Disentangling carbon flow across microbial kingdoms in the rhizosphere of maize. *Soil Biology and Biochemistry* 134, 122-130 (2019).

8 Kuzyakov, Y. & Razavi, B. S. Rhizosphere size and shape: temporal dynamics and spatial stationarity. *Soil Biology and Biochemistry* 135, 343-360 (2019).

9 Jones, D. L., Nguyen, C. & Finlay, R. D. Carbon flow in the rhizosphere: carbon trading at the soil–root interface. *Plant and Soil* 321, 5-33 (2009).

10 Rüger, L. *et al*. Assembly patterns of the rhizosphere microbiome along the longitudinal root axis of maize (*Zea mays* L.). *Frontiers in Microbiology* 12, 237 (2021).

11 Kawasaki, A. *et al*. The microbiomes on the roots of wheat (*Triticum aestivum* L.) and rice (*Oryza sativa* L.) exhibit significant differences in structure between root types and along root axes. *Functional Plant Biology* 48(9), 871-888 (2021).

12 Cotton, T. A. *et al*. Metabolic regulation of the maize rhizobiome by benzoxazinoids. *The ISME Journal* 13, 1647-1658 (2019).

13 King, W. L. *et al*. The hierarchy of root branching order determines bacterial composition, microbial carrying capacity and microbial filtering. *Communications biology* 4, 483 (2021).

14 Becker, M. F., Hellmann, M. & Knief, C. Spatio-temporal variation in the root-associated microbiota of orchard-grown apple trees. *Environmental microbiome* 17, 1-21 (2022).

15 Keel, S. G. *et al*. Allocation of carbon to fine root compounds and their residence times in a boreal forest depend on root size class and season. *New Phytologist* 194, 972-981 (2012).

16 Galindo-Castañeda, T., Hartmann, M. & Lynch, J. P. Location: root architecture structures rhizosphere microbial associations. *Journal of experimental botany* 75, 594-604 (2024).

17 Waller, S., Wilder, S. L., Schueller, M. J., Housh, A. B. & Ferrieri, R. A. Quantifying plant-borne carbon assimilation by root-associating bacteria. *Microorganisms* 8, 700 (2020).

18 Trivedi, P., Leach, J. E., Tringe, S. G., Sa, T. & Singh, B. K. Plant–microbiome interactions: from community assembly to plant health. *Nature reviews microbiology* 18, 607-621 (2020).

19 Hochholdinger, F., Park, W. J., Sauer, M. & Woll, K. From weeds to crops: genetic analysis of root development in cereals. *Trends in Plant Science* 9, 42-48 (2004).

20 Haichar, F. e. Z., Roncato, M.-A. & Achouak, W. Stable isotope probing of bacterial community structure and gene expression in the rhizosphere of Arabidopsis thaliana. *FEMS Microbiology Ecology* 81, 291-302 (2012).

21 Jahnke, S. *et al*. Combined MRI–PET dissects dynamic changes in plant structures and functions. *The Plant Journal* 59, 634-644 (2009).

22 Metzner, R. *et al*. In vivo imaging and quantification of carbon tracer dynamics in nodulated root systems of pea plants. *Plants* 11, 632 (2022).

23 Yu, P. *et al*. Seedling root system adaptation to water availability during maize domestication and global expansion. *Nature Genetics* 56, 1245-1256 (2024).

24 Fiore-Donno, A. M. *et al*. Functional traits and spatio-temporal structure of a major group of soil protists (Rhizaria: Cercozoa) in a temperate grassland. *Frontiers in Microbiology* 10, 1332 (2019).

25 Enns, L. C., McCully, M. E. & Canny, M. J. Branch roots of young maize seedlings, their production, growth, and phloem supply from the primary root. *Functional Plant Biology* 33, 391-399 (2006).

26 Dennis, P. G., Miller, A. J. & Hirsch, P. R. Are root exudates more important than other sources of rhizodeposits in structuring rhizosphere bacterial communities? *FEMS Microbiolgy Ecology* 72, 313-327 (2010).

27 Pausch, J. & Kuzyakov, Y. Photoassimilate allocation and dynamics of hotspots in roots visualized by ^{14}C phosphor imaging. *Journal of Plant Nutrition and Soil Science* 174, 12-19 (2011).

28 Darwent, M. J., Paterson, E., McDonald, A. J. S. & Tomos, A. D. Biosensor reporting of root exudation from *Hordeum vulgare* in relation to shoot nitrate concentration. *Jorunal of Experimental Botany* 54, 325-334 (2003).

29 Watt, M., Kirkegaard, J. & Passioura, J. Rhizosphere biology and crop productivity—a review. *Soil Research* 44, 299-317 (2006).

30 Orman-Ligeza, B. *et al*. Post-embryonic root organogenesis in cereals: branching out from model plants. *Trends in Plant Science* 18, 459-467 (2013).

31 Lynch, J. P. Root phenes that reduce the metabolic costs of soil exploration: opportunities for 21st century agriculture. *Plant, Cell & Environment* 38, 1775-1784 (2015).

32 Farrar, J., Hawes, M., Jones, D. & Lindow, S. How roots control the flux of carbon to the rhizosphere. *Ecology* 84, 827-837 (2003).

33 Poorter, H. *et al*. Biomass allocation to leaves, stems and roots: meta-analyses of interspecific variation and environmental control. *New Phytologist* 193, 30-50 (2012).

34 Marschner, P., Crowley, D. & Rengel, Z. Rhizosphere interactions between microorganisms and plants govern iron and phosphorus acquisition along the root axis–model and research methods. *Soil Biology and Biochemistry* 43, 883-894 (2011).

35 Dupuy, L. X. & Silk, W. K. Mechanisms of early microbial establishment on growing root surfaces. *Vadose Zone Journal* 15 (2016).

36 Kuzyakov, Y. & Blagodatskaya, E. Microbial hotspots and hot moments in soil: concept & review. *Soil Biology and Biochemistry* 83, 184-199 (2015).

37 Loo, E. P.-I. *et al*. Sugar transporters spatially organize microbiota colonization along the longitudinal root axis of Arabidopsis. *Cell Host & Microbe* 32, 543-556. e546 (2024).

38 Van Diepeningen, A. D., De Vos, O. J., Zelenev, V. V., Semenov, A. M. & Van Bruggen, A. H. DGGE fragments oscillate with or counter to fluctuations in cultivable bacteria along wheat roots. *Microbial Ecology* 50, 506-517 (2005).

39 Van Bruggen, A., Semenov, A. & Zelenev, V. Wavelike distributions of microbial populations along an artificial root moving through soil. *Microbial Ecology* 40, 250-259 (2000).

40 Van Vuurde, J. & Schippers, B. Bacterial colonization of seminal wheat roots. *Soil Biology and Biochemistry* 12, 559-565 (1980).

41 Bonkowski, M. *et al*. Spatiotemporal Dynamics of Maize (*Zea mays* L.) Root Growth and Its Potential Consequences for the Assembly of the Rhizosphere Microbiota. *Frontiers in Microbiology* 12, 461 (2021).

42 Sivasithamparam, K., Parker, C. & Edwards, C. Rhizosphere micro-organisms of seminal and nodal roots of wheat grown in pots. *Soil Biology and Biochemistry* 11, 155-160 (1979).

43 Kawasaki, A. *et al*. Microbiome and exudates of the root and rhizosphere of *Brachypodium distachyon*, a model for wheat. *PLoS One* 11 (2016).

44 Watt, M., Silk, W. & Passioura, J. Rates of root and organism growth, soil conditions, and temporal and spatial development of the rhizosphere. *Annals of Botany* 97, 839-855 (2006).

45 Bell, J. K., Mamet, S. D., Helgason, B. & Siciliano, S. D. Brassica napus bacterial assembly processes vary with plant compartment and growth stage but not between lines. *Applied and Environmental Microbiology* 88, e00273-00222 (2022).

46 Garrido-Sanz, D. *et al*. Changes in structure and assembly of a species-rich soil natural community with contrasting nutrient availability upon establishment of a plant-beneficial Pseudomonas in the wheat rhizosphere. *Microbiome* 11, 214 (2023).

47 Xie, J. *et al*. Strategies and structure feature of the aboveground and belowground microbial community respond to drought in wild rice (Oryza longistaminata). *Rice* 14, 1-17 (2021).

48 Hannula, S. E. *et al*. Shifts in rhizosphere fungal community during secondary succession following abandonment from agriculture. *The ISME Journal* 11, 2294-2304 (2017).

49 Hannula, S., Morrien, E., Van der Putten, W. & De Boer, W. Rhizosphere fungi actively assimilating plant-derived carbon in a grassland soil. *Fungal Ecology* 48, 100988 (2020).

50 Potshangbam, M., Devi, S. I., Sahoo, D. & Strobel, G. A. Functional characterization of endophytic fungal community associated with Oryza sativa L. and Zea mays L. *Frontiers in microbiology* 8, 325 (2017).

51 Gesteiro, N. *et al*. Effects of seed infection by Fusarium verticillioides on maize performance against Sesamia nonagrioides attack. *Physiologia plantarum* 176, e14649 (2024).

52 Blacutt, A. A., Gold, S. E., Voss, K. A., Gao, M. & Glenn, A. E. Fusarium verticillioides: Advancements in understanding the toxicity, virulence, and niche adaptations of a model mycotoxigenic pathogen of maize. *Phytopathology* 108, 312-326 (2018).

53 Okello, P. N., Petrović, K., Kontz, B. & Mathew, F. M. Eight species of Fusarium cause root rot of corn (Zea mays) in South Dakota. *Plant Health Progress* 20, 38-43 (2019).

54 Ye, J. *et al*. Cytological and molecular characterization of quantitative trait locus qRfg1, which confers resistance to Gibberella stalk rot in maize. *Molecular Plant-Microbe Interactions* 26, 1417-1428 (2013).

55 Modrzewska, M., Bryła, M., Kanabus, J. & Pierzgalski, A. Trichoderma as a biostimulator and biocontrol agent against Fusarium in the production of cereal crops: Opportunities and possibilities. *Plant Pathology* 71, 1471-1485 (2022).

56 Afzal, M. Y., Das, B. K., Valappil, V. T., Scaria, J. & Brözel, V. S. Root exudate compounds change the bacterial community in bulk soil. *Rhizosphere* 30, 100885 (2024).

57 Bosshard, P. P., Zbinden, R. & Altwegg, M. Paenibacillus turicensis sp. nov., a novel bacterium harbouring heterogeneities between 16S rRNA genes. *International Journal of Systematic and Evolutionary Microbiology* 52, 2241-2249 (2002).

58 Hamasaki, Y. *et al*. Paenibacillus macerans possesses two types of 16S rDNA copies in a genome with a length difference of twelve base pairs. *Bioscience, Biotechnology, and Biochemistry* 69, 1995-1998 (2005).

59 el Zahar Haichar, F. *et al*. Plant host habitat and root exudates shape soil bacterial community structure. *The ISME Journal* 2, 1221 (2008).

60 Ahmad, M. *et al*. Combating iron and zinc malnutrition through mineral biofortification in maize through plant growth promoting Bacillus and Paenibacillus species. *Frontiers in Plant Science* 13, 1094551 (2023).

61 Bag, S., Mondal, A., Majumder, A., Mondal, S. K. & Banik, A. Flavonoid mediated selective cross-talk between plants and beneficial soil microbiome. *Phytochemistry Reviews* 21, 1739-1760 (2022).

62 Jaeger, C. H., Lindow, S. E., Miller, W., Clark, E. & Firestone, M. Mapping of sugar and amino acid availability in soil around roots with bacterial sensors of sucrose and tryptophan. *Applied and Environmental Microbiology* 65, 2685-2690 (1999).

63 Hungate, B. A. *et al*. The functional significance of bacterial predators. *Mbio* 12, 10.1128/mbio. 00466-00421 (2021).

64 Glücksman, E., Bell, T., Griffiths, R. I. & Bass, D. Closely related protist strains have different grazing impacts on natural bacterial communities. *Environmental Microbiology* 12, 3105-3113 (2010).

65 Flues, S., Bass, D. & Bonkowski, M. Grazing of leaf-associated Cercomonads (Protists: Rhizaria: Cercozoa) structures bacterial community composition and function. *Environmental Microbiology* 19, 3297-3309 (2017).

66 Vetterlein, D. *et al*. Experimental platforms for the investigation of spatiotemporal patterns in the rhizosphere - laboratory and field scale. *Jorunal of Plant Nutrition and Soil Science* 184, 35-50 (2021).

67 Hinz, C. *et al*. Setup and characterisation according to NEMA NU 4 of the phenoPET scanner, a PET system dedicated for plant sciences. *Physics in Medicine & Biology* 69, 055019 (2024).

68 van Dusschoten, D. *et al*. Quantitative 3D analysis of plant roots growing in soil using magnetic resonance imaging. *Plant Physiology*, pp. 01388.02015 (2016).

69 Teste, F. P. *et al*. Access to mycorrhizal networks and roots of trees: importance for seedling survival and resource transfer. *Ecology* 90, 2808-2822 (2009).

70 Tournier, E. *et al*. Modification of a commercial DNA extraction kit for safe and rapid recovery of DNA and RNA simultaneously from soil, without the use of harmful solvents. *MethodsX* 2, 182-191 (2015).

71 Lueders, T. in *Handbook of hydrocarbon and lipid microbiology* (2010).

72 Frindte, K. *et al*. Evidence for signatures of ancient microbial life in paleosols. *Scientific Reports* 10, 1-11 (2020).

73 Martin, M. Cutadapt removes adapter sequences from high-throughput sequencing reads. *EMBnet Journal* 17, 10-12 (2011).

74 Bolyen, E. *et al*. Reproducible, interactive, scalable and extensible microbiome data science using QIIME 2. *Nature Biotechnolgy* 37, 852-857 (2019).

75 Callahan, B. J. *et al*. DADA2: high-resolution sample inference from Illumina amplicon data. *Nature Methods* 13, 581 (2016).

76 Katoh, K. & Standley, D. M. MAFFT multiple sequence alignment software version 7: improvements in performance and usability. *Molecular Biology and Evolution* 30, 772-780 (2013).

77 Quast, C. *et al*. The SILVA ribosomal RNA gene database project: improved data processing and web-based tools. *Nucleic Acids Research* 41, D590-D596 (2012).

78 Abarenkov, K. *et al*. The UNITE database for molecular identification and taxonomic communication of fungi and other eukaryotes: sequences, taxa and classifications reconsidered. *Nucleic Acids Research* 52, D791-D797 (2024).

79 McMurdie, P. J. & Holmes, S. phyloseq: an R package for reproducible interactive analysis and graphics of microbiome census data. *PLoS One* 8 (2013).

80 Dixon, P. VEGAN, a package of R functions for community ecology. *Journal of Vegetation Science* 14, 927-930 (2003).

81 Lahti, L. & Shetty, S. Introduction to the microbiome R package. *Preprint at* https://microbiome. *github. io/tutorials* (2018).

82 Schloss, P. D. *et al*. Introducing mothur: open-source, platform-independent, community-supported software for describing and comparing microbial communities. *Applied and Environmental Microbiology* 75, 7537-7541 (2009).

83 Rognes, T., Flouri, T., Nichols, B., Quince, C. & Mahé, F. VSEARCH: a versatile open source tool for metagenomics. *PeerJ* 4, e2584 (2016).

84 Camacho, C. *et al*. BLAST+: architecture and applications. *BMC Bioinformatics* 10, 1-9 (2009).

85 Guillou, L. *et al*. The Protist Ribosomal Reference database (PR2): a catalog of unicellular eukaryote small sub-unit rRNA sequences with curated taxonomy. *Nucleic Acids Research* 41, D597-D604 (2012).

86 Edgar, R. C., Haas, B. J., Clemente, J. C., Quince, C. & Knight, R. UCHIME improves sensitivity and speed of chimera detection. *Bioinformatics* 27, 2194-2200 (2011).

87 Youngblut, N. D., Barnett, S. E. & Buckley, D. H. HTSSIP: an R package for analysis of high throughput sequencing data from nucleic acid stable isotope probing (SIP) experiments. *PLoS One* 13, e0189616 (2018).

88 Love, M. I., Huber, W. & Anders, S. Moderated estimation of fold change and dispersion for RNA-seq data with DESeq2. *Genome Biology* 15, 1-21 (2014).

89 Röttjers, L. & Faust, K. From hairballs to hypotheses–biological insights from microbial networks. *FEMS Microbiology Reviews* 42, 761-780 (2018).

90 Tackmann, J., Rodrigues, J. F. M. & von Mering, C. Rapid inference of direct interactions in large-scale ecological networks from heterogeneous microbial sequencing data. *Cell Systems* 9, 286-296. e288 (2019).

91 Shannon, P. *et al*. Cytoscape: a software environment for integrated models of biomolecular interaction networks. *Genome Research* 13, 2498-2504 (2003).

92 Assenov, Y., Ramírez, F., Schelhorn, S.-E., Lengauer, T. & Albrecht, M. Computing topological parameters of biological networks. *Bioinformatics* 24, 282-284 (2008).

6 Acknowledgments

We would like to thank Marius Röder (Molecular Biology of the Rhizosphere, University of Bonn) for excellent technical assistance. Esther Breuer, Marco Dautzenberg and Gregor Huber (Enabling Technologies, IBG-2, Forschungszentrum Jülich GmbH) are acknowledged for their valuable assistance during labeling experiments. We furthermore thank Kirsten Unger (Soil Sciences, University of Bonn) for performing the EA-IRMS measurements. Caroline Marcon and Frank Hochholdinger (Crop Functional Genomics, University of Bonn) are acknowledged for providing maize seeds for this study. The Next Generation Sequencing Core Facility of the Medical Faculty at the University of Bonn is acknowledged for providing the instrumentation for MiSeq sequencing. This work was conducted within the framework of the priority program 2089, funded by the Deutsche Forschungsgemeinschaft (DFG, German Research Foundation) – P18 (Project ID 403637614, C.K. and M.W.) and P14 (Project ID 403635931, M.B.). Michelle Watt currently holds the Adrienne Clarke Chair of Botany, which is supported through the University of Melbourne Botany Foundation.

7 Author contributions

S.R.S., R.K., M.W. and C.K. conceptualized the study.

S.R.S. performed the experiments and data analysis.

L.R., D.N., and K.F. contributed to amplicon and qPCR data generation and analysis.

M.F.B., K.F., J.F., M.B. and S.L.B. contributed to data analysis and interpretation.

A.C. and S.R.S. performed $^{13}CO_2$ labeling.

D.P. and D.v.D. performed MRI measurements and contributed to the data analysis.

R.M., C.H. and A.C. performed ^{11}C-PET labeling and contributed to the data analysis.

S.R.S., R.K. and C.K. wrote the manuscript with input from all authors.

8 Competing interests statement

The authors declare no competing interests.

9 Material

Tab 1 Influence of root type and photosynthate level on microbial community composition. Influence of both factors as well as their interaction on total community composition (study I) and photosynthate consumer community, reflected by the ^{13}C-heavy fraction of the DNA-SIP analysis (study II), was assessed by PERMANOVA based on 999 permutations. R^2 values are given in the table, detailed test statistics *in* Table S 1. *Significance* code: *** indicates p-values ≤ 0.001, ** p-values ≤ 0.01 and * p-values ≤ 0.05.

Study	PERMANOVA model	Factor	Bacteria	Fungi	Cercozoa
Study I: Total community	Root type * ^{11}C level	Root type	0.20***	0.13***	0.18***
		^{11}C level (categorical)	0.07***	0.08***	0.09***
		Interaction	0.07***	0.08**	0.04
		Residuals	0.66	0.71	0.69
Study II: ^{13}C-heavy fraction community	Root type * ^{11}C level	Root type	0.26***	0.14*	0.17**
		^{11}C level (categorical)	0.34***	0.35***	0.47***
		Interaction	0.13***	0.14**	0.05
		Residuals	0.27	0.37	0.31
	Root type * ^{13}C level	Root type	0.26***	0.14	0.17*
		^{13}C level (numeric)	0.31***	0.34***	0.37***
		Interaction	0.11**	0.10	0.05
		Residuals	0.32	0.42	0.41

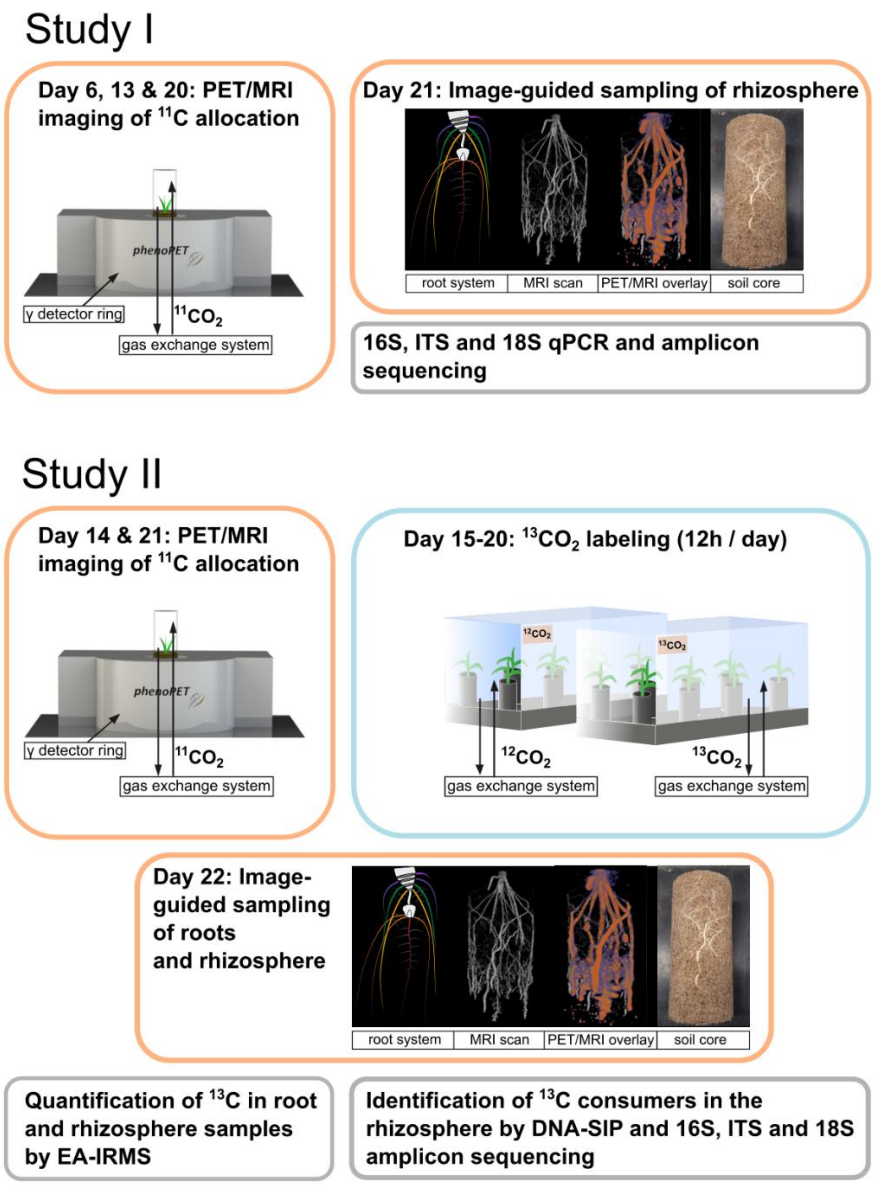

Fig 1 Conceptual study design. In Study I we investigated temporal changes in photosynthate allocation and the effect of small-scale spatial heterogeneity in photosynthate allocation on the prokaryotic, fungal and cercozoan rhizosphere communities. PET-MRI imaging (orange boxes) enabled us to define root regions with distinct photosynthate levels (low, medium, high) and to consider root architecture at high spatial resolution for identifying root types and sections during sampling. Study II combines this approach with $^{13}CO_2$ labeling (blue box) to specifically identify photosynthate consumers and investigate their response to spatially heterogeneous photosynthate distribution. Analyses upon destructive sampling (grey boxes) included elemental analysis coupled to isotope ratio mass spectrometry (EA-IRMS) to obtain quantitative data on photosynthate contents of root and rhizosphere samples and DNA-based microbial community compositional analyses.

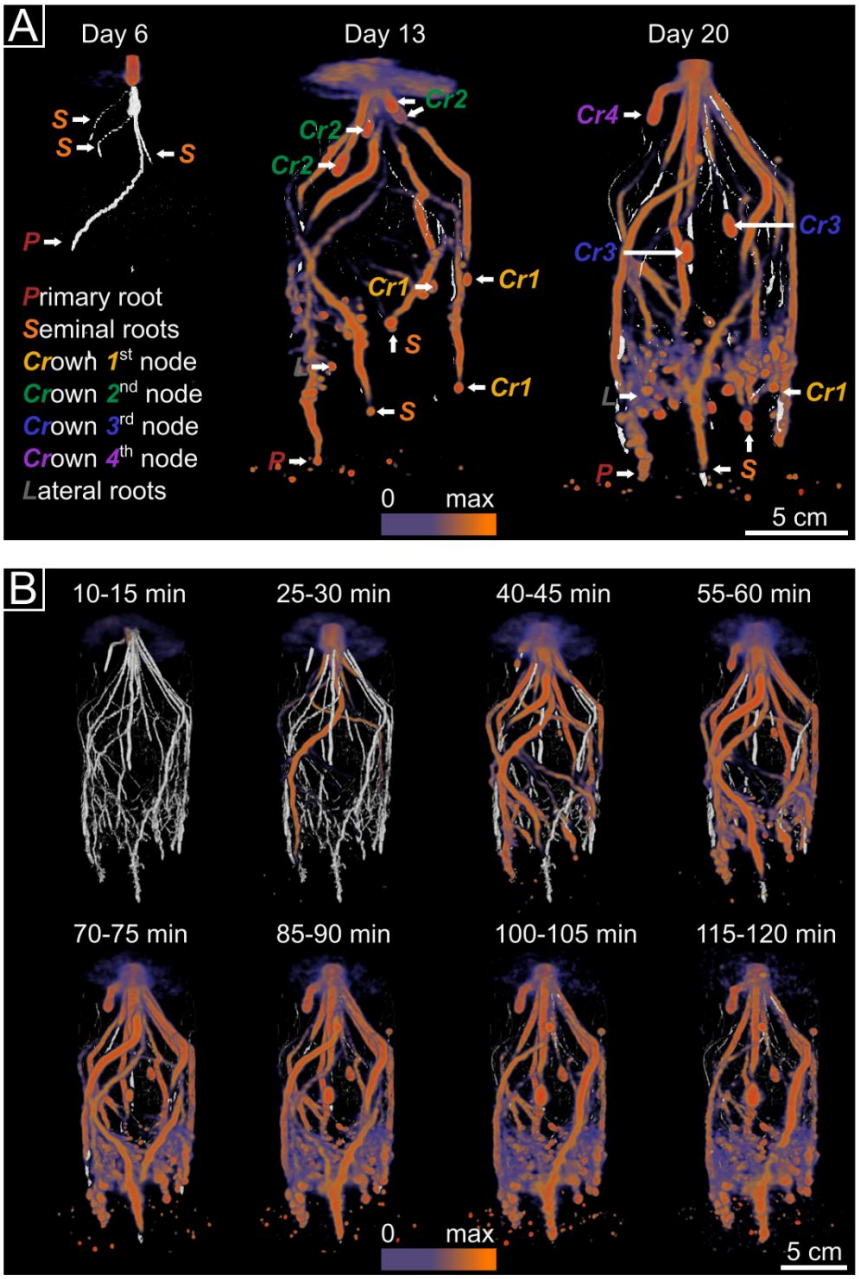

Fig 2 Allocation of recently fixed carbon in roots visualized by co-registered PET-MRI scans. The same maize plants were imaged in study I at three time points by PET (colored) and MRI (grey) over a period of 120 min. a Co-registered PET-MRI scans were obtained for 6-, 13-, and 20-day old plants at 85-90 min after labeling start. Prominently visible representatives of the different root types are marked with letters: P = primary root, S = seminal roots, Cr = crown roots of nodes 1-4, L = lateral roots. On day 6, the root system consisted of the primary root and three seminal roots. On day 20, around 10-12 crown roots from up to four different consecutive nodes had developed in all plants. b Belowground allocation of ^{11}C-labeled photosynthates in a 20-day old plant over the measurement period of 2 h. Images are integrals calculated over 5 min of measurement. A time-lapse video showing ^{11}C-photosynthate allocation is available as Video S 1.

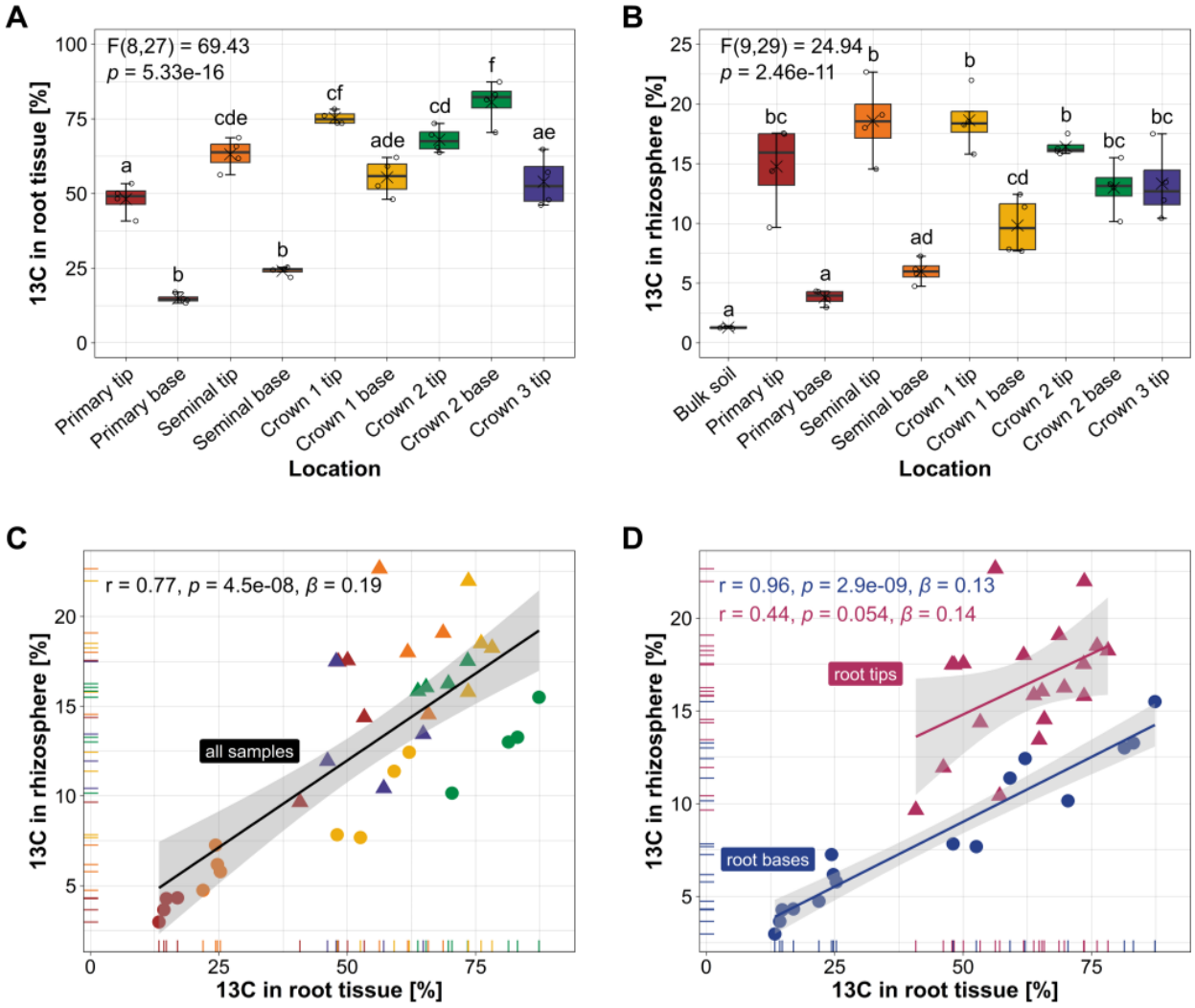

Fig 3 ^{13}C tracer allocation in different root types and root sections and their associated rhizosphere soil samples. The mass fraction of ^{13}C in percent in a root tissue and b rhizosphere soil samples as measured by EA-IRMS and visualized in box plots across different locations in the root system. Boxes span from the first to the third quartiles, the line inside each box represents the median; x represents the mean and the whiskers extend to the last data point within 1.5 times the inter quartile range. Data points outside of whiskers represent outliers. Significance of differences was tested by one-way ANOVA (two-sided), and distinct lowercase letters indicate significant differences between groups (n = 4 biological replicates) as tested by Tukey HSD post hoc tests ($p < 0.05$). Scatter plots illustrate the relationship (Pearson correlation coefficient r with significance (p) between mass fraction ^{13}C in root tissue and the rhizosphere for c all samples colored by root type (n = 36 biological replicates) and d for root tip (n = 20) and root base samples (n = 16) separately. β indicates the slope. A linear regression model was fitted (solid black line), and the shaded area represents the 95 % confidence interval around the best fit (based on the standard error of the estimate). Source data are provided as a Source Data file.

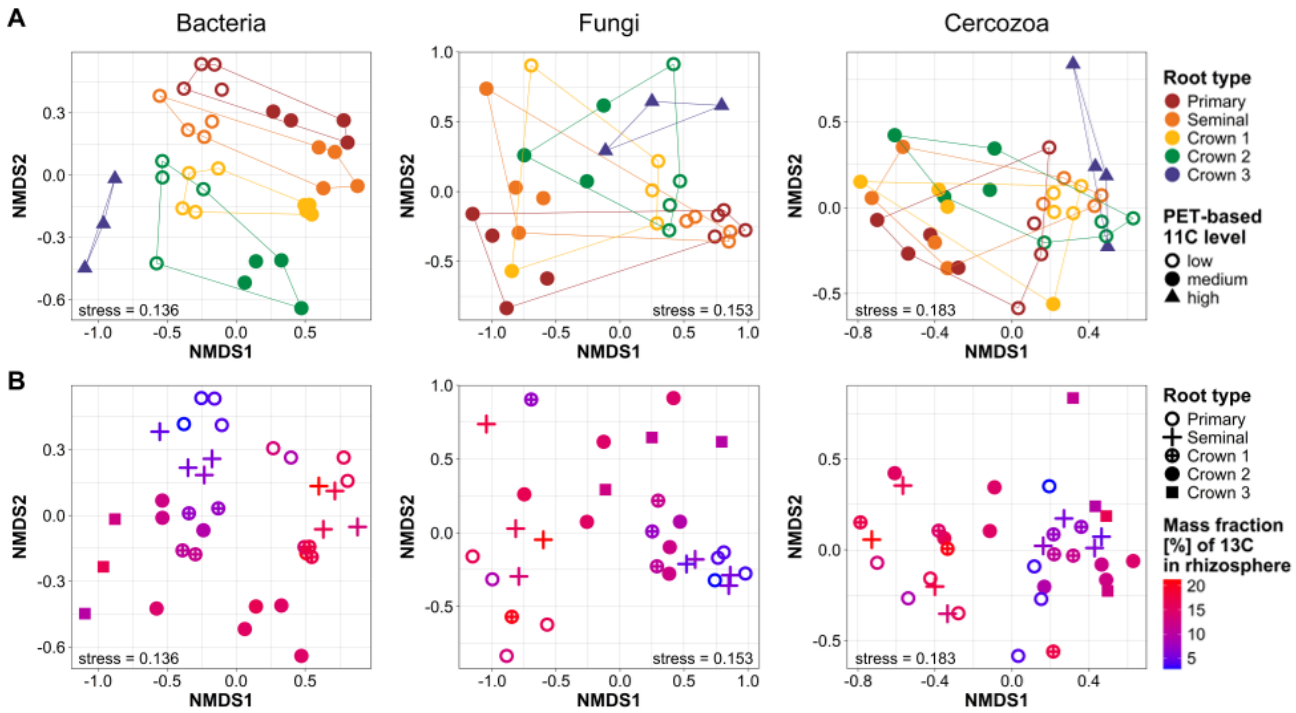

Fig 4 Variation in microbial community composition related to root type, root section and belowground carbon allocation (study II). Variation in community composition was assessed after $^{13}CO_2$ labeling in the DNA of the ^{13}C-heavy fraction, representing predominantly ^{13}C consumers. Variation is visualized by non-metric multidimensional scaling (NMDS) plots based on Bray-Curtis dissimilarities, highlighting the dependence on root type and a categorical photosynthate levels defined by ^{11}C-PET or b the mass fraction of ^{13}C measured in the rhizosphere soil by EA-IRMS. Information on root sections can be inferred from the plots in a, with root tip samples being represented by closed symbols, whereas root base samples are represented by open symbols. Source data are provided as a Source Data file.

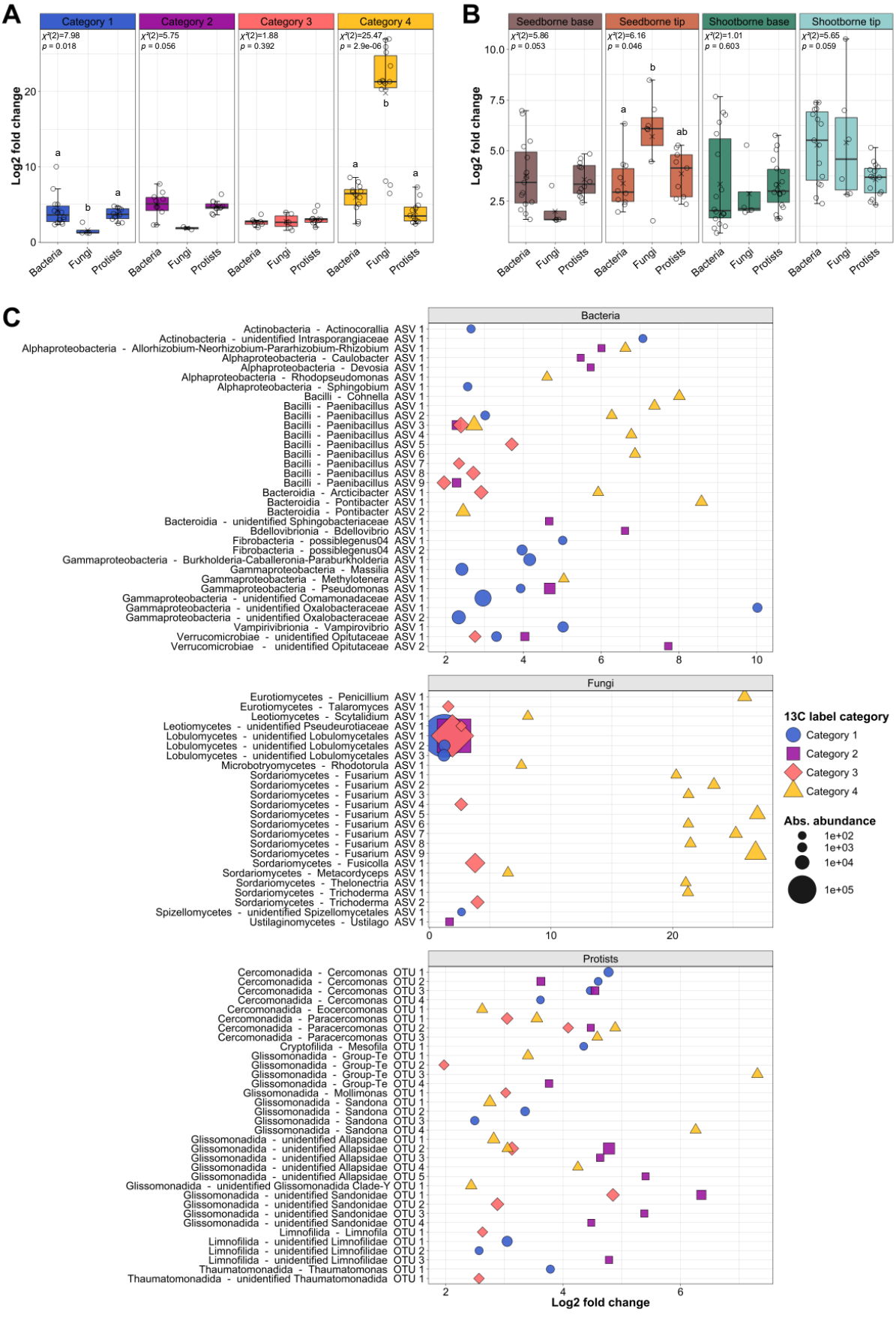
A
Category 1
Category 2
Category 3
Category 4
Log2 fold change
Bacteria
Fungi
Protists
B
Seedborne base
Seedborne tip
Shootborne base
Shootborne tip
C
Bacteria
Fungi
Protists
13C label category
Category 1
Category 2
Category 3
Category 4
Abs. abundance
1e+02
1e+03
1e+04
1e+05
Log2 fold change

Fig 5 ^{13}C label intensity and identity of microbial taxa with significant label incorporation. Significantly labeled taxa were identified using the DESeq2 algorithm of the HTSSIP package. For this analysis, samples were grouped into four categories, either a and c according to the mass fraction of ^{13}C quantified in the rhizosphere soil (Category 1: 1.5 % - 6.9 %; Category 2: 6.9 % - 12.3 %, Category 3: 12.3 % - 17.7 %; Category 4: 17.7 % - 23.1 %; Figure S 12) or b based on the sample origin within the root system (seed-borne root tips, seed-borne root bases, shoot-borne root tips, shoot-borne root bases). a and b show the label intensity of significantly labeled taxa according to the fold-change in sequence read abundance between the ^{13}C-heavy and ^{12}C-heavy fraction. Boxes span from the first to the third quartiles, the line inside each box represents the median; x represents the mean and the whiskers extend to the last data point within 1.5 times the inter quartile range. Data points outside of whiskers represent outliers. Significance of differences within subsets was tested by Kruskal-Wallis rank sum test. Distinct lowercase letters indicate significant differences between groups as tested by Dunn's post hoc tests with Benjamini-Hochberg correction ($p < 0.05$). From left to right, a consists of n = 14, 4, 10, 10, 2, 11, 7, 6, 9, 12, 14, 12 biological replicates and b of n = 15, 4, 12, 10, 7, 9, 18, 4, 18, 15, 6, 15 biological replicates. c illustrates the identity of the labeled taxa along with the enrichment in the ^{13}C-heavy fraction over the ^{12}C-heavy fraction based on log2 fold changes and the summed abundance of the ^{13}C-labeled taxa in the ^{13}C-heavy fraction based on read counts. Absolute abundance equals the sum of all reads of a labeled ASV over all samples of a label category. Bacteria and fungi are labeled as Class_Genus_ASV and protists as Order_Genus_OTU. Source data are provided as a Source Data file.

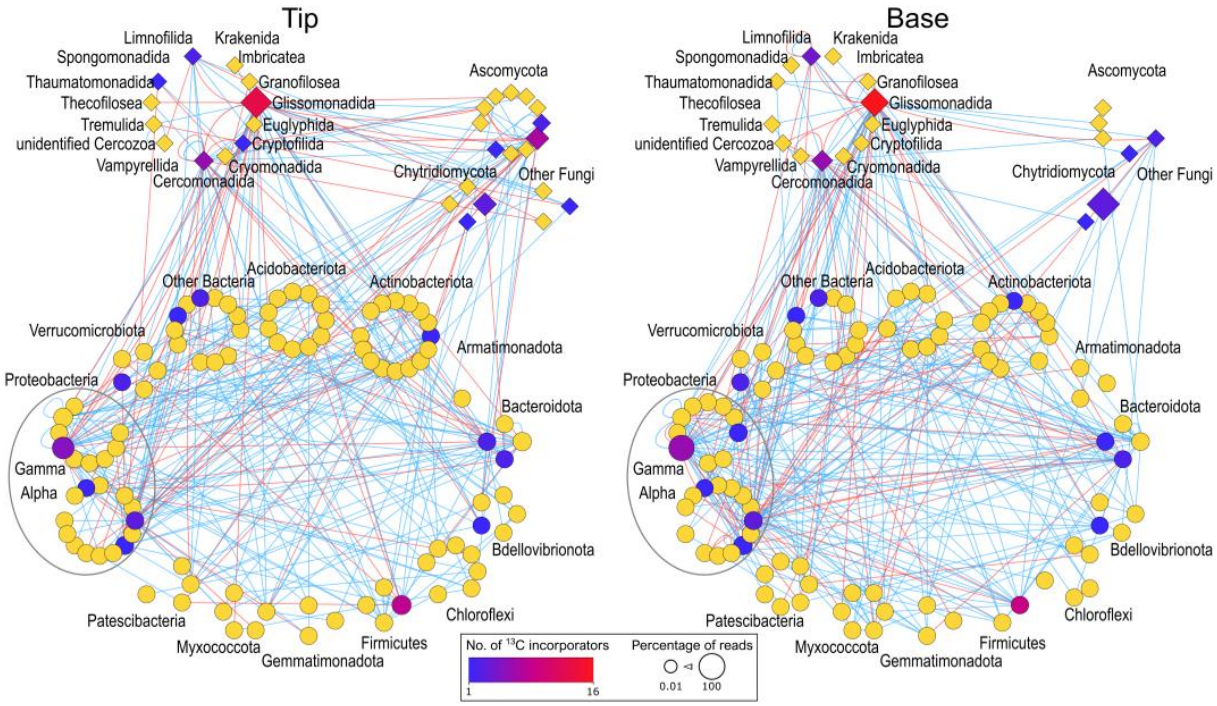

Fig 6 Core networks illustrating the associations between bacterial, fungal and cercozoan taxa and the positioning of ^{13}C labeled taxa. Networks were independently calculated for the root tip and root base microbiota based on ^{13}C amplicon sequence data of study II. Nodes are arranged at phylum (bacteria, fungi) and order level (Cercozoa). Positive associations are indicated by blue lines, negative associations by red lines. Network taxa are colored according to the number of ^{13}C incorporators (blue to red) or non-incorporators (yellow) as determined by DESeq2 analysis. The node size is proportional to the percentage of reads. Source data are provided as a Source Data file.

10 Supplementary material

The supplementary material for Chapter II can be viewed and downloaded here:
https://uni-koeln.sciebo.de/s/DK1NsXCQPfXK4WD

10.1 Supplementary video

Video S 1 Allocation of recently fixed carbon in maize roots. Allocation of ^{11}C-labeled carbon into the maize root system as visualized by PET/MRI imaging for an individual plant in study I.

10.2 Supplementary figures

Figure S 1 Sampling concept in both studies. a Conceptual drawing of a) maize root system on harvesting day. B) The sampling scheme: Root tips and bases of all root types including crown roots from consecutive nodes were collected.

Figure S 2 The distribution of fresh, ^{11}C-labelled photosynthates in all plants of study I on day 6, day 13 and day 20 after sowing.

Figure S 3 The distribution of fresh, ^{11}C-labelled photosynthates in plants of study II on day 14 and day 21 after sowing.

Figure S 4 Mass fraction of ^{13}C [%] in the rhizosphere (a) and root tissue (b) of unlabeled control plants as measured by EA-IRMS (n=4).

Figure S 5 Community composition of the maize rhizosphere microbiota (prokaryotes, fungi, Cercozoa) in study I.

Figure S 6 Heatmaps illustrating results for pairwise PERMANOVA applied to compare microbial community composition between different root types in the ^{13}C-heavy fraction of study II.

Figure S 7 Heatmaps displaying the relative abundance of dominant (>0.25 % relative abundance) (a) bacterial and (b) fungal genera that showed a significant response to photosynthate level or root type.

Figure S 8 Bar plots showing the relative contribution (%) of five ecological processes to bacterial and fungal community assembly.

Figure S 9 The Shannon diversity index, ASV richness and eveness for prokaryotes, fungi and Cercozoa in dependence on root type, root section or categorical photosynthate levels according to ^{11}C-PET.

Figure S 10 Boxplots presenting the qPCR results for prokaryotic 16S rRNA gene and fungal ITS1 copy numbers and their variation in dependence on root type, root section or categorical photosynthate levels according to ^{11}C-PET.

Figure S 11 Relationship between the prokaryotic (a) and fungal (b) diversity and their population size as determined by qPCR targeting a 16S rRNA gene fragment (prokaryotes) or the ITS1 region (fungi).

Figure S 12 Grouping of samples for HR-SIP analyses into four categories based on their ^{13}C proportion relative to total C mass in the rhizosphere soil as determined by EA-IRMS.

Figure S 13 ^{13}C label intensity and abundance of microbial taxa with significant label incorporation.

Figure S 14 Relative abundance of ^{13}C-labeled taxa at different locations in the root system.

Figure S 15 Microbial co-occurrence networks resolved at genus level.

Figure S 16 Automatically regulated gas flow during a labelling day in the ^{13}CO2 labelling chamber (chamber II) and the ^{12}CO2 control chamber (chamber I).

Figure S 17 Mean root length (mm) of the examined primary, seminal and crown root types from the four different leaf nodes, as determined by MRI measurements and NMRooting analysis at day 6, 13 and 20 after sowing (study I).

Figure S 18 A ^{13}C-labeled sample and its corresponding 12C-control sample from the crown root 1 tip as an example for SIP fraction selection prior to amplicon sequencing.

10.3 Supplementary tables

Table S 1 Detailed test statistics accompanying the PERMANOVA results in Table 1.

Table S 2 The effect of root type and photosynthate allocation on responsive fungal genera in study I as identified by one-way ANOVA.

Table S 3 Influence of photosynthate level and root type on microbial community composition of DNA fractions collected during DNA-SIP in study II.

Table S 4 Number of different ASVs/OTUs detected as “labelled” by DESeq2 analysis within each taxon and per category.

Table S 5 Comparison of microbial co-occurrence network parameters between ^{13}C incorporators and non-incorporators.

Table S 6 Number of roots per root type of each plant on days 14 and 21 after sowing as determined by MRI in study II. Plant pairs xA and xB were pooled for sampling on day 22.

Table S 7 Primers used to generate standards and cycling conditions for qPCR. Primer sequences available via reference list for bacteria/archaea1, fungi2 and Cercozoa3.

Table S 8 Primers for amplicon sequencing and qPCR of prokaryotes (bacteria and archaea)4, fungi5, 6 and protists (Cercozoa)3. BC indicates barcoded primers.

Table S 9 Two-step PCR conditions for amplicon sequencing of prokaryotes, fungi and Cercozoa.

Table S 10 PCR reaction composition for amplicon sequencing.

Table S 11 Total and mean read number per sample remaining for downstream analyses after initial quality filtering.

Chapter III: Protist community shifts under maize monoculture

Continuous maize cropping reshapes rhizosphere protist communities through soil legacy effects

Reference:

Niedeggen, D., Clayton, J., Schreiter, S., Tarkka, M., Vetterlein, D., Bonkowski, M. Under Review. Continuous maize cropping reshapes rhizosphere protist communities through soil legacy effects. Biology and Fertility of Soils manuscript ID BFSO-D-25-00898.

Author contributions:

DV, MB and MT contributed to the conception and design of the study. Material preparation, fieldwork, and data collection were carried out by **DN**, SS, and MT. Data analysis and interpretation were performed by **DN** and MB. The first draft of the manuscript was written by **DN**, and all authors critically revised and commented on previous versions.

Continuous maize cropping reshapes rhizosphere protist communities through soil legacy effects

Running title: Protist community shifts under continuous maize cultivation

Daniela Niedeggen[1,2], Jessica Clayton[3], Susanne Schreiter[3], Mika Tarkka[4], Doris Vetterlein[3], Michael Bonkowski[1,2]

[1]University of Cologne, Institute of Zoology, Terrestrial Ecology, Cologne, Germany
[2] Cluster of Excellence on Plant Sciences (CEPLAS), University of Cologne, Germany

[3]Helmholtz Centre for Environmental Research GmbH –UFZ, Dept. Soil System Science, Halle/Saale, Germany

[4]Helmholtz Centre for Environmental Research GmbH –UFZ, Dept. Soil Ecology, Halle/Saale, Germany

Corresponding Author:

Prof. Dr. Michael Bonkowski	m.bonkowski@uni-koeln.de +492214703152
Daniela Niedeggen	daniela.niedeggen@uni-koeln.de

Abstract

Soil protists, especially potential plant pathogens such as Oomycota and Phytomyxea, are increasingly recognised as key players in rhizosphere dynamics, yet their role in the formation of agricultural soil legacies remains under-explored. In a five-year field experiment involving the continuous cultivation of maize in loam and sand, we used high-throughput amplicon sequencing to track temporal changes in protist communities, focusing on Oomycota and Cercozoa/Phytomyxea. Two contrasting trajectories were observed: the enrichment of potential maize-specific pathogenic oomycetes (e.g., *Pythium arrhenomanes* and *P. monospermum*), and increased variability among heterotrophic cercozoan consumers, including potential pathogen antagonists such as *Platyreta* and Trinematidae. These patterns were modulated by soil texture and interannual climate variability (precipitation and temperature). Loam fostered an increasing soil legacy effect with compositional shifts in protist communities. In sand, legacy development was more stochastic and sensitive to drought disturbance. Rhizosphere alpha diversity declined with soil legacy, whereas bulk soil communities showed partial resilience over time. Environmental variables drove significant changes in beta diversity, indicating layered interactions between plant traits, abiotic drivers, and microbial feedbacks. Our findings demonstrate that protists are responsive indicators and key players in the formation of maize rhizosphere legacies, with significant implications for plant–soil feedbacks.

Key words: Soil legacy effects, continuous cropping, rhizosphere microbiota, protist pathogens, microbial grazers

1 Introduction

1.1 Soil legacy effects under monoculture and the role of protists

Root-associated microbiomes assemble and co-evolve over a plant's lifetime (Donn et al. 2015, Bonkowski et al. 2021), and their propagules often persist in the soil as resting stages. This creates 'soil-legacy effects' that influence the performance of subsequent crops, typically via the accumulation of host-specific microbial consortia (Bever et al. 1997, terHorst et al. 2016, Bakker et al. 2018, Schmid et al. 2019).

Modern studies confirm that the effects of conspecific legacies are intensified by continuous monoculture. Repeated planting of the same crop reduces microbial diversity, disrupts nutrient cycling, often encouraging the presence and activity of soil-borne pathogens. This has an impact on plant phenotype and productivity (Li et al. 2019, Yang et al. 2020). By contrast, crop rotation, practised for centuries (Bullock 1992), is an empirical evolved management strategy that disrupts root-pathogen build-up and thus mitigates negative legacies (Krupinsky et al. 2002, Bever et al. 2015). Additionally, diversified systems such as intercropping can dilute specialist pathogens and enhance plant immunity by lowering host density and broadening root-exudate chemistry, which together reshape microbial interaction networks (Li et al. 2021, Pelissier et al. 2021, Oburger et al. 2022). Diverse microbial communities and stable belowground networks can buffer plant performance under environmental stress (Toju et al. 2018, Wagg et al. 2019), making them key targets for climate-smart agriculture. Yet, the composition of microbial communities is also influenced by abiotic factors such as temperature, water availability, and soil texture (Williams and Rice 2007, Bauke et al. 2022, Yim et al. 2022, Zhao et al. 2024). As climate variability intensifies, it is becoming increasingly important to understand how microbial legacies develop and influence plant function in order to ensure the resilience of crop production.

As most legacy research has focused on bacteria and fungi (Hannula et al. 2021, Epp Schmidt et al. 2022, Kuerban et al. 2023), the eukaryotic realm outside the fungal kingdom remains largely unexplored. This is surprising given that protists — unicellular microbial eukaryotes — contain major plant pathogens (Neuhauser et al. 2014, Thines 2014, Bass et al. 2018, Schwelm et al. 2018, Rodenburg et al. 2024) and occupy pivotal trophic positions that couple microbial turnover to nutrient fluxes (Clarholm 1985, Bonkowski 2004). Protists are a polyphyletic and immensely diverse group that encompass a wide range of trophic strategies and ecological functions (Pawlowski et al. 2012, Geisen et al. 2018). Protistan consumers drive the microbial loop in the rhizosphere, thereby accelerating nitrogen turnover, while predation imposes deterministic pressures on community assembly (Rosenberg et al. 2009, Rüger et al. 2021, Rüger et al. 2023).

Some protist groups, however, evolved to become parasites of plants and animals with worldwide economic importance (Dixon 2009, Neuhauser et al. 2010, Derevnina et al. 2016). Free-living Cercozoa fulfil both functions: predominantly bacterivorous or fungivorous consumers graze on the root-associated microbiome, and shape the community structure of the rhizosphere micorbiota (Bonkowski 2004, Geisen et al. 2018), while Phytomyxea are a subgroup containing a broad variety of obligate plant pathogens, including the genera *Plasmodiophora* and *Spongospora* (Neuhauser et al. 2014). Hemibiotrophic protists can alternate between saprotrophic growth in soil and pathogenic infection of plant roots (Kamoun et al. 2015). Among them, oomycetes such as *Pythium arrhenomanes* and *P. ultimum* cause damping-off and root-rot in *Zea mays*. Their oospores have a long lifespan and persist in the soil, germinating when a suitable host reappears and promoting their accumulation under continuous cropping.

1.2 Study system, hypothesis and objectives

To explore how protist communities respond to soil legacy development, we analysed a five-season *Zea mays* monoculture on newly established field plots without a history of maize cultivation (Vetterlein et al. 2020, Vetterlein et al. 2021). The field experiment was initiated in autumn 2018 with 24 homogeneously packed plots of loam or sand, each measuring 11 x 3,1 metres. The plots were arranged in a randomised design and managed identically (no tillage and only mineral fertiliser). This set-up provided uniform starting conditions yet contrasting soil textures, creating a unique chronosequence (2019–2023) under a shared climate (Vetterlein et al. 2021).

Targeted amplicon markers captured the protistan groups Cercozoa and Oomycota. Cercozoan primers amplified the full diversity of Cercozoa, including the plant-pathogenic Phytomyxea (Dumack et al. 2019, Fiore-Donno et al. 2020) and oomycete primers retrieved the breadth of Oomycota, a lineage rich in maize pathogens such as *Pythium* and *Phytophthora* (Telle et al. 2011, Schmidt et al. 2020, Fiore-Donno and Bonkowski 2021).

We hypothesised that continuous maize cultivation selects for conspecific, directional shifts in rhizosphere protist communities, resulting in a progressive diversity decline and a cumulative enrichment of host-associated microbial consortia, including potential root pathogens (Bass et al. 2018, Schmidt et al. 2020, Bickel and Koehler 2021). These patterns would result in a temporal intensification of plant–soil feedbacks and the formation of persistent soil legacy effects. We profiled Cercozoa (including Phytomyxea) and Oomycota communities across five seasons to (i) determine how soil texture modulates legacy-driven trajectories, (ii) relate changes in alpha- and

beta-diversity to abiotic drivers, and (iii) quantify shifts in the balance between pathogenic and heterotrophic protists in bulk soil and rhizosphere.

2 Methods

2.1 Field experiment and study site

The field experiment is situated at the Bad Lauchstädt Research Station in central Germany (51.3904 °N, 11.8759 °E). Long-term climate records for 1993–2013 report a mean annual precipitation of around 525 mm and a mean temperature of 9.7 °C (Schädler et al. 2019). In 2018, twenty-four plots (11 m × 3.1 m) were excavated to 1 m depth and refilled with homogenised soil. Loam, taken from the upper 50 cm of a local Haplic Phaeozem, was sieved to 20 mm and compacted with a vibrating plate to a bulk density of 1.36 g cm^{-3}. The sand substrate comprised 83 % industrial quartz sand blended with 17 % of the same loam and settled to a bulk density of 1.50 g cm^{-3} without mechanical compaction. Each plot contained a 25 cm gravel layer beneath a 75 cm soil layer to ensure uniform drainage. The design is two-factorial, with twelve loam and twelve sand plots. Within each texture, six plots were sown with wild-type *Zea mays* L. B73 and six with its root-hairless mutant *rth3*, giving six replicates per treatment level. Since April 2019 maize has been grown annually under identical management (no tillage, mineral fertiliser only; no heavy machinery). The maize crop was always harvested in October; stubble remained on the plots, which were covered with a permeable tarp from October to March to suppress winter weeds, remaining weeds were removed by hand (Vetterlein et al. 2021).

2.2 Sample collection and processing

Sampling was performed once per growing season at the maize growth stage BBCH 19, when the maize plant had produced nine or more leaves, typically in late June or early July. The 24 plots (loam/wild-type, loam/*rth3*, sand/wild-type, sand/*rth3*; six replicates each) were sampled in random order. The sampling locations were established using soil cores taken to determine root length density. These cores were positioned 10 cm from a randomly selected maize plant and perpendicular to the row orientation. A 20 × 20 × 20 cm soil cube was then extracted around each of these boreholes. To avoid resampling areas that had previously been disturbed, sampling points in subsequent years were randomly selected while ensuring a distance of at least 50 cm from any earlier destructive sampling. All sampling points were georeferenced and recorded in a GIS. The soil cube was transported to the field laboratory within 15 min. There the block was weighed, gently crumbled by hand, and roots were separated. Rhizosphere adhering to the roots

was removed with sterile toothbrushes over sterile Petri dishes. The detached rhizosphere and the remaining bulk soil were homogenised and stored at 4 °C for DNA extraction.

2.3 Environmental and plant covariates

Daily weather records were used to derive cumulative rainfall from sowing to BBCH-19 and the corresponding temperature sum expressed as growing-degree days (GDD). Across the chronosequence, rainfall between sowing and sampling ranged from a minimum of 22 mm in 2020 to a maximum of 50 mm in 2021, whereas GDD varied between about 124 °C d (2020) and 156 °C d (2022) (Fig. S 1). Thus 2021 represented the wettest growth season, while 2022 combined the lowest rainfall with the highest thermal peak. Plant traits were measured on the same day as microbiome sampling. In each plot three shoots were harvested and oven dried. Root traits were obtained from three soil cores per plot. After washing and scanning, root length was corrected for decomposition with depth-specific factors. The spatio-temporal framework served as the foundation for evaluating the dynamics of protistan communities.

2.4 DNA extraction, amplicon sequencing and processing

DNA extraction and purification were performed using the FastDNA® SPIN Kit for Soil (MP Biomedicals, CA, USA) according to the manufacturer's protocol. Extractions for the 2019, 2022, and 2023 samples were conducted in Cologne, while DNA from the 2021 samples was extracted by a collaborating research group in Braunschweig using the same protocol. Separate two-step PCR protocols were used to target the regions of interest for Oomycota and Cercozoa.

For oomycete communities, the ITS1 region was amplified using the primer pair S1777F and 58SOomR (Fiore-Donno and Bonkowski 2020) in the first PCR, followed by a semi-nested PCR with barcoded primers S1786StraF and 58SOomR with an annealing temperature of 58°C under similar conditions. For cercozoan community profiling, the hypervariable V4 region of the 18S rRNA gene was amplified. In the initial PCR, the forward primers S615F_Cerco and S615F_Phyt (1:1 mixture) were used together with the reverse primer S963R_Phyt (Fiore-Donno et al. 2020). A semi-nested PCR followed, using an equimolar mixture of the barcoded primers S615F_Cer and S947R_Cer. Both PCR steps began with an initial denaturation at 95°C for 2 min, followed by 24 cycles of 95°C for 30 s, annealing at 52°C (first PCR) or 58°C (semi-nested PCR) for 30 s, extension at 72°C for 30 s, and finished with a final elongation at 72°C for 5 min. In both protocols, 1 µl of template DNA was used in the initial PCR and 1 µl of the amplicon was used for the semi-nested step; tagged primers (as described in Fiore-Donno et al. (2018)) were incorporated during the second PCR. Final reaction mixtures included DreamTaq polymerase (Thermo Fisher Scientific, Dreieich,

Germany) at 0.01 units, Thermo Scientific DreamTaq Green Buffer, 0.2 mM dNTPs, and 1 µM primers. To mitigate potential effects of PCR competition, each reaction was performed in duplicate, and at least two negative controls were included per PCR batch. Both duplicates of the second PCR were pooled (12.5 µl each) before purification and normalization using the SequalPrep Normalization Plate Kit (Invitrogen, Thermo Fisher Scientific, USA) to obtain a concentration of 1 - 2 ng/µl per sample. The purified PCR products were then sequenced on an Illumina MiSeq platform (Illumina Inc., San Diego, CA, United States) were performed at the Cologne Center for Genomics (Cologne, Germany), using the MiSeq v3 Reagent kit with 2 × 300 cycles.

For Oomycota and Cercozoa the raw paired end reads were processed through a customized mothur (v.1.45.3) pipeline (Schloss et al. 2009): reads were merged under stringent criteria (no mismatches allowed in primer or barcode regions, zero ambiguities), with a minimum overlap of 200 bp for Cercozoa and 70 bp for Oomycota, contigs failing these thresholds were discarded. After demultiplexing and trimming of primer and tag sequences, sequences were de novo clustered at 97 % similarity via abundance-based greedy clustering (agc) (Rognes et al. 2016), with chimeras identified and removed by VSEARCH and singleton OTUs below 0.005 % total abundance filtered out (fewer than 142 reads for Cercozoa and 127 reads for Oomycota). Taxonomy was then assigned by BLAST+ (Camacho et al. 2009), using an e value cutoff of 1×10^{-50} against the PR^2 database for Cercozoa (Guillou et al. 2013) and 1×10^{-10} against a custom Oomycota ITS reference database for Oomycetes based on NCBI GenBank (Solbach et al. 2025 [unpublished]); in both cases, only the top hit was retained and non target sequences excluded. OTUs with ≥ 95 % identity to a reference were assigned to species level, with lower identity matches assigned at higher taxonomic ranks. Chimeras were identified using UCHIME (Edgar et al. 2011) as implemented in mothur and the abovementioned reference template (Fiore-Donno et al. 2018). Since chimera detection of Oomycetes often led to false positives or negatives with UCHIME, all sequences with an alignment to sequence length ratio of less than 0.7 were discarded instead. The taxonomic assignment of both OTU databases was manually checked. The final Cercozoa dataset comprised 850 OTUs at a mean depth of 33,697 reads per sample and the final Oomycota dataset comprised 208 OTUs at a mean depth of 7,282 reads per sample.

2.5 Statistical analysis

All statistical analyses were conducted using R (v4.3.2, R Core Team, 2023), final data visualisations were produced using ggplot2 (Wickham 2016) and RcolorBrewer (Neuwirth 2022). Data wrangling and reshaping were carried out with dplyr for filtering (Wickham et al. 2023), tidyr

(Wickham et al. 2024) and reshape2 (Wickham 2007) for pivoting tables, forcats (Wickham 2023) for recoding of categorical variables.

Spearman correlations of covariates were calculated between sampling year (time) and each predictor (GDD, rainfall, root length, shoot dry weight). Root and shoot traits were further analysed with two-way ANOVA followed by Tukey contrasts.

To ensure data quality, OTU tables for Cercozoa (including Phytomyxea), Phytomyxea alone and Oomycota were filtered to ≥ 5,000 reads per sample and extreme outliers were excluded based on ordination space (maximum one sample per protistan group). After filtering, a maximum of 24 samples per condition (i.e., one per field plot) could be retained. Phytomyxea and Cercozoa showed full or near-full retention across most years and soil types. However, no rhizosphere samples remained for either group in 2023 due to quality filtering. Oomycota retention was more variable, with lower sample numbers particularly in sandy soils. No bulk soil samples were sequenced for either group in 2021, neither for Oomycota in 2022. Full sample counts per group, year, soil type, and sampling location are available in Tab. S 1.

Calculations of α-diversity were based on Hill numbers (Chao et al. 2014) with OTU richness (Hill #0), diversity (Hill #1; exponential Shannon) and evenness (Hill #2; inverse Simpson) and performed in vegan (Oksanen et al. 2024). For these analyses, bulk soil and rhizosphere samples were analysed separately. Log-normalised richness was compared among years with one-way ANOVA followed by Tukey's HSD (agricolae; de Mendiburu (2023)) or, where assumptions failed, Kruskal–Wallis with Dunn's post hoc test (FSA; Ogle et al. (2025)).

Bray–Curtis dissimilarities of relative abundances were ordinated with NMDS (vegan::metaMDS); solutions with stress < 0.20 were retained. Bulk soil and rhizosphere samples were pooled for NMDS to increase statistical power and capture overall community trajectories. Environmental vectors were fitted using envfit (999 permutations), and the five strongest predictors (R^2, $P < 0.05$) were added to biplots. When sampling plot accounted for significant variation among samples, a partial fitting approach was applied to control for this block effect. Environmental vectors were then fitted with permutations stratified by sampling plot. Growing degree days (GDD) were used to represent temperature effects, while rainfall and irrigation were summed to represent total precipitation input. For root traits, root length was fitted as a representative variable. Community differences were assessed with PERMANOVA (adonis2); heterogeneous dispersions (betadisper) were handled by pairwise PERMANOVAs with Bonferroni- and FDR-adjusted P values and, if necessary, by refitting the model without the most dispersed year(s). Despite two maize

genotypes being included in the experiment, PERMANOVA analysis revealed that plant genotype had no significant influence on protist community composition (Cercozoa: p = 0.598; Phytomyxea: p = 0.407; Oomycota: p = 0.759). Genotype was therefore grouped together for all analyses.

For eight focal genera (Trinematidae, *Platyreta*, *Spongospora*, *Plasmodiophorida* sp., *Myzocytiopsis lenticularis*, *Phytophthora undulata*, *Pythium arrhenomanes*, *P. monospermum*) $\log_2$-transformed abundances were regressed against time with separate quasi-Poisson GLMs (glm, family = quasipoisson(link = "log")) for loam and sand. Model slopes, pseudo-R^2, dispersion, quasi-AIC and FDR-corrected P values guided interpretation.

Differentially abundant OTUs were identified with DESeq2 (Love et al. 2014). Size factors were estimated by the “poscounts” method. Wald tests calculated $\log_2$ fold changes for each year relative to 2019, with adjusted p-values (Benjamini–Hochberg) ≤ 0.05 indicating significance.

3 Results

3.1 Plant performance across seasons

Plant growth metrics, calculated as the plot-level averages of three plants or cores, varied considerably over the five-year monoculture period. Root length showed a gradual accumulation over time (Fig. S 2, top), while shoot dry mass closely tracked seasonal climatic patterns, peaking in the wet year of 2021, declining during the 2022 drought, and partially recovering in the moderate year 2023 (Fig. S 2, bottom).

3.2 Alpha diversity reveals lineage specific legacy effects

Clear but lineage-specific trends in protist α-diversity emerged across the five years sequence (Fig. 1,Fig. S 3). Cercozoan richness (Hill #0) dropped after the first year: OTU richness fell to roughly 65 % of the 2019 baseline (ANOVA: $F_{(1,145)} = 119.08$, $p < 0.001$). However, richness in bulk soil recovered to approximately 90 % of the initial level by 2023 (ANOVA: $F_{(1,138)} = 41.89$, $p < 0.001$). These changes were accompanied by declines in diversity (Hill #1) and evenness (Hill #2) in both the rhizosphere and the bulk soil, suggesting that specific OTUs became dominant in the bulk soil over time.

The obligate plant-parasitic subgroup Phytomyxea comprised 12 OTUs and largely mirrored the broader cercozoan pattern. Rhizosphere richness declined and stayed low after the first year. In contrast, after an interim decline, bulk soil richness returned to the 2019 baseline by 2023 ($F_{(1,286)}$

= 117.58, p < 0.001). This was accompanied by a decrease in diversity (Hill #1) and evenness (Hill #2), both of which recovered to initial levels by 2023, in both bulk soil and rhizosphere (Fig. S 3).

The behaviour of Oomycota, which includes key plant pathogens, was different. Bulk soil richness remained unchanged over the years (ANOVA: $F_{(1,57)}$ = 0.45, p = 0.50). However, increasing dominance of specific oomycete taxa was evident in loam bulk soil, where evenness (Hill #1) declined over time (Fig. S 3). In the rhizosphere, the Oomycota richness declined to ~80 % of that in 2019 over time (ANOVA: $F_{(1,112)}$ = 9.72, p < 0.002), but diversity (Hill #1) and evenness (Hill #2) remained stable, indicating that the decline was mainly due to low-abundance taxa rather than the dominant community members.

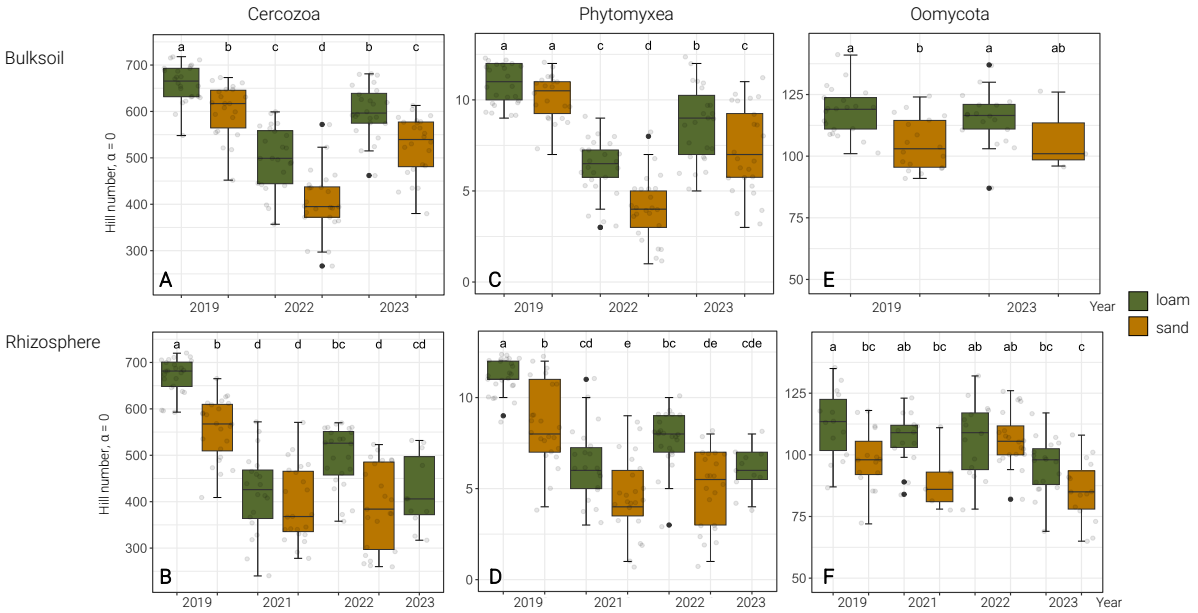

Fig. 1 Boxplots of temporal changes in OTU richness (Hill number, α = 0) under continuous maize cultivation for Cercozoa, Phytomyxea, and Oomycota across four sampling years. Richness declined over time in the rhizosphere for all groups. Different letters indicate statistically significant differences between years (Tukey's HSD, p < 0.05).

3.3 Shifts in community composition driven by time and environment

Non-metric multidimensional scaling (NMDS, stress <0.2) indicated lineage-specific temporal shifts in the composition of protists across the bulk soil and rhizosphere (Fig. 2, Tab. 1,Fig. S 5, Fig. S 6). Soil texture significantly modified these trajectories for Cercozoa (PERMANOVA: R^2 = 0.02, p = 0.001) and Oomycota (R^2 = 0.02, p = 0.002), whereas Phytomyxea were unaffected by texture (p = 0.434). The texture dependence was also reflected by the contrasting directions and strengths of the environmental vectors fitted to the NMDS ordinations (Fig. S 4). While cercozoan consumer communities primarily exhibited variability in beta dispersion, Oomycota—including the plant pathogenic genus *Pythium* spp. —showed clear compositional shifts over time.

Beta-dispersion of cercozoan communities increased significantly after the first year and variation on community composition remained high in subsequent years. The communities in both soil types were structured by time (both soils: p = 0.001), temperature (both soils: p = 0.001), precipitation (sand: p = 0.001; loam: p = 0.003), shoot biomass (both soils: p = 0.001), and root length (sand: p = 0.001; loam: p= 0.41) (Fig. S 4). In loam the variation in cercozoan community composition increased year by year, whereas in sand, community variation decreased in 2023.

Obligate plant parasitic Phytomyxea also underwent significant temporal shifts in beta diversity. Beta dispersion increased from 2019 to 2022, but decreased in 2023, corresponding with the decline and partial recovery of alpha diversity in 2023. Community structure was primarily shaped by time (sand: p = 0.002; loam: p = 0.001) and precipitation (sand: p = 0.001; loam: p = 0.004). Root length also influenced community composition, but only marginally (sand: p = 0.083; loam: p = 0.001) (Fig. S 4).

Oomycota displayed a pronounced directional shift in community structure across the five-year monoculture period, forming a temporal gradient in ordination space. This shift was evident in both soil types and was not associated with beta dispersion. Despite relatively stable alpha diversity patterns, oomycete community composition changed markedly over time (both soils: p = 0.001), with precipitation (both soils: p = 0.001), temperature (sand: p=0.021; loam: p = 0.001), and root length (sand: p=0.001; loam: p = 0.001) identified as key drivers.

To identify the taxa that contributed to these community-level patterns, we analysed taxa specific abundance trends across the years (Fig. 3, Fig. S 7,Fig. S 8). Within Cercozoa, changes in community structure were marked by a decline in plant-pathogenic Phytomyxea and an increase in heterotrophic genera (Fig. S 7). Obligate plant pathogenic Phytomyxea, including the genera *Spongospora* and *Plasmodiophorida*, showed a clear decrease after the first year, while

heterotrophic cercozoan genera such as Trinematidae and mycophagus *Platyreta* amoeba increased markedly in 2022 (Fig. 3). In Oomycota, a decline in potential non-pathogenic taxa (*Myzocytiopsis lenticularis*, *Phytophthora undulata*) was evident shortly after the first year (Fig. 3, Fig. S 8), whereas the proportions of known maize pathogens—especially *Pythium arrhenomanes* and *P. monospermum*—increased progressively over the years (Fig. S 7, Fig. S 8). These linear increases were clearly reflected in the $\log_2$-transformed yearly abundance trends (Fig. 3), consistent with the directional compositional shifts observed in beta diversity.

Together, ordination and differential-abundance analyses depict two contrasting compositional trajectories: a shift towards heterotroph consumers in Cercozoa, and a progressive enrichment of potential plant pathogenic *Pythium* in Oomycota.

Tab. 1 Permanova results for temporal community shifts (2019–2023). PERMANOVA (R^2, F-values, and p-values) on Bray–Curtis distances for Cercozoa, Phytomyxea, and Oomycota communities. Analyses for all plots combined and separated for sand and loam soils. Asterisks in the beta dispersion (BetaDisper) row denote significant differences of community variability between years (***p < 0.001).

~ year

		R^2	F-value	p-value	BetaDisper
Cercozoa	Sand	0.123	19.36	0.001	***
	Loam	0.137	23.58	0.001	***
Phytomyxea	Sand	0.048	6.93	0.001	***
	Loam	0.104	17.24	0.001	
Oomycota	Sand	0.094	7.69	0.001	***
	Loam	0.174	20.80	0.001	

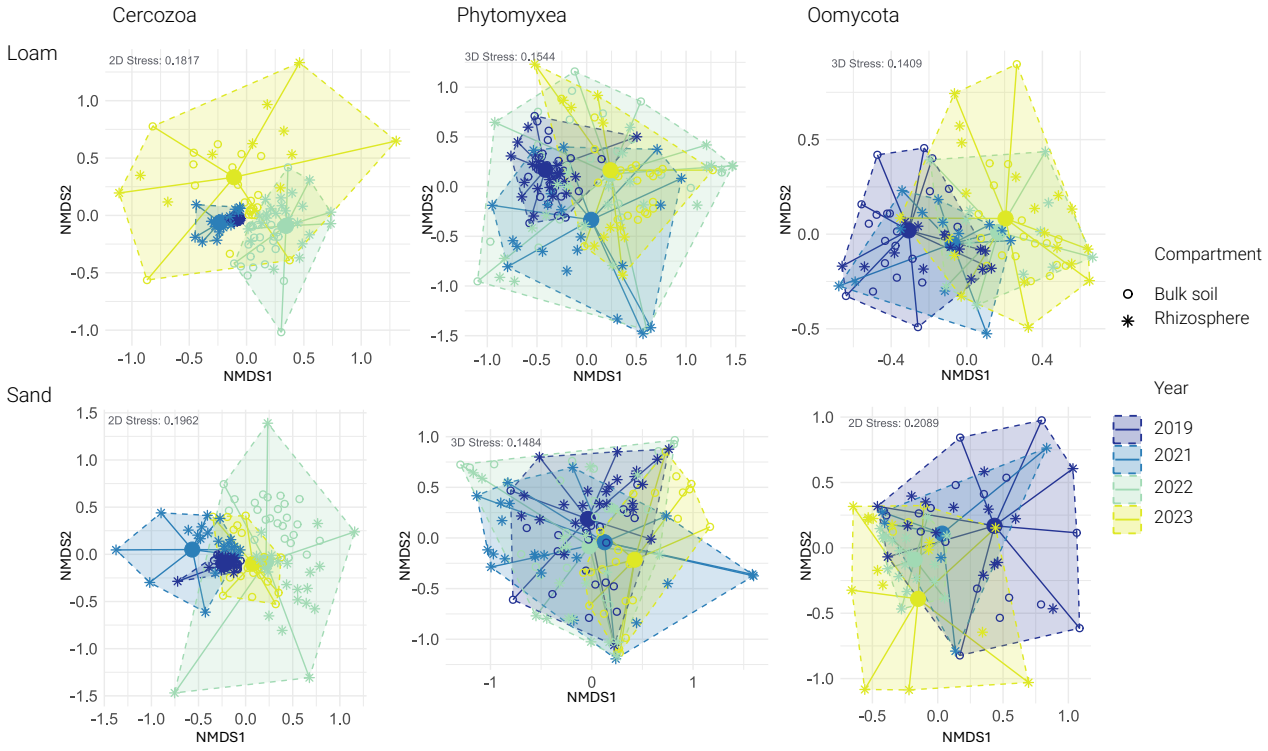

Fig. 2 Shifts of protist community composition (Cercozoa, Phytomyxea and Oomycota) over five years of continuous maize cultivation. NMDS ordinations of Bray–Curtis dissimilarities for Cercozoa (left), Phytomyxea (center), and Oomycota (right), shown separately for loam (top) and sand (bottom). Each polygon encloses samples from a given year (colour-coded). The ordinations were performed in two or three dimensions, depending on the stress (threshold = 0.2) and only the first two NMDS axes are shown.

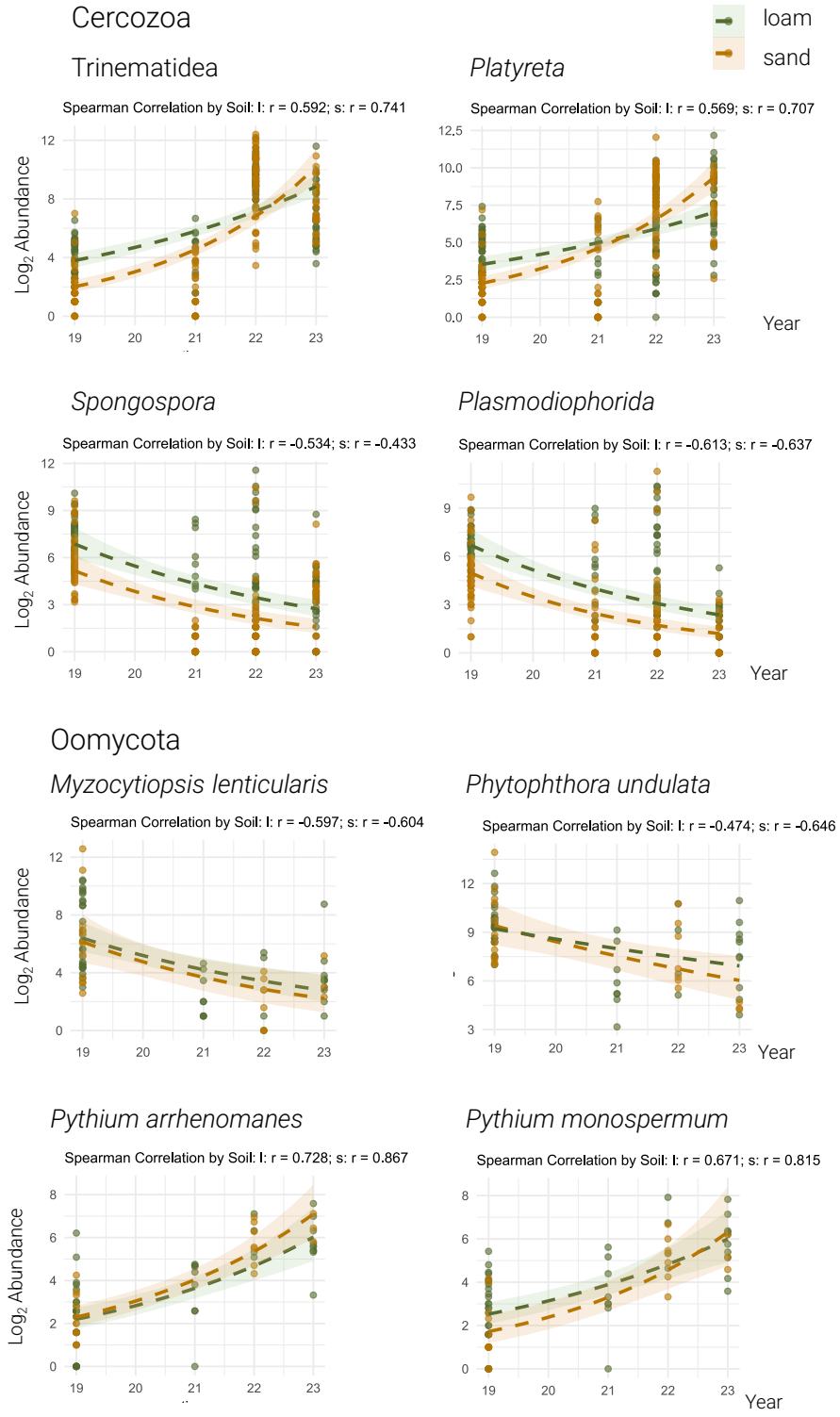

Fig. 3 Abundance trends of selected protistan taxa over five maize seasons. The panels show the year-wise $\log_2$ transformed abundance ($\log_2$[abundance + 1]) of representative taxa from the phyla Cercozoa (including Phytomyxea) and Oomycota, split by soil type (loam = green; sand = orange). The curves reflect quasi-Poisson generalised linear models (GLMs); the Spearman correlation coefficients (r) are shown for each soil type.

4 Discussion

4.1 Legacy effects of maize-pathogens and the rise of microbial antagonists

The alternating wet and dry seasons of 2021 and 2022, respectively, acted as natural pulses of perturbations, restructuring protist communities in distinct ways. While cercozoan communities showed increased variation following the 2022 drought, suggesting opportunistic priority effects causing more diverse trajectories in community assembly after rewetting, oomycete communities were largely unaffected by drought and exhibited coherent, directional compositional shifts, consistent with gradual accumulation and maize-specific pathogen enrichment.

Generally, over the course of the five consecutive maize seasons, the OTU richness of both protist lineages in the rhizosphere declined, mirroring the loss of diversity typically reported for bacterial communities in monoculture (Li et al. 2019, Liu et al. 2024). In contrast, rotation systems are known to sustain richer microbiomes and limit pathogen pressure (Venter et al. 2016). However, the persistent decline in the abundance of the dominant Phytomyxean genera *Plasmodiophora* and *Spongospora* can likely be attributed to the absence of their respective former host plants - Brassicaceae and potatoes - in the agricultural soil, as these pathogens are known to produce propagules capable of surviving in soil for multiple years (Balendres et al. 2017, Zahr et al. 2021). Although a certain promiscuity in host specificity of Phytomyxea does exist (Neuhauser et al. 2014), and e.g. *Polymyxa graminis* being a common pathogen of cereals (Kanyuka et al. 2003), maize cultivation apparently did not lead to an enrichment of these phytomyxid pathogens over time. During the five-year period, there was a steady increase in the dominance of the maize-specific hemiobiotrophic pathogens *Pythium arrhenomanes* and P. *monospermum*, with a concurrent disappearance of rare oomycete taxa. In parallel, the abundance of heterotrophic cercozoan consumers (e.g., small flagellate glissomonads and testate Trinematidae amoebae) increased, while the abundance of obligate phytomyxean plant parasites declined. It is not known whether beneficial heterotrophic Cercozoa can be directly recruited by plants (Bonkowski 2004, Gao et al. 2019, Amacker et al. 2020), but mycophagous vampyrellid amoebae, such as the genus *Playtreta*, are well known to suppress fungal and oomycete pathogens through direct grazing (Old and Darbyshire 1978, Chakraborty and Old 1982, Old and Chakraborty 1986, Hess and Suthaus 2022). Their significantly increasing abundance over time suggests increasing top-down control. Maize roots dynamically adjust their exudate composition throughout the growing season (Santangeli et al. 2024), altering microbial habitats and selectively influencing microbial colonizers and their grazers (Bais et al. 2006, Hartmann et al. 2009, Rüger et al. 2023, Niedeggen

et al. 2024, Schultes et al. in review). Although root-secreted secondary metabolites may act as signalling molecules to recruit beneficial rhizosphere microbes, they can also increase the risk of attracting root pathogens or herbivores (Oldroyd 2013, Santhanam et al. 2015). Consequently, the parallel increase in both heterotrophic cercozoans and potential maize-pathogenic oomycetes suggests an ecological trade-off within the rhizosphere community.

Over time, however, the two physically divergent substrates, loam and sand, differentiated not only in their microbial response dynamics but even further diverged in soil structure. Phalempin et al. (2025) demonstrated, within this field experiment, that old root channels in loam remained intact but not in sand. Consequently, roots and their co-evolved microbiomes transitioned to a decomposer system during root decay. Root biopore recycling, whereby new roots of subsequent crops re-use old root channels of the previous crop, is thus characterised by the legacy of the former decomposer communities. Hemibiotrophic pathogens, such as *Pythium* oomycetes, which spend part of their life cycle as decomposers appear to derive significant advantage from the decomposition phase. Especially bacterial rhizosphere microbiomes, as well as their cercozoan consumers, tend to diversify during the decomposition stage (Niedeggen et al. in prep). Thus, loam likely promoted microbial legacy effects through biopore recycling, favouring the recolonisation of new roots by residual propagules or enriched microsites. This structural continuity may have also fostered the gradual build-up of maize-specific oomycete pathogens. Established populations thus likely gained an advantage during colonisation in successive seasons, progressively displacing rare taxa. Also the gradual increase in cercozoan dispersion in loam (Fig. S 4) may be explained by biopore recycling, because microbial niches diversify through recurrent changes between the rhizosphere and root decomposer communities. Changes in cercozoan community composition were significantly influenced by shoot biomass, strongly indicating that belowground energy input from rhizodeposition through shoot photosynthetic activity drives belowground foodweb interactions. A recent study of Santangeli et al. (2024) confirmed that C exudation per maize plant increased with increasing shoot biomass production over time, but the C exudation rate per unit root surface area decreased as plants matured, so that also qualitative changes in rhizodeposition cannot be excluded. By contrast, the communities of Phytomyxea and Oomycota were not affected by aboveground plant traits, but rather by root length, reflecting the direct dependence of these potential plant pathogens with plant roots. In sand, the decomposition of dead roots was slow and sand was unable to support stable biopores, which strongly restricted biopore recycling and likely hindered the transmission of microbial propagules from old to new roots. Cercozoan communities showed a strong response to the 2022 drought in sand (Fig. S 4), exhibiting a sudden increase in community

dispersion, which suggests a strong pulse disturbance. Loam soils are likely more buffered due to their greater moisture-holding capacity (Hillel 2003, Libohova et al. 2018).

Ultimately, the observed patterns reflect a dynamic interplay of decomposers and pathogen accumulation, driven by complex interactions among plant, microbial, and soil-structural legacies conditioned by climate variability.

4.2 Conclusion

Continuous maize cultivation leaves distinct biological legacies in the rhizosphere, shaping protist community composition and function over time. The polyphyletic nature and resulting divergent functional adaptations of protists were reflected in contrasting trajectories of taxon-specific responses unfolding during continuous maize monoculture: enrichment of potential maize-specific pathogenic Oomycota and increased variability among of heterotrophic, and partly potentially antagonistic Cercozoa, while maize was not the right host for Phytomyxea. Soil texture and climate extremes further influenced these responses. In loam, stable biopore networks of old root channels, and greater moisture retention likely led to gradual microbial shifts. In sand, weaker structural cohesion led to more sudden community shifts after a drought year. These patterns emphasize the critical influence of the abiotic context on rhizosphere feedback and soil legacies. Given the critical roles of protists as both, potential plant pathogens and antagonists in plant-soil feedbacks, their inclusion in agroecological strategies is vital for maintaining microbial functionality and supporting resilient crop systems under climate stress.

5 Acknowledgements

We gratefully acknowledge all SPP members taking part in the Complex Sampling campaigns, as their dedicated efforts were essential for the successful acquisition of samples over multiple years. This project was carried out in the framework of the DFG Priority Programme 2089 “Rhizosphere spatiotemporal organization – a key to rhizosphere functions” funded by the Deutsche Forschungsgemeinschaft (project numbers 403635931, 403641192).

6 Conflict of interest statement

None declared.

7 Author contributions

DV, MB and MT contributed to the conception and design of the study. Material preparation, fieldwork, and data collection were carried out by DN, SS, and MT. Data analysis and interpretation were performed by DN and MB. The first draft of the manuscript was written by DN, and all authors critically revised and commented on previous versions.

8 Data availability statement

The data that support the findings of this study are available from the corresponding author upon request.

9 References

Amacker, N., Z. Gao, B. C. Agaras, E. Latz, G. A. Kowalchuk, C. F. Valverde, A. Jousset, and S. Weidner. 2020. Biocontrol Traits Correlate With Resistance to Predation by Protists in Soil Pseudomonads. Front Microbiol 11:614194.

Bais, H. P., T. L. Weir, L. G. Perry, S. Gilroy, and J. M. Vivanco. 2006. The role of root exudates in rhizosphere interactions with plants and other organisms. Annual Review of Plant Biology 57:233-266.

Bakker, P., C. M. J. Pieterse, R. de Jonge, and R. L. Berendsen. 2018. The Soil-Borne Legacy. Cell 172:1178-1180.

Balendres, M. A., R. S. Tegg, and C. R. Wilson. 2017. Resting Spore Dormancy and Infectivity Characteristics of the Potato Powdery Scab Pathogen Spongospora subterranea. Journal of Phytopathology 165:323-330.

Bass, D., C. van der Gast, S. Thomson, S. Neuhauser, S. Hilton, and G. D. Bending. 2018. Plant Rhizosphere Selection of Plasmodiophorid Lineages from Bulk Soil: The Importance of "Hidden" Diversity. Frontiers in Microbiology Volume 9 - 2018.

Bauke, S. L., W. Amelung, R. Bol, L. Brandt, N. Brüggemann, E. Kandeler, N. Meyer, D. Or, A. Schnepf, M. Schloter, S. Schulz, N. Siebers, C. von Sperber, and H. Vereecken. 2022. Soil water status shapes nutrient cycling in agroecosystems from micrometer to landscape scales. Journal of Plant Nutrition and Soil Science 185:773-792.

Bever , J., K. Westover, and J. Antonovics. 1997. Incorporating the soil community into plant population dynamics: the utility of the feedback approach. Journal of Ecology 85:561-573.

Bever, J. D., S. A. Mangan, and H. M. Alexander. 2015. Maintenance of plant species diversity by pathogens. Annual Review of Ecology, Evolution, and Systematics 46:305-325.

Bickel, J. T., and A. M. Koehler. 2021. Review of Pythium Species Causing Damping-Off in Corn. Plant Health Progress 22:219-225.

Bonkowski, M. 2004. Protozoa and plant growth: the microbial loop in soil revisited. New Phytologist 162:617-631.

Bonkowski, M., M. Tarkka, B. S. Razavi, H. Schmidt, E. Blagodatskaya, R. Koller, P. Yu, C. Knief, F. Hochholdinger, and D. Vetterlein. 2021. Spatiotemporal Dynamics of Maize (Zea mays L.) Root Growth and Its Potential Consequences for the Assembly of the Rhizosphere Microbiota. Front Microbiol 12:619499.

Bullock, D. G. 1992. Crop rotation. Critical Reviews in Plant Sciences 11:309-326.

Camacho, C., G. Coulouris, V. Avagyan, N. Ma, J. Papadopoulos, K. Bealer, and e. al. 2009. BLAST+: architecture and applications. . BMC Bioinformatics 10:421.

Chakraborty, S., and K. M. Old. 1982. Mycophagous soil amoeba: Interactions with three plant pathogenic fungi. Soil Biology and Biochemistry 14:247-255.

Chao, A., C.-H. Chiu, and L. Jost. 2014. Unifying Species Diversity, Phylogenetic Diversity, Functional Diversity, and Related Similarity and Differentiation Measures Through Hill Numbers. Annual Review of Ecology, Evolution, and Systematics 45:297-324.

Clarholm, M. 1985. Interactions of bacteria, protozoa and plants leading to mineralization of soil nitrogen. Soil Biology and Biochemistry 17:181-187.

de Mendiburu, F. 2023. agricolae: Statistical Procedures for Agricultural Research. R package version 1.3-7.

Derevnina, L., B. Petre, R. Kellner, Y. F. Dagdas, M. N. Sarowar, A. Giannakopoulou, J. C. De la Concepcion, A. Chaparro-Garcia, H. G. Pennington, P. van West, and S. Kamoun. 2016. Emerging oomycete threats to plants and animals. Philos Trans R Soc Lond B Biol Sci 371.

Dixon, G. R. 2009. The Occurrence and Economic Impact of Plasmodiophora brassicae and Clubroot Disease. Journal of Plant Growth Regulation 28:194-202.

Donn, S., J. A. Kirkegaard, G. Perera, A. E. Richardson, and M. Watt. 2015. Evolution of bacterial communities in the wheat crop rhizosphere. Environ Microbiol 17:610-621.

Dumack, K., A. M. Fiore-Donno, Bass. D., and M. Bonkowski. 2019. Making sense of environmental sequencing data: ecologically important functional traits of the protistan groups Cercozoa and Endomyxa (Rhizaria). . Mol Ecol Resour 20:398– 403.

Edgar, R. C., B. J. Haas, J. C. Clemente, C. Quince, and R. Knight. 2011. UCHIME improves sensitivity and speed of chimera detection. Bioinformatics 27:2194-2200.

Epp Schmidt, D., G. Dlott, M. Cavigelli, S. Yarwood, and J. E. Maul. 2022. Soil microbiomes in three farming systems more affected by depth than farming system. Applied Soil Ecology 173.

Fiore-Donno, A. M., and M. Bonkowski. 2020. Different community compositions between obligate and facultative oomycete plant parasites in a landscape-scale metabarcoding survey. Biology and Fertility of Soils 57:245-256.

Fiore-Donno, A. M., and M. Bonkowski. 2021. Different community compositions between obligate and facultative oomycete plant parasites in a landscape-scale metabarcoding survey. Biology and Fertility of Soils 57:245-256.

Fiore-Donno, A. M., T. Richter-Heitmann, and M. Bonkowski. 2020. Contrasting Responses of Protistan Plant Parasites and Phagotrophs to Ecosystems, Land Management and Soil Properties. Front Microbiol 11:1823.

Fiore-Donno, A. M., C. Rixen, M. Rippin, K. Glaser, E. Samolov, U. Karsten, B. Becker, and M. Bonkowski. 2018. New barcoded primers for efficient retrieval of cercozoan sequences in high-throughput environmental diversity surveys, with emphasis on worldwide biological soil crusts. Mol Ecol Resour 18:229-239.

Gao, Z., I. Karlsson, S. Geisen, G. Kowalchuk, and A. Jousset. 2019. Protists: Puppet Masters of the Rhizosphere Microbiome. Trends in Plant Science 24:165-176.

Geisen, S., E. A. D. Mitchell, S. Adl, M. Bonkowski, M. Dunthorn, F. Ekelund, L. D. Fernandez, A. Jousset, V. Krashevska, D. Singer, F. W. Spiegel, J. Walochnik, and E. Lara. 2018. Soil protists: a fertile frontier in soil biology research. FEMS Microbiology Reviews 42:293-323.

Guillou, L., D. Bachar, S. Audic, D. Bass, C. Berney, L. Bittner, and e. al. 2013. The protist ribosomal reference database (PR2): a catalog of unicellular eukaryote small sub-unit rRNA sequences with curated taxonomy. Nucleic Acids Research 41.

Hannula, S. E., R. Heinen, M. Huberty, K. Steinauer, J. R. De Long, R. Jongen, and T. M. Bezemer. 2021. Persistence of plant-mediated microbial soil legacy effects in soil and inside roots. . Nat Commun 12.

Hartmann, A., M. Schmid, D. van Tuinen, and G. Berg. 2009. Plant-driven selection of microbes. Plant and Soil 321:235-257.

Hess, S., and A. Suthaus. 2022. The Vampyrellid Amoebae (Vampyrellida, Rhizaria). Protist 173:125854.

Hillel, D. 2003. Introduction to environmental soil physics. Elsevier.

Kamoun, S., O. Furzer, J. D. G. Jones, H. S. Judelson, G. S. Ali, R. J. D. Dalio, S. G. Roy, L. Schena, A. Zambounis, F. Panabières, D. Cahill, M. Ruocco, A. Figueiredo, X.-R. Chen, J. Hulvey, R. Stam, K. Lamour, M. Gijzen, B. M. Tyler, N. J. Grünwald, M. S. Mukhtar, D. F. A. Tomé, M. Tör, G. Van Den Ackerveken, J. McDowell, F. Daayf, W. E. Fry, H. Lindqvist-Kreuze, H. J. G. Meijer, B. Petre, J. Ristaino, K. Yoshida, P. R. J. Birch, and F. Govers. 2015. The Top 10 oomycete pathogens in molecular plant pathology. Molecular Plant Pathology 16:413-434.

Kanyuka, K., E. Ward, and M. J. Adams. 2003. Polymyxa graminis and the cereal viruses it transmits: a research challenge. Molecular Plant Pathology 4:393-406.

Krupinsky, J. M., K. L. Bailey, M. P. McMullen, B. D. Gossen, and T. K. Turkington. 2002. Managing Plant Disease Risk in Diversified Cropping Systems. Agronomy Journal 94:198-209.

Kuerban, M., W. F. Cong, J. Jing, and T. M. Bezemer. 2023. Microbial soil legacies of crops under different water and nitrogen levels determine succeeding crop performance. Plant Soil 485.

Li, X.-F., Z.-G. Wang, X.-G. Bao, J.-H. Sun, S.-C. Yang, P. Wang, C.-B. Wang, J.-P. Wu, X.-R. Liu, X.-L. Tian, Y. Wang, J.-P. Li, Y. Wang, H.-Y. Xia, P.-P. Mei, X.-F. Wang, J.-H. Zhao, R.-P. Yu, W.-P. Zhang, Z.-X. Che, L.-G. Gui, R. M. Callaway, D. Tilman, and L. Li. 2021. Long-term increased grain yield and soil fertility from intercropping. Nature Sustainability 4:943-950.

Li, X., A. Jousset, W. de Boer, V. J. Carrion, T. Zhang, X. Wang, and E. E. Kuramae. 2019. Legacy of land use history determines reprogramming of plant physiology by soil microbiome. ISME J 13:738-751.

Libohova, Z., C. Seybold, D. Wysocki, S. Wills, P. Schoeneberger, C. Williams, D. Lindbo, D. Stott, and P. R. Owens. 2018. Reevaluating the effects of soil organic matter and other properties on available water-holding capacity using the National Cooperative Soil Survey Characterization Database. Journal of Soil and Water Conservation 73:411-421.

Liu, C., J. Wang, Y. Wang, L. Li, Z. Feng, Y. Xian, Y. Jiang, J. Yu, T. Tong, X. Li, and M. Yao. 2024. Crop rotation and fertilization shape the microbiomes of maize rhizosphere soil with distinct mechanisms. Plant and Soil 507:89-108.

Love, M. I., W. Huber, and S. Anders. 2014. Moderated estimation of fold change and dispersion for RNA-seq data with DESeq2. Genome Biology 15:550.

Neuhauser, S., S. Bulman, and M. Kirchmair. 2010. Plasmodiophorids: The Challenge to Understand Soil-Borne, Obligate Biotrophs with a Multiphasic Life Cycle. Pages 51-78 in Y. Gherbawy and K. Voigt, editors. Molecular Identification of Fungi. Springer Berlin Heidelberg, Berlin, Heidelberg.

Neuhauser, S., M. Kirchmair, S. Bulman, and D. Bass. 2014. Cross-kingdom host shifts of phytomyxid parasites. BMC Evolutionary Biology 14:33.

Neuwirth, E. 2022. RColorBrewer: ColorBrewer Palettes. R package version 1.1-3.

Niedeggen, D., D. Pflugfelder, D. van Dusschoten, A. Hakobyan, A. Wendel, C. Knief, R. Koller, and M. Bonkowski. in prep. Root decay legacies and biopore recycling drive rhizosphere microbiome assembly under continuous maize cropping.

Niedeggen, D., L. Rüger, E. Oburger, M. Santangeli, M. Ahmed, D. Vetterlein, S. Blagodatsky, and M. Bonkowski. 2024. Microbial utilisation of maize rhizodeposits applied to agricultural soil at a range of concentrations. European Journal of Soil Science 75.

Oburger, E., H. Schmidt, and C. Staudinger. 2022. Harnessing belowground processes for sustainable intensification of agricultural systems. Plant and Soil 478:177-209.

Ogle, D. H., J. C. Doll, A. P. Wheeler, and A. Dinno. 2025. FSA: Simple Fisheries Stock Assessment Methods. R package version 0.9.6.

Oksanen, J., G. Simpson, F. Blanchet, R. Kindt, P. Legendre, P. Minchin, R. O'Hara, P. Solymos, M. Stevens, E. Szoecs, H. Wagner, M. Barbour, M. Bedward, B. Bolker, D. Borcard, G. Carvalho, M. Chirico, M. De Caceres, S. Durand, H. Evangelista, R. FitzJohn, M. Friendly, B. Furneaux, G. Hannigan, M. Hill, L. Lahti, D. McGlinn, M. Ouellette, E. Ribeiro Cunha, T. Smith, A. Stier, C. Ter Braak, and J. Weedon. 2024. vegan: Community Ecology Package. R package version 2.6-8.

Old, K. M., and S. Chakraborty. 1986. Mycophagous soil amoebae: their biology and significance in the ecology of soil-borne plant pathogens. . Progress in protistology 1:163-194.

Old, K. M., and J. F. Darbyshire. 1978. Soil fungi as food for giant amoebae. Soil Biology and Biochemistry 10:93-100.

Oldroyd, G. E. 2013. Speak, friend, and enter: signalling systems that promote beneficial symbiotic associations in plants. Nature Reviews Microbiology 11:252-263.

Pawlowski, J., S. Audic, S. Adl, D. Bass, L. Belbahri, C. Berney, S. S. Bowser, I. Cepicka, J. Decelle, M. Dunthorn, A. M. Fiore-Donno, G. H. Gile, M. Holzmann, R. Jahn, M. Jirků, P. J. Keeling, M. Kostka, A. Kudryavtsev, E. Lara, J. Lukeš, D. G. Mann, E. A. D. Mitchell, F. Nitsche, M. Romeralo, G. W. Saunders, A. G. B. Simpson, A. V. Smirnov, J. L. Spouge, R. F. Stern, T. Stoeck, J. Zimmermann, D. Schindel, and C. de Vargas. 2012. CBOL Protist Working Group: Barcoding Eukaryotic Richness beyond the Animal, Plant, and Fungal Kingdoms. PLoS Biology 10:e1001419.

Pelissier, R., L. Buendia, A. Brousse, C. Temple, E. Ballini, F. Fort, C. Violle, and J. B. Morel. 2021. Plant neighbour-modulated susceptibility to pathogens in intraspecific mixtures. Journal of Experimental Botany 72:6570-6580.

Phalempin, M., N. Jentzsch, J. M. Köhne, S. Schreiter, R. Gründling, D. Vetterlein, and S. Schlüter. 2025. Soil structure development in a five-year chronosequence of maize cropping on two contrasting soil textures. Soil and Tillage Research 251.

Rodenburg, S. Y. A., D. de Ridder, F. Govers, and M. F. Seidl. 2024. Oomycete Metabolism Is Highly Dynamic and Reflects Lifestyle Adaptations. Mol Plant Microbe Interact 37:571-582.

Rognes, T., T. Flouri, B. Nichols, C. Quince, and F. Mahé. 2016. VSEARCH: a versatile open source tool for metagenomics. PeerJ 4 4:e2584. .

Rosenberg, K., J. Bertaux, K. Krome, A. Hartmann, S. Scheu, and M. Bonkowski. 2009. Soil amoebae rapidly change bacterial community composition in the rhizosphere of Arabidopsis thaliana. The ISME Journal 3:675-684.

Rüger, L., K. Feng, K. Dumack, J. Freudenthal, Y. Chen, R. Sun, M. Wilson, P. Yu, B. Sun, Y. Deng, F. Hochholdinger, D. Vetterlein, and M. Bonkowski. 2021. Assembly Patterns of the Rhizosphere Microbiome Along the Longitudinal Root Axis of Maize (Zea mays L.). Frontiers in Microbiology 12:614501.

Rüger, L., M. Ganther, J. Freudenthal, J. Jansa, A. Heintz-Buschart, M. T. Tarkka, and M. Bonkowski. 2023. Root cap is an important determinant of rhizosphere microbiome assembly. New Phytologist 239:1434-1448.

Santangeli, M., T. Steininger-Mairinger, D. Vetterlein, S. Hann, and E. Oburger. 2024. Maize (Zea mays L.) root exudation profiles change in quality and quantity during plant development – A field study. Plant Science 338.

Santhanam, R., V. T. Luu, A. Weinhold, J. Goldberg, Y. Oh, and I. T. Baldwin. 2015. Native root-associated bacteria rescue a plant from a sudden-wilt disease that emerged during continuous cropping. Proceedings of the National Academy of Sciences of the United States of America 112:E5013-5020.

Schädler, M., F. Buscot, S. Klotz, T. Reitz, W. Durka, J. Bumberger, I. Merbach, S. G. Michalski, K. Kirsch, P. Remmler, E. Schulz, and H. Auge. 2019. Investigating the consequences of climate change under different land-use regimes: a novel experimental infrastructure. Ecosphere 10:e02635.

Schloss, P. D., S. L. Westcott, T. Ryabin, J. R. Hall, M. Hartmann, E. B. Hollister, and e. al. 2009. Introducing mothur : open-source, platform-independent, community-supported software for describing and comparing microbial communities. Applied Environmental Microbiology 75:7537-7541.

Schmid, M. W., T. Hahl, S. J. van Moorsel, C. Wagg, G. B. De Deyn, and B. Schmid. 2019. Feedbacks of plant identity and diversity on the diversity and community composition of rhizosphere microbiomes from a long-term biodiversity experiment. Molecular Ecology 28:863-878.

Schmidt, C. S., A. Leclerque, T. Pfeiffer, J. W. Goessling, M. Orlik, B. Jamshidi, K. Saar, J. Sellmann, I. Siepe, and E. Koch. 2020. Pathogenicity of Pythium species to maize. . European Journal of Plant Pathology 158:335-347.

Schultes, S., L. Rüger, D. Niedeggen, J. Freudenthal, K. Frindte, M. Becker, R. Metzner, D. Pflugfelder, A. Chlubek, C. Hinz, D. van Dusschoten, S. Bauke, M. Bonkowski, M. Watt, R. Koller, and C. Knief. in review. Photosynthate distribution determines spatial patterns in the rhizosphere microbiota of the maize root system. Nature Communications manuscript ID NCOMMS-24-55118A.

Schwelm, A., J. Badstöber, S. Bulman, N. Desoignies, M. Etemadi, R. E. Falloon, C. M. M. Gachon, A. Legreve, J. Lukeš, U. Merz, A. Nenarokova, M. Strittmatter, B. K. Sullivan, and S. Neuhauser. 2018. Not in your usual Top 10: protists that infect plants and algae. Molecular Plant Pathology 19:1029-1044.

Solbach, M. D., C. Albracht, K. Dumack, N. Eisenhauer, A. M. Fiore-Donno, A. Vogel, C. Wagg, and M. Bonkowski. 2025 [unpublished]. Legacies of consecutive summer droughts on soil-borne potential plant pathogenic protists and protistan consumers [Preprint].

Telle, S., R. G. Shivas, M. J. Ryley, and M. Thines. 2011. Molecular phylogenetic analysis of Peronosclerospora (Oomycetes) reveals cryptic species and genetically distinct species parasitic to maize. European Journal of Plant Pathology 130:521-528.

terHorst, C. P., P. C. Zee, and J. K. Bailey. 2016. Eco-evolutionary dynamics in plant-soil feedbacks. Functional Ecology 30:1062-1072.

Thines, M. 2014. Phylogeny and evolution of plant pathogenic oomycetes—a global overview. European Journal of Plant Pathology 138:431-447.

Toju, H., K. G. Peay, M. Yamamichi, K. Narisawa, K. Hiruma, K. Naito, S. Fukuda, M. Ushio, S. Nakaoka, Y. Onoda, K. Yoshida, K. Schlaeppi, Y. Bai, R. Sugiura, Y. Ichihashi, K. Minamisawa, and E. T. Kiers. 2018. Core microbiomes for sustainable agroecosystems. Nat Plants 4:247-257.

Venter, Z. S., K. Jacobs, and H.-J. Hawkins. 2016. The impact of crop rotation on soil microbial diversity: A meta-analysis. Pedobiologia 59:215-223.

Vetterlein, D., A. Carminati, I. Kögel-Knabner, G. P. Bienert, K. Smalla, E. Oburger, A. Schnepf, T. Banitz, M. T. Tarkka, and S. Schlüter. 2020. Rhizosphere Spatiotemporal Organization–A Key to Rhizosphere Functions. Frontiers in Agronomy 2.

Vetterlein, D., E. Lippold, S. Schreiter, M. Phalempin, T. Fahrenkampf, F. Hochholdinger, C. Marcon, M. Tarkka, E. Oburger, M. Ahmed, M. Javaux, and S. Schlüter. 2021. Experimental platforms for the investigation of spatiotemporal patterns in the rhizosphere—Laboratory and field scale. Journal of Plant Nutrition and Soil Science 184:35-50.

Wagg, C., K. Schlaeppi, S. Banerjee, E. E. Kuramae, and M. G. A. van der Heijden. 2019. Fungal-bacterial diversity and microbiome complexity predict ecosystem functioning. Nat Commun 10:4841.

Wickham, H. 2007. Reshaping Data with the reshape Package. Journal of Statistical Software 21(12):1-20.

Wickham, H. 2016. ggplot2: Elegant Graphics for Data Analysis. Springer-Verlag New York.

Wickham, H. 2023. forcats: Tools for Working with Categorical Variables (Factors). R package version 1.0.0.

Wickham, H., R. François, L. Henry, K. Müller, and D. Vaughan. 2023. dplyr: A Grammar of Data Manipulation. R package version 1.1.4.

Wickham, H., D. Vaughan, and M. Girlich. 2024. tidyr: Tidy Messy Data. R package version 1.3.1.

Williams, M. A., and C. W. Rice. 2007. Seven years of enhanced water availability influences the physiological, structural, and functional attributes of a soil microbial community. Applied Soil Ecology 35:535-545.

Yang, T., K. H. M. Siddique, and K. Liu. 2020. Cropping systems in agriculture and their impact on soil health-A review. Global Ecology and Conservation 23.

Yim, B., Z. Ibrahim, L. Rüger, M. Ganther, L. Maccario, S. J. Sørensen, A. Heintz-Buschart, M. T. Tarkka, D. Vetterlein, M. Bonkowski, E. Blagodatskaya, and K. Smalla. 2022. Soil texture is a stronger driver of the maize rhizosphere microbiome and extracellular enzyme activities than soil depth or the presence of root hairs. Plant and Soil.

Zahr, K., A. Sarkes, Y. Yang, H. Ahmed, Q. Zhou, D. Feindel, M. W. Harding, and J. Feng. 2021. Plasmodiophora brassicae in Its Environment: Effects of Temperature and Light on Resting Spore Survival in Soil. Phytopathology® 111:1743-1750.

Zhao, J., X. Xie, Y. Jiang, J. Li, Q. Fu, Y. Qiu, X. Fu, Z. Yao, Z. Dai, Y. Qiu, and H. Chen. 2024. Effects of simulated warming on soil microbial community diversity and composition across diverse ecosystems. Science of the Total Environment 911:168793.

10 Supplementary material

Tab. S 1 Sample counts retained after filtering, by year, soil type, and compartment. Numbers of samples retained for analysis per protist group (Cercozoa, Phytomyxea, Oomycota), year, soil (loam vs. sand), and compartment (bulk vs. rhizosphere). Maximum possible per group = 24 (1 per plot). Dashes (–) indicate no sequencing was performed for that group × compartment × year combination. Note: no rhizosphere data available in 2023 for Cercozoa or Phytomyxea due to filtering losses.

Protist Group	Year	Bulk Loam	Rhizo Loam	Bulk Sand	Rhizo Sand
Phytomyxea	2019	24	24	22	24
	2020	–	–	–	–
	2021	–	20	–	23
	2022	24	24	24	22
	2023	24	11	24	0
Cercozoa	2019	24	24	22	24
	2020	–	–	–	–
	2021	–	19	–	23
	2022	24	24	24	23
	2023	24	11	24	0
Oomycota	2019	22	14	18	15
	2020	–	–	–	–
	2021	–	13	–	5
	2022	–	15	–	20
	2023	18	19	3	15

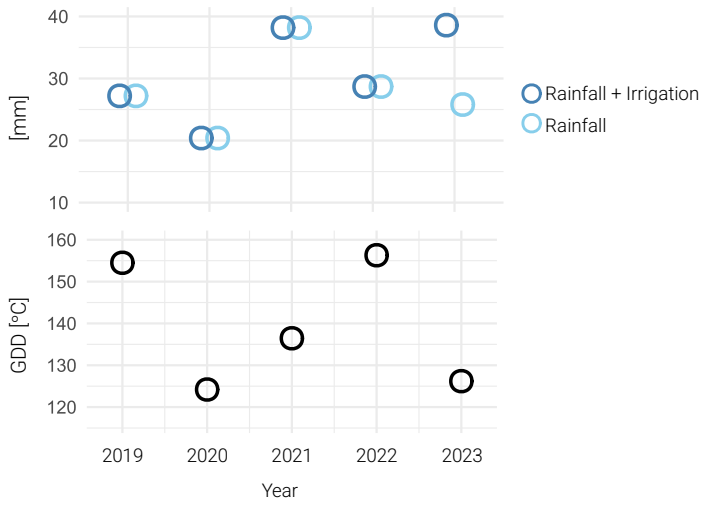

Fig. S 1 Climatic conditions across the five maize seasons. Top: cumulative rainfall (mm) and combined rainfall and irrigation (mm) from sowing to microbial sampling based on daily records from the German Weather Service (DWD). Bottom: Growing degree days (GDD, °C), calculated as the cumulative daily temperature exceeding the base temperature threshold from sowing to sampling.

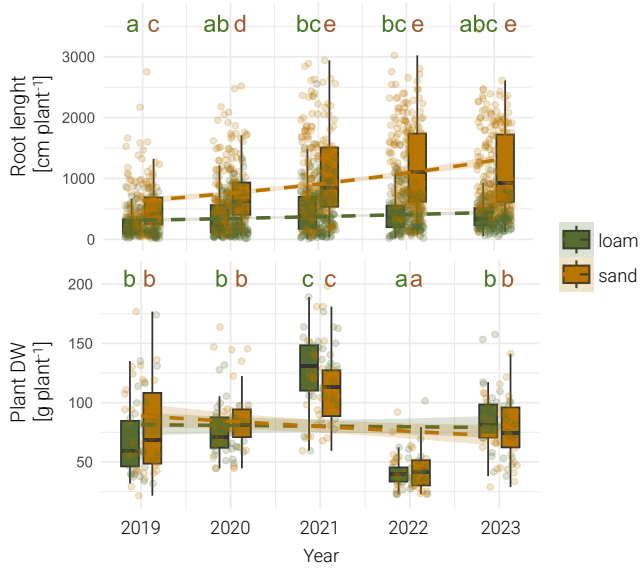

Fig. S 2 Seasonal changes in plant performance metrics, shown separately for sand (orange) and loam (green) plots. Top: root length (cm), corrected for degraded roots. Bottom: Plant dry weight at harvest (g). Statistical analysis was performed using Quasi-Poisson GLMs and ANOVA with the model structure variable ~ time * soil, followed by Tukey's HSD post hoc tests. Different letters denote statistically significant differences between years and soil types ($p < 0.05$).

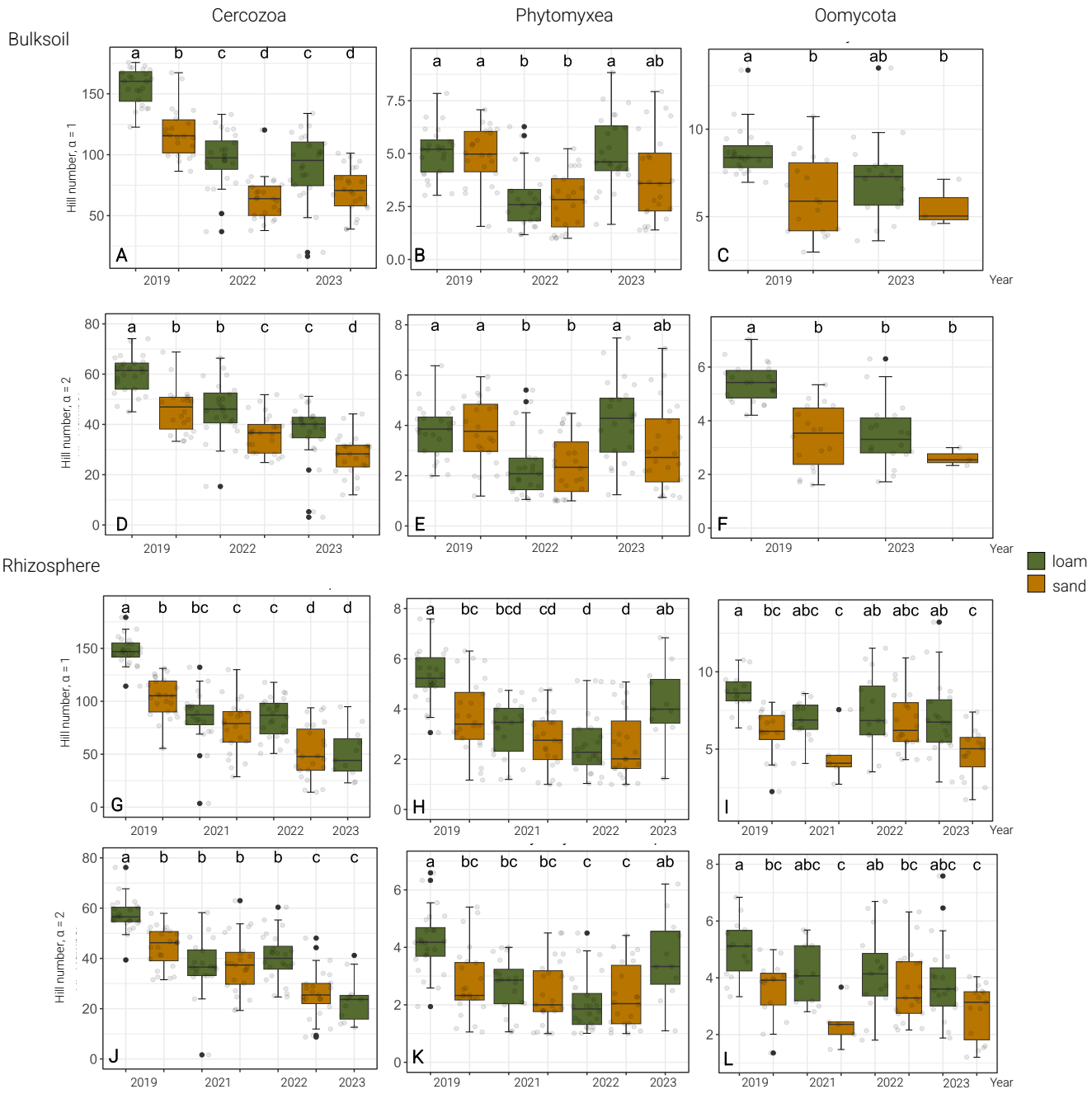

Fig. S 3 Boxplots of temporal changes in α-diversity as exponential Shannon entropy (Hill number, α = 1) and evenness as inverse Simpson index (Hill number, α = 2) for Cercozoa, Phytomyxea, and Oomycota communities across four sampling years. A-F show bulk soil, G-L rhizosphere, Generally, α-diversity tended to decline over time. Different letters indicate statistically significant differences between years (Tukey's HSD, $p < 0.05$).

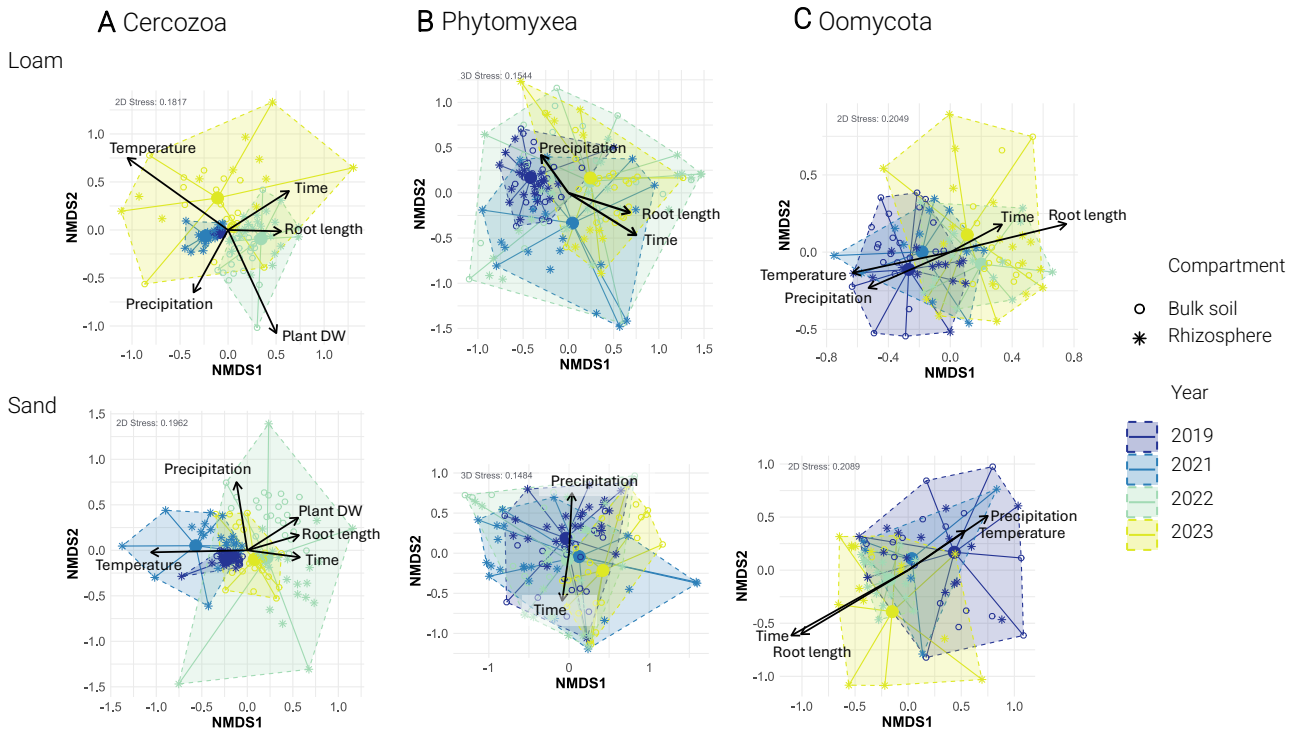

Fig. S 4 Soil-type–specific community shifts across five years of continuous maize as in Fig. 2, including vectors of the most influential environmental factors. NMDS ordinations depict changes in beta diversity for Cercozoa (left), Phytomyxea (centre), and Oomycota (right) communities from 2019 to 2023, shown separately for loam (upper panel) and sand (lower panel) soils. Polygons enclose samples from each year, with point shapes differentiating sampling compartments (bulk soil vs. rhizosphere). Statistically significant environmental variables are fitted as vectors. Temperature = GDD, cumulative growing degree days; Plant DW = shoot dry weight; Time, Root length; Precipitation = combined rainfall and irrigation. Ordinations were performed in two or three dimensions depending on stress (threshold = 0.2); only the first two NMDS axes are shown.

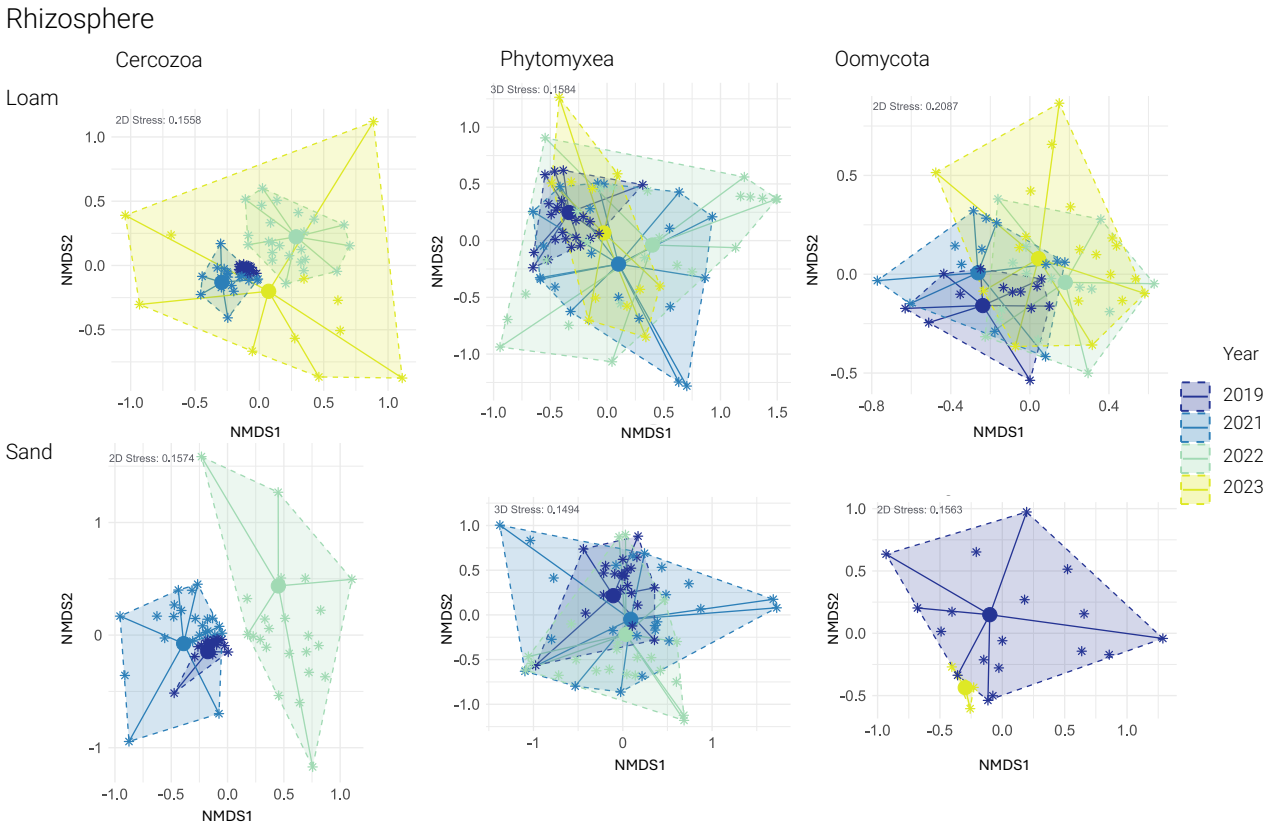

Fig. S 5 Rhizosphere specific protist community composition shifts (Cercozoa, Phytomyxea and Oomycota) over five years of continuous maize cultivation. NMDS ordinations of Bray–Curtis dissimilarities for Cercozoa (left), Phytomyxea (center), and Oomycota (right), shown separately for loam (upper panel) and sand (lower panel) soils. Each polygon encloses samples from a given year. The ordinations were performed in two or three dimensions, depending on the stress (threshold = 0.2) and only the first two NMDS axes are shown.

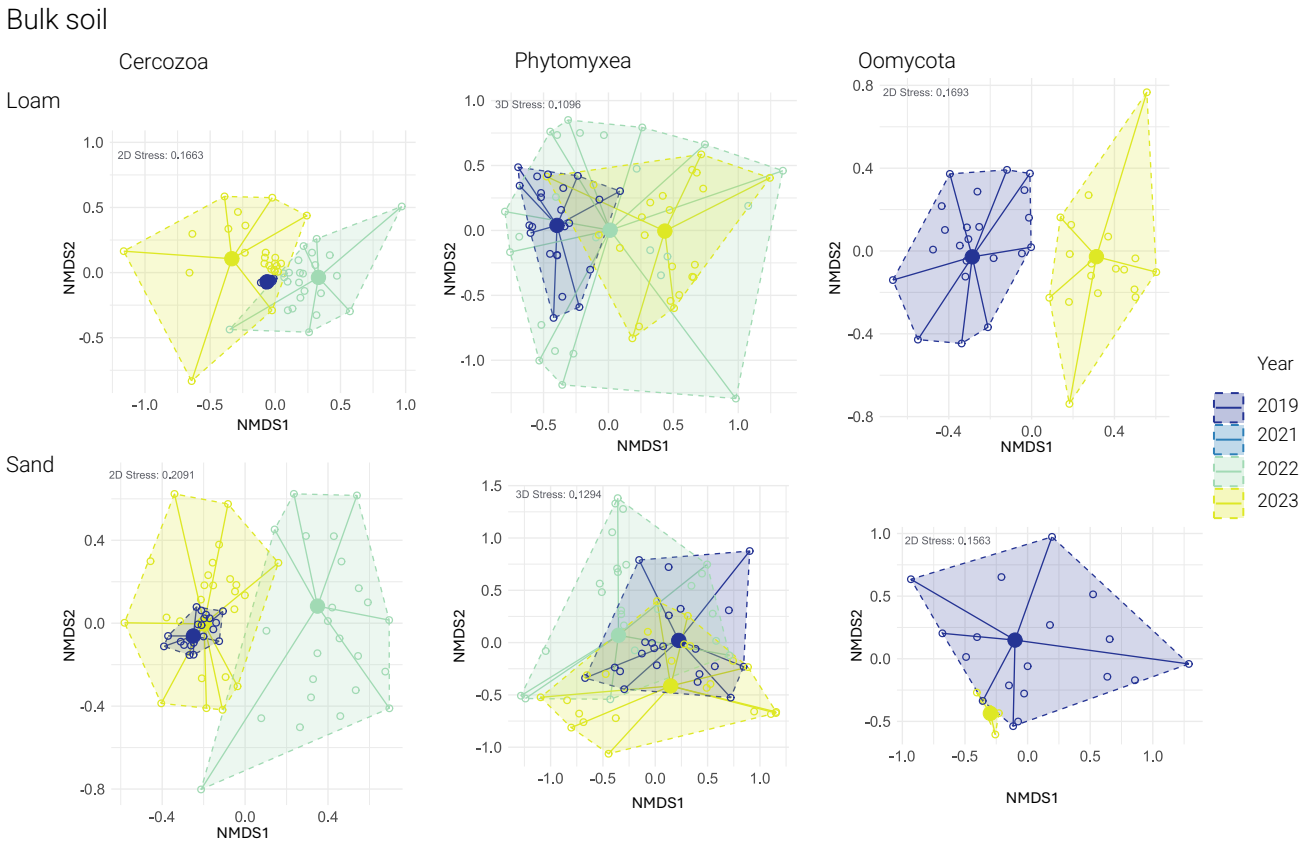

Fig. S 6 Bulk soil specific protist community composition shifts (Cercozoa, Phytomyxea and Oomycota) over five years of continuous maize cultivation. NMDS ordinations of Bray–Curtis dissimilarities for Cercozoa (left), Phytomyxea (center), and Oomycota (right), shown separately for loam (upper panel) and sand (lower panel). Each polygon encloses samples from a given year. The ordinations were performed in two or three dimensions, depending on the stress (threshold = 0.2) and only the first two NMDS axes are shown.

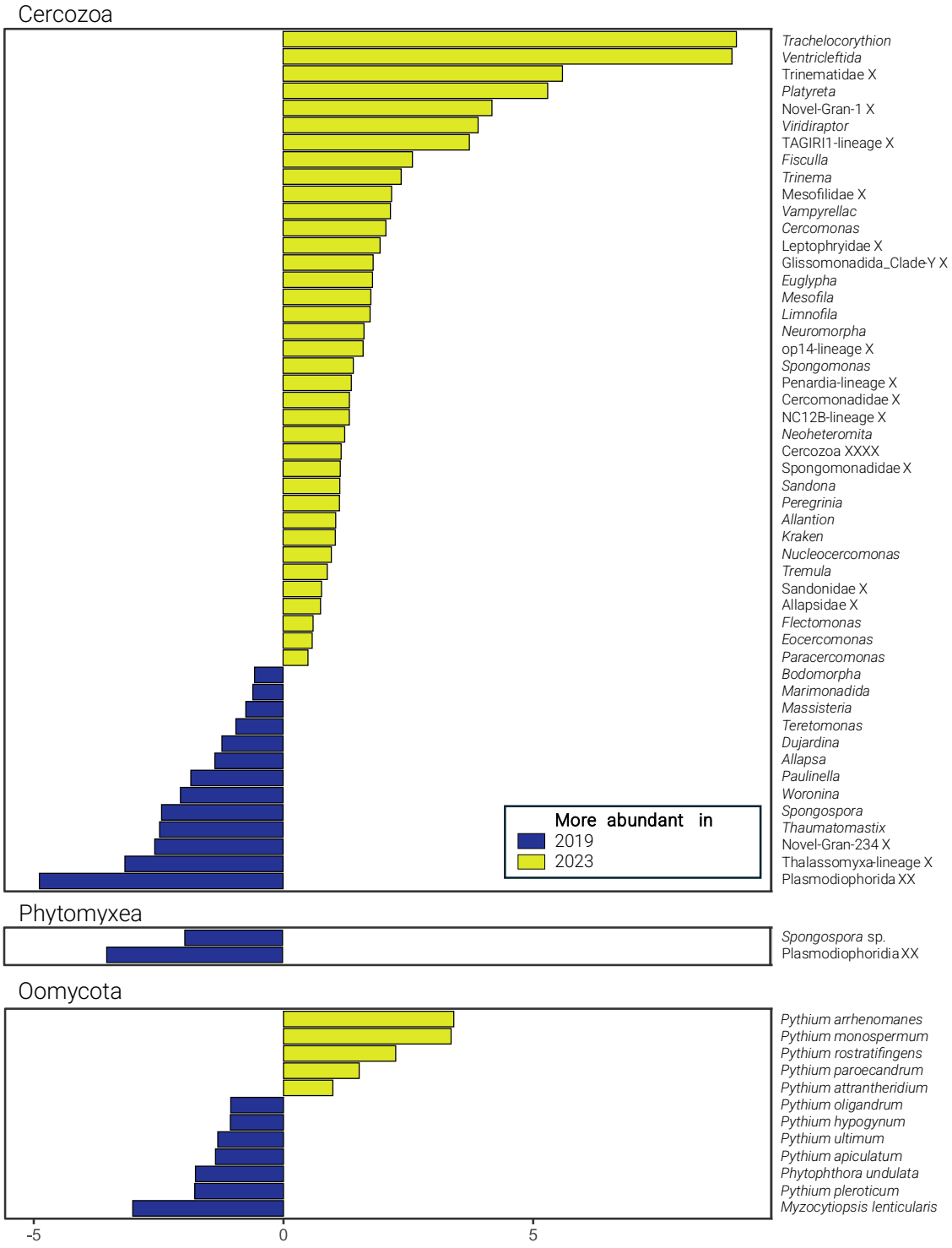

Fig. S 7 Differentially abundant protistan taxa between 2019 and 2023. Bar plots show $\log_2$ fold changes in taxon abundance between 2023 and 2019, based on DESeq2 analysis at the genus level (Cercozoa) and species level (Phytomyxea, Oomycota). Yellow bars indicate taxa more abundant in 2023; blue bars those more abundant in 2019. Only statistically significant changes (adjusted $p < 0.05$) are shown. Taxa are ordered by effect size within each microbial group.

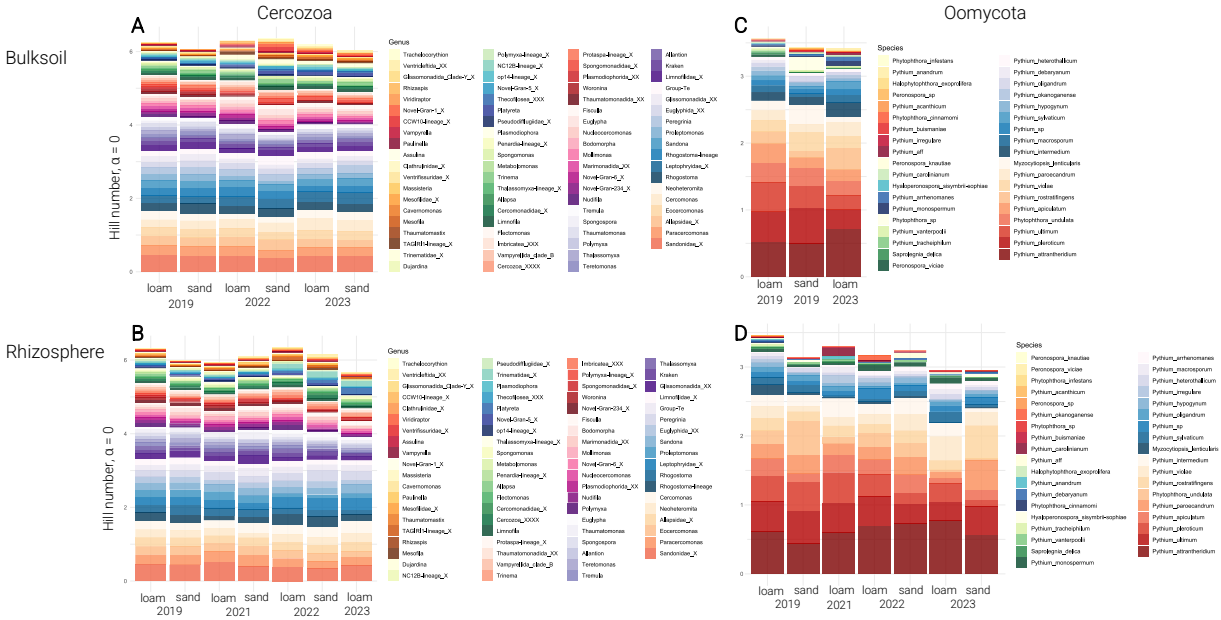

Fig. S 8 Trends in relative-abundance of protistan taxa in bulk vs. rhizosphere compartments. The stacked bar plots show the square-root transformed relative abundances of all Cercozoa taxa (left, including Phytomyxea) and Oomycota (right) taxa from 2019 to 2023. Data are shown separately for the bulk soil (top panels) and the rhizosphere (bottom panels). Taxa are colour-coded by group and ordered by abundance within each dataset. Square-root transformation reduces the effects of dominance while preserving the visibility of less abundant taxa.

Chapter IV: Root legacies govern the maize rhizosphere

Decay legacies and biopore recycling drive rhizosphere succession in maize monocultures

Reference:

Niedeggen, D., Pfugfelder, D., van Dusschoten, D., Hakobyan, A., Wendel, A. Knief, C., Koller, R., Bonkowski, M. Submitted. Decay legacies and biopore recycling drive rhizosphere succession in maize monocultures. New Phytologist manuscript ID NPH-MS-2025-52358.

Author contributions:

DN, CK, and RK and MB planned and designed the research. **DN**, DP, DD, AH and AW performed the experiments. **DN**, DP, AH and AW analysed and interpreted the data. **DN** and MB wrote the manuscript. **DN**, CK, RK and MB revised the manuscript.

Decay legacies and biopore recycling drive rhizosphere succession in maize monocultures

Daniela Niedeggen[1,2], Daniel Pflugfelder[3], Dagmar van Dusschoten[3], Anna Hakobyan[4], Anna Wendel[4], Claudia Knief[4], Robert Koller[3], Michael Bonkowski[1,2]

[1]University of Cologne, Institute of Zoology, Terrestrial Ecology, University of Cologne, 50674 Köln, Germany;

[2] Cluster of Excellence on Plant Sciences (CEPLAS), University of Cologne, 50674 Köln, Germany;

[3] Institute of Bio- and Geosciences, Plant Sciences (IBG-2), Forschungszentrum Juelich GmbH, Juelich, Germany;

[4] Institute of Crop Science and Resource Conservation, Molecular Biology of the Rhizosphere, University of Bonn, 53115 Bonn, Germany.

Key words: Soil legacy effects, biopore recycling, rhizosphere microbiome, microbial succession, MRI, *Zea mays*

Corresponding Author:

Prof. Dr. Michael Bonkowski	m.bonkowski@uni-koeln.de +492214703152
Daniela Niedeggen	daniela.niedeggen@uni-koeln.de

Summary

• Rhizosphere microbial succession and biopore recycling were traced through a growth → decay → regrowth cycle of maize to disentangle how biological legacies (resident microbiota) and physical legacies (root biopores) influence rhizosphere assembly and plant performance.

• A column experiment compared 'fresh' soil with maize monoculture-conditioned 'legacy' soil. High-resolution MRI mapped root architecture in situ, tracking root channels through decay and regrowth, identifying re-entered biopores. Guided sampling along recycled biopores and free growing roots, followed by 16S, ITS and 18S amplicon sequencing profiled bacteria, fungi, Oomycota, Cercozoa and Phytomyxea.

• Microbial succession followed three phases: (i) distinct rhizosphere microbiomes during growth; (ii) a community shift after decomposition; and (iii) an imperfect return to rhizosphere microbiomes during regrowth since root decay shifted rhizosphere community composition. About 10 % of new roots re-entered existing biopores, boosting rooting depth and microbial heterogeneity. Communities in legacy and fresh soil were always distinct, demonstrating the influence of previous cropping history.

• The microbial maize rhizosphere composition alternates between living-root and decomposer states, while biopore recycling increases community heterogeneity.

1 Introduction

Plant–soil interactions are inherently dynamic. Through coordinated biological, chemical, and physical mechanisms, plants continuously remodel the soil surrounding their roots (Bever 1994, Berg and Smalla 2009). Over time, these modifications accumulate to create a distinctive soil legacy that persists beyond plant senescence (Kardol et al. 2007, Frouz 2024). This legacy is formed at the plant–soil interface, particularly in the rhizosphere — the narrow zone directly influenced by living roots (Hartmann et al. 2009). Host-specific microbial consortia (i.e. microbiomes) assemble and co-evolve here along the developing roots (Friman et al. 2013, Bonkowski et al. 2021). These consortia leave behind a legacy through their propagules in the soil, a persistent microbial signature, once the roots have decayed.

Soil legacy effects manifest through multiple pathways. Biologically, plants selectively assemble specific microbial taxa, creating distinctive microbiome signatures, revealing that plants can effectively "condition" soils through selective recruitment and enrichment of specific microbial taxa (van der Putten et al. 2013, Gundale and Kardol 2021). Physically, root growth reorganizes the soil matrix, creating biopores that alter soil structure (Ehlers et al. 1983, Lucas et al. 2019, Wu et al. 2021, Wendel et al. 2022). Chemically, root exudation and litter decomposition modify soil nutrient profiles and organic matter composition. These processes interact synergistically, collectively influencing subsequent plant generations and shaping plant community composition and ecosystem dynamics at various spatial and temporal scales (Petermann et al. 2008, Kinkel et al. 2011, Bever et al. 2012, Kardol et al. 2013, Schnepf et al. 2022).

Research on soil microbial legacies has revealed their significant impact on plant growth. The plant associated microbiomes can create positive, neutral or negative feedback effects. Positive legacy effects occur when subsequent plants benefit from enhanced nutrient availability or protection against pathogens (Mariotte et al. 2018, Wubs and Bezemer 2018, Hannula et al. 2021). Conversely, negative legacy effects emerge when plant growth is hindered by the accumulation of pathogens or altered nutrient cycling (Kardol et al. 2007, van der Putten et al. 2013). These legacy effects have particular relevance in agricultural systems, where the rhizosphere microbiome assembled by one crop can substantially influence the productivity of subsequent crops (Hu et al. 2018, Roy et al. 2021, Liu et al. 2023). Continuous cropping systems, such as maize monocultures, often demonstrate altered microbial community structures with increased pathogen abundance and reduced crop performance (Frindte et al. 2020, Mao et al. 2021, Zhao et al. 2021).

Despite the growing appreciation for the importance of soil microbial legacies in agricultural sustainability, a critical knowledge gap exists in understanding the specific mechanisms

governing microbiome transmission between crop generations. This gap is particularly significant given the increasing interest in microbiome engineering as a sustainable alternative to conventional agricultural inputs (Oyserman et al. 2018). An important shortcoming of current experimental approaches is that most microbial rhizosphere consortia are reassembled from scratch in sieved experimental soil. Under field conditions without tillage, biopores created by roots of previous crops remain (Stirzaker et al. 1996), and maintain a distinct spatial arrangement of microbial propagules along former root channels, even after the roots have decomposed.

These old root channels are frequently reused by subsequent crops (Rasse and Smucker 1998), serving as 'root highways', reducing the mechanical impedance and thereby facilitating deeper root penetration into subsoil layers (Passioura 2002). This is enhancing resource acquisition (Athmann et al. 2013), but also exposes new roots to both beneficial microbiome legacies and potentially harmful decomposer communities. While the decay of roots partly restores soil nutrients (Eissenstat and Yanai 1997), the decaying root material may also enrich harmful microorganisms (Watt et al. 2006), including hemibiotrophic pathogens such as Phytophthora and Pythium species during their saprophytic life stage (Kamoun et al. 2015). Understanding the persistence of beneficial microbial assemblages after crop removal and identifying which microbial taxa exhibit the strongest legacy effects in a subsequent rhizosphere, represents a crucial research frontier.

Building on our ongoing research examining the spatiotemporal organization of the maize rhizosphere (Vetterlein et al. 2020), we focus on two central research questions: (1) How do biological legacies influence the structure and function of the maize rhizosphere microbiome? (2) How does biopore recycling, as a physical legacy, mediate the reassembly and functional potential of these communities across successive growth phases? We hypothesize that soils conditioned by previous crop growth exhibit significant modifications in microbial diversity during regrowth, primarily driven by pre-established microbial consortia in root channels.

To address these questions, we integrated modern sequencing technologies with non-invasive MRI root phenotyping in a controlled experimental system. Our study contrasts two soil treatments with identical composition but different management histories (Vetterlein et al. 2021): (1) fresh soil with no prior plant history, and (2) legacy soil exposed to four consecutive seasons of maize monoculture in the field. We implement a three-phase experimental study to capture dynamic changes in root architecture and microbial community composition: (1) Initial microbiome assembly on roots of a first-generation maize plant, (2) root decay period, and (3) microbiome assembly on roots of a second generation maize plant, with or without biopore recycling.

Through molecular profiling, we elucidate how microbial communities shift between growth stages under the influence of management history and biopore recycling. By linking microbial legacies to biopore recycling, we aim to clarify how these legacy effects collectively shape the spatio-temporal organisation of the maize rhizosphere and maize growth.

2 Material and Methods

2.1 Soil history treatments

Two soil history treatments were used to study the effects of soil legacy on the composition of the maize rhizosphere microbiome: (i) Fresh soil, a mix of 83% quartz sand (WF33, Quarzwerke Weferlingen, Germany) and 17% 1 mm-sieved loam collected from the top 50 cm of a haplic Phaeozem in Schladebach, Germany, where it had been under continuous agricultural use and last cultivated with oilseed rape; and (ii) Legacy soil, derived from the same quartz/loam mixture, but installed in the field at the Bad Lauchstädt research station in October 2018 and cultivated with maize (Zea mays L., inbred line B73) over four consecutive seasons from April 2019 to June 2022 (Vetterlein et al. 2021).

2.2 Three-phase column experiment design

The experiment comprised three distinct growth phases designed to examine how legacy effects and biopore recycling influence rhizosphere microbial community dynamics and root architecture over time: (a) Phase 1 – Establishment of the primary root system; (b) *Decay phase* and (c) Phase 2 – Legacy phase with second generation of root growth in the presence of biopores (with a control set of freshly prepared columns).

2.2.1 Phase 1- establishment of a primary root system

Maize seeds (inbred line B73) were surface sterilised in a 10% H_2O_2 solution followed by a three-hour soak in a calcium sulphate solution. The seeds were then sown in 30 cm x 8 cm cylindrical PVC columns filled with either fresh or legacy soil. Prior to packing, both soil types were fertilised with N, P, K, Mg, Ca and micronutrients as described in Vetterlein et al. (2021). The soil columns were compacted to a bulk density of 1.5 g cm^{-3} and irrigated to maintain a volumetric water content of 18%. Following sowing, the columns were placed in a climate chamber at 20°C during the day (14h) and 16°C at night, with 60% relative humidity. Plants were grown for 24 days until the first roots reached the bottom of the column. Out of the initial 18 columns per treatment, viable plants developed in 13 columns with fresh soil and in 16 columns with legacy soil, of which the shoots were then harvested. This phase established the primary root system, forming the foundation for the next experimental stages.

2.2.2 Decay phase- root system decomposition

Following growth phase 1, the soil columns were incubated for seven months (205 days) under controlled conditions (20°C and 40% water holding capacity) to allow the roots to decompose. Root decomposition was monitored in a subset of columns using MRI imaging at one, four, and six months after the end of Phase 1. After the end of the incubation period – referred to as the *decay phase* - five columns per treatment (fresh and legacy soil) were opened and destructively sampled for rhizosphere samples (see section 3.5). Following data collection, the remaining columns containing biopores left by the decayed roots were ready to be reseeded in Phase 2.

2.2.3 Phase 2 - regrowth of a consecutive root system

In Phase 2, we compared two treatments to examine root growth and rhizosphere development under different legacy conditions: (i) *First growth* columns – newly prepared controls for this phase, and (ii) *Second growth* columns – reseeded columns containing biopores from Phase 1 and the subsequent decay phase. A total of 37 columns were set up: The *first growth* control group included 23 new columns (12 with fresh soil, 11 with legacy soil), while the *second growth* group comprised 14 reused columns (6 fresh soil, 8 legacy soil) that had undergone both Phase 1 and Decay.

Maize seeds were then sown in all columns under identical environmental conditions as in Phase 1. To preserve the integrity of the soil matrix of reused columns, no additional fertilizer was added to the *second growth* columns. Newly prepared *first growth* columns as control, received the same fertiliser formulation as in Phase 1, but rates were reduced by 19 % (legacy soil) and 14 % (fresh soil) reflecting the nitrogen removed with shoot biomass in Phase 1; other nutrients were scaled proportionally.

Plants were grown until roots reached the bottom of the column, which occurred after 21 days. At harvest, shoot parameters and rhizosphere samples were collected for further analysis.

2.3 MRI-based root trait analysis

Maize root architecture was assessed non-invasively using high-resolution MRI, which generated 3D images of roots within the soil columns (van Dusschoten et al. 2016). MRI data were processed using NMRooting software to extract key root traits, including total root length (mm), maximum rooting depth (mm), and digital root fresh weight (g). In replanted columns, MRI scans taken after Phase 2 were precisely aligned with those of Phase 1, enabling us to differentiate roots growing in undisturbed soil matrix from those reusing existing biopores (Fig. SI 3). This alignment allowed for

quantification of biopore recycling by calculating the root length within these pre-existing channels.

2.4 Shoot-trait measurements

At harvest, number of leaves per plant, leaf length (measured as the length of the longest leaf), and photosynthetic activity as indicated by SPAD values were quantified for shoots. Photosynthetic activity was measured using a SPAD-502Plus (Konica Minolta) device at three positions on the shoot. Shoots were then cut above the root crown, dried at 60 °C until constant weight, and weighed to determine shoot dry biomass.

2.5 MRI-guided rhizosphere sampling

Soil cores were loosened by gently tapping the columns and carefully pushed out onto a sterile surface. Precise sampling locations for molecular analysis were guided by the corresponding 3D MRI images. Rhizosphere sampling focused on collecting soil tightly adhering to root surfaces, achieved by carefully scraping soil from roots immediately after extraction.

In *first growth* columns (without biopores), samples were taken along growing seminal roots. In *decay phase* columns, pre-decay MRI scans were used to locate biopores and associated seminal roots, from which soil was collected using a small spatula. In *second growth* columns (with established biopores), rhizosphere samples were collected from two distinct regions: (i) along seminal roots growing in the undisturbed soil matrix (*free growing seminal root*), and (ii) along seminal roots growing within biopores (*legacy root*). All samples were stored at 4°C and processed for DNA extraction within one week.

2.6 DNA extraction, PCR and sequencing

DNA extraction and purification were performed using the FastDNA® SPIN Kit for Soil (MP Biomedicals, CA, USA) according to the manufacturers' protocols. Separate two-step PCR protocols were used for each taxonomic group to target the regions of interest for bacteria, fungi, Oomycota, and Cercozoa.

Prokaryotic 16S rRNA and fungal ITS1 amplicons were generated using established two-step PCR protocols with the 515f-806r primer set (Caporaso et al. 2011) and the ITS1F-ITS2 primer set (White et al. 1990, Gardes and Bruns 1993), respectively, as described by Schultes et al. (in review) with 8mer barcoded primers in the second PCR. For the fungal ITS1 amplicons, unspecific bands were observed on 1.5 % agarose gels after the first PCR. Correct bands were excised, incubated in 30 µl of sterile water at 60 °C for 10 min and stored at 4 °C overnight before doing the second PCR with 10 µl of this DNA suspension. Amplification products were quantified using the

QuantiFluor dsDNA System on a QuantusTM Fluorometer and pooled at equimolar concentrations. Pooled PCR products were purified with PEG (20 % PEG8000 in 2.5 M NaCl. Library preparation and sequencing on a NovASeq instrument was conducted by Novogene.

For oomycete communities, the ITS1 region was amplified using the primer pair S1777F and 58SOomR (Fiore-Donno and Bonkowski 2020) in the first PCR, followed by a semi-nested PCR with barcoded primers S1786StraF and 58SOomR under similar conditions (with an annealing temperature of 58°C). For cercozoan community profiling, the hypervariable V4 region of the 18S rRNA gene was amplified. In the initial PCR, the forward primers S615F_Cerco and S615F_Phyt (1:1 mixture) were used together with the reverse primer S963R_Phyt (Fiore-Donno et al. 2020). A semi-nested PCR followed, using an equimolar mixture of the barcoded primers S615F_Cer and S947R_Cer. Both PCR steps began with an initial denaturation at 95°C for 2 min, followed by 24 cycles of 95 °C for 30 s, annealing at 52°C (first PCR) or 58°C (semi-nested PCR) for 30 s, extension at 72 °C for 30 s, and finished with a final elongation at 72 °C for 5 min. In both protocols, 1 µl of template DNA was used in the initial PCR and 1 µl of the amplicon was used for the semi-nested step; tagged primers (as described in Fiore-Donno et al. (2018)) were incorporated during the second PCR. Final reaction mixtures included DreamTaq polymerase (Thermo Fisher Scientific, Dreieich, Germany) at 0.01 units, Thermo Scientific DreamTaq Green Buffer, 0.2 mM dNTPs, and 1 µM primers. To mitigate PCR competition, each reaction was performed in duplicate, and at least two negative controls were included per PCR batch. Both duplicates of the second PCR were pooled (12.5 µl each) before purification and normalization using the SequalPrep Normalization Plate Kit (Invitrogen, Thermo Fisher Scientific, USA) to obtain a concentration of 1 - 2 ng/µl per sample. The purified PCR products were then sequenced on an Illumina MiSeq platform (Illumina Inc., San Diego, CA, United States) at the Cologne Center for Genomics (Cologne, Germany). With the MiSeq v3 Reagent kit, 2 × 300 cycles were performed.

2.7 Sequence processing and bioinformatics

For prokaryotes and fungi the raw sequence reads were initially demultiplexed using Cutadapt (Martin 2011) and primer sequences were trimmed using QIIME 2 (version 2024.2 (Bolyen et al. 2019)). Quality-filtered reads were processed using default parameters of DADA2 (Callahan et al. 2016), implemented in QIIME2. The taxonomic assignment of operational taxonomic units (OTUs) was done using a custom classify-sklearn plugin classifier against the SILVA SSU138.2 Ref NR99 database for bacteria (Quast et al. 2013) and, the UNITE 10.0 dynamic database for fungi (Abarenkov et al. 2024), respectively. The databases were customized by sub-setting to the amplicon region. The classified reads were quality filtered by removing rare OTUs that appeared

less than 20 times and in less than five samples in a given dataset. Sequence alignment was executed with MAFFT (Katoh and Standley 2013).

For Oomycota and Cercozoa the raw paired end reads were processed through a customized mothur (v.1.45.3) pipeline (Schloss et al. 2009): reads were merged under stringent criteria (no mismatches in primer or barcode regions, zero ambiguities), with a minimum overlap of 200 bp for Cercozoa and 70 bp for Oomycota, contigs failing these thresholds were discarded. After demultiplexing and trimming of primer and tag sequences, sequences were de novo clustered at 97 % similarity via abundance-based greedy clustering (agc) (Rognes et al. 2016), with chimeras identified and removed by VSEARCH and singleton OTUs below 0.005 % total abundance filtered out (fewer than 452 reads for Cercozoa and 218 reads for Oomycota). Taxonomy was then assigned by BLAST+ (Camacho et al. 2009), using an e value cutoff of 1×10^{-50} against the PR^2 database for Cercozoa (Guillou et al. 2013) and 1×10^{-10} against a custom Oomycota ITS reference database for Oomycetes based on NCBI GenBank (Solbach et al. 2025 [unpublished]); in both cases, only the top hit was retained and non target sequences excluded. OTUs with ≥ 95 % identity to a reference were assigned to species level, with lower identity matches assigned at higher taxonomic ranks. Chimeras were identified using UCHIME (Edgar et al. 2011) as implemented in mothur and the abovementioned reference template (Fiore-Donno et al. 2018). Since chimera detection of Oomycetes often led to false positives or negatives with UCHIME, all sequences with an alignment to sequence length ratio of less than 0.7 were discarded instead. The taxonomic assignment of both OTU databases was manually checked. The final Cercozoa dataset comprised 629 OTUs at a mean depth of 40,379 reads per sample and the final Oomycota dataset comprised 81 OTUs at a mean depth of 5,730 reads per sample.

2.8 Statistical analysis

All statistical analyses were conducted using R (v4.3.2, R Core Team, 2023), final data visualisations were produced using ggplot2 (Wickham 2016) and RcolorBrewer (Neuwirth 2022). OTU count tables for bacteria, fungi, Oomycota, Phytomyxea and Cercozoa were converted to relative abundances. Relative abundances were aggregated to the required taxonomic ranks, then square root transformed to account for compositionality (Greenacre 2021). Data wrangling and reshaping were carried out with dplyr for filtering (Wickham et al. 2023), tidyr (Wickham et al. 2024) and reshape2 (Wickham 2007) for pivoting tables, forcats (Wickham 2023) for recoding of categorical variables.

Calculations of α-diversity were based on Hill numbers (Chao et al. 2014) with OTU richness (Hill #0), diversity (Hill #1; exponential Shannon) and evenness (Hill #2; inverse Simpson) and executed

in vegan (Oksanen et al. 2024). Sampling completeness was evaluated from species accumulation and rarefaction curves. Normality was tested with the Anderson–Darling test (nortest; Gross and Ligges (2015)) and homogeneity of variances with Levene's test (car; Fox and Weisberg (2019). When one-way ANOVA assumptions were met, pairwise comparisons were performed with Tukey's HSD (agricolae; de Mendiburu (2023)). Otherwise, a non parametric Kruskal–Wallis test followed by Dunn's post hoc test (FSA; Ogle et al. (2025)), with p values tidied by broom (Robinson et al. 2024) and adjusted for multiple comparisons using the Benjamini–Hochberg FDR procedure.

Community composition based on Bray–Curtis distances was assessed by non-metric multidimensional scaling (NMDS) (vegan::metaMDS). Stress plots guided the choice of dimensionality (stress < 0.2 accepted). Treatment groupings were overlaid with standard vegan functions. Homogeneity of multivariate dispersion among treatments was evaluated with vegan::betadisper on the same distance matrix and tested for significance with permutest (999 permutations); significant contrasts are depicted as 95 % confidence ellipses in the ordinations.

Differentially abundant OTUs were identified with DESeq2 (Love et al. 2014). Low depth samples (determined by rarefaction) were removed. Counts were analysed in a negative binomial GLM after adding a pseudocount (+1) and log2 transformation. Wald tests were used for contrasts, and p values were Benjamini–Hochberg adjusted. Shared and unique OTUs among and plant growth/decay phases and rhizosphere locations (*free growing seminal root*, *legacy root* or biopore) were visualised in VennDiagram (Chen 2022). OTUs absent from all samples in a phase x location subset were excluded before diagram construction.

3 Results

Plant performance and rhizosphere composition differed markedly between fresh and legacy soils across the growth-decay phases.

3.1 Legacy soil restricted plant performance but promoted deeper rooting

Plants responded differently to soil legacy conditions aboveground and belowground, showing reduced overall growth but adaptive rooting behaviour (Figure 1). Aboveground, leaf length measurements indicated no significant difference in shoot performance due to soil history during the *first growth* phase. However, during the *second growth* phase, plants grown in legacy soil with no additional fertilization developed significantly shorter leaves compared to those in fresh soil or compared to those during the *first growth* phase (Figure 1A). This was further supported by lower SPAD values (chlorophyll content) observed in legacy soil treatments during the second phase (Fig. SI 1). Also belowground, plants grown in legacy soil displayed smaller digital root fresh weights than those grown in fresh soil, but in both growth phases (Figure 1B). Across soil histories, there was a trend toward a further reduction of root system size in the *second growth* phase. Notably, plants in legacy soil reached deeper maximum rooting depth than those in fresh soil during the *first growth* phase (Figure 1C). In the *second growth* phase, however, roots in both soils, legacy and fresh, reached the bottom of the column within the 21-day growth period. Soil legacy had no effect on biopore recycling. With both soil histories, approximately 10% of the old root channels that were established during the *first growth* phase were re-used during the *second growth* phase (Fig. SI 2), which corresponds to about 20% of all roots growing during the *second growth* phase.

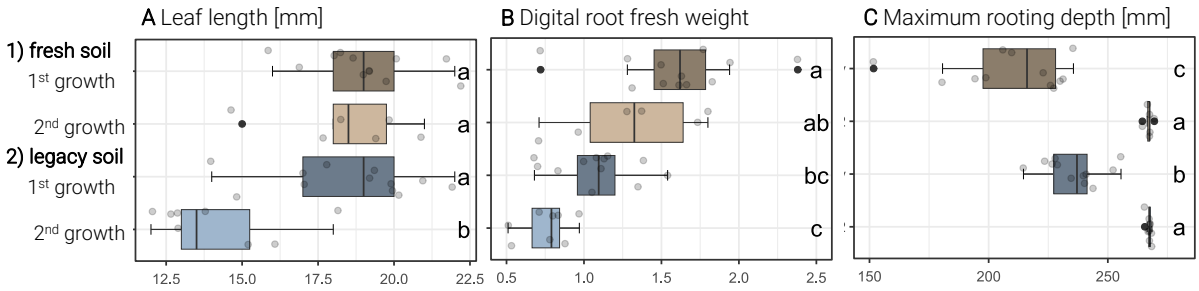

Figure 1 Effects of soil history and growth phase on plant performance. (A) Leaf length [mm], (B) digital root fresh weight and (C) maximum rooting depth [mm] of plants grown in 1) fresh soil (no maize history) and 2) legacy soil (four years of maize cultivation) during the two successive growth phases. Leaf length was measured from the shoot base to the tip of the longest leaf and root characteristics were assessed using MRI imaging. Different letters indicate statistically significant differences (Tukey's HSD $p < 0.05$). Each point represents a single plant replicate.

3.2 Root decay transiently lowers pathogen diversity

The α-diversity patterns of the different microbial groups showed contrasting responses to root decomposition, in both fresh soil and legacy soil, reflecting their distinct ecological strategies and trophic positions. Fungal and oomycete communities, including taxa from pathogen-rich lineages such as Hypocreales and *Pythium* (Fig. SI 4), exhibited similar patterns of transiently reduced OTU richness during the decomposition phase (Figure 2). For fungi, this reduction was statistically significant in fresh soil (ANOVA $F_{(5,64)} = 6.02$, $p < 0.001$) and was accompanied dominance of specific taxa reflected by strongly reduced evenness (Hill #2), and resulting in overall reduced diversity (Hill #1) (Fig. SI 5). The reduction of oomycete richness occurred in legacy soil (ANOVA: $F_{(5,204)} = 7.00$, $p < 0.001$), while their Hill #1 and Hill #2 values remained unchanged, indicating that the decline concerned mainly low-abundance taxa rather than the dominant community members (Fig. SI 5).

Obligate biotrophic Phytomyxea showed a contrasting response pattern. Phytomyxea richness increased during decomposition in fresh soil (ANOVA: $F_{(5,196)} = 7.35$, $p < 0.001$) and remained elevated in the *second growth* phase, whereas legacy soil showed no significant changes across phases. The Evenness (Hill #2) remained unaffected by the growth phase, indicating that the diversity (Hill #1) increase after decomposition was mainly due to the increased OTU richness (Fig. SI 5).

Also, Cercozoan richness peaked during the *decay phase* in both soil history types (ANOVA: $F_{(5,65)} = 5.69$, $p < 0.001$), but diversity and evenness remained unaffected (Fig. SI 5). The increase of cercozoan consumer richness was particularly pronounced among the less abundant Cercozoan orders Cryptofilida, Marmimonadida, and Imbricatea (K.-W. on relative abundance, all $p<0.01$; Dunn's post-hoc, all $p<0.03$), indicating that decomposition creates opportunities for subordinate taxa to flourish.

This rise in cercozoan consumer richness during decay coincided with increased bacterial evenness (Hill #2) and marginally increased OTU richness ($p= 0.09$), resulting in significantly increased diversity after decay (Figure 2, Fig. SI 5).

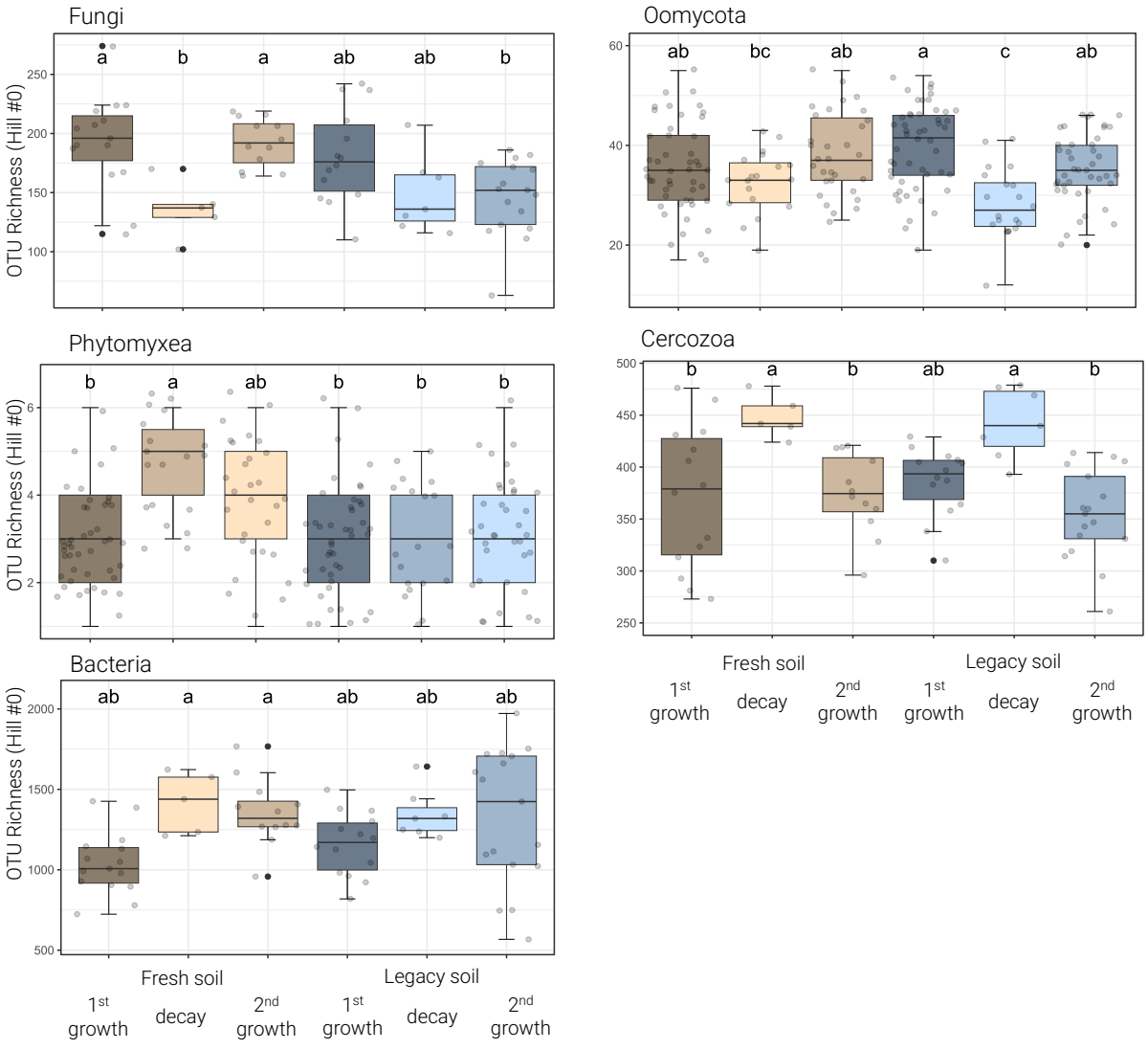

Figure 2 Shifts in rhizosphere species richness following root decomposition. Boxplots with OTU richness (Hill #0) of fungi, Oomycota, Phytomyxea, Cercozoa and bacteria. Different letters indicate significant differences (Tukey's HSD).

3.3 Root decay and soil legacy jointly reshape community composition

The rhizosphere microbiome underwent significant community shifts as it transitioned through the succession of root growth, decay, and regrowth phases, with patterns that differed between fresh soil and legacy soil. During the *first growth* phase, plants assembled distinct rhizosphere communities in both soil types, creating a characteristic living root-associated microbiome (Figure 3). This living rhizosphere effect was evident across all microbial groups studied— fungi, Oomycota, Phytomyxea, Cercozoa and bacteria —demonstrating the influence of living roots on

microbial community assembly. However, communities in legacy soil were always distinct from those in fresh soil (Table 1), demonstrating the influence of previous cropping history.

After the decay of roots, the rhizosphere microbiomes had shifted towards specific decomposer communities. This transition was particularly pronounced among primary decomposers (fungi, bacteria) and their consumers (Cercozoa) (Table 1). The magnitude of this shift varied by taxonomic group, with bacteria showing the strongest response to phase transitions (R^2 = 0.499), followed by Cercozoa (R^2 = 0.334) and fungi (R^2 = 0.299, see Table 1).

When new roots colonized the soil during the *second growth* phase, they encountered a microbial environment still bearing the legacy of decomposer communities. Rather than reverting completely to the original rhizosphere composition, *second growth* phase root communities maintained significant differences from *first growth* phase communities (Table 1). Microbial communities developing inside pre-existing biopores in both soil types showed remarkably higher variability than those colonizing adjacent mineral soil, particularly bacteria (β-dispersion: F = 5.19, p < 0.001) and Cercozoa (β-dispersion: F = 5.63, p < 0.001, Figure 3). The obligate pathogenic Phytomyxea showed a clear succession from root microbiome to decomposer communities in legacy soil, but in fresh soil their composition remained unchanged across growth phases (β-dispersion: F = 0.365, p = 0.696). Oomycota were the least affected by soil history (R2 = 0.085, see Table 1), only in fresh soil their communities diverged during decay and partly shifted back during regrowth, whereas in legacy soil no significant community change across growth phases occurred.

Table 1 PERMANOVA, Bray-Curtis dissimilarity - Effects of soil history and growth and decay phases on beta diversity. Separate models were run for each microbial group. Variance explained (R^2), and p-value for the effect of soil history and the interaction term soil history × growth/decay phase.

Group	**~ soil history**			**~ soil history * phase**		
	R^2	F	p-value	R^2	F	p-value
Fungi	0.169	4.473	0.001	0.299	5.451	0.001
Bacteria	0.239	6.900	0.001	0.499	12.730	0.001
Cercozoa	0.151	3.906	0.001	0.334	6.416	0.001
Phytomyxea	0.167	4.345	0.001	0.222	3.588	0.001
Oomycota	0.085	2.041	0.005	0.145	2.164	0.001

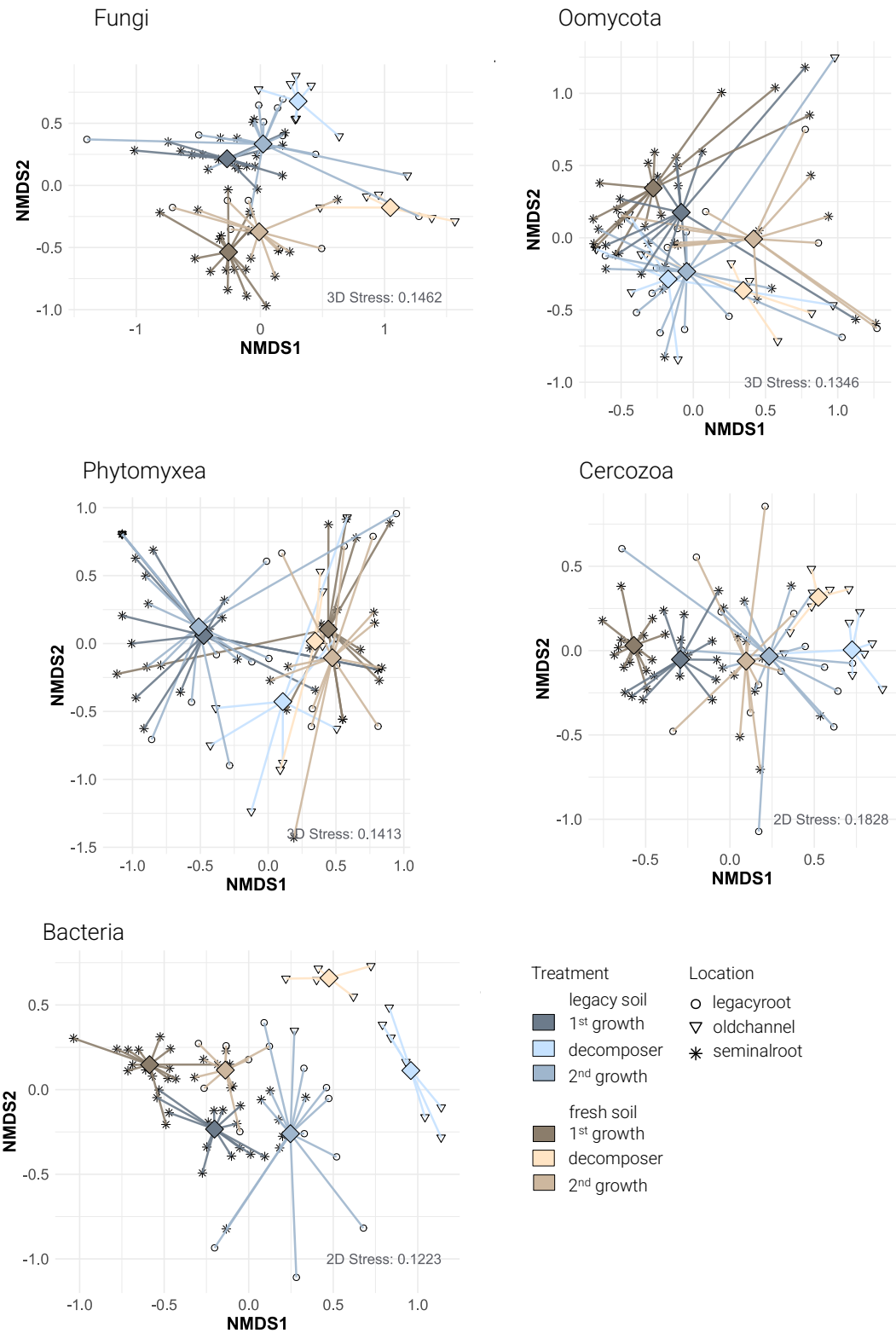

Figure 3 Shifts in community composition: Non-metric multidimensional scaling (NMDS) plots of Bray Curtis diversity for fungi, Oomycota, Phytomyxea, Cercozoa and bacteria. Each data point represents one sample, with different shapes indicating sampling locations. Spider plots connect samples within each phase for the respective soil history (fresh vs. legacy).

3.4 Decomposer legacy redirects second-phase microbiome assembly

The decomposition of roots created lasting microbial legacies that influenced community assembly in the *second growth* phase, with effects that varied by microbial group and soil history. Analysis of the most influential taxa for the NMDS fit and phase-specific responders revealed consistent patterns of succession across the growth-decay-regrowth cycle (Fig. SI 7). For fungi, saprotrophic Ascomycota lineages increased significantly after root decay. Oomycete responses were particularly distinctive, DESeq2 agreed with the relative abundances, both reporting a strong increase of *Myzocytopsis lenticularis* and *Lagenidium* spp. during decay, especially in legacy soil. Cercozoan succession patterns revealed complex trophic interactions, with different flagellate and amoeboid taxa increasing during specific phases of the growth-decay cycle. Notably, sandonid flagellates flourished on living roots in legacy soil, while *Thaumatomonas* species proliferated on decomposed roots in legacy soil and *Neuromorpha vorax* dominated decomposed roots in fresh soil. Across both soil histories *Paracercomonas metabolicus* was identified as the most consistent responder in the *decay phase* by indicator-taxa analysis (DESeq2). Bacterial succession was characterized by a shift from fast-growing copiotrophs like *Pseudomonas* during active root growth to specialized decomposers such as the Actinomycete *Sporichthya* during decay.

3.5 Core taxa persist, with limited phase-specific turnover

Despite the substantial community shifts observed across growth and decomposition phases, a significant proportion of microbial taxa persisted throughout the experiment, forming a stable core microbiome in both fresh soil and legacy soil. Bacteria and fungi showed similar patterns of core community structure, with approximately 32.5 % and 26% of their total OTUs, respectively, being shared across all phases and sampling locations (Fig. SI 6). These core taxa were countered by substantial phase-specific diversity, particularly along free-growing seminal roots during the *first growth* phase, which harboured about 13% of bacterial and 20 % of fungal OTUs exclusively. In contrast, Oomycota, Phytomyxea and Cercozoa exhibited much larger core microbiomes, with 63 %, 75 % and 81.5 % of their OTUs, respectively, being shared across all rhizosphere samples regardless of phase. Despite this overall stability, our MRI-guided sampling approach revealed specialized ecological niches within these groups. Remarkably, 12.5 % of oomycete OTUs and only 1.6 % of cercozoan OTUs were exclusively associated with living roots across both growth phases, underscoring oomycetes roles as potential plant pathogens, while cercozoan are consumers. Conversely, a small proportion of "strict decomposer" OTUs (2.5 % in Oomycota and 1 % in Cercozoa) occurred exclusively in decayed biopores.

4 Discussion

4.1 Biological legacies restrict growth and increase microbial heterogeneity

Biological legacy from four seasons of monoculture maize (legacy soil), as well as the biological and physical legacies that were already established during one growth phase, altered plant performance (Figure 1). Plants grown in legacy soil consistently developed smaller root systems, but roots grew deeper (Figure 1B-C). During the *second growth* phase, which received no additional fertiliser, plants in legacy soil displayed an expected reduction in shoot performance, evidenced by shorter leaves and lower SPAD values (Figure 1A, Fig. SI 1). This outcome reinforces our first research question, showing that the biological legacy accumulated in legacy soil increasingly constrained plant growth, especially when external nutrient inputs were withheld. As root systems in both soil history types reached the bottom of the column during the regrowth phase (Figure 1C), a physical legacy effect through biopores facilitating deeper root growth was observed. Accordingly, biopore recycling emerged as a shared trait independent of soil history, underlining biopore recycling as a key mechanism by which root systems in both soils achieved deeper rooting, as discussed below.

4.2 Biopore recycling: Reused biopores guide deep rooting

Clear separation of living and residual roots in the MRI scans enabled in-situ quantification of newly elongated roots (Fig. SI 3). We found that 10 % of biopores were reused by new roots in the *second growth* phase, corresponding to approximately 20% of all roots developed in this phase, consistent to previous reports (Nakamoto 1997, Athmann et al. 2013, Han et al. 2017). Our approach revealed how biopores can act as 'root highways' (Passioura 2002), providing zones of low penetration resistance and rapid routes for deeper soil exploration (Figure 1C). Beyond facilitating root penetration and potentially influencing nutrient uptake, microbial biomass in the rhizosphere is typically higher than in the surrounding undisturbed soil matrix (Alphei et al. 1996, Vinther 1999, Pankhurst 2002). These coevolved rhizosphere communities contain beneficial (e.g., PGPB or mycorrhizal fungi) or detrimental (e.g., pathogens) microorganisms whose propagules persist even after root death. As the rhizosphere microbiome transitioned from active root growth to decay and subsequent root system regrowth, these microbial communities responded dynamically to changing qualities of C inputs and structural niches. This broader interplay between root legacies and microbial communities set the stage for the following patterns of microbial succession.

4.3 Microbiome succession was cyclical but not fully reversible

The living plant co-organizes its own rhizosphere microbiome by favouring certain taxa and inhibiting others (Bais et al. 2006, Rüger et al. 2021, Yim et al. 2022, Rüger et al. 2023, He et al. 2024), but shoot harvest and subsequent root death initiate decomposition processes. This transfer alters key parameters for microbial growth and community organization, especially concerning changes in the quality and availability of carbon and nutrients (Personeni and Loiseau 2004, Bauke et al. 2017, Pan et al. 2023). This resulted in a general shift in rhizosphere composition across all microbial groups between the growth phases (Figure 3). It corresponded to transitions from rhizosphere microbiomes developed during the *first growth* phase to distinct decomposer communities during root decay, as reported for decay of plant litter (Bastian et al. 2009, Esperschütz et al. 2013). In particular, the results of the present study provide new evidence that although root-growth-associated microbiomes reassemble during plant growth following root decay, the rhizosphere microbiome of a subsequent plant still bears a distinctive signature of the preceding decomposer community. Thus root decomposition marked a clear inflection point in rhizosphere community composition, as shown by our alpha and beta diversity metrics (Figure 2, Figure 3, Fig. SI 5). Fungal and oomycete alpha diversity declined after root decay and only partially recovered during the *second growth* phase (Figure 2). Since most fungi as well as hemibiotrophic oomycetes are opportunistic saprophytes (Ballhausen and de Boer 2016, Rodenburg et al. 2024), this likely reflects priority effects and pre-emptive competition on decomposing roots, where the first colonizer occupies most resources, effectively preventing other species from establishing. As these opportunistic taxa thrived during the decay phase, they may have gained a competitive advantage when root growth resumed, which in some cases could have hindered the full restoration of the original community.

The high amount of easily available carbon sources in the rhizosphere favours copiotrophs, causing sharp declines in bacterial richness as compared to bulk soil (Bonkowski et al. 2021). Roots in contrast are a poor resource for decomposers (Bertrand et al. 2006), but offer a wider variety of resource qualities that likely provide more niches for a broader diversity of taxa (Machinet et al. 2009). Thus, Cercozoan OTU richness increased following root decay but declined again during the subsequent regrowth phase (Figure 2). This temporary rise in richness likely reflects a response to the temporal variability in the availability and composition of prey and decomposing root material.

Cercozoa encompass a range of trophic strategies (Dumack et al. 2020), with different species exhibiting the capacity to consume specific microbial taxa at successive stages of root decay. Communities of bacterivorous cercozoa often closely match the diversity of bacterial rhizosphere

microbiomes, suggesting that these communities can adapt quickly to changes in their bacterial food sources (Dumack et al. 2022). As root regrowth progressed, the microbial niche likely shifted back toward taxa associated with living roots, resulting in reduced diversity. Although bacterial OTU richness showed only a marginal increase during decay (Fig. SI 4, Figure 2), both Shannon and Simpson-based Hill numbers increased significantly after decay (Fig. SI 5). This indicates that while few new taxa appeared, the community became more evenly structured, with reduced dominance. Such reorganisation reflects the metabolic flexibility and competitive–cooperative interactions of bacterial communities (Freilich et al. 2011), enabling them to rapidly adapt to decomposition by balancing abundances among taxa.

Most OTUs persisted throughout all phases, resulting in a robust core microbiome, as demonstrated by the overlap in the Venn diagrams (Fig. SI 6). Consequently, phase-related diversity shifts were primarily driven by changes in relative abundance rather than by significant gains or losses of OTUs. By contrast, the cores of fungi and bacteria were smaller indicating that their community structure is more sensitive to host availability and resource fluctuations. Hence, while higher trophic levels and potential pathogens adapted to environmental fluctuations by adjusting proportions within a common core, fungi and bacteria underwent more fundamental changes in OTU membership.

Communities in the *decay phase* clustered separately from the growth phase communities (Figure 3), which confirms substantial microbial community turnover and supports the hypothesis that root decomposition promotes a community distinct from the microbiome associated with living plant roots. The decay period creates a short-lived “window of opportunity” in which opportunistic saprotrophs and low-abundance copiotrophs (r-strategists) bloom in response to the change in the quality and availability of organic substrates (Fierer et al. 2007, Bastian et al. 2009). During subsequent regrowth, the fungal, Phytomyxea, Cercozoa and bacterial communities largely returned to their original structures. However, oomycete assemblages were only partially recovered, with a significant proportion being obligate host-dependent specialists, as Venn diagram analysis showed that 12.5 % of oomycete OTUs rely on living roots for maintenance, creating a diversity bottleneck (Fig. SI 6). The lack of living roots and shifts in substrate quality during decay appears to grant opportunistic taxa a lasting competitive edge, partially hindering the full reassembly of the original community once plant growth resumes. Collectively, these patterns indicate that legacy-induced microbial networks drive a cyclical, yet not fully reversible, succession in the maize rhizosphere.

Despite these clear overall patterns, soil history modulated both the intensity and trajectory of microbial succession and plant root development (Figure 3). Dispersion of beta diversity was

significantly higher in legacy soils during regrowth for bacteria and cercozoans, implying more heterogeneous or unpredictable regrowth patterns. Thus, legacy soil, already conditioned by repeated maize monoculture, appears to introduce significant variability after decay, thereby reducing the host specificity of rhizosphere microbiomes.

According to community-selection theory (Goodnight 2011) and recent experimental evidence in maize (Rüger et al. 2021, Schultes et al. in review), the individual microbiomes of single roots within the root system differ in species composition, and consequently selection acts at the level of many semi-independent sub-communities. Across both soils, phase-specific OTUs appeared in distinct root zones—for example, the 1 % of cercozoan "strict decomposer associated taxa" confined to decaying biopores and the 12.5 % of oomycete OTUs found exclusively on living roots. These patch-restricted taxa show that the fitness and traits of an individual microbe can become a function of community membership (Goodnight et al. 1992, Weidner et al. 2015). In the *second growth* phase, the mosaic of root-patch legacies meant that each biopore inherited a slightly different inoculum, widening dispersion of beta diversity and introducing substantially increased variability in consecutive bacterial and cercozoan rhizosphere microbiomes. Together, these highly heterogeneous root-patch legacies explain how a stable core microbiome can coexist alongside the phase-specific turnover and heightened variability observed in legacy soil. Especially in legacy soil, the coupling of reduced plant performance (Figure 1) with this microbial succession could point to a feedback loop between plant development and community dynamics—a loop driven not only by biological history and resource exploitation but also by the biopore network that links past root systems to future growth cycles.

4.4 Conclusion

This study shows that biological legacy from four seasons of continuous maize and the physical legacy of pre-existing biopores jointly determine both plant performance and rhizosphere assembly. Plants grown in legacy soil formed smaller root systems. 10 % of biopores were reused by new roots, exploiting them as low-resistance pathways for deeper rooting. Microbial communities followed a reproducible but incomplete growth → decay → regrowth loop: root-associated consortia shifted to decomposer dominance after root death and only partly re-assembled during the *second growth* phase, leaving (i) a persistent core of ≥ 63 % of cercozoan and oomycete OTUs, (ii) zone-restricted groups such as saprotrophic fungi confined to decayed biopores and oomycetes restricted to living roots, and (iii) a metabolically flexible bacterial community whose membership turned over between rhizosphere and decay. In legacy soil, this mosaic of root-patch legacies enlarged the dispersion of beta diversity during regrowth, producing greater heterogeneity within cercozoan and bacterial microbiomes, and coinciding with a

reduction in root growth. Together, the data demonstrate a feedback loop in which past crop history shapes the spatial inoculum (biopores plus microbial patches), which in turn modulates current plant vigour and further sculpts the rhizosphere.

5 Acknowledgements

We thank Merle Noschinski-Reetz for her technical support. This project was carried out in the framework of the priority programme 2089 “Rhizosphere spatiotemporal organization – a key to rhizosphere functions” funded by the Deutsche Forschungsgemeinschaft (project numbers 403635931 and 403637614).

6 Conflict of interest statement

None declared.

7 Author contributions

DN, CK, and RK and MB planned and designed the research. DN, DP, DD, AH and AW performed the experiments. DN, DP, AH and AW analysed and interpreted the data. DN and MB wrote the manuscript. DN, CK, RK and MB revised the manuscript.

8 Data availability statement

The data that support the findings of this study are available from the corresponding author upon request.

9 References

Abarenkov, K., R. H. Nilsson, K.-H. Larsson, Andy F. S. Taylor, Tom W. May, T. G. Frøslev, J. Pawlowska, B. Lindahl, K. Põldmaa, C. Truong, D. Vu, T. Hosoya, T. Niskanen, T. Piirmann, F. Ivanov, A. Zirk, M. Peterson, Tanya E. Cheeke, Y. Ishigami, Arnold T. Jansson, Thomas S. Jeppesen, E. Kristiansson, V. Mikryukov, Joseph T. Miller, R. Oono, Francisco J. Ossandon, J. Paupério, I. Saar, D. Schigel, A. Suija, L. Tedersoo, and U. Kõljalg. 2024. The UNITE database for molecular identification and taxonomic communication of fungi and other eukaryotes: sequences, taxa and classifications reconsidered. Nucleic Acids Research 52:D791-D797.

Alphei, J., M. Bonkowski, and S. Scheu. 1996. Protozoa, Nematoda and Lumbricidae in the rhizosphere of Hordelymus europaeus (Poaceae): Faunal interactions, response of microorganisms and effects on plant growth. Oecologia 106:111-126.

Athmann, M., T. Kautz, R. Pude, and U. Köpke. 2013. Root growth in biopores—evaluation with in situ endoscopy. Plant and Soil 371:179-190.

Bais, H. P., T. L. Weir, L. G. Perry, S. Gilroy, and J. M. Vivanco. 2006. The role of root exudates in rhizosphere interactions with plants and other organisms. Annual Review of Plant Biology 57:233-266.

Ballhausen, M.-B., and W. de Boer. 2016. The sapro-rhizosphere: Carbon flow from saprotrophic fungi into fungus-feeding bacteria. Soil Biology and Biochemistry 102:14-17.

Bastian, F., L. Bouziri, B. Nicolardot, and L. Ranjard. 2009. Impact of wheat straw decomposition on successional patterns of soil microbial community structure. Soil Biology and Biochemistry 41:262-275.

Bauke, S. L., M. Landl, M. Koch, D. Hofmann, K. A. Nagel, N. Siebers, A. Schnepf, and W. Amelung. 2017. Macropore effects on phosphorus acquisition by wheat roots – a rhizotron study. Plant and Soil 416:67-82.

Berg, G., and K. Smalla. 2009. Plant species and soil type cooperatively shape the structure and function of microbial communities in the rhizosphere. FEMS Microbiology Ecology 68.

Bertrand, I., B. Chabbert, B. Kurek, and S. Recous. 2006. Can the Biochemical Features and Histology of Wheat Residues Explain their Decomposition in Soil? Plant and Soil 281:291-307.

Bever, J. D. 1994. Feeback between plants and their soil communities in an old field community. Ecology 75.7:1965-1977.

Bever, J. D., T. G. Platt, and E. R. Morton. 2012. Microbial population and community dynamics on plant roots and their feedbacks on plant communities. Annual Review of Microbiology 66:265-283.

Bolyen, E., J. R. Rideout, M. R. Dillon, N. A. Bokulich, C. C. Abnet, G. A. Al-Ghalith, H. Alexander, E. J. Alm, M. Arumugam, F. Asnicar, Y. Bai, J. E. Bisanz, K. Bittinger, A. Brejnrod, C. J. Brislawn, C. T. Brown, B. J. Callahan, A. M. Caraballo-Rodríguez, J. Chase, E. K. Cope, R. Da Silva, C. Diener, P. C. Dorrestein, G. M. Douglas, D. M. Durall, C. Duvallet, C. F. Edwardson, M. Ernst, M. Estaki, J. Fouquier, J. M. Gauglitz, S. M. Gibbons, D. L. Gibson, A. Gonzalez, K. Gorlick, J. Guo, B. Hillmann, S. Holmes, H. Holste, C. Huttenhower, G. A. Huttley, S. Janssen, A. K. Jarmusch, L. Jiang, B. D. Kaehler, K. B. Kang, C. R. Keefe, P. Keim, S. T. Kelley, D. Knights, I. Koester, T. Kosciolek, J. Kreps, M. G. I. Langille, J. Lee, R. Ley, Y.-X. Liu, E. Loftfield, C. Lozupone, M. Maher, C. Marotz, B. D. Martin, D. McDonald, L. J. McIver, A. V. Melnik, J. L. Metcalf, S. C. Morgan, J. T. Morton, A. T. Naimey, J. A. Navas-Molina, L. F. Nothias, S. B. Orchanian, T. Pearson, S. L. Peoples, D. Petras, M. L. Preuss, E. Pruesse, L. B. Rasmussen, A. Rivers, M. S. Robeson, P. Rosenthal, N. Segata, M. Shaffer, A. Shiffer, R. Sinha, S. J. Song, J. R. Spear, A. D. Swafford, L. R. Thompson, P. J. Torres, P. Trinh, A. Tripathi, P. J. Turnbaugh, S. Ul-Hasan, J. J. J. van der Hooft, F. Vargas, Y. Vázquez-Baeza, E. Vogtmann, M. von Hippel, W. Walters, Y. Wan, M. Wang, J. Warren, K. C. Weber, C. H. D. Williamson, A. D. Willis, Z. Z. Xu, J. R. Zaneveld, Y. Zhang, Q. Zhu, R. Knight, and J. G. Caporaso. 2019. Reproducible, interactive, scalable and extensible microbiome data science using QIIME 2. Nature Biotechnology 37:852-857.

Bonkowski, M., M. Tarkka, B. S. Razavi, H. Schmidt, E. Blagodatskaya, R. Koller, P. Yu, C. Knief, F. Hochholdinger, and D. Vetterlein. 2021. Spatiotemporal Dynamics of Maize (Zea mays L.) Root Growth and Its Potential Consequences for the Assembly of the Rhizosphere Microbiota. Front Microbiol 12:619499.

Callahan, B. J., P. J. McMurdie, M. J. Rosen, A. W. Han, A. J. A. Johnson, and S. P. Holmes. 2016. DADA2: High-resolution sample inference from Illumina amplicon data. Nature Methods 13:581-583.

Camacho, C., G. Coulouris, V. Avagyan, N. Ma, J. Papadopoulos, K. Bealer, and e. al. 2009. BLAST+: architecture and applications. . BMC Bioinformatics 10:421.

Caporaso, J. G., C. L. Lauber, W. A. Walters, D. Berg-Lyons, C. A. Lozupone, P. J. Turnbaugh, N. Fierer, and R. Knight. 2011. Global patterns of 16S rRNA diversity at a depth of millions of sequences per sample. Proceedings of the National Academy of Sciences 108:4516-4522.

Chao, A., C.-H. Chiu, and L. Jost. 2014. Unifying Species Diversity, Phylogenetic Diversity, Functional Diversity, and Related Similarity and Differentiation Measures Through Hill Numbers. Annual Review of Ecology, Evolution, and Systematics 45:297-324.

Chen, H. 2022. VennDiagram: Generate High-Resolution Venn and Euler Plots. R package version 1.7.3.

de Mendiburu, F. 2023. agricolae: Statistical Procedures for Agricultural Research. R package version 1.3-7.

Dumack, K., K. Feng, S. Flues, M. Sapp, S. Schreiter, R. Grosch, L. E. Rose, Y. Deng, K. Smalla, and M. Bonkowski. 2022. What Drives the Assembly of Plant-associated Protist Microbiomes? Investigating the Effects of Crop Species, Soil Type and Bacterial Microbiomes. Protist 173.

Dumack, K., A. M. Fiore-Donno, D. Bass, and M. Bonkowski. 2020. Making sense of environmental sequencing data: Ecologically important functional traits of the protistan groups Cercozoa and Endomyxa (Rhizaria). Mol Ecol Resour 20:398-403.

Edgar, R. C., B. J. Haas, J. C. Clemente, C. Quince, and R. Knight. 2011. UCHIME improves sensitivity and speed of chimera detection. Bioinformatics 27:2194-2200.

Ehlers, W., U. Köpke, F. Hesse, and W. Böhm. 1983. Penetration resistance and root growth of oats in tilled and untilled loess soil. Soil and Tillage Research 3:261-275.

Eissenstat, D. M., and R. D. Yanai. 1997. The Ecology of Root Lifespan. In: M Begon, AH Fitter (eds) Advances in Ecological Research. Academic Press.

Esperschütz, J., C. Zimmermann, A. Dümig, G. Welzl, F. Buegger, M. Elmer, J. C. Munch, and M. Schloter. 2013. Dynamics of microbial communities during decomposition of litter from pioneering plants in initial soil ecosystems. Biogeosciences 10:5115-5124.

Fierer, N., M. A. Bradford, and R. B. Jackson. 2007. Toward an ecological classification of soil bacteria. Ecology 88:1354-1364.

Fiore-Donno, A. M., and M. Bonkowski. 2020. Different community compositions between obligate and facultative oomycete plant parasites in a landscape-scale metabarcoding survey. Biology and Fertility of Soils 57:245-256.

Fiore-Donno, A. M., T. Richter-Heitmann, and M. Bonkowski. 2020. Contrasting Responses of Protistan Plant Parasites and Phagotrophs to Ecosystems, Land Management and Soil Properties. Front Microbiol 11:1823.

Fiore-Donno, A. M., C. Rixen, M. Rippin, K. Glaser, E. Samolov, U. Karsten, B. Becker, and M. Bonkowski. 2018. New barcoded primers for efficient retrieval of cercozoan sequences in high-throughput environmental diversity surveys, with emphasis on worldwide biological soil crusts. Mol Ecol Resour 18:229-239.

Fox, J., and S. Weisberg. 2019. An R Companion to Applied Regression, Third edition. Sage, Thousand Oaks CA.

Freilich, S., R. Zarecki, O. Eilam, E. S. Segal, C. S. Henry, M. Kupiec, U. Gophna, R. Sharan, and E. Ruppin. 2011. Competitive and cooperative metabolic interactions in bacterial communities. Nat Commun 2:589.

Friman, V. P., A. Jousset, and A. Buckling. 2013. Rapid prey evolution can alter the structure of predator–prey communities. Journal of Evolutionary Biology 27:374-380.

Frindte, K., S. A. Zoche, and C. Knief. 2020. Development of a Distinct Microbial Community Upon First Season Crop Change in Soils of Long-Term Managed Maize and Rice Fields. Front Microbiol 11.

Frouz, J. 2024. Plant-soil feedback across spatiotemporal scales from immediate effects to legacy. Soil Biology and Biochemistry 189:109289.

Gardes, M., and T. D. Bruns. 1993. ITS primers with enhanced specificity for basidiomycetes - application to the identification of mycorrhizae and rusts. Molecular Ecology 2:113-118.

Goodnight, C. J. 2011. Evolution in metacommunities. Philos Trans R Soc Lond B Biol Sci 366:1401-1409.

Goodnight, C. J., J. M. Schwartz, and L. Stevens. 1992. Contextual analysis of models of group selection, soft selection, hard selection, and the evolution of altruism. American Naturalist:743-761.

Greenacre, M. 2021. Compositional data analysis. Annual Review of Statistics and Its Application 8:271-299.

Gross, J., and U. Ligges. 2015. nortest: Tests for Normality. R package version 1.0-4.

Guillou, L., D. Bachar, S. Audic, D. Bass, C. Berney, L. Bittner, and e. al. 2013. The protist ribosomal reference database (PR2): a catalog of unicellular eukaryote small sub-unit rRNA sequences with curated taxonomy. Nucleic Acids Research 41.

Gundale, M. J., and P. Kardol. 2021. Multi-dimensionality as a path forward in plant-soil feedback research. . Journal of Ecology 109:3446-3465.

Han, E., T. Kautz, N. Huang, and U. Köpke. 2017. Dynamics of plant nutrient uptake as affected by biopore-associated root growth in arable subsoil. Plant and Soil 415:145-160.

Hannula, S. E., R. Heinen, M. Huberty, K. Steinauer, J. R. De Long, R. Jongen, and T. M. Bezemer. 2021. Persistence of plant-mediated microbial soil legacy effects in soil and inside roots. . Nat Commun 12.

Hartmann, A., M. Schmid, D. van Tuinen, and G. Berg. 2009. Plant-driven selection of microbes. Plant and Soil 321:235-257.

He, X., D. Wang, Y. Jiang, M. Li, M. Delgado-Baquerizo, C. McLaughlin, C. Marcon, L. Guo, M. Baer, Y. A. T. Moya, N. von Wiren, M. Deichmann, G. Schaaf, H. P. Piepho, Z. Yang, J. Yang, B. Yim, K. Smalla, S. Goormachtig, F. T. de Vries, H. Huging, M. Baer, R. J. H. Sawers, J. C. Reif, F. Hochholdinger, X. Chen, and P. Yu. 2024. Heritable microbiome variation is correlated with source environment in locally adapted maize varieties. . Nature Plants 10:598-617.

Hu, L., C. A. M. Robert, S. Cadot, X. Zhang, M. Ye, B. Li, D. Manzo, N. Chervet, T. Steinger, M. G. A. van der Heijden, K. Schlaeppi, and M. Erb. 2018. Root exudate metabolites drive plant-soil feedbacks on growth and defense by shaping the rhizosphere microbiota. Nat Commun 9:2738.

Kamoun, S., O. Furzer, J. D. G. Jones, H. S. Judelson, G. S. Ali, R. J. D. Dalio, S. G. Roy, L. Schena, A. Zambounis, F. Panabières, D. Cahill, M. Ruocco, A. Figueiredo, X.-R. Chen, J. Hulvey, R. Stam, K. Lamour, M. Gijzen, B. M. Tyler, N. J. Grünwald, M. S. Mukhtar, D. F. A. Tomé, M. Tör, G. Van Den Ackerveken, J. McDowell, F. Daayf, W. E. Fry, H. Lindqvist-Kreuze, H. J. G. Meijer, B. Petre, J. Ristaino, K. Yoshida, P. R. J. Birch, and F. Govers. 2015. The Top 10 oomycete pathogens in molecular plant pathology. Molecular Plant Pathology 16:413-434.

Kardol, P., N. J. Cornips, M. M. L. van Kempen, J. M. T. Bakx-Schotman, and v. d. P. WH. 2007. Microbe-mediated plant-soil feedback causes historical contingency effects in plant community assembly. . Ecological Monographs 77:147-162.

Kardol, P., G. B. De Deyn, E. Laliberté, P. Mariotte, and C. V. Hawkes. 2013. Biotic plant–soil feedbacks across temporal scales. Journal of Ecology 101:309-315.

Katoh, K., and D. M. Standley. 2013. MAFFT Multiple Sequence Alignment Software Version 7: Improvements in Performance and Usability. Molecular Biology and Evolution 30:772-780.

Kinkel, L. L., M. G. Bakker, and D. C. Schlatter. 2011. A coevolutionary framework for managing disease-suppressive soils. . Annual Review of Phytopathology.

Liu, C., X. Feng, Y. Xu, A. Kumar, Z. Yan, J. Zhou, Y. Yang, L. Peixoto, Z. Zeng, and H. Zang. 2023. Legume-based rotation enhances subsequent wheat yield and maintains soil carbon storage. . Agronomy for Sustainable Development.

Love, M. I., W. Huber, and S. Anders. 2014. Moderated estimation of fold change and dispersion for RNA-seq data with DESeq2. Genome Biology 15:550.

Lucas, M., S. Schluter, H. J. Vogel, and D. Vetterlein. 2019. Roots compact the surrounding soil depending on the structures they encounter. Sci Rep 9:16236.

Machinet, G. E., I. Bertrand, B. Chabbert, F. Watteau, G. Villemin, and S. Recous. 2009. Soil biodegradation of maize root residues: Interaction between chemical characteristics and the presence of colonizing micro-organisms. Soil Biology and Biochemistry 41:1253-1261.

Mao, L., Y. Liu, J. Zhang, J. Okerblad, S. Chen, and N. C. Johnson. 2021. Soil biota suppress maize growth and influence root traits under continuous monoculture. . Plant and Soil 461:441-455.

Mariotte, P., Z. Mehrabi, T. M. Bezemer, G. B. De Deyn, A. Kulmatiski, B. Drigo, G. F. C. Veen, M. G. A. van der Heijden, and P. Kardol. 2018. Plant-Soil Feedback: Bridging Natural and Agricultural Sciences. . Trends in Ecology & Evolution 33:129-142.

Martin, M. 2011. Cutadapt removes adapter sequences from high-throughput sequencing reads. EMBnet.journal; Vol 17, No 1: Next Generation Sequencing Data Analysis.

Nakamoto, T. 1997. The distribution of maize roots as influenced by artificial vertical macropores. Japanese Journal of Crop Science 66:331-332.

Neuwirth, E. 2022. RColorBrewer: ColorBrewer Palettes. R package version 1.1-3.

Ogle, D. H., J. C. Doll, A. P. Wheeler, and A. Dinno. 2025. FSA: Simple Fisheries Stock Assessment Methods. R package version 0.9.6.

Oksanen, J., G. Simpson, F. Blanchet, R. Kindt, P. Legendre, P. Minchin, R. O'Hara, P. Solymos, M. Stevens, E. Szoecs, H. Wagner, M. Barbour, M. Bedward, B. Bolker, D. Borcard, G. Carvalho, M. Chirico, M. De Caceres, S. Durand, H. Evangelista, R. FitzJohn, M. Friendly, B. Furneaux, G. Hannigan, M. Hill, L. Lahti, D. McGlinn, M. Ouellette, E. Ribeiro Cunha, T. Smith, A. Stier, C. Ter Braak, and J. Weedon. 2024. vegan: Community Ecology Package. R package version 2.6-8.

Oyserman, B. O., M. H. Medema, and J. M. Raaijmakers. 2018. Road MAPs to engineer host microbiomes. Current Opinion in Microbiology 43:46-54.

Pan, J., C. R. See, R. Wang, J. Luan, J. Wang, F. Liu, X. Quan, H. Chen, X. Wang, and C. Wang. 2023. Decoupling of nitrogen, phosphorus, and carbon release from fine and coarse roots during 7 years of decomposition. Journal of Ecology 112:348-359.

Pankhurst, C. E., Pierret, A., Hawke, B.G., Kirby, J.M. 2002. Microbiological and chemical properties of soil associated with macropores at different depths in a red-duplex soil in NSW Australia. Plant and Soil 238:11-20.

Passioura, J. B. 2002. Soil conditions and plant growth'. Plant Cell and Environment 25:311-318.

Personeni, E., and P. Loiseau. 2004. How does the nature of living and dead roots affect the residence time of carbon in the root litter continuum? Plant and Soil 267:129-141.

Petermann, J. S., A. J. F. Fergus, L. A. Turnbull, and B. Schmid. 2008. Janzen-Connell effects are widespread and strong enough to maintain diversity in grasslands. Ecology 89:2399-2406.

Quast, C., E. Pruesse, P. Yilmaz, J. Gerken, T. Schweer, P. Yarza, J. Peplies, and F. O. Glöckner. 2013. The SILVA ribosomal RNA gene database project: improved data processing and web-based tools. Nucleic Acids Research 41:D590-D596.

Rasse, D. P., and A. J. M. Smucker. 1998. Root recolonization of previous root channels in corn and alfalfa rotations. Plant and Soil 204:203-212.

Robinson, D., A. Hayes, and S. Couch. 2024. broom: Convert Statistical Objects into Tidy Tibbles. R package version 1.0.6.

Rodenburg, S. Y. A., D. de Ridder, F. Govers, and M. F. Seidl. 2024. Oomycete Metabolism Is Highly Dynamic and Reflects Lifestyle Adaptations. Mol Plant Microbe Interact 37:571-582.

Rognes, T., T. Flouri, B. Nichols, C. Quince, and F. Mahé. 2016. VSEARCH: a versatile open source tool for metagenomics. PeerJ 4 4:e2584. .

Roy, J., R. van Duijnen, E. F. Leifheit, S. Mbedi, V. M. Temperton, and M. C. Rillig. 2021. Legacy effects of pre-crop plant functional group on fungal root symbionts of barley. Ecological Applications.

Rüger, L., K. Feng, K. Dumack, J. Freudenthal, Y. Chen, R. Sun, M. Wilson, P. Yu, B. Sun, Y. Deng, F. Hochholdinger, D. Vetterlein, and M. Bonkowski. 2021. Assembly Patterns of the Rhizosphere Microbiome Along the Longitudinal Root Axis of Maize (Zea mays L.). Frontiers in Microbiology 12:614501.

Rüger, L., M. Ganther, J. Freudenthal, J. Jansa, A. Heintz-Buschart, M. T. Tarkka, and M. Bonkowski. 2023. Root cap is an important determinant of rhizosphere microbiome assembly. New Phytologist 239:1434-1448.

Schloss, P. D., S. L. Westcott, T. Ryabin, J. R. Hall, M. Hartmann, E. B. Hollister, and e. al. 2009. Introducing mothur : open-source, platform-independent, community-supported software for describing and comparing microbial communities. Applied Environmental Microbiology 75:7537-7541.

Schnepf, A., A. Carminati, M. A. Ahmed, M. Ani, P. Benard, J. Bentz, M. Bonkowski, M. Knott, D. Diehl, P. Duddek, E. Kröner, M. Javaux, M. Landl, E. Lehndorff, E. Lippold, A. Lieu, C. W. Mueller, E. Oburger, W. Otten, X. Portell, M. Phalempin, A. Prechtel, R. Schulz, J. Vanderborght, and D. Vetterlein. 2022. Linking rhizosphere processes across scales: Opinion. Plant and Soil.

Schultes, S., L. Rüger, D. Niedeggen, J. Freudenthal, K. Frindte, M. Becker, R. Metzner, D. Pflugfelder, A. Chlubek, C. Hinz, D. van Dusschoten, S. Bauke, M. Bonkowski, M. Watt, R. Koller, and C. Knief. in review. Photosynthate distribution

determines spatial patterns in the rhizosphere microbiota of the maize root system. Nature Communications manuscript ID NCOMMS-24-55118A.

Solbach, M. D., C. Albracht, K. Dumack, N. Eisenhauer, A. M. Fiore-Donno, A. Vogel, C. Wagg, and M. Bonkowski. 2025 [unpublished]. Legacies of consecutive summer droughts on soil-borne potential plant pathogenic protists and protistan consumers [Preprint].

Stirzaker, R. J., J. B. Passioura, and Y. Wilms. 1996. Soil structure and plant growth: Impact of bulk density and biopores. Plant and Soil 185.

van der Putten, W. H., R. D. Bardgett, J. D. Bever, T. M. Bezemer, B. B. Casper, T. Fukami, P. Kardol, J. N. Klironomos, A. Kulmatiski, J. A. Schweitzer, K. N. Suding, T. F. J. Van de Voorde, and D. A. Wardle. 2013. Plant–soil feedbacks: the past, the present and future challenges. Journal of Ecology 101:265-276.

van Dusschoten, D., R. Metzner, J. Kochs, J. A. Postma, D. Pflugfelder, J. Buhler, U. Schurr, and S. Jahnke. 2016. Quantitative 3D Analysis of Plant Roots Growing in Soil Using Magnetic Resonance Imaging. Plant Physiol 170:1176-1188.

Vetterlein, D., A. Carminati, I. Kögel-Knabner, G. P. Bienert, K. Smalla, E. Oburger, A. Schnepf, T. Banitz, M. T. Tarkka, and S. Schlüter. 2020. Rhizosphere Spatiotemporal Organization–A Key to Rhizosphere Functions. Frontiers in Agronomy 2.

Vetterlein, D., E. Lippold, S. Schreiter, M. Phalempin, T. Fahrenkampf, F. Hochholdinger, C. Marcon, M. Tarkka, E. Oburger, M. Ahmed, M. Javaux, and S. Schlüter. 2021. Experimental platforms for the investigation of spatiotemporal patterns in the rhizosphere—Laboratory and field scale. Journal of Plant Nutrition and Soil Science 184:35-50.

Vinther, F. P., Eiland, F., Lind, A. M., & Elsgaard, L. 1999. Microbial biomass and numbers of denitrifiers related to macropore channels in agricultural and forest soils. Soil Biology and Biochemistry 31:603-611.

Watt, M., P. Hugenholtz, R. White, and K. Vinall. 2006. Numbers and locations of native bacteria on field-grown wheat roots quantified by fluorescence in situ hybridization (FISH). Environmental Microbiology 8(5).

Weidner, S., R. Koller, E. Latz, G. Kowalchuk, M. Bonkowski, S. Scheu, and A. Jousset. 2015. Bacterial diversity amplifies nutrient-based plant-soil feedbacks. Functional Ecology.

Wendel, A. S., S. L. Bauke, W. Amelung, and C. Knief. 2022. Root-rhizosphere-soil interactions in biopores. Plant and Soil 475:253-277.

White, T. J., T. Bruns, S. J. W. T. Lee, and J. Taylor. 1990. Amplification and direct sequencing of fungal ribosomal RNA genes for phylogenetics. PCR protocols: a guide to methods and applications 18:315-322.

Wickham, H. 2007. Reshaping Data with the reshape Package. Journal of Statistical Software 21(12):1-20.

Wickham, H. 2016. ggplot2: Elegant Graphics for Data Analysis. Springer-Verlag New York.

Wickham, H. 2023. forcats: Tools for Working with Categorical Variables (Factors). R package version 1.0.0.

Wickham, H., R. François, L. Henry, K. Müller, and D. Vaughan. 2023. dplyr: A Grammar of Data Manipulation. R package version 1.1.4.

Wickham, H., D. Vaughan, and M. Girlich. 2024. tidyr: Tidy Messy Data. R package version 1.3.1.

Wu, G. L., C. Jia, Z. Huang, M. López-Vicente, and Y. Liu. 2021. Plant litter crust appear as a promising measure to combat desertification in sandy land ecosystem. CATENA 206.

Wubs, E. R. J., and T. M. Bezemer. 2018. Temporal carry-over effects in sequential plant–soil feedbacks. Oikos 127:220-229.

Yim, B., Z. Ibrahim, L. Rüger, M. Ganther, L. Maccario, S. J. Sørensen, A. Heintz-Buschart, M. T. Tarkka, D. Vetterlein, M. Bonkowski, E. Blagodatskaya, and K. Smalla. 2022. Soil texture is a stronger driver of the maize rhizosphere microbiome and extracellular enzyme activities than soil depth or the presence of root hairs. Plant and Soil.

Zhao, Y., W. Fu, C. Hu, G. Chen, Z. Xiao, Y. Chen, Z. Wang, and H. Cheng. 2021. Variation of rhizosphere microbial community in continuous mono-maize seed production. Sci Rep 11.

10 Supporting Information

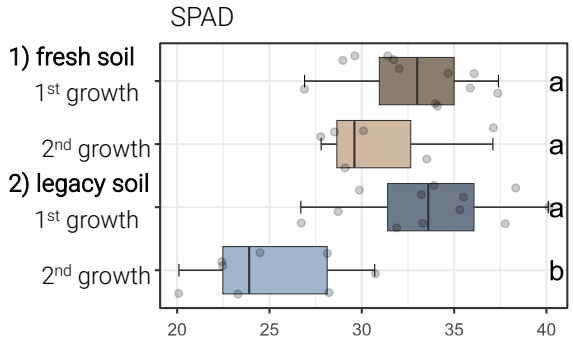

Fig. SI 1 SPAD values (chlorophyll content) in leaves across both soil histories (fresh and legacy) and growth phases (first and second growth). Boxplots show SPAD measurements taken at harvest for plants grown in fresh and legacy soils. Letters indicate statistically significant differences between treatments based on Tukey's HSD test ($p < 0.05$). Each point represents an individual plant replicate.

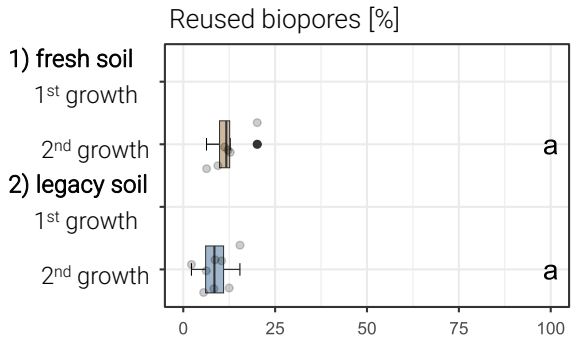

Fig. SI 2 Reuse of biopores: old root channels from the *first growth* phase during the *second growth* phase. The percentage was calculated by dividing the root length found in biopores during the *second growth* phase by the total root length measured after the *first growth* phase. Letters indicate statistically significant differences between treatments based on Tukey's HSD test ($p < 0.05$). Each point represents an individual plant replicate.

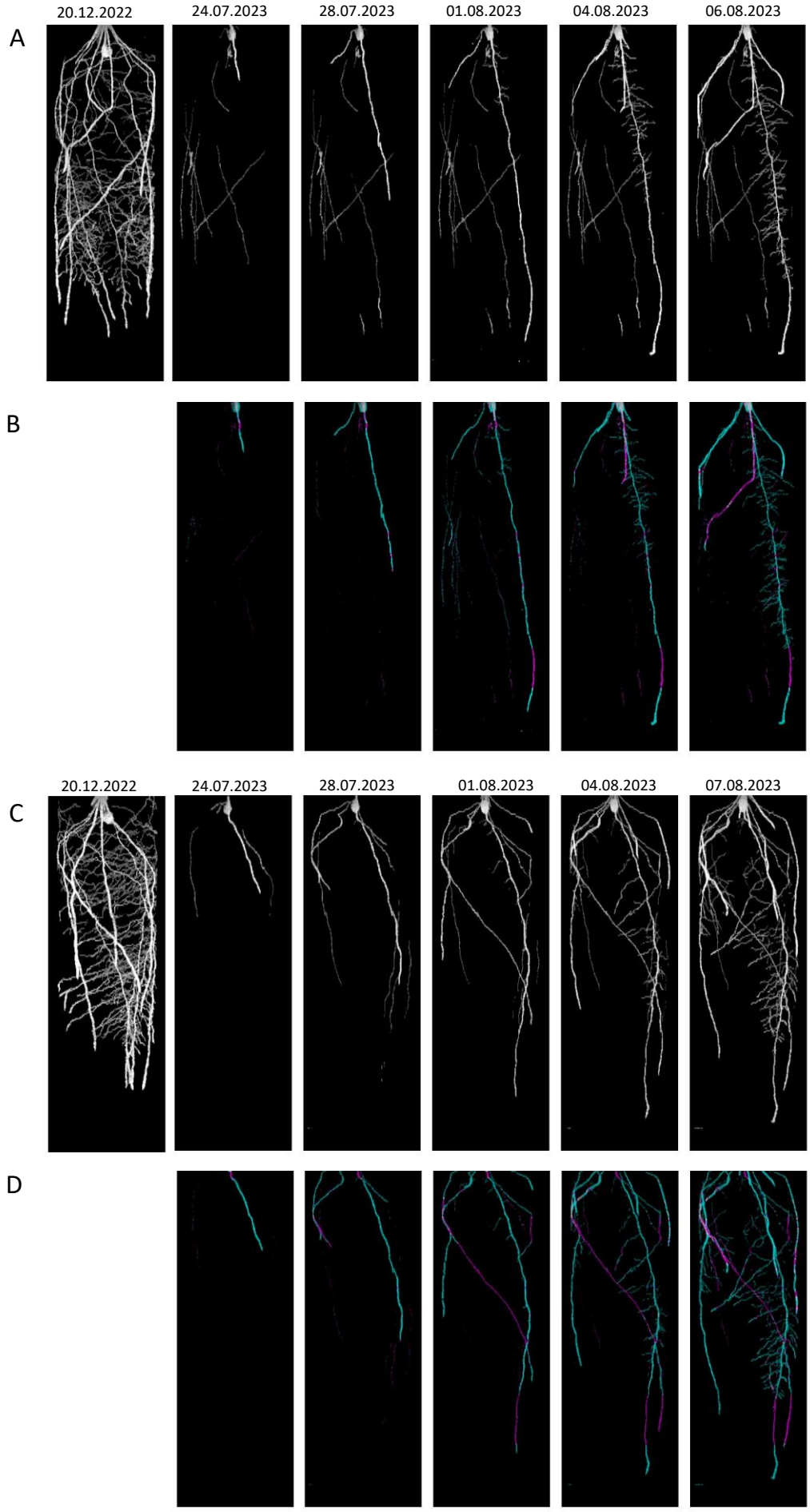
A
20.12.2022
24.07.2023
28.07.2023
01.08.2023
04.08.2023
06.08.2023
B
C
20.12.2022
24.07.2023
28.07.2023
01.08.2023
04.08.2023
07.08.2023
D

Fig. SI 3 MRI-based visualization of root decomposition and re-use in legacy and fresh soil. Panels (A) and (B) depict a soil column with legacy soil, while panels (C) and (D) represent a fresh-soil column. In each case, the first panel (A or C) shows a raw MRI scan acquired at the end of the *first growth* phase and five scans during the *second growth* phase. The second panel (B or D) overlays newly formed roots (cyan) and old root channels (pink), revealing how biopores from the *first growth* phase persist and potentially guide root development in the subsequent phase.

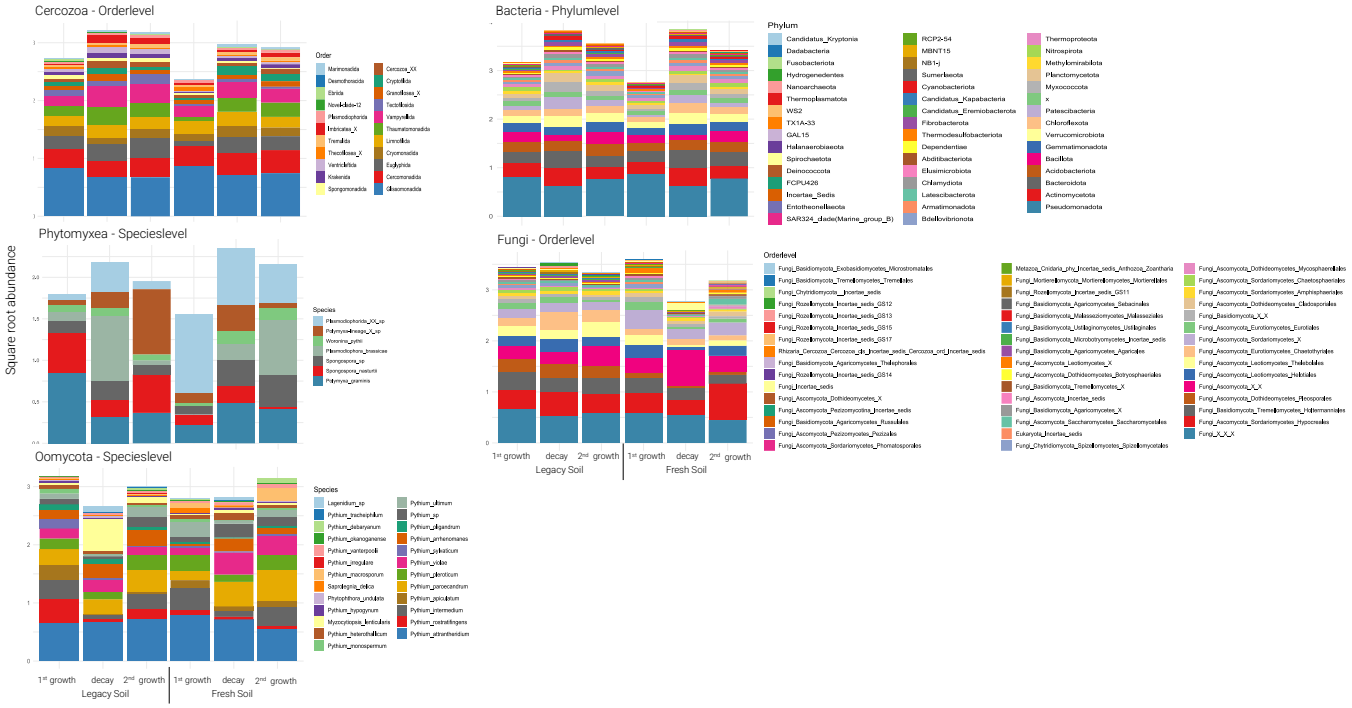

Fig. SI 4 Relative abundances of Protistan, bacterial and fungal taxa across phases. Stacked bar plots show square root transformed relative abundances of taxa at different taxonomic levels: Cercozoa (order level), Phytomyxea (species level), Oomycota (species level), Bacteria (phylum level) and Fungi (order level). Taxa are colour coded according to their respective groups. The bars are ordered by abundance within each dataset to highlight dominant and less abundant taxa. The y-axis represents relative abundance, allowing variation between phases to be visualised.

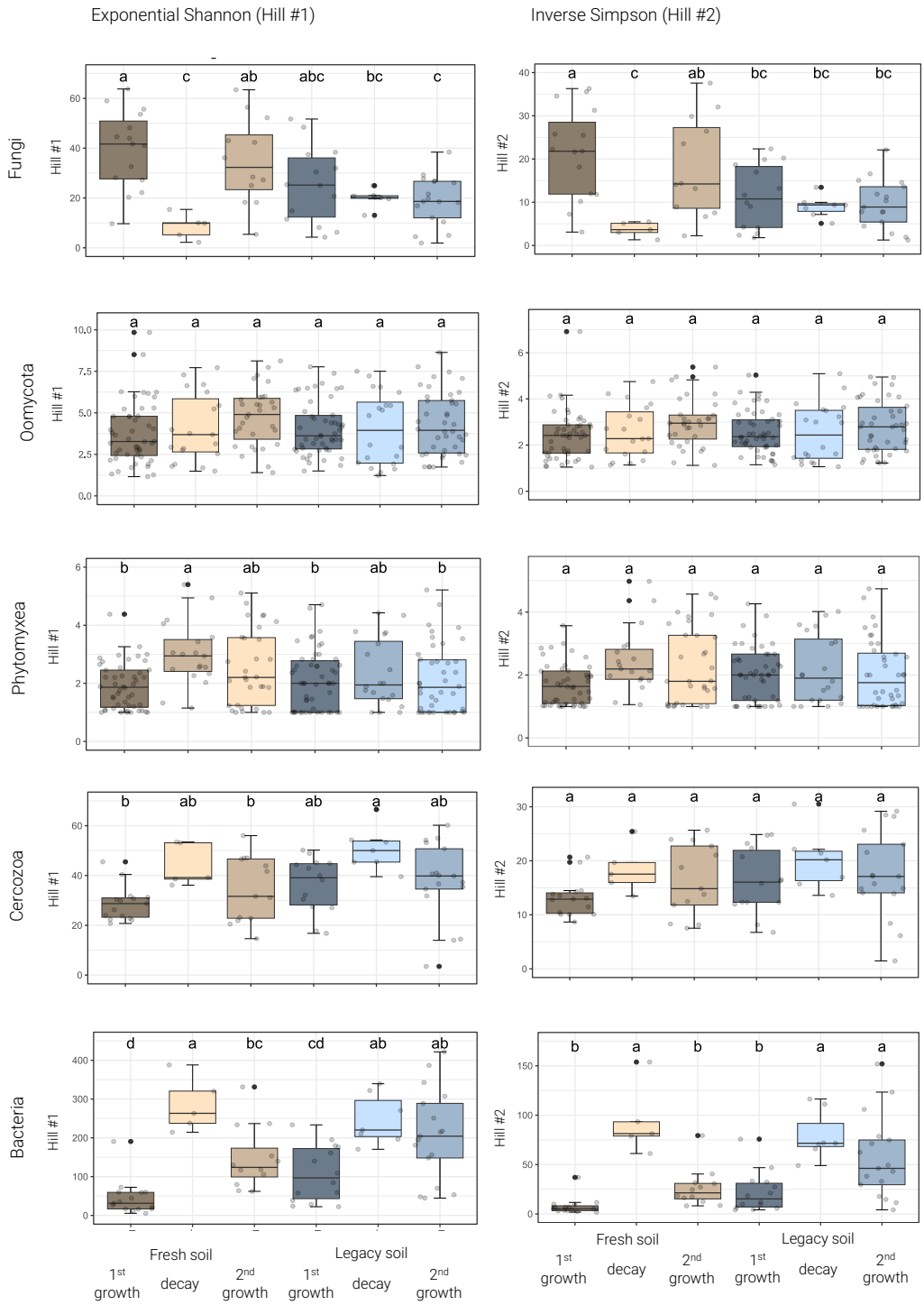

Fig. SI 5 Shifts in α-diversity following root decomposition. The boxplots show the diversity as exponential Shannon entropy (Hill #1) and the evenness as inverse Simpson index (Hill #2) for fungi, Oomycota, Phytomyxea, Cercozoa and bacteria. Different letters indicate significant differences (Tukey's HSD test).

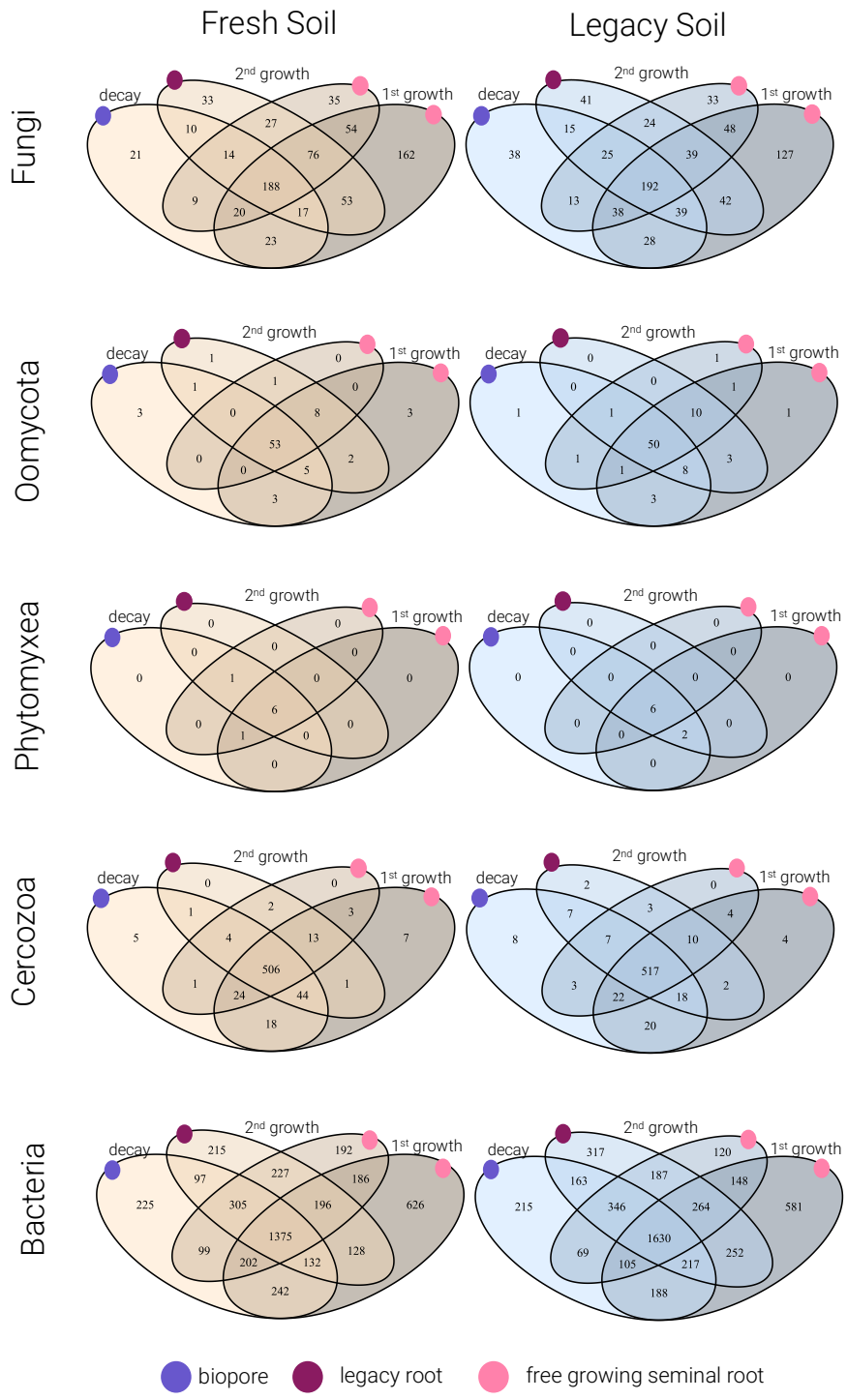

Fig. SI 6 Overlap of rhizosphere OTUs across plant growth phases. Venn diagrams illustrate shared and unique OTU counts between the three growth phases (first growth, decay, and second growth) for microbial communities in the rhizosphere: Fungi, Oomycota, Phytomyxea, Cercozoa and bacteria. Diagrams on the left represent samples from fresh soil, while those on the right show legacy soil. Colour coding above each diagram indicates the sampling location: *free growing seminal root*, *legacy root* (seminal roots growing inside a biopore) or biopore. Numbers within each sector represent the number of OTUs specific to, or shared between, growth phases.

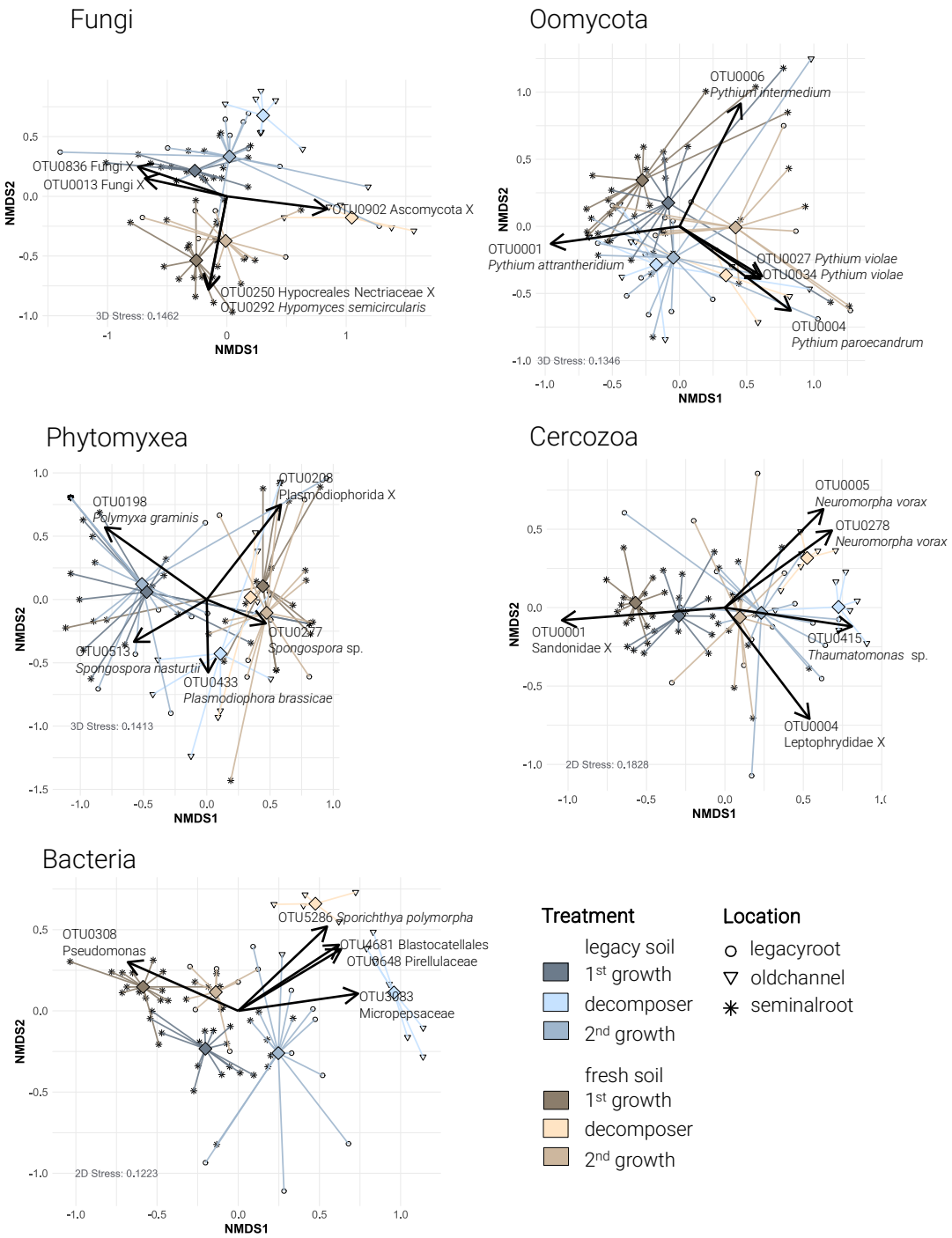

Fig. SI 7 Taxa contributing to shifts in community composition: Non-metric multidimensional scaling (NMDS) plots depict beta diversity of Fungi, Bacteria, Cercozoa, Phytomyxea, and Oomycota communities, as in Figure 3, with vectors fitted for the most explanatory OTUs. Arrows represent OTUs significantly associated with community variation (envfit, $p < 0.05$), with direction indicating the gradient and length proportional to the strength of correlation (R^2). Only the top five taxa (based on R^2 values) per community are shown. Labels correspond to species-level taxonomic assignments where available. NMDS dimensionality and stress values follow the same thresholds as in the main figure.

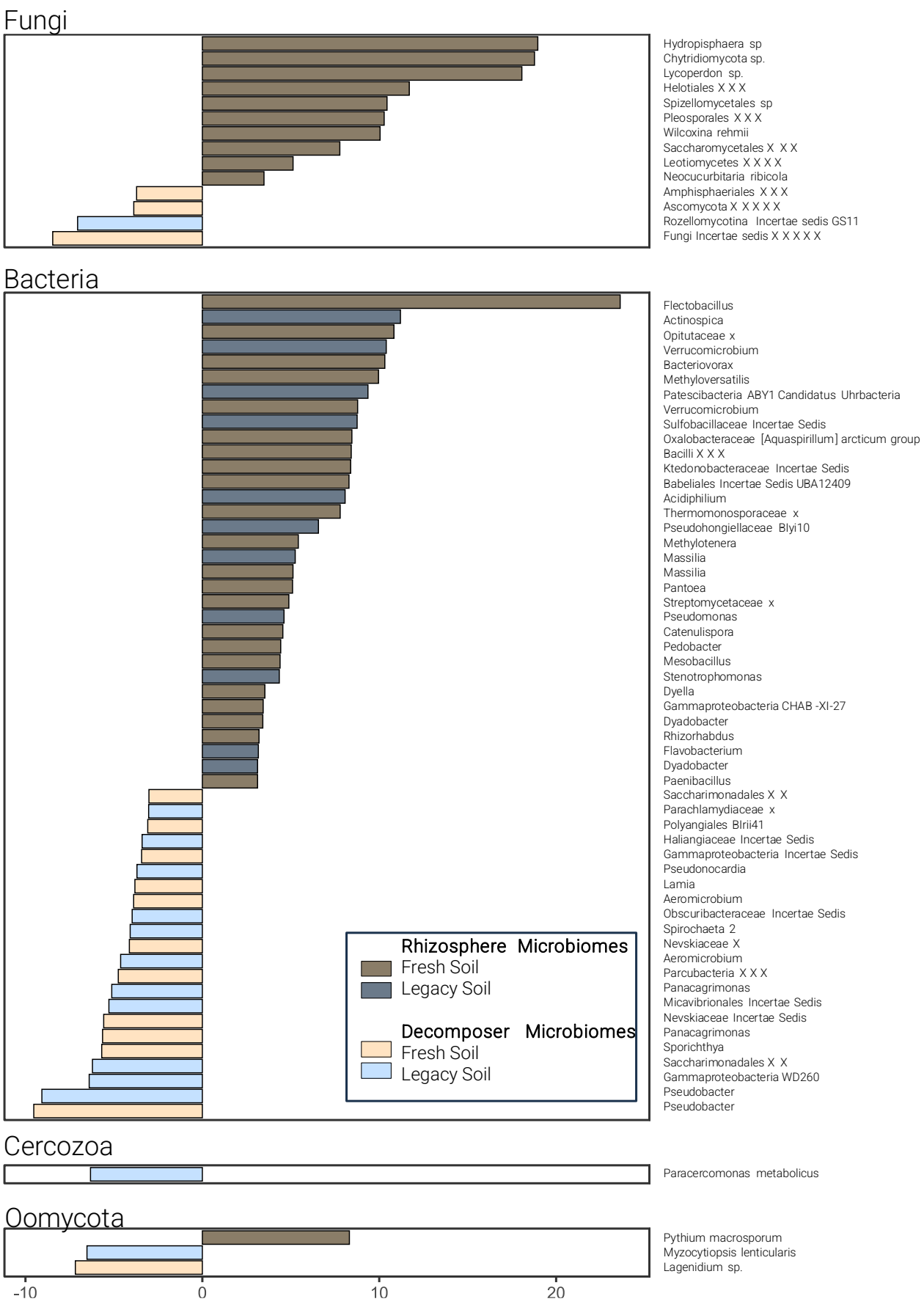
Fungi
Hydropisphaera sp
Chytridiomycota sp.
Lycoperdon sp.
Helotiales X X X
Spizellomycetales sp
Pleosporales X X X
Wilcoxina rehmii
Saccharomycetales X X X
Leotiomycetes X X X X
Neocucurbitaria ribicola
Amphisphaeriales X X X
Ascomycota X X X X X
Rozellomycotina Incertae sedis GS11
Fungi Incertae sedis X X X X X
Bacteria
Flectobacillus
Actinospica
Opitutaceae x
Verrucomicrobium
Bacteriovorax
Methyloversatilis
Patescibacteria ABY1 Candidatus Uhrbacteria
Verrucomicrobium
Sulfobacillaceae Incertae Sedis
Oxalobacteraceae [Aquaspirillum] arcticum group
Bacilli X X X
Ktedonobacteraceae Incertae Sedis
Babeliales Incertae Sedis UBA12409
Acidiphilium
Thermomonosporaceae x
Pseudohongiellaceae Blyi10
Methylotenera
Massilia
Massilia
Pantoea
Streptomycetaceae x
Pseudomonas
Catenulispora
Pedobacter
Mesobacillus
Stenotrophomonas
Dyella
Gammaproteobacteria CHAB -XI-27
Dyadobacter
Rhizorhabdus
Flavobacterium
Dyadobacter
Paenibacillus
Saccharimonadales X X
Parachlamydiaceae x
Polyangiales BIrii41
Haliangiaceae Incertae Sedis
Gammaproteobacteria Incertae Sedis
Pseudonocardia
Lamia
Aeromicrobium
Obscuribacteraceae Incertae Sedis
Spirochaeta 2
Nevskiaceae X
Aeromicrobium
Parcubacteria X X X
Panacagrimonas
Micavibrionales Incertae Sedis
Nevskiaceae Incertae Sedis
Panacagrimonas
Sporichthya
Saccharimonadales X X
Gammaproteobacteria WD260
Pseudobacter
Pseudobacter
Rhizosphere Microbiomes
Fresh Soil
Legacy Soil
Decomposer Microbiomes
Fresh Soil
Legacy Soil
Cercozoa
Paracercomonas metabolicus
Oomycota
Pythium macrosporum
Myzocytiopsis lenticularis
Lagenidium sp.
-10
0
10
20

Fig. SI 8 Differentially abundant taxa in fungal, cercozoan, oomycete, and bacterial communities. Differential abundance analysis was performed using DESeq2 on count data aggregated at different taxonomic levels: species level for fungi, Cercozoa, and Oomycota, and genus level for bacteria. The log2fold change represents differences in taxon abundance between the growing and decomposer communities across two soil histories: fresh soil and legacy soil. Bars extending to the right indicate higher abundance in communities at the growing root, and bars extending to the left indicate higher abundance in communities in decomposed root channels. Colour coding indicates soil history and community composition: Dark brown = Rhizosphere microbiome (fresh soil), dark blue = Rhizosphere microbiome (legacy soil), light brown = Decomposer microbiomes (fresh soil), bright blue = Decomposer microbiome (legacy soil). Taxa are sorted by effect size within each microbial group. Only significantly differentially abundant taxa (based on adjusted p-value thresholds) are shown.

General Discussion

Linking aims and hypotheses to findings

Root systems are dynamic interfaces where the continuous interaction of bottom-up carbon release and top-down trophic control forms the rhizosphere microbiome. Carbon is secreted in the form of mucilage at the growing tips, while exudates are passively released at older root zones; these pulsed inputs initiate bacterial and fungal growth. Protist grazers then restructure the emerging microbial assemblage, and the altered prey field feeds back on the predators themselves. This coupled, bidirectional loop likely promotes rhizosphere self-organisation and is influenced by two legacy dimensions inherited from previous crops: microbial propagules and reused biopores.

Based on this, the thesis aimed to investigate how the interaction between C supply and soil legacies promotes self-organisation in the rhizosphere under continuous maize cultivation. Five working hypotheses guided the experimental programme: H1, that microbial activity begins only when local C exceeds substrate-specific thresholds; H2, that photosynthate allocation mosaics define the spatial template for microbial niches; H3 and H4, that biological residues and recycled biopores, respectively, shape community succession; and H5, that pathogenic protists accumulate during continuous maize cultivation, thereby reinforcing negative plant–soil feedback loops.

Carbon thresholds as the first biochemical gate

Over the past decade, it has become clear that the C released by roots represents a strategic investment. Ideally, it should encourage the growth of microbial communities to protect the host plant, mobilise nutrients, and stabilise the plant–soil system (Vandenkoornhuyse et al. 2015, Spooren et al. 2024). This process can be divided into two steps: (i) pre-selection in C hotspots, followed by (ii) host-mediated selection. Pre-selection through C input into the soil creates local micro-environmental hotspots where fast-growing, root-compatible taxa can outcompete the bulk soil background (Bulgarelli et al. 2012, Kuzyakov and Blagodatskaya 2015). These hotspots attract both beneficial microorganisms, such as plant growth promoting PGPR and mycorrhizal fungi, and detrimental microorganisms, such as pathogens (Bais et al. 2006). C-threshold gating therefore acts as a biochemical rather than immunological first filter. This is followed by host-mediated selection, turning this stochastic colonisation into a more deterministic rhizosphere microbiome. During this immune-gated phase, the composition of root exudates is modified through the addition of flavonoids, riboflavin and other signalling molecules (Santangeli et al.

2024). These molecules may encourage the growth of beneficial microbes, which improve plant nutrition and growth (Wang et al. 2024), increase plant tolerance to abiotic stresses (Nozari et al. 2021, Notununu et al. 2022), and trigger systemic resistance against a broad spectrum of pathogens and insect herbivores (Neal et al. 2012, Pieterse et al. 2014).

Our respiration-kinetics assays quantified step one (Chapter I: Microbial utilization of maize rhizodeposits (Niedeggen et al. 2024)). Microbial growth was initiated above 60 % of C_{mic} for simple sugars and late-season exudates but required 250 % and 630 % of C_{mic} for early-season exudates and mucilage, respectively. Multi-peaked respiration curves for complex substrates implied that secondary metabolites delay microbial growth in the rhizosphere, hindering the rapid degradation of functionally relevant plant compounds (Bais et al. 2006, Sasse et al. 2018, Khashi u Rahman 2019). By restraining fast-growing copiotrophs, these compounds may simultaneously facilitate the subsequent enrichment of plant-selected taxa. Accordingly, community structure shifts from the largely stochastic assemblages seen at root tips to the more deterministic, plant-directed structure observed further along the root axis (Rüger et al. 2021). Spatial imaging linked these kinetics to *in-situ* gradients. PET–MRI of ^{11}C photosynthate showed pronounced tip-centred hotspots, with signal intensity, and thus C availability dropping along the root axis (Chapter II: Photosynthate hotspots structure rhizosphere microbiota). The high relative tracer signal shown and existing literature suggest that the C supply at the root exceeds the activation threshold, whereas concentrations drop below it within a few millimetres of the surface (Ahmed et al. 2015, Zickenrott et al. 2016, Lohse et al. 2021). This multi-step process was supported by DNA-SIP, which revealed that strongly ^{13}C-labelled, copiotroph-dominated consortia occupied carbon-rich tips, whereas older segments hosted weaker-labelled, more diverse assemblages. Further microscale data by Ghaderi et al. (2025) showed the same pattern: metabolically active zones are restricted to a narrow sheath around the root; as enzyme and microbial activity drop steeply beyond 1–2 mm. Taken together, this reinforces our hypothesis (H1) that, due to substrate-specific activation thresholds, microbial activity, and therefore the zones modulated by plants, are confined to the immediate rhizosphere. Furthermore, it leads to spatiotemporal niche partitioning across the root system, supporting our hypothesis (H2) that patchy C release creates distinct *carbon niches* resulting in selection acting at the level of many semi-independent sub-communities.

However, exudate profiles change markedly during plant development and in response to stress (Gargallo-Garriga et al. 2018, Santangeli et al. 2024, Hartwig et al. 2025). Therefore, the dynamic chemistry of rhizodeposits must be considered alongside plant growth dynamics. During active

vegetative growth plants invest in specialised metabolites that help assemble protective soil microbiomes (Rolfe et al. 2019). However, after flowering resources are redirected towards seed formation, resulting in a reduction in such selective signals (Keith et al. 1986, Swinnen et al. 1994). Thus, the selection of microbes by roots is a dynamic process influenced by ontogeny and the environment.

In summary, plants do not passively tolerate microbes surviving the C gradient; rather, they actively interact with the soil microbiome to assemble a rhizosphere microbiome that maximises their own benefit. This process begins with C provisioning and continues with an evolved chemical and immunological dialogue. Our findings showed that the functional rhizosphere is defined by C-thresholds and substrate composition, as microbes respired rather than proliferated beyond these hotspot zones. These empirically derived thresholds and kinetic functions therefore provided a quantitative context for the dialogue between plants, soil and microbes. Incorporating microbial growth kinetics and exudate chemistry into rhizosphere models will refine predictions of rhizosphere width, C turnover and microbial activity. Specifically, replacing the standard first-order decay terms with kinetic functions and incorporating spatial confinement with concentration gradients enables microbial activity to be incorporated into models ranging from µm-scale pores to 3D root architecture and field-scale platforms (Vetterlein et al. 2020, Landl et al. 2021, Schnepf et al. 2022). Such multi-scale integration will help to understand how the rhizosphere self-organises, as well as the soil-borne legacies, that arise there.

Dual legacies: biological and physical filters

During active growth, maize roots and the rhizosphere microbiota, together develop a characteristic 'rhizosphere signature': an interconnected community, that transitions from fast-growing pioneer taxa at the advancing tip to host-mediated, function-rich partners along older root segments. This spatially organised pattern, which is shaped by C supply, immune signals and environmental context, does not disappear when the crop is harvested. Instead, its physical structure remains as a matrix of former root channels, known as biopores (Ehlers et al. 1983), and its biological components persist (Stenström et al. 2001). Together, these form a dual legacy on which the next generation must establish itself.

Imaging studies confirmed that such intact biopores persist over growing seasons and that subsequent roots preferentially re-enter them (Rasse and Smucker 1998, Banfield et al. 2017, Han et al. 2017, Wendel et al. 2022). By acting as 'root highways', biopores reduce penetration costs (Passioura 2002) and improve the acquisition of resources (Athmann et al. 2013). Inside the developing biopores, the resident community experiences a second, decomposition-driven

succession (Blagodatskaya et al. 2021). After a root dies, the hotspot shifts from a rhizosphere fuelled by exudates to a detritusphere fuelled by increasingly recalcitrant root tissue. First, labile compounds are consumed by fast-growing copiotrophs (Herzog et al. 2019). Once these pools have been depleted, resources become more complex (cellulose, lignin) and the community turns over to slower-growing, enzyme-rich specialists (often filamentous fungi) before activity eventually subsides and most taxa return to dormancy (de Boer et al. 2005).

Our field chronosequence showed how microbial legacy builds up over five consecutive maize seasons, influencing the rhizosphere microbiome of subsequent crops under realistic agricultural conditions (Chapter III: Protist community shifts under maize monoculture). Over time, the rhizosphere protist community gradually diverged from the initial baseline as the abundance of potentially plant-pathogenic oomycetes and cercozoan predators increased, supporting the hypothesis (H3) that microbial residues direct microbial succession over successive growth seasons. As the rhizosphere is spatially limited, this biological legacy is physically bound to biopores. Therefore, soil texture determines the boundary conditions for this legacy loop. In sandy soils, roots tended to be thicker, resulting in larger pores, as observed in loamy soils (Lippold et al. 2021, Rüger et al. 2023a). However, Phalempin et al. (2025) found that only loamy soil preserved a well-connected biopore network. In sandy plots, biopores collapsed and root residues were accumulated rather than decomposed. We therefore suggest that the biopore network preserved in the loam supported gradual, cumulative shifts in community composition. In contrast, the unstable sand environment led to more seasonally driven shifts. This supports the hypothesis (H4), that biopore recycling transmits legacy-borne microbes, which could potentially intensify negative plant–soil feedback.

The subsequent column study examined the impact of biological and physical legacies by comparing 'fresh' soil with 'legacy' soil conditioned by maize monoculture from the field experiment, over a cycle of maize growth, decay and regrowth (Chapter IV: Root legacies govern the maize rhizosphere). Thus, it linked drivers at the field level with microscale habitat structure and enabled microbial succession to be traced along the original pore network. High-resolution MRI was employed to map root architecture *in situ*, track root channels through decay and regrowth, and identify re-entered biopores. Approximately one in five new roots recycled an old biopore. Legacy-driven, rhizosphere microbiomes with increased β-dispersion were then established in these biopores, supporting H4. This was particularly evident in pre-conditioned legacy soil, where prior monoculture had already diversified the inoculum, supporting H3.

Crucially, the second-generation rhizosphere community recovered, but did not fully converge with the first-generation community. Consequently, the microbial composition of the rhizosphere in continuous maize cultivation fluctuates between living-root and decomposer states while retaining traces of the past. This illustrates how the fallow period between crop cycles alters plant-mediated biological legacies and enables the cyclical changes seen in continuously cultivated maize (Dhungana and Nguyen 2025). On the one hand, bacterial and bacterivorous cercozoan communities flourished in terms of alpha diversity during decay, taking advantage of the diverse carbon sources available. However, the arrival of a fresh root probably resulted in plant selection, which reduced the diversity of bacterial and cercozoan communities. As this selection is initially stochastic, beta dispersion between different communities increased in the second-generation rhizosphere. On the other hand, groups of root-associated pathogenic oomycetes and fungi, which share many functional traits (Dodds et al. 2009) experienced a bottleneck when living plant roots were unavailable, resulting in a loss of diversity. This diversity was only regained when the next root appeared. The reduction in alpha diversity was even more pronounced for fungi. In addition to a bottleneck caused by the unavailability of living plant roots, this suggests an increase in rare species specialised in decomposing dead plant material (i.e. saprotrophs) (de Boer et al. 2005). The recovery of successive rhizosphere microbiomes across bacteria, fungi, Cercozoa and Oomycota suggests strong plant-mediated recruitment pressures, that can override the effects of decomposers. However, the initial stage is not fully restored as the legacy inocula in individual biopores gradually guide and diversify regrowth trajectories.

Trophic feedbacks: predators, pathogens and plant signals

The dual physical and biological legacies of biopores and microbial residues in the soil shape the encounter between a new root and its microbiome. Continuously growing the same crop in the same field leads to the accumulation of host-specific soil-borne pathogens, while reducing the diversity and functionality of the microbial community (Shipton 1977, McDonald and Stukenbrock 2016, Strom et al. 2020, Yang et al. 2020). Field surveys showed that it is continuous cultivation rather than crop identity, that drives cyclic but directional turnover, ultimately shifting soils towards distinct microbial communities biased towards the host crop (Dhungana and Nguyen 2025). Such soil-borne legacies further impact plant performance and agricultural yield. Mao et al. (2021) confirmed a strong, soil biota-mediated negative feedback loop under continuous maize monoculture, demonstrating that living soil from such plots suppresses biomass and yield in subsequent crops.

When pathogen pressure increases, plants activate a multilayered immune network to defend themselves (Dodds et al. 2024). Two stages can be distinguished: pattern-triggered immunity (PTI), which recognises conserved pathogen-associated molecular patters, and effector-triggered immunity (ETI), which targets secreted effector proteins. Cell-surface receptors activate defence pathways, triggering broad-spectrum resistance against a wide range of pathogens. These pathways include the production of reactive oxygen species (ROS), Ca^{2+} influx, mitogen-activated protein kinase (MAPK) cascades, the induction of defence genes and the hormonal signalling, most notably salicylic acid (SA) and jasmonic acid (JA) (Bari and Jones 2009). Further, altering quorum sensing and other microbial signalling processes, that direct the formation of protective partnerships in the rhizosphere (Wang and Song 2022). Although the primary aim is pathogen suppression, this plant-mediated enrichment of antagonistic microbes has been framed as the plant's 'cry for help' (Bakker et al. 2018, Rizaludin et al. 2021, Mesny et al. 2023).

A coupling between pathogen build-up and antagonist acquisition by the plant is shown for *Arabidopsis* plants in soil preconditioned with the oomycete pathogen *Hyaloperonospora arabidopsidis*, which assembled a protective bacterial consortium (Berendsen et al. 2018, Goossens et al. 2023). Likewise, cucurbit roots exuded bitter triterpenes, that attracted Enterobacter and Bacillus strains which are antagonistic to *Fusarium oxysporum* (Zhong et al. 2022), and dune grass (*Carex arenaria*) emitted pathogen-induced volatiles, that attracted anti-fungal bacteria (Schulz-Bohm et al. 2018). Similarly, in crops, durum wheat, that was naturally infected with the *Fusarium graminearum* crown-rot pathogen recruited the *Stenotrophomonas rhizophila* bacterium, inducing resistance to the disease and promoting wheat growth (Liu et al. 2021). Our five-year maize chronosequence pointed to a similar pattern, with potentially beneficial heterotrophic Cercozoa co-enriching alongside rising pathogen pressure, although direct plant recruitment of heterotrophic Cercozoa cannot be confirmed (Gao et al. 2019, Amacker et al. 2020). Pathogenic oomycetes adapted to maize, notably *Pythium arrhenomanes* and *P. monospermum*, accumulated steadily over time, supporting the hypothesis (H5), that protist pathogens strengthen negative plant–soil feedbacks under monoculture. However, heterotrophic cercozoans, including mycophagous vampyrellid amoebae such as *Platyreta* and testate Trinematidae amoebae, also flourished. These consumers can suppress fungal and oomycete pathogens through direct grazing (Old and Darbyshire 1978, Chakraborty and Old 1982, Old and Chakraborty 1986, Hess and Suthaus 2022). The specific enrichment of predatory protists, like Cercozoa, in response to pathogen pressure was also shown by a recent study on chilli pepper (Gao et al. 2024). Taken together with our maize data, these observations appear to support the concept of an underground 'cry for help', whereby shifts in root exudation driven by

defence mechanisms restrain pathogens by sustaining populations of their microbial predators. Over successive cycles, supporting pathogen antagonists could mature into disease-suppressive soils (DSS) (Raaijmakers and Mazzola 2016, Jayaraman et al. 2021). While these soils do not eradicate soil-borne pathogens, the resident microbiome keeps disease expression minimal, even when both the pathogen and a susceptible host are present (Weller et al. 2002, Mazzola 2007, Schlatter et al. 2017). Therefore, disease pressure is mitigated even under continuous monoculture.

Spatiotemporal feedbacks in the self-organising rhizosphere of maize

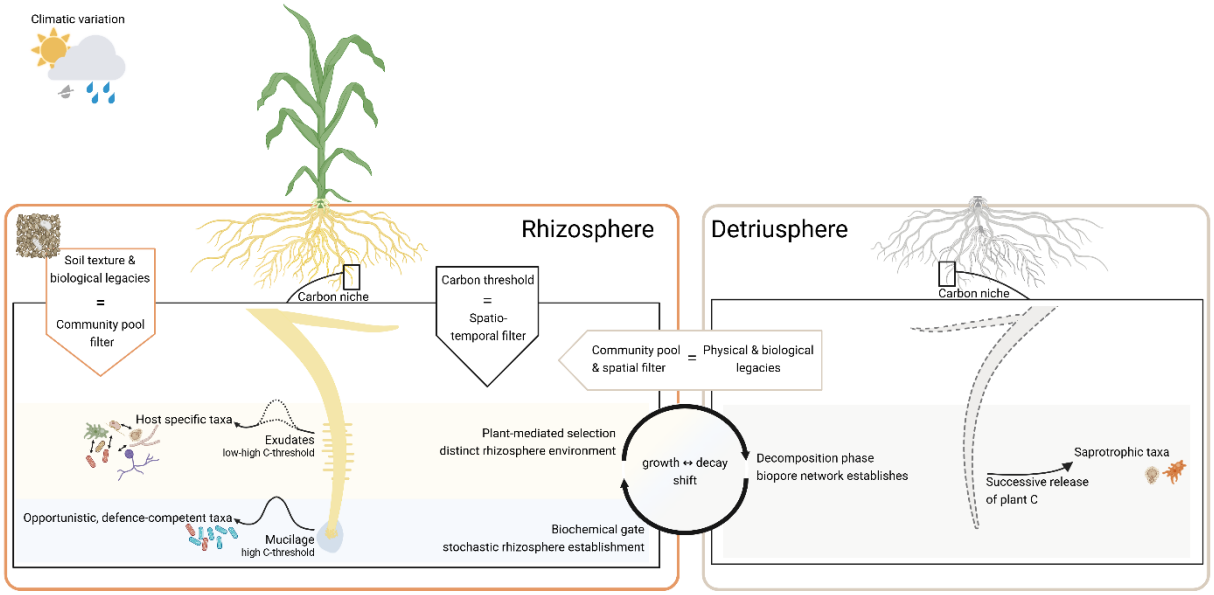

Figure 1 Soil legacies shape maize rhizosphere microbiomes - microbial assembly along the root life cycle. During plant growth, plant-derived C creates spatiotemporal *carbon niches* in which plant–microbe interactions occur. Microbial assembly in these niches is guided by three filters: (1) a community-pool filter, defined by soil texture and accumulated biological legacies in the bulk soil; (2) a temporal filter, which is imposed by the plant's pulsed C release; and (3) a spatial filter, created by root architecture and C-allocation patterns. Biopores provide an additional physical spatial filter that directs root elongation and microbial recolonisation. Climatic variation (e.g. moisture and temperature fluctuations) modulates all filters. Along the root, microbial succession proceeds. First, a biochemical gate at the root tip, where highly concentrated mucilage favours opportunistic, defence-competent copiotrophs, leading to an initially stochastic community. In older root segments, plant-mediated selection occurs, where exudates (including secondary metabolites) and trophic interactions shape a host-specific rhizosphere environment. When the plant dies, the system undergoes a growth ↔ decay shift: during decomposition, plant C is successively released, favouring saprotrophic taxa in the detritusphere and establishing a biopore network that stores physical and biological legacies. These legacies subsequently feed back to the next root generation, forming a growth ↔ decay feedback loop that couples rhizosphere and detritusphere dynamics, linking soil legacies, C-thresholds and root architecture to the assembly and turnover of the maize rhizosphere microbiome. The figure was created in https://BioRender.com and can be viewed and downloaded here: https://uni-koeln.sciebo.de/s/DK1NsXCQPfXK4WD

Collectively, this thesis provided insight into how the rhizosphere microbiome of maize develops and evolves through a series of locally constrained processes. Along the growing root, pulsed photosynthate appeared to create temporary, millimetre-scale *carbon niches* (Chapter I: Microbial utilization of maize rhizodeposits). At the root tip, C release is likely high enough to exceed activation thresholds, favouring opportunistic, defence-competent copiotrophs (Chapter II: Photosynthate hotspots structure rhizosphere microbiota). As the root elongates, these hotspots seem to transition into a more mediated rhizosphere environment. C concentrations decrease, secondary metabolites increase, and the community shifts towards slower-cycling, plant-mediated taxa. These bottom-up, C-mediated microbial niches are further modulated by trophic control (Rüger et al. 2021, Rüger et al. in prep). The result is probably a spatial patchwork comprising mutualists, cheaters, pathogens and regulators.

Legacy processes added a temporal dimension to this patchwork. When roots decomposed, the food web shifted towards a detritusphere: saprotrophs flourished, plant-pathogen specialists lost their hosts and declined (Chapter IV: Root legacies govern the maize rhizosphere). During the next growth cycle, these inocula could function as an initial filter, affecting the early stages of microbial community assembly. Our field chronosequence demonstrated that under continuous maize cultivation, this feedback can drift towards a state biased towards pathogens (*Pythium* spp.) (Chapter III: Protist community shifts under maize monoculture). However, the concurrent increase in potentially antagonistic heterotrophic cercozoans suggested that plants may actively sustain antagonists, that moderate disease levels. When viewed as an interactive unit, the plant and its microbiota appear to collectively form a distinct rhizosphere community, supplemented by phase-specific functional blooms. This reflects a dynamic consortium, that is assembled, pruned, and recovered each season.

In summary, C-thresholds determine where microbial niches can form. Physical and biological legacies, alongside trophic interactions, define the available inoculum and the taxa, that ultimately thrive. Together, these local processes generate the spatiotemporal feedback loops, that organise the maize rhizosphere microbiome.

Although modelling tools are becoming more sophisticated, incorporating multiple layers and their interactions, the rhizosphere remains an intricately layered system whose feedback loops defy simple generalisations. Continued integration of empirical data into predictive models is

essential to ensure that each conclusion, however precise, fits the dynamic complexity of the soil ecosystem, rather than imposing a false simplification.

Legacy-aware rhizosphere engineering for sustainable agriculture

One of the main objectives of understanding the spatio-temporal feedbacks between soil legacies and the maize rhizosphere microbiome is to discover key traits, that can be harnessed from this fundamentally layered below-ground system to reliably support sustainable crop production. Since the mid-20th century, the introduction of mineral fertilisers, pesticides and mechanisation has led to increased productivity, economic development and social transformation in modern intensive agriculture worldwide (FAO 2013). While these technologies stabilise production in the short term, they have also accelerated soil-organic-matter (SOM) loss, nutrient imbalances and biodiversity decline, pushing many agro-ecosystems towards biophysical tipping points (Pimm and Raven 2000, Foley et al. 2005, Vitousek et al. 2009, Liu et al. 2010, Panettieri et al. 2014). The stability of soil organic matter (SOM) primarily depends on microbial necromass (Miltner et al. 2012, Kallenbach et al. 2016, Liang et al. 2017). Once soil organic carbon (SOC) falls below ~1 % this necromass-driven pool becomes unstable, with microbial fractions drifting out of stoichiometric equilibrium and becoming inefficient at immobilising C (Loveland and Webb 2003, Clayton et al. 2021). Long-term trials show that organic agricultural systems, displaying higher SOM and better soil structure, deliver more stable soil functions, such as lower nitrate leaching and fewer plant-parasitic nematodes, and a yield gap to conventional farming, that narrows over time, underscoring the link between SOM maintenance and yield resilience (Schrama et al. 2018). Hence, maintaining SOM above this tipping point is critical for yield stability, water retention and nutrient supply (Philip Robertson et al. 2014, Oldfield et al. 2019).

Consequently, targeted approaches through soil microbiome engineering are proposed as a possible route forward. There is a growing consensus, that breeding strategies should select plant varieties based on their ability to foster beneficial microbes, creating resilient crops, that can withstand abiotic and biotic stresses (Bender et al. 2016, Oburger et al. 2022). Therefore, breeding approaches should take a holobiont perspective into account, incorporating root traits, that could attract beneficial partners or protect against pathogens (Nerva et al. 2022, Salse et al. 2024). Another factor to consider when breeding is root exudates: the chemical footprint released by crops into the soil. While exudates can support a diverse microbiome, that can trigger induced systemic resistance responses, mucilage hydrogels can maintain water connectivity in the rhizosphere and improve drought tolerance (Zarebanadkouki et al. 2019). However, exudates are also linked to soil-borne pathogen infections (Yuan et al. 2018). Therefore, choosing crop rotations and cover crops based on the chemical footprint they leave is crucial (Jing et al. 2022).

Another method of soil microbiome engineering uses inoculation of the roots with PGPR, arbuscular mycorrhizal fungi (AMF), protists, or entomopathogenic nematodes. Enhanced nutrient acquisition and protection against pathogens and insects are anticipated to reduce the use of fertiliser, pesticides and herbicides (Ehlers 2001, Vessey 2003, Asiloglu et al. 2020, Amacker et al. 2025). For example, protist inoculation has been shown to increase plant above-ground biomass by enhancing the activity and survival of PGPR (Jousset 2017), which stimulate nutrient acquisition (Levrat et al. 1992, Alphei et al. 1996) or produce antimicrobial and antifungal compounds (Mazzola et al. 2009, Jousset and Bonkowski 2010). However, the success of this method varies depending on the local environment and so diagnostic-guided inoculation seems to be a key step in ensuring its application is successful. Large-scale field trials have shown that soil microbiome indicators can predict 86 % of the variation in how plants growth respond to AMF inoculation, whereas the abundance of pathogenic fungi explains a third (Lutz et al. 2023). Further ideas to improve the success of microbiome inoculations include strain improvement through genome editing of single bioinoculants (Wen et al. 2021) and shifting whole microbial communities through soil transplantation (Raaijmakers and Kiers 2022, Gerrits et al. 2023). Recent reviews demonstrated the potential and success of microbial applications, while also highlighting the need to properly consider the ecological side effects (Trivedi et al. 2020, Oburger et al. 2022, Compant et al. 2025). They emphasise the need for a better understanding of how inoculants evolve in the natural environment, in order to address their potential effects on non-target organisms, antibiotic resistance, horizontal gene transfer, invasiveness, and pathogenicity.

An extensive agricultural approach to creating a beneficial soil environment would involve combining knowledge from various levels of research on microbes, soil structure, and exudates within a legacy-aware soil management system. This would implicate (i) the diversification of crop rotation practices, thereby shifting the balance of microbial succession away from an accumulation of crop-specific pathogens and increasing the diversity of exudates and (ii) reduced tillage to limit compaction and preserve biopores, thereby enabling deep rooting and enhancing rhizosphere reassembly.

Organic agricultural systems incorporate legacy-aware management, where diversified rotations, minimal tillage and restrained chemical use work with, rather than against, soil legacies (Gunapala and Scow 1998, Bonanomi et al. 2016). The diversity of crop rotations, which involves alternating nutrient-demanding crops with species that require fewer nutrients, followed by regenerative phases of deep-rooted, nitrogen-fixing legumes or multi-species cover crops, prevents the accumulation of negative feedback loops (Olesen et al. 2000, Bond and Grundy

2001, Stockdale et al. 2001). It dilutes host-specific pathogen pools, expands the chemical and functional breadth of root exudates, thereby supporting the development of DSS (Peters et al. 2003, Peralta et al. 2018, Seitz et al. 2024). Furthermore, organic management improves the physical properties of soil, primarily because higher SOM reduces compaction, increases aggregate stability, and improves the availability of water to plants (Williams et al. 2017). Stability of soil biotic and abiotic properties and soil processes are linked to more stable soil functions (Schrama et al. 2018). Consequently, the mechanisms that soil-ecological engineering now seeks to capture, such as trait-based crop design and exudate steering to encourage beneficial legacies and support DSS, cannot be considered revolutionary.

Contemporary research is deepening our understanding of the underlying processes that influence soil legacies, demonstrating that managing these legacies is a logical approach to sustainable agriculture. Rather than being exploited for short-term results, which risks SOM loss and destabilises feedback loops, this knowledge and advancing methods should be used to create site-specific, predictive interventions that support the long-term reduction of resource use and negative consequences of intensive land use, as well as the restoration of degraded soils. Consequently, working with soil legacies rather than against them transforms the rhizosphere into a resilient buffer, that can sustain yield with minimal external inputs.

Closing remarks

The work presented here indicates that spatiotemporal feedback loops between soil legacies and the maize rhizosphere microbiome generate a self-organising interface, which is characterised by cyclical transitions between living-root and decomposer states. The initiation of microbial growth is determined by carbon release patterns, while root-derived legacies supply the historical inoculum and pore architecture, that direct their assembly. By providing quantitative descriptors such as microbial activation thresholds and kinetic functions, this thesis offers parameters, that can be incorporated into multi-scale models. Overall, it suggests that deliberate, legacy-aware soil management could help to create a resilient rhizosphere system with low input requirements, that supports consistent yields.

General References

Ahmed, M. A., M. Holz, S. K. Woche, J. Bachmann, and A. Carminati. 2015. Effect of soil drying on mucilage exudation and its water repellency: a new method to collect mucilage. Journal of Plant Nutrition and Soil Science 178:821-824.

Alphei, J., M. Bonkowski, and S. Scheu. 1996. Protozoa, Nematoda and Lumbricidae in the rhizosphere of Hordelymus europeaus (Poaceae): faunal interactions, response of microorganisms and effects on plant growth. Oecologia 106:111-126.

Amacker, N., Z. Gao, B. C. Agaras, E. Latz, G. A. Kowalchuk, C. F. Valverde, A. Jousset, and S. Weidner. 2020. Biocontrol Traits Correlate With Resistance to Predation by Protists in Soil Pseudomonads. Front Microbiol 11:614194.

Amacker, N., Z. Gao, L. C. Jousset Alexandre, S. Geisen, and A. Kowalchuk George. 2025. Identity and timing of protist inoculation affect plant performance largely irrespective of changes in the rhizosphere microbial community. Applied and Environmental Microbiology 91:e00240-00225.

Anderson, J. P. E., and K. H. Domsch. 1978. A physiological method for the quantitative measurement of microbial biomass in soils. Soil Biology and Biochemistry 10:215-221.

Anderson, T. H., and K. H. Domsch. 1985. Maintenance carbon requirements of actively-metabolizing microbial populations under in situ conditions. Soil Biology & Biochemistry 17:pp. 197 -203.

Asiloglu, R., K. Shiroishi, K. Suzuki, O. C. Turgay, J. Murase, and N. Harada. 2020. Protist-enhanced survival of a plant growth promoting rhizobacteria, Azospirillum sp. B510, and the growth of rice (Oryza sativa L.) plants. Applied Soil Ecology 154:103599.

Athmann, M., T. Kautz, R. Pude, and U. Köpke. 2013. Root growth in biopores—evaluation with in situ endoscopy. Plant and Soil 371:179-190.

Atkinson, J. A., M. J. Hawkesford, W. R. Whalley, H. Zhou, and S. J. Mooney. 2020. Soil strength influences wheat root interactions with soil macropores. Plant Cell and Environment 43:235-245.

Bacic, A., S. F. Moody, J. A. McComb, J. M. Hinch, and A. E. Clarke. 1987. Extracellular polysaccharides from shaken liquid cultures of Zea mays. Functional Plant Biology 14:633-641.

Bais, H. P., T. L. Weir, L. G. Perry, S. Gilroy, and J. M. Vivanco. 2006. The role of root exudates in rhizosphere interactions with plants and other organisms. Annual Review of Plant Biology 57:233-266.

Bakker, P. A. H. M., C. M. J. Pieterse, R. de Jonge, and R. L. Berendsen. 2018. The Soil-Borne Legacy. Cell 172:1178-1180.

Banfield, C. C., M. A. Dippold, J. Pausch, D. T. T. Hoang, and Y. Kuzyakov. 2017. Biopore history determines the microbial community composition in subsoil hotspots. Biology and Fertility of Soils 53:573-588.

Bari, R., and J. D. G. Jones. 2009. Role of plant hormones in plant defence responses. Plant Molecular Biology 69:473-488.

Bauke, S. L., W. Amelung, R. Bol, L. Brandt, N. Brüggemann, E. Kandeler, N. Meyer, D. Or, A. Schnepf, M. Schloter, S. Schulz, N. Siebers, C. von Sperber, and H. Vereecken. 2022. Soil water status shapes nutrient cycling in agroecosystems from micrometer to landscape scales. Journal of Plant Nutrition and Soil Science 185:773-792.

Bender, S. F., C. Wagg, and M. G. A. van der Heijden. 2016. An Underground Revolution: Biodiversity and Soil Ecological Engineering for Agricultural Sustainability. Trends in Ecology & Evolution 31:440-452.

Berendsen, R. L., G. Vismans, K. Yu, Y. Song, R. de Jonge, W. P. Burgman, M. Burmølle, J. Herschend, P. A. H. M. Bakker, and C. M. J. Pieterse. 2018. Disease-induced assemblage of a plant-beneficial bacterial consortium. The ISME Journal 12:1496-1507.

Bever, J. D., T. G. Platt, and E. R. Morton. 2012. Microbial population and community dynamics on plant roots and their feedbacks on plant communities. Annual Review of Microbiology 66:265-283.

Bever, J. D., K. M. Westover, and J. Antonovics. 1997. Incorporating the Soil Community into Plant Population Dynamics: The Utility of the Feedback Approach. Journal of Ecology 85:561-573.

Blagodatskaya, E., M. Tarkka, C. Knief, R. Koller, S. Peth, V. Schmidt, S. Spielvogel, D. Uteau, M. Weber, and B. S. Razavi. 2021. Bridging Microbial Functional Traits With Localized Process Rates at Soil Interfaces. Front Microbiol 12:625697.

Bonanomi, G., F. De Filippis, G. Cesarano, A. La Storia, D. Ercolini, and F. Scala. 2016. Organic farming induces changes in soil microbiota that affect agro-ecosystem functions. Soil Biology and Biochemistry 103:327-336.

Bond, W., and A. C. Grundy. 2001. Non-chemical weed management in organic farming systems. Weed Research 41:383-405.

Bonkowski, M. 2004. Protozoa and plant growth: the microbial loop in soil revisited. New Phytologist 162:617-631.

Bonkowski, M., M. Tarkka, B. S. Razavi, H. Schmidt, E. Blagodatskaya, R. Koller, P. Yu, C. Knief, F. Hochholdinger, and D. Vetterlein. 2021. Spatiotemporal Dynamics of Maize (Zea mays L.) Root Growth and Its Potential Consequences for the Assembly of the Rhizosphere Microbiota. Front Microbiol 12:619499.

Bouffaud, M.-L., M.-A. Poirier, D. Muller, and Y. Moënne-Loccoz. 2014. Root microbiome relates to plant host evolution in maize and other Poaceae. Environmental Microbiology 16:2804-2814.

Bremer, E., and P. Kuikman. 1994. Microbial utilization of 14C[U]glucose in soil is affected by the amount and timing of glucose additions. Soil Biology & Biochemistry 26:511-517.

Brimecombe, M. J., F. A. De Leij, and J. M. Lynch. 2000. The effect of root exudates on rhizosphere microbial populations. The Rhizosphere, Biochemistry and Organic Substances at the Soil–Plant Interface (eds R. Pinton, Z. Varini & P. Nannipieri):95-140.

Bulgarelli, D., M. Rott, K. Schlaeppi, E. Ver Loren van Themaat, N. Ahmadinejad, F. Assenza, P. Rauf, B. Huettel, R. Reinhardt, E. Schmelzer, J. Peplies, F. O. Gloeckner, R. Amann, T. Eickhorst, and P. Schulze-Lefert. 2012. Revealing structure and assembly cues for Arabidopsis root-inhabiting bacterial microbiota. Nature 488:91-95.

Bullock, D. G. 1992. Crop rotation. Critical Reviews in Plant Sciences 11:309-326.

Chakraborty, S., and K. M. Old. 1982. Mycophagous soil amoeba: Interactions with three plant pathogenic fungi. Soil Biology and Biochemistry 14:247-255.

Clarholm, M. 1981. Protozoan Grazing of Bacteria in Soil--lmpact and Importance. Microbial Ecology 7:343-350.

Clarholm, M. 1985. Interactions of bacteria, protozoa and plants leading to mineralization of soil nitrogen. Soil Biology and Biochemistry 17:181-187.

Clayton, J., K. Lemanski, and M. Bonkowski. 2021. Shifts in soil microbial stoichiometry and metabolic quotient provide evidence for a critical tipping point at 1% soil organic carbon in an agricultural post-mining chronosequence. Biology and Fertility of Soils 57:435-446.

Collins, J. C., and E. J. Reilly. 1968. Chemical composition of the exudate from excised maize roots. Planta 83:218-222.

Compant, S., F. Cassan, T. Kostic, L. Johnson, G. Brader, F. Trognitz, and A. Sessitsch. 2025. Harnessing the plant microbiome for sustainable crop production. Nature Reviews Microbiology 23:9-23.

de Boer, W., L. B. Folman, R. C. Summerbell, and L. Boddy. 2005. Living in a fungal world: impact of fungi on soil bacterial niche development. FEMS Microbiology Reviews 29:795-811.

Denison, R. F., C. Bledsoe, M. Kahn, F. O'Gara, E. L. Simms, and L. S. Thomashow. 2003. COOPERATION IN THE RHIZOSPHERE AND THE “FREE RIDER” PROBLEM. Ecology 84:838-845.

Dhungana, I., and N. H. Nguyen. 2025. Legacy of Repeated Cultivation Drives Cyclical Microbial Community Development in a Tropical Oxisol Soil. Microbial Ecology 88:30.

Dixon, G. R. 2009. The Occurrence and Economic Impact of Plasmodiophora brassicae and Clubroot Disease. Journal of Plant Growth Regulation 28:194-202.

Dodds, P. N., J. Chen, and M. A. Outram. 2024. Pathogen perception and signaling in plant immunity. Plant Cell 36:1465-1481.

Dodds, P. N., M. Rafiqi, P. H. P. Gan, A. R. Hardham, D. A. Jones, and J. G. Ellis. 2009. Effectors of biotrophic fungi and oomycetes: pathogenicity factors and triggers of host resistance. New Phytologist 183:993-1000.

Donn, S., J. A. Kirkegaard, G. Perera, A. E. Richardson, and M. Watt. 2015. Evolution of bacterial communities in the wheat crop rhizosphere. Environmental Microbiology 17:610-621.

Ehlers, R.-U. 2001. Mass production of entomopathogenic nematodes for plant protection. Applied Microbiology and Biotechnology 56:623-633.

Ehlers, W., U. Köpke, F. Hesse, and W. Böhm. 1983. Penetration resistance and root growth of oats in tilled and untilled loess soil. Soil and Tillage Research 3:261-275.

Epp Schmidt, D., G. Dlott, M. Cavigelli, S. Yarwood, and J. E. Maul. 2022. Soil microbiomes in three farming systems more affected by depth than farming system. Applied Soil Ecology 173.

FAO. 2013. The State of Food Insecurity in the World 2013: Food Systems for Better Nutrition. FAO, Rome, Italy.

Fierer, N., M. A. Bradford, and R. B. Jackson. 2007. Toward an ecological classification of soil bacteria. Ecology 88:1354-1364.

Fiore-Donno, A. M., C. Rixen, M. Rippin, K. Glaser, E. Samolov, U. Karsten, B. Becker, and M. Bonkowski. 2018. New barcoded primers for efficient retrieval of cercozoan sequences in high-throughput environmental diversity surveys, with emphasis on worldwide biological soil crusts. Mol Ecol Resour 18:229-239.

Foley, J. A., R. DeFries, G. P. Asner, C. Barford, G. Bonan, S. R. Carpenter, F. S. Chapin, M. T. Coe, G. C. Daily, H. K. Gibbs, J. H. Helkowski, T. Holloway, E. A. Howard, C. J. Kucharik, C. Monfreda, J. A. Patz, I. C. Prentice, N. Ramankutty, and P. K. Snyder. 2005. Global Consequences of Land Use. Science 309:570-574.

Frindte, K., S. A. Zoche, and C. Knief. 2020. Development of a Distinct Microbial Community Upon First Season Crop Change in Soils of Long-Term Managed Maize and Rice Fields. Front Microbiol 11.

Frouz, J. 2024. Plant-soil feedback across spatiotemporal scales from immediate effects to legacy. Soil Biology and Biochemistry 189.

Gao, Z., I. Karlsson, S. Geisen, G. Kowalchuk, and A. Jousset. 2019. Protists: Puppet Masters of the Rhizosphere Microbiome. Trends in Plant Science 24:165-176.

Garcia Arredondo, M., W. Kew, R. Chu, M. E. Jones, R. M. Boiteau, Z. G. Cardon, and M. Keiluweit. 2024. Differential Exudation Creates Biogeochemically Distinct Microenvironments during Rhizosphere Evolution. Environmental Science & Technology.

Gargallo-Garriga, A., C. Preece, J. Sardans, M. Oravec, O. Urban, and J. Peñuelas. 2018. Root exudate metabolomes change under drought and show limited capacity for recovery. Scientific Reports 8:12696.

Geisen, S., E. A. D. Mitchell, S. Adl, M. Bonkowski, M. Dunthorn, F. Ekelund, L. D. Fernandez, A. Jousset, V. Krashevska, D. Singer, F. W. Spiegel, J. Walochnik, and E. Lara. 2018. Soil protists: a fertile frontier in soil biology research. FEMS Microbiology Reviews 42:293-323.

Geisen, S., E. A. D. Mitchell, D. M. Wilkinson, S. Adl, M. Bonkowski, M. W. Brown, A. M. Fiore-Donno, T. J. Heger, V. E. J. Jassey, V. Krashevska, D. J. G. Lahr, K. Marcisz, M. Mulot, R. Payne, D. Singer, O. R. Anderson, D. J. Charman, F. Ekelund, B. S. Griffiths, R. Rønn, A. Smirnov, D. Bass, L. Belbahri, C. Berney, Q. Blandenier, A. Chatzinotas, M. Clarholm, M. Dunthorn, A. Feest, L. D. Fernández, W. Foissner, B. Fournier, E. Gentekaki, M. Hájek, J. Helder, A. Jousset, R. Koller, S. Kumar, A. La Terza, M. Lamentowicz, Y. Mazei, S. S. Santos, C. V. W. Seppey, F. W. Spiegel, J. Walochnik, A. Winding, and E. Lara. 2017. Soil protistology rebooted: 30 fundamental questions to start with. Soil Biology and Biochemistry 111:94-103.

Gerrits, G. M., R. Waenink, A. L. Aradottir, E. Buisson, T. Dutoit, M. C. Ferreira, J. B. Fontaine, R. Jaunatre, P. Kardol, R. Loeb, S. Magro Ruiz, M. Maltz, M. Pärtel, B. Peco, J. Piqueray, N. A. L. Pilon, I. Santa-Regina, K. T. Schmidt, P. Sengl, R. van Diggelen, D. L. M. Vieira, W. von Brackel, P. Waryszak, T. J. Wills, R. H. Marrs, and E. R. J. Wubs. 2023. Synthesis on the effectiveness of soil translocation for plant community restoration. Journal of Applied Ecology 60:714-724.

Ghaderi, N., Z. Ibrahim, A. Guber, S. Khosrozadeh, V. Guliyev, M. Tarkka, and E. Blagodatskaya. 2025. High-resolution sampling for enhanced spatial analysis of microbial growth and enzyme activity in the rhizosphere. Rhizosphere 34.

Gong, X., Y. Feng, K. Dang, Y. Jiang, H. Qi, and B. Feng. 2023. Linkages of microbial community structure and root exudates: Evidence from microbial nitrogen limitation in soils of crop families. Science of the Total Environment 881:163536.

Goossens, P., J. Spooren, K. C. M. Baremans, A. Andel, D. Lapin, N. Echobardo, C. M. J. Pieterse, G. Van den Ackerveken, and R. L. Berendsen. 2023. Obligate biotroph downy mildew consistently induces near-identical protective microbiomes in Arabidopsis thaliana. Nature microbiology 8:2349-2364.

Gunapala, N., and K. M. Scow. 1998. Dynamics of soil microbial biomass and activity in conventional and organic farming systems. Soil Biology and Biochemistry 30:805-816.

Guo, S., C. Tao, A. Jousset, W. Xiong, Z. Wang, Z. Shen, B. Wang, Z. Xu, Z. Gao, S. Liu, R. Li, Y. Ruan, Q. Shen, G. A. Kowalchuk, and S. Geisen. 2022. Trophic interactions between predatory protists and pathogen-suppressive bacteria impact plant health. ISME J 16:1932-1943.

Han, E., T. Kautz, N. Huang, and U. Köpke. 2017. Dynamics of plant nutrient uptake as affected by biopore-associated root growth in arable subsoil. Plant and Soil 415:145-160.

Hannula, S. E., R. Heinen, M. Huberty, K. Steinauer, J. R. De Long, R. Jongen, and T. M. Bezemer. 2021. Persistence of plant-mediated microbial soil legacy effects in soil and inside roots. . Nat Commun 12.

Hartwig, R. P., M. Santangeli, H. Würsig, M. Martín Roldán, B. Yim, E. Lippold, A. Tasca, E. Oburger, M. Tarkka, D. Vetterlein, P. Bienert, E. Blagodatskaya, K. Smalla, B. Hause, and M. A. Wimmer. 2025. Drought response of

the maize plant–soil–microbiome system is influenced by plant size and presence of root hairs. Annals of Botany:mcaf033.

Hassani, M. A., P. Duran, and S. Hacquard. 2018. Microbial interactions within the plant holobiont. Microbiome 6:58.

Herzog, C., M. Hartmann, B. Frey, B. Stierli, C. Rumpel, N. Buchmann, and I. Brunner. 2019. Microbial succession on decomposing root litter in a drought-prone Scots pine forest. The ISME Journal 13:2346-2362.

Hess, S., and A. Suthaus. 2022. The Vampyrellid Amoebae (Vampyrellida, Rhizaria). Protist 173:125854.

Hiltner, L. 1904. Über neuere Erfahrungen und Probleme auf dem Gebiete der Bodenbakteriologie und unter besonderer Berücksichtigung der Gründüngung und Brache. Arb. Deut. Landw. Gesell 98:59-78.

Hinsinger, P., A. G. Bengough, D. Vetterlein, and I. M. Young. 2009. Rhizosphere: biophysics, biogeochemistry and ecological relevance. Plant and Soil 321:117-152.

Jahnke, S., M. I. Menzel, D. Van Dusschoten, G. W. Roeb, J. Bühler, S. Minwuyelet, P. Blümler, V. M. Temperton, T. Hombach, M. Streun, S. Beer, M. Khodaverdi, K. Ziemons, H. H. Coenen, and U. Schurr. 2009. Combined MRI–PET dissects dynamic changes in plant structures and functions. The Plant Journal 59:634-644.

Jayaraman, S., A. K. Naorem, R. Lal, R. C. Dalal, N. K. Sinha, A. K. Patra, and S. K. Chaudhari. 2021. Disease-Suppressive Soils-Beyond Food Production: a Critical Review. J Soil Sci Plant Nutr 21:1437-1465.

Jing, J., W. F. Cong, and T. M. Bezemer. 2022. Legacies at work: plant-soil-microbiome interactions underpinning agricultural sustainability. Trends in Plant Science 27:781-792.

Jousset, A. 2012. Ecological and evolutive implications of bacterial defences against predators. Environ Microbiol 14:1830-1843.

Jousset, A. 2017. Application of Protists to Improve Plant Growth in Sustainable Agriculture. Pages 263-273 *in* S. Mehnaz, editor. Rhizotrophs: Plant Growth Promotion to Bioremediation. Springer Singapore, Singapore.

Jousset, A., and M. Bonkowski. 2010. The model predator Acanthamoeba castellanii induces the production of 2,4, DAPG by the biocontrol strain Pseudomonas fluorescens Q2-87. Soil Biology and Biochemistry 42:1647-1649.

Jousset, A., L. Rochat, M. Péchy-Tarr, C. Keel, S. Scheu, and M. Bonkowski. 2009. Predators promote defence of rhizosphere bacterial populations by selective feeding on non-toxic cheaters. The ISME Journal 3:666-674.

Kallenbach, C. M., S. D. Frey, and A. S. Grandy. 2016. Direct evidence for microbial-derived soil organic matter formation and its ecophysiological controls. Nature Communications 7:13630.

Kamoun, S., O. Furzer, J. D. G. Jones, H. S. Judelson, G. S. Ali, R. J. D. Dalio, S. G. Roy, L. Schena, A. Zambounis, F. Panabières, D. Cahill, M. Ruocco, A. Figueiredo, X.-R. Chen, J. Hulvey, R. Stam, K. Lamour, M. Gijzen, B. M. Tyler, N. J. Grünwald, M. S. Mukhtar, D. F. A. Tomé, M. Tör, G. Van Den Ackerveken, J. McDowell, F. Daayf, W. E. Fry, H. Lindqvist-Kreuze, H. J. G. Meijer, B. Petre, J. Ristaino, K. Yoshida, P. R. J. Birch, and F. Govers. 2015. The Top 10 oomycete pathogens in molecular plant pathology. Molecular Plant Pathology 16:413-434.

Kardol, P., N. J. Cornips, M. M. L. van Kempen, J. M. T. Bakx-Schotman, and v. d. P. WH. 2007. Microbe-mediated plant-soil feedback causes historical contingency effects in plant community assembly. . Ecological Monographs 77:147-162.

Keith, H., J. M. Oades, and J. K. Martin. 1986. Input of carbon to soil from wheat plants. . Soil Biology & Biochemistry 18:445-449.

Khashi u Rahman, M., Zhou, X., & Wu, F. 2019. The role of root exudates, CMNs, and VOCs in plant–plant interaction. Journal of Plant Interactions, 14:630-636.

Krupinsky, J. M., K. L. Bailey, M. P. McMullen, B. D. Gossen, and T. K. Turkington. 2002. Managing Plant Disease Risk in Diversified Cropping Systems. Agronomy Journal 94:198-209.

Kuzyakov, Y., and E. Blagodatskaya. 2015. Microbial hotspots and hot moments in soil: Concept & review. Soil Biology and Biochemistry 83:184-199.

Kuzyakov, Y., and G. Domanski. 2000. Carbon input by plants into the soil. Review. Journal of Plant Nutrition and Soil Science 163:421-431.

Kuzyakov, Y., and B. S. Razavi. 2019. Rhizosphere size and shape: Temporal dynamics and spatial stationarity. Soil Biology and Biochemistry 135:343-360.

Landl, M., A. Haupenthal, D. Leitner, E. Kroener, D. Vetterlein, R. Bol, H. Vereecken, J. Vanderborght, A. Schnepf, J. Evers, and S. P. Long. 2021. Simulating rhizodeposition patterns around growing and exuding root systems. in silico Plants 3.

Levrat, P., M. Pussard, and C. Alabouvette. 1992. Enhanced bacterial metabolism of a Pseudomonas strain in response to the addition of culture filtrate of a bacteriophagous amoeba. European Journal of Protistology 28:79-84.

Li, X.-F., Z.-G. Wang, X.-G. Bao, J.-H. Sun, S.-C. Yang, P. Wang, C.-B. Wang, J.-P. Wu, X.-R. Liu, X.-L. Tian, Y. Wang, J.-P. Li, Y. Wang, H.-Y. Xia, P.-P. Mei, X.-F. Wang, J.-H. Zhao, R.-P. Yu, W.-P. Zhang, Z.-X. Che, L.-G. Gui, R. M. Callaway, D. Tilman, and L. Li. 2021. Long-term increased grain yield and soil fertility from intercropping. Nature Sustainability 4:943-950.

Li, X., A. Jousset, W. de Boer, V. J. Carrion, T. Zhang, X. Wang, and E. E. Kuramae. 2019. Legacy of land use history determines reprogramming of plant physiology by soil microbiome. ISME J 13:738-751.

Liang, C., J. P. Schimel, and J. D. Jastrow. 2017. The importance of anabolism in microbial control over soil carbon storage. Nature microbiology 2:17105.

Lippold, E., M. Phalempin, S. Schlüter, and D. Vetterlein. 2021. Does the lack of root hairs alter root system architecture of Zea mays? Plant and Soil 467:267-286.

Liu, C., X. Feng, Y. Xu, A. Kumar, Z. Yan, J. Zhou, Y. Yang, L. Peixoto, Z. Zeng, and H. Zang. 2023. Legume-based rotation enhances subsequent wheat yield and maintains soil carbon storage. . Agronomy for Sustainable Development.

Liu, H., J. Li, L. C. Carvalhais, C. D. Percy, J. Prakash Verma, P. M. Schenk, and B. K. Singh. 2021. Evidence for the plant recruitment of beneficial microbes to suppress soil-borne pathogens. New Phytologist 229:2873-2885.

Liu, X., X. Zhang, Y. Wang, Y. Sui, S. Zhang, S. Herbert, and G. Ding. 2010. Soil degradation: a problem threatening the sustainable development of agriculture in Northeast China. Plant, Soil and Environment 56:87-97.

Lohse, M., R. Haag, E. Lippold, D. Vetterlein, T. Reemtsma, and O. J. Lechtenfeld. 2021. Direct Imaging of Plant Metabolites in the Rhizosphere Using Laser Desorption Ionization Ultra-High Resolution Mass Spectrometry. Frontiers in plant science 12.

Loveland, P., and J. Webb. 2003. Is there a critical level of organic matter in the agricultural soils of temperate regions: a review. Soil and Tillage Research 70:1-18.

Lucas, M., S. Schluter, H. J. Vogel, and D. Vetterlein. 2019. Roots compact the surrounding soil depending on the structures they encounter. Sci Rep 9:16236.

Lundberg, D. S., S. L. Lebeis, S. H. Paredes, S. Yourstone, J. Gehring, S. Malfatti, J. Tremblay, A. Engelbrektson, V. Kunin, T. G. d. Rio, R. C. Edgar, T. Eickhorst, R. E. Ley, P. Hugenholtz, S. G. Tringe, and J. L. Dangl. 2012. Defining the core Arabidopsis thaliana root microbiome. Nature 488:86-90.

Lutz, S., N. Bodenhausen, J. Hess, A. Valzano-Held, J. Waelchli, G. Deslandes-Herold, K. Schlaeppi, and M. G. A. van der Heijden. 2023. Soil microbiome indicators can predict crop growth response to large-scale inoculation with arbuscular mycorrhizal fungi. Nat Microbiol 8:2277-2289.

Mao, L., Y. Liu, J. Zhang, J. Okerblad, S. Chen, and N. C. Johnson. 2021. Soil biota suppress maize growth and influence root traits under continuous monoculture. . Plant and Soil 461:441-455.

Mariotte, P., Z. Mehrabi, T. M. Bezemer, G. B. De Deyn, A. Kulmatiski, B. Drigo, G. F. C. Veen, M. G. A. van der Heijden, and P. Kardol. 2018. Plant-Soil Feedback: Bridging Natural and Agricultural Sciences. . Trends in Ecology & Evolution 33:129-142.

Mazzola, M. 2007. Manipulation of rhizosphere bacterial communities to induce suppressive soils. Journal of Nematology 39:213-220.

Mazzola, M., I. de Bruijn, F. Cohen Michael, and M. Raaijmakers Jos. 2009. Protozoan-Induced Regulation of Cyclic Lipopeptide Biosynthesis Is an Effective Predation Defense Mechanism for Pseudomonas fluorescens. Applied and Environmental Microbiology 75:6804-6811.

McDonald, B. A., and E. H. Stukenbrock. 2016. Rapid emergence of pathogens in agro-ecosystems: global threats to agricultural sustainability and food security. Philosophical Transactions of the Royal Society B: Biological Sciences 371:20160026.

Mesny, F., S. Hacquard, and B. P. Thomma. 2023. Co-evolution within the plant holobiont drives host performance. EMBO Reports 24:e57455.

Miltner, A., P. Bombach, B. Schmidt-Brücken, and M. Kästner. 2012. SOM genesis: microbial biomass as a significant source. Biogeochemistry 111:41-55.

Neal, A. L., S. Ahmad, R. Gordon-Weeks, and J. Ton. 2012. Benzoxazinoids in Root Exudates of Maize Attract Pseudomonas putida to the Rhizosphere. PLoS ONE 7:e35498.

Nerva, L., M. Sandrini, L. Moffa, R. Velasco, R. Balestrini, and W. Chitarra. 2022. Breeding toward improved ecological plant–microbiome interactions. Trends in Plant Science 27:1134-1143.

Neuhauser, S., M. Kirchmair, S. Bulman, and D. Bass. 2014. Cross-kingdom host shifts of phytomyxid parasites. BMC Evolutionary Biology 14:33.

Niedeggen, D., L. Rüger, E. Oburger, M. Santangeli, M. Ahmed, D. Vetterlein, S. Blagodatsky, and M. Bonkowski. 2024. Microbial utilisation of maize rhizodeposits applied to agricultural soil at a range of concentrations. European Journal of Soil Science 75.

Notununu, I., L. Moleleki, A. Roopnarain, and R. Adeleke. 2022. Effects of plant growth-promoting rhizobacteria on the molecular responses of maize under drought and heat stresses: A review. Pedosphere 32:90-106.

Nozari, R. M., F. Ortolan, L. V. Astarita, and E. R. Santarem. 2021. Streptomyces spp. enhance vegetative growth of maize plants under saline stress. Brazilian Journal of Microbiology 52:1371-1383.

Oburger, E., D. Leitner, D. L. Jones, K. C. Zygalakis, A. Schnepf, and T. Roose. 2011. Adsorption and desorption dynamics of citric acid anions in soil. European Journal of Soil Science 62:733-742.

Oburger, E., H. Schmidt, and C. Staudinger. 2022. Harnessing belowground processes for sustainable intensification of agricultural systems. Plant and Soil 478:177-209.

Ofek, M., M. Voronov-Goldman, Y. Hadar, and D. Minz. 2014. Host signature effect on plant root-associated microbiomes revealed through analyses of resident vs. active communities. Environmental Microbiology 16:2157-2167.

Old, K. M., and S. Chakraborty. 1986. Mycophagous soil amoebae: their biology and significance in the ecology of soil-borne plant pathogens. . Progress in protistology 1:163-194.

Old, K. M., and J. F. Darbyshire. 1978. Soil fungi as food for giant amoebae. Soil Biology and Biochemistry 10:93-100.

Oldfield, E. E., M. A. Bradford, and S. A. Wood. 2019. Global meta-analysis of the relationship between soil organic matter and crop yields. SOIL 5:15-32.

Olesen, J. E., M. Askegaard, and I. A. Rasmussen. 2000. Design of an Organic Farming Crop-Rotation Experiment. Acta Agriculturae Scandinavica, Section B — Soil & Plant Science 50:13-21.

Panettieri, M., H. Knicker, J. M. Murillo, E. Madejón, and P. G. Hatcher. 2014. Soil organic matter degradation in an agricultural chronosequence under different tillage regimes evaluated by organic matter pools, enzymatic activities and CPMAS ^{13}C NMR. Soil Biology and Biochemistry 78:170-181.

Panikov, N. S. 1995. Microbial growth kinetics. Chapman and Hall, London, Glasgow.

Passioura, J. B. 2002. Soil conditions and plant growth'. Plant Cell and Environment 25:311-318.

Pausch, J., and Y. Kuzyakov. 2018. Carbon input by roots into the soil: Quantification of rhizodeposition from root to ecosystem scale. Glob Chang Biol 24:1-12.

Pawlowski, J., S. Audic, S. Adl, D. Bass, L. Belbahri, C. Berney, S. S. Bowser, I. Cepicka, J. Decelle, M. Dunthorn, A. M. Fiore-Donno, G. H. Gile, M. Holzmann, R. Jahn, M. Jirků, P. J. Keeling, M. Kostka, A. Kudryavtsev, E. Lara, J. Lukeš, D. G. Mann, E. A. D. Mitchell, F. Nitsche, M. Romeralo, G. W. Saunders, A. G. B. Simpson, A. V. Smirnov, J. L. Spouge, R. F. Stern, T. Stoeck, J. Zimmermann, D. Schindel, and C. de Vargas. 2012. CBOL Protist Working Group: Barcoding Eukaryotic Richness beyond the Animal, Plant, and Fungal Kingdoms. PLoS Biology 10:e1001419.

Pelissier, R., L. Buendia, A. Brousse, C. Temple, E. Ballini, F. Fort, C. Violle, and J. B. Morel. 2021. Plant neighbour-modulated susceptibility to pathogens in intraspecific mixtures. Journal of Experimental Botany 72:6570-6580.

Peralta, A. L., Y. Sun, M. D. McDaniel, and J. T. Lennon. 2018. Crop rotational diversity increases disease suppressive capacity of soil microbiomes. Ecosphere 9:e02235.

Peters, R. D., A. V. Sturz, M. R. Carter, and J. B. Sanderson. 2003. Developing disease-suppressive soils through crop rotation and tillage management practices. Soil and Tillage Research 72:181-192.

Phalempin, M., N. Jentzsch, J. M. Köhne, S. Schreiter, R. Gründling, D. Vetterlein, and S. Schlüter. 2025. Soil structure development in a five-year chronosequence of maize cropping on two contrasting soil textures. Soil and Tillage Research 251.

Philip Robertson, G., K. L. Gross, S. K. Hamilton, D. A. Landis, T. M. Schmidt, S. S. Snapp, and S. M. Swinton. 2014. Farming for Ecosystem Services: An Ecological Approach to Production Agriculture. Bioscience 64:404-415.

Pieterse, C. M. J., C. Zamioudis, R. L. Berendsen, D. M. Weller, S. C. M. Van Wees, and P. A. H. M. Bakker. 2014. Induced Systemic Resistance by Beneficial Microbes. Annual Review of Phytopathology 52:347-375.

Pimm, S. L., and P. Raven. 2000. Extinction by numbers. Nature 403:843-845.

Raaijmakers, J. M., and E. T. Kiers. 2022. Rewilding plant microbiomes. Science 378:599-600.

Raaijmakers, J. M., and M. Mazzola. 2016. Soil immune responses. Science 352:1392-1393.

Raaijmakers, J. M., T. C. Paulitz, C. Steinberg, C. Alabouvette, and Y. Moënne-Loccoz. 2009. The rhizosphere: a playground and battlefield for soilborne pathogens and beneficial microorganisms. Plant and Soil 321:341-361.

Rasse, D. P., and A. J. M. Smucker. 1998. Root recolonization of previous root channels in corn and alfalfa rotations. Plant and Soil 204:203-212.

Reischke, S., M. G. K. Kumar, and E. Bååth. 2015. Threshold concentration of glucose for bacterial growth in soil. Soil Biology and Biochemistry 80:218-223.

Rizaludin, M. S., N. Stopnisek, J. M. Raaijmakers, and P. Garbeva. 2021. The Chemistry of Stress: Understanding the 'Cry for Help' of Plant Roots. Metabolites 11.

Rolfe, S. A., J. Griffiths, and J. Ton. 2019. Crying out for help with root exudates: adaptive mechanisms by which stressed plants assemble health-promoting soil microbiomes. Current Opinion in Microbiology 49:73-82.

Rosenberg, K., J. Bertaux, K. Krome, A. Hartmann, S. Scheu, and M. Bonkowski. 2009. Soil amoebae rapidly change bacterial community composition in the rhizosphere of Arabidopsis thaliana. The ISME Journal 3:675-684.

Roy, J., R. van Duijnen, E. F. Leifheit, S. Mbedi, V. M. Temperton, and M. C. Rillig. 2021. Legacy effects of pre-crop plant functional group on fungal root symbionts of barley. Ecological Applications.

Rüger, L., K. Feng, Y. Chen, R. Sun, B. Sun, Y. Deng, D. Vetterlein, and M. Bonkowski. 2023a. Responses of root architecture and the rhizosphere microbiome assembly of maize (Zea mays L.) to a soil texture gradient. Soil Biology and Biochemistry 181:109026.

Rüger, L., K. Feng, K. Dumack, J. Freudenthal, Y. Chen, R. Sun, M. Wilson, P. Yu, B. Sun, Y. Deng, F. Hochholdinger, D. Vetterlein, and M. Bonkowski. 2021. Assembly Patterns of the Rhizosphere Microbiome Along the Longitudinal Root Axis of Maize (Zea mays L.). Frontiers in Microbiology 12:614501.

Rüger, L., M. Ganther, J. Freudenthal, J. Jansa, A. Heintz-Buschart, M. T. Tarkka, and M. Bonkowski. 2023b. Root cap is an important determinant of rhizosphere microbiome assembly. New Phytologist 239:1434-1448.

Rüger, L., M. Wilson, J. Jansa, J. Huang, N. Eisenhauer, and M. Bonkowski. in prep. Effects of protist species richness on the composition of the rhizosphere bacterial microbiome and plant performance.

Salse, J., R. L. Barnard, C. Veneault-Fourrey, and H. Rouached. 2024. Strategies for breeding crops for future environments. Trends in Plant Science 29:303-318.

Santangeli, M., T. Steininger-Mairinger, D. Vetterlein, S. Hann, and E. Oburger. 2024. Maize (Zea mays L.) root exudation profiles change in quality and quantity during plant development – A field study. Plant Science 338.

Sasse, J., E. Martinoia, and T. Northen. 2018. Feed Your Friends: Do Plant Exudates Shape the Root Microbiome? Trends in Plant Science 23:25-41.

Sawada, K., S. Funakawa, and T. Kosaki. 2008. Soil microorganisms have a threshold concentration of glucose to increase the ratio of respiration to assimilation. Soil Science and Plant Nutrition 54:216-223.

Schlaeppi, K., N. Dombrowski, R. G. Oter, E. Ver Loren van Themaat, and P. Schulze-Lefert. 2014. Quantitative divergence of the bacterial root microbiota in Arabidopsis thaliana relatives. Proceedings of the National Academy of Sciences of the United States of America 111:585-592.

Schlatter, D., L. Kinkel, L. Thomashow, D. Weller, and T. Paulitz. 2017. Disease Suppressive Soils: New Insights from the Soil Microbiome. Phytopathology® 107:1284-1297.

Schnepf, A., A. Carminati, M. A. Ahmed, M. Ani, P. Benard, J. Bentz, M. Bonkowski, M. Knott, D. Diehl, P. Duddek, E. Kröner, M. Javaux, M. Landl, E. Lehndorff, E. Lippold, A. Lieu, C. W. Mueller, E. Oburger, W. Otten, X. Portell, M. Phalempin, A. Prechtel, R. Schulz, J. Vanderborght, and D. Vetterlein. 2022. Linking rhizosphere processes across scales: Opinion. Plant and Soil.

Schrama, M., J. J. de Haan, M. Kroonen, H. Verstegen, and W. H. Van der Putten. 2018. Crop yield gap and stability in organic and conventional farming systems. Agriculture, Ecosystems & Environment 256:123-130.

Schulz-Bohm, K., S. Gerards, M. Hundscheid, J. Melenhorst, W. de Boer, and P. Garbeva. 2018. Calling from distance: attraction of soil bacteria by plant root volatiles. The ISME Journal 12:1252-1262.

Schwelm, A., J. Badstöber, S. Bulman, N. Desoignies, M. Etemadi, R. E. Falloon, C. M. M. Gachon, A. Legreve, J. Lukeš, U. Merz, A. Nenarokova, M. Strittmatter, B. K. Sullivan, and S. Neuhauser. 2018. Not in your usual Top 10: protists that infect plants and algae. Molecular Plant Pathology 19:1029-1044.

Seitz, V. A., B. B. McGivern, M. A. Borton, J. M. Chaparro, M. E. Schipanski, J. E. Prenni, and K. C. Wrighton. 2024. Cover crop root exudates impact soil microbiome functional trajectories in agricultural soils. Microbiome 12:183.

Shipton, P. J. 1977. Monoculture and Soilborne Plant Pathogens. Annual Review of Phytopathology 15:387-407.

Spooren, J., S. van Bentum, L. S. Thomashow, C. M. J. Pieterse, D. M. Weller, and R. L. Berendsen. 2024. Plant-Driven Assembly of Disease-Suppressive Soil Microbiomes. Annual Review of Phytopathology 62:1-30.

Stenström, J., K. Svensson, and M. Johansson. 2001. Reversible transition between active and dormant microbial states in soil. FEMS Microbial Ecology 36:93-104.

Stockdale, E. A., N. H. Lampkin, M. Hovi, R. Keatinge, E. K. M. Lennartsson, D. W. Macdonald, S. Padel, F. H. Tattersall, M. S. Wolfe, and C. A. Watson. 2001. Agronomic and environmental implications of organic farming systems. Pages 261-327 Advances in Agronomy. Academic Press.

Strom, N., W. Hu, D. Haarith, S. Chen, and K. Bushley. 2020. Interactions between soil properties, fungal communities, the soybean cyst nematode, and crop yield under continuous corn and soybean monoculture. Applied Soil Ecology 147:103388.

Swinnen, J., J. A. Van Veen, and R. J. S. B. Merckx. 1994. 14C pulse-labelling of field-grown spring wheat: an evaluation of its use in rhizosphere carbon budget estimations. Soil Biology & Biochemistry 26:161-170.

Tai, H., X. Lu, N. Opitz, C. Marcon, A. Paschold, A. Lithio, D. Nettleton, and F. Hochholdinger. 2016. Transcriptomic and anatomical complexity of primary, seminal, and crown roots highlight root type-specific functional diversity in maize (Zea mays L.). Journal of Experimental Botany 67:1123-1135.

Thines, M. 2014. Phylogeny and evolution of plant pathogenic oomycetes—a global overview. European Journal of Plant Pathology 138:431-447.

Toju, H., K. G. Peay, M. Yamamichi, K. Narisawa, K. Hiruma, K. Naito, S. Fukuda, M. Ushio, S. Nakaoka, Y. Onoda, K. Yoshida, K. Schlaeppi, Y. Bai, R. Sugiura, Y. Ichihashi, K. Minamisawa, and E. T. Kiers. 2018. Core microbiomes for sustainable agroecosystems. Nat Plants 4:247-257.

Trivedi, P., J. E. Leach, S. G. Tringe, T. Sa, and B. K. Singh. 2020. Plant-microbiome interactions: from community assembly to plant health. Nature Reviews Microbiology 18:607-621.

van der Putten, W. H., R. D. Bardgett, J. D. Bever, T. M. Bezemer, B. B. Casper, T. Fukami, P. Kardol, J. N. Klironomos, A. Kulmatiski, J. A. Schweitzer, K. N. Suding, T. F. J. Van de Voorde, and D. A. Wardle. 2013. Plant–soil feedbacks: the past, the present and future challenges. Journal of Ecology 101:265-276.

van Dusschoten, D., R. Metzner, J. Kochs, J. A. Postma, D. Pflugfelder, J. Buhler, U. Schurr, and S. Jahnke. 2016. Quantitative 3D Analysis of Plant Roots Growing in Soil Using Magnetic Resonance Imaging. Plant Physiol 170:1176-1188.

Vandenkoornhuyse, P., A. Quaiser, M. Duhamel, A. Le Van, and A. Dufresne. 2015. The importance of the microbiome of the plant holobiont. New Phytologist 206:1196-1206.

Vessey, J. K. 2003. Plant growth promoting rhizobacteria as biofertilizers. Plant and Soil 255:571-586.

Vetterlein, D., A. Carminati, I. Kögel-Knabner, G. P. Bienert, K. Smalla, E. Oburger, A. Schnepf, T. Banitz, M. T. Tarkka, and S. Schlüter. 2020. Rhizosphere Spatiotemporal Organization–A Key to Rhizosphere Functions. Frontiers in Agronomy 2.

Vetterlein, D., E. Lippold, S. Schreiter, M. Phalempin, T. Fahrenkampf, F. Hochholdinger, C. Marcon, M. Tarkka, E. Oburger, M. Ahmed, M. Javaux, and S. Schlüter. 2021. Experimental platforms for the investigation of spatiotemporal patterns in the rhizosphere—Laboratory and field scale. Journal of Plant Nutrition and Soil Science 184:35-50.

Vitousek, P. M., R. Naylor, T. Crews, M. B. David, L. E. Drinkwater, E. Holland, P. J. Johnes, J. Katzenberger, L. A. Martinelli, P. A. Matson, G. Nziguheba, D. Ojima, C. A. Palm, G. P. Robertson, P. A. Sanchez, A. R. Townsend, and F. S. Zhang. 2009. Nutrient Imbalances in Agricultural Development. Science 324:1519-1520.

Wagg, C., K. Schlaeppi, S. Banerjee, E. E. Kuramae, and M. G. A. van der Heijden. 2019. Fungal-bacterial diversity and microbiome complexity predict ecosystem functioning. Nat Commun 10:4841.

Walter, A., R. Feil, and U. Schurr. 2003. Expansion dynamics, metabolite composition and substance transfer of the primary root growth zone of Zea mays L. grown in different external nutrient availabilities. . Plant, Cell & Environment 26:1451-1466.

Wang, X., Y. Chi, and S. Song. 2024. Important soil microbiota's effects on plants and soils: a comprehensive 30-year systematic literature review. Front Microbiol 15:1347745.

Wang, Z., and Y. Song. 2022. Toward understanding the genetic bases underlying plant-mediated "cry for help" to the microbiota. Imeta 1:e8.

Watt, M., P. Hugenholtz, R. White, and K. Vinall. 2006. Numbers and locations of native bacteria on field-grown wheat roots quantified by fluorescence in situ hybridization (FISH). Environmental Microbiology 8(5).

Watt, M., M. E. McCully, and J. A. Kirkegaard. 2003. Soil strength and rate of root elongation alter the accumulation of Pseudomonas spp. and other bacteria in the rhizosphere of wheat. . Functional Plant Biology 30:483-491.

Weller, D. M., J. M. Raaijmakers, B. B. M. Gardener, and L. S. Thomashow. 2002. MICROBIAL POPULATIONS RESPONSIBLE FOR SPECIFIC SOIL SUPPRESSIVENESS. Annual Review of Phytopathology 40:309-348.

Wen, A., K. L. Havens, S. E. Bloch, N. Shah, D. A. Higgins, A. G. Davis-Richardson, J. Sharon, F. Rezaei, M. Mohiti-Asli, A. Johnson, G. Abud, J.-M. Ane, J. Maeda, V. Infante, S. S. Gottlieb, J. G. Lorigan, L. Williams, A. Horton, M. McKellar, D. Soriano, Z. Caron, H. Elzinga, A. Graham, R. Clark, S.-M. Mak, L. Stupin, A. Robinson, N. Hubbard, R. Broglie, A. Tamsir, and K. Temme. 2021. Enabling Biological Nitrogen Fixation for Cereal Crops in Fertilized Fields. ACS Synthetic Biology 10:3264-3277.

Wendel, A. S., S. L. Bauke, W. Amelung, and C. Knief. 2022. Root-rhizosphere-soil interactions in biopores. Plant and Soil 475:253-277.

Williams, D. M., H. Blanco-Canqui, C. A. Francis, and T. D. Galusha. 2017. Organic Farming and Soil Physical Properties: An Assessment after 40 Years. Agronomy Journal 109:600-609.

Williams, M. A., and C. W. Rice. 2007. Seven years of enhanced water availability influences the physiological, structural, and functional attributes of a soil microbial community. Applied Soil Ecology 35:535-545.

Wubs, E. R. J., and T. M. Bezemer. 2018. Temporal carry-over effects in sequential plant–soil feedbacks. Oikos 127:220-229.

Yang, T., K. H. M. Siddique, and K. Liu. 2020. Cropping systems in agriculture and their impact on soil health-A review. Global Ecology and Conservation 23.

Yim, B., Z. Ibrahim, L. Rüger, M. Ganther, L. Maccario, S. J. Sørensen, A. Heintz-Buschart, M. T. Tarkka, D. Vetterlein, M. Bonkowski, E. Blagodatskaya, and K. Smalla. 2022. Soil texture is a stronger driver of the maize rhizosphere microbiome and extracellular enzyme activities than soil depth or the presence of root hairs. Plant and Soil.

Yuan, J., J. Zhao, T. Wen, M. Zhao, R. Li, P. Goossens, Q. Huang, Y. Bai, J. M. Vivanco, G. A. Kowalchuk, R. L. Berendsen, and Q. Shen. 2018. Root exudates drive the soil-borne legacy of aboveground pathogen infection. Microbiome 6:156.

Zarebanadkouki, M., T. Fink, P. Benard, and C. C. Banfield. 2019. Mucilage Facilitates Nutrient Diffusion in the Drying Rhizosphere. Vadose Zone Journal 18:190021.

Zhalnina, K., K. B. Louie, Z. Hao, N. Mansoori, U. N. Da Rocha, S. Shi, and E. L. Brodie. 2018. Dynamic root exudate chemistry and microbial substrate preferences drive patterns in rhizosphere microbial community assembly. . Nature microbiology 3:470-480.

Zhao, J., X. Xie, Y. Jiang, J. Li, Q. Fu, Y. Qiu, X. Fu, Z. Yao, Z. Dai, Y. Qiu, and H. Chen. 2024. Effects of simulated warming on soil microbial community diversity and composition across diverse ecosystems. Science of the Total Environment 911:168793.

Zhao, Y., W. Fu, C. Hu, G. Chen, Z. Xiao, Y. Chen, Z. Wang, and H. Cheng. 2021. Variation of rhizosphere microbial community in continuous mono-maize seed production. Sci Rep 11.

Zhao, Z.-B., J.-Z. He, S. Geisen, L.-L. Han, J.-T. Wang, J.-P. Shen, W.-X. Wei, Y.-T. Fang, P.-P. Li, and L.-M. Zhang. 2019. Protist communities are more sensitive to nitrogen fertilization than other microorganisms in diverse agricultural soils. Microbiome 7:33.

Zhong, Y., W. Xun, X. Wang, S. Tian, Y. Zhang, D. Li, Y. Zhou, Y. Qin, B. Zhang, G. Zhao, X. Cheng, Y. Liu, H. Chen, L. Li, A. Osbourn, W. J. Lucas, S. Huang, Y. Ma, and Y. Shang. 2022. Root-secreted bitter triterpene modulates the rhizosphere microbiota to improve plant fitness. Nature Plants 8:887-896.

Zickenrott, I. M., S. K. Woche, J. Bachmann, M. A. Ahmed, and D. Vetterlein. 2016. An efficient method for the collection of root mucilage from different plant species—A case study on the effect of mucilage on soil water repellency. Journal of Plant Nutrition and Soil Science 179:294-302.

Zilber-Rosenberg, I., and E. Rosenberg. 2008. Role of microorganisms in the evolution of animals and plants: the hologenome theory of evolution. FEMS Microbiology Reviews 32:723-735.